PHD

An ultrasonic study of the elastic properties and acoustic mode vibrational anharmonicity in glasses and crystals

Sidek, Hj. Ab. Aziz

Award date:
1989

Awarding institution:
University of Bath

AN ULTRASONIC STUDY OF THE ELASTIC PROPERTIES AND ACOUSTIC MODE VIBRATIONAL ANHARMONICITY IN GLASSES AND CRYSTALS.

submitted by

Hj. Ab. Aziz SIDEK

for the degree of Doctor of Philosophy

of the University of Bath

1989

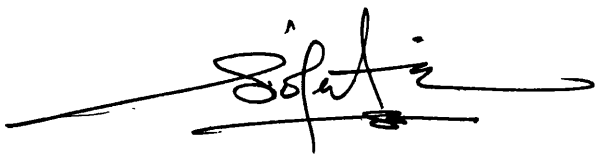

ProQuest LLC
789 East Eisenhower Parkway
P.O. Box 1346
Ann Arbor, MI 48106-1346

IN THE NAME OF ALLAH, THE BENEFICIENT, THE MERCIFUL

This thesis is dedicated to

my parents

my wife - Siti Jauyah

my son - Amir Sidek

ACKNOWLEDGEMENTS

First and foremost I would like to express my sincere gratitude to Professor G. A. Saunders for his constant supervision, interest, encouragement and support during the period of this research. Working in Professor Saunders' research team has provided me with some enormous theoretical and experimental experiences from which I will continue to draw benefit in the future.

I owe a particular debt of thanks to many others especially to our technical staff; Mrs. W. A. Lambson for her carefully alignment, cutting and polishing all my ultrasonic samples, Mr. E. F. Lambson for his efficiency in dealing with high pressure ultrasonic system, Mr. R. C. J. Draper for his quick-reaction in solving any technical problem, Mr. B. Chapman for his guidance in using the X-ray facilities, Dr. R. N. Hampton for useful discussions and my research colleaques - Noureddine, Ian, Sheikh, Ali, Haitham and Wang.

I am really grateful to the Agriculture University (UPM) and Public Service Department of Malaysia for their study leave and financial support. "Jutaan terima kasih" for them.

Abstract

Measurements of ultrasonic wave velocities and their hydrostatic pressure and temperature dependences have enabled determination of linear and nonlinear elastic properties of a number of glasses and single crystals. In each material studied, some form of softening of acoustic modes occurs either with pressure or temperature or both. To quantify this softening, the zone centre acoustic phonon mode vibrational anharmonicities are expressed in terms of the mode Grüneisen parameters γ_i $(= -\mathrm{d}\ln\omega_i/\mathrm{d}\ln V)$.

(i) Softening the shear modes under pressure is found in $(Ag_2O)_y(B_2O_3)_{1-y}$ and $(AgI)_x[(Ag_2O)_y(B_2O_3)_{1-y}]_{1-x}$ superionic glasses: dC_{44}/dP and γ_S are negative. Differences between dC_{IJ}/dP in the binary and ternary glasses implies that silver ions introduced via Ag_2O and AgI occupy different microscopic sites.

(ii) In $(Sm_2O_3)_x(P_2O_5)_{1-x}$ glasses, an unusual compositional dependence of the elastic behaviour is correlated with the microscopic structure changes. As pressure is increased, these glasses become easier to compress: their longitudinal and shear modes soften with pressure whilst a reduction of temperature causes slight mode softening. A relaxation process of two-level systems

affects the elastic constants at low temperatures.

(iii) The pressure dependences of the elastic constants of the cubic Ce_3S_4 crystal have been measured. Although this material has positive temperature derivatives of C_{11} and C' ($=(C_{11}-C_{12})/2$): evidence of a phase transition at low temperatures, application of pressure does not result in mode softening.

(iv) In the two piezoelectric crystals, rhombohedral $AlPO_4$ and tetragonal $Li_2B_4O_7$, application of pressure does induce shear mode softening: dC_{66}/dP and the respective γ_i are negative. For $AlPO_4$, this is consistent with a positive temperature dependence of C_{66} associated with interaction between the transverse-acoustic and the optic phonons.

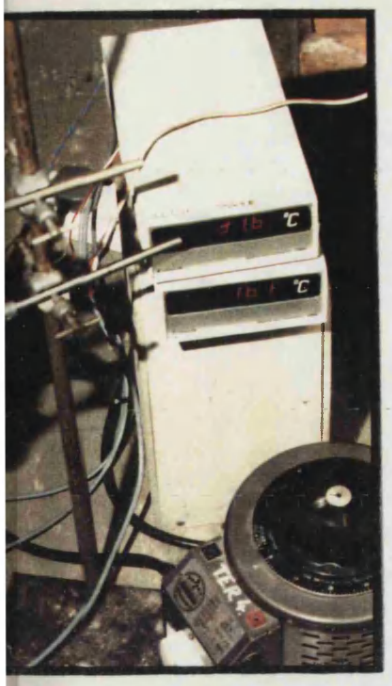

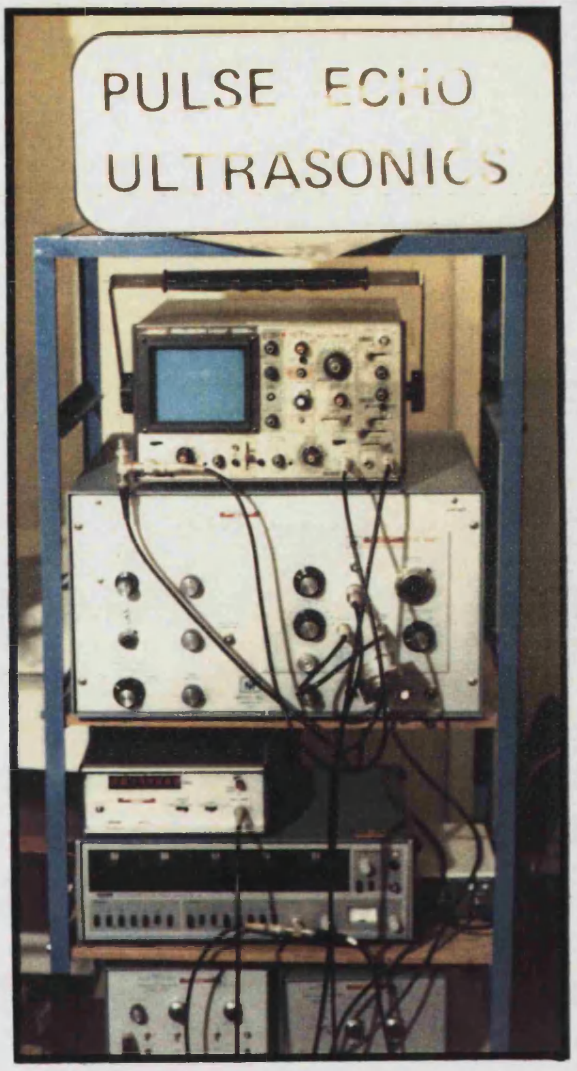
PULSE ECHO
ULTRASONICS

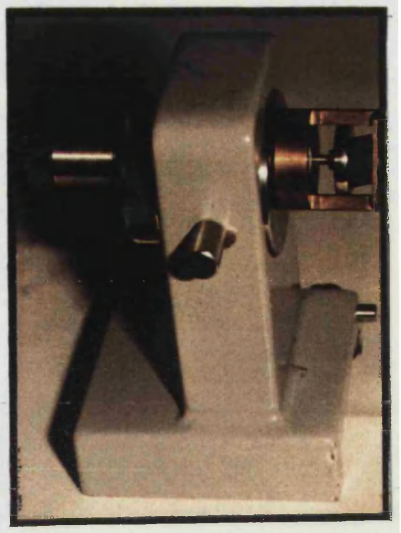

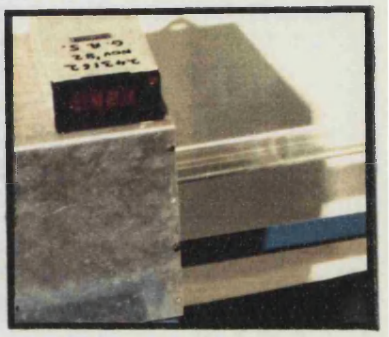

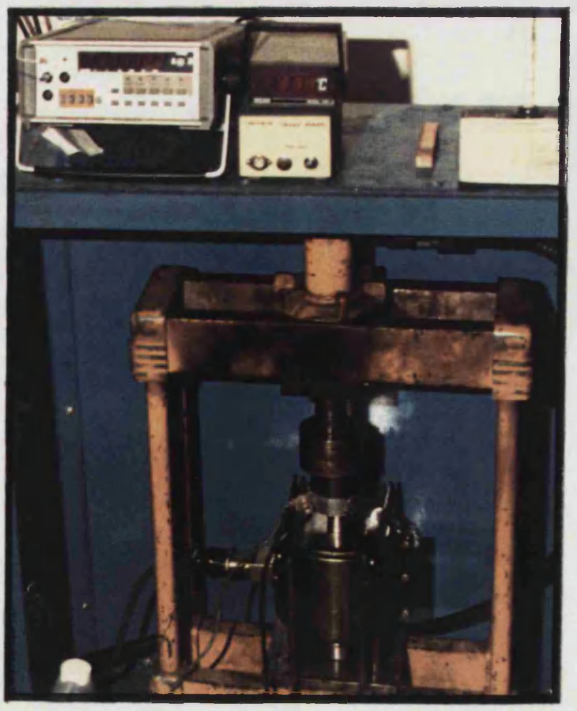

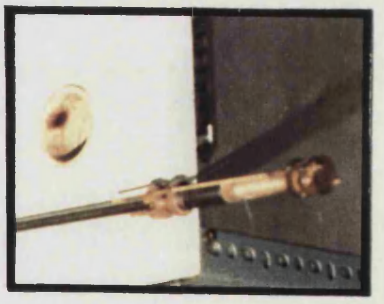

CONTENTS

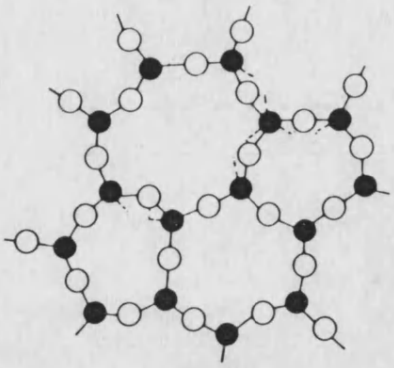

1

GENERAL INTRODUCTION

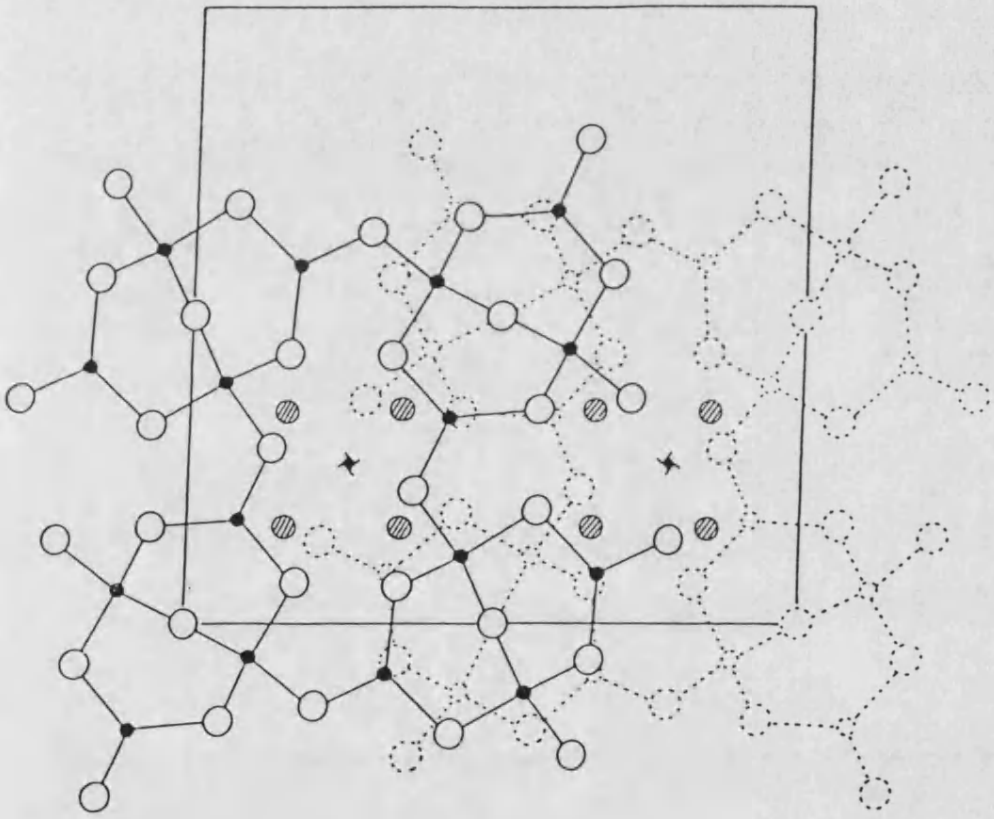

CHAPTER ONE

GENERAL INTRODUCTION

The main objective of this research is to investigate the elasticity and vibrational anharmonicity of the long wavelength acoustic phonons modes in a number of solids which can show interesting phonon properties. Study of ultrasonic wave propagation in solid materials has been recognized as a most effective way of evaluating their elastic properties especially under pressure. The emphasis has been placed here on measurement of the effect of hydrostatic pressure and temperature on the velocities of ultrasonic wave propagation. These measurements have been accomplished by using the well established pulse-echo overlap system. In general the fundamental elastic parameters which control many of the mechanical properties of solids are given by the second order elastic constants (SOEC) which describe macroscopically the resistance of a solid body to strain. They constitute the coefficient in the linear relationship between stress and strain. Since the SOEC relate directly to the second derivative of the total energy of a solid with respect to strain, they lead to an insight into the nature of the interatomic binding

forces. For instance a description of the interatomic long-range attractive and short-range repulsive interactions which make up the total internal energy of solid materials is provided through the macroscopic bulk modulus (a linear combination of elastic constants). Knowledge of elastic constants is also of central importance in theoretical investigations of the vibrational properties of solids because they define the slopes of the acoustic branches of the phonon dispersion curves near to the Brillouin zone centre.

The concept of anharmonicity, defined as the nonlinearity of interatomic forces with respect to atomic displacements, has also to be involved when the vibrational properties of solids are discussed. Even at absolute zero the atomic vibrations which govern the thermal behaviour of solids are not linear (i.e. Hooke's law is not obeyed). Studies of the effect of hydrostatic pressure and temperature upon the elastic constants of solids have the aim of providing details of the acoustic mode vibrational anharmonicity. The pressure dependences of the elastic constants themselves provide information on the shift of the mode energies with compression and characterize the acoustic mode vibrational anharmonicity. In the long wavelength limit the acoustic mode Grüneisen parameters quantify the volume dependence $(-d\ln\omega_i/d\ln V)$ of the normal mode frequencies ω_i, or in other words the strain dependences of the lattice vibrational frequencies, accruing from the effect of hydrostatic

pressure upon lattice potential. The temperature dependences of the second order elastic stiffness constants also provide useful information on the anharmonicity of lattice vibrations of solids. Especially at high temperatures, all physical properties which depend upon thermal motion are greatly influenced by anharmonicty so that its knowledge is fundamental to an understanding of material properties such as mechanical strength, thermal expansion, lattice instability and soft phonon modes. In chapter 2, the general concepts of elasticity and anharmonicity are reviewed, serving as a basic introduction for the development of the subject of the rest of the work. An outline of the experimental techniques and relevant systems employed is given in chapter 3.

Chapter 4 through 6 deal specifically with glasses while the three subsequent chapters are concerned with three different crystalline solids. The experimental results obtained on each type of solid are presented intentionally for convenience, in separate chapters avoiding any complexity due to the different physical nature of each sample studied.

In chapter 4, we present a brief review of some aspects of the nature of amorphous materials which include the essentials of making the glasses and aspects of their microscopic stuctures. The essential difference between a glass and a crystal is explained by the random network theory proposed by Zachariasen (1932). It is now

realized that most amorphous materials show distinctive features of acoustic and thermal properties in the low temperatures region, for example vitreous silica has larger specific heat than a quartz crystal (Zeller and Pohl 1971). Such behaviour has been accounted for using the concept of two-level systems (Phillips 1972, Anderson et al. 1972) where in addition to phonons, amorphous materials contains low frequency vibrational states. In this connection, an anomalous behaviour of the ultrasonic wave velocity in many glasses as the temperature is reduced towards absolute zero can be quite well described by utilizing the model of two-level systems. Interest in the series of Ag_2O-B_2O_3 (binary) and AgI-Ag_2O-B_2O_3 (ternary) silver borate glasses arises from their being superionic conducting glasses: their electrical properties show high ionic conductivity. The beginning of this work arose from the question of how the ease of ionic motion might be related to the ion vibrational states in ionic glass. So for this reason we have made the first measurements of elastic behaviour under hydrostatic pressure in a series of superionic glasses in order to acquire information about the anharmonicity of the long wavelength acoustic modes in these materials (chapter 5). The ultrasonic measurements in these glasses have not only provided their elastic properties but also lead to information about the behaviour of the mobile ions contributed from two different sources in the glassy matrix of such materials. The chemical compositional

dependence upon the ultrasonic wave velocity can also be used to help in evaluate the possible of glass structure.

The presence of a variable valence rare-earth element is known to promote a valence instability state in certain crystals and usually causes some striking physical behaviour. For example crystalline SmS crystal exhibits a pressure induced transformation which can influence the occurence of soft acoustic phonons modes (Tu Hailing, Saunders and Bach 1984). To search for the possibility that the intermediate valence state can occur for a rare earth ion in a glassy matrix, an ultrasonic study has been made of a series of samarium phosphate glasses in the composition range 5 mole% to 25 mole% of Sm_2O_3. The compositional dependences of the elastic constants and their hydrostatic pressure and temperature derivatives of these glasses do show anomalous behaviour (chapter 6). For example, their bulk and shear moduli unlike other phosphate glasses, decrease under hydrostatic pressure which lead to negative values of longitudinal and transverse mode Grüneisen parameters: an indication of acoustic mode softening.

A previous study on rare-earth cerium chalcogenide Ce_3S_4 crystal (Futterer et al. 1988) has shown that this crystal (unlike La_3S_4) does not undergo a phase transition when temperature is lowered to 16K, however it its elastic stiffnesses $(C_{11} - C_{12})/2$ and C_{11} reveal the fact that the associated acoustic phonons soften with temperature. One of our aims is to see whether the

acoustic phonon mode softening can also be disclosed by the application of hydrostatic pressure to this particular compound containing a variable valence rare-earth element (chapter 7).

The piezolectric crystal berlinite ($AlPO_4$) has also been reported to display a softening acoustic phonon mode which resulted in an anomalous positive temperature dependence of C_{66}. Furthermore this rhombohedral $AlPO_4$ and its isomorphic quartz crystals exhibit the α-β structural transformation which results in softening of certain zone centre optic phonons at room temperature. So measurements have been made for the ultrasonic wave velocity as a function of hydrostatic pressure in $AlPO_4$ (embodied of chapter 8) to answer the question whether the possible structural transformation has any effect in residual softening of the long wavelength phonons, especially of the transverse acoustic phonons which propagate along [010] with [100] polarisation directions. Piezoelectric crystals often show mode softening so this study the soft acoustic phonon mode has been extended to include lithium tetraborate. Lithium tetraborate ($Li_2B_4O_7$) is a non-centrosymmetric piezoelectric crystal which has potential in electronic engineering and high frequency devices. The experimental work of chapter 9, which contributes a substantial portion of this thesis, is designed to study the elastic behaviour of lithium tetraborate $Li_2B_4O_7$ tetragonal single crystal as a function of temperature and hydrostatic pressure for the

first time. Effort has been made to study of each pure- and quasi-modes elastic wave propagation in this tetragonal crystal in order to obtained the temperature dependences of each elastic stiffness constants down to 4.2K. Present measurements of this non-cubic crystal indeed reveal that some of the transverse acoustic phonons of long wavelength soften either with temperature or hydrostatic pressure.

Finally, in chapter 10, a summary is presented to portray the important findings of our work and discuss the generality of the conclusions in this study of elasticity and acoustic mode vibrational anharmonicity of several solids which exhibit aspects of mode softening.

2

GENERAL DESCRIPTION OF THE ELASTICITY OF SOLIDS AND ACOUSTIC VIBRATIONAL ANHARMONICITY.

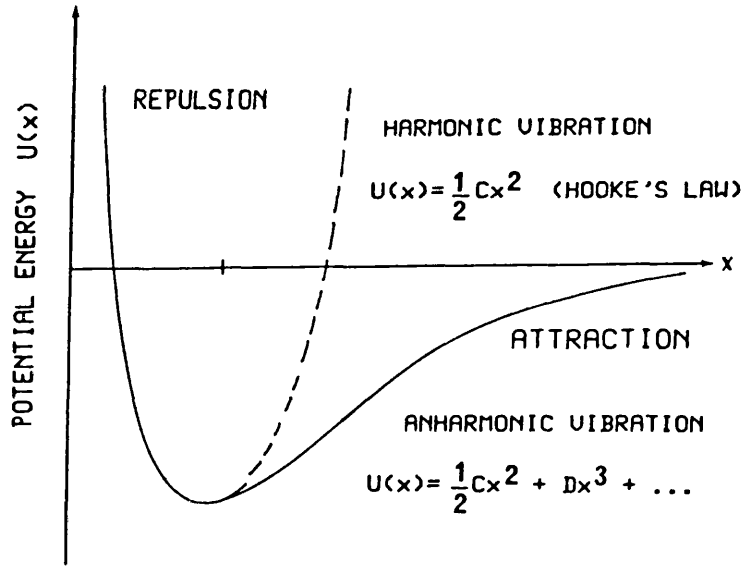

CHAPTER TWO

GENERAL DESCRIPTION OF THE ELASTICITY OF SOLIDS AND ACOUSTIC VIBRATIONAL ANHARMONICITY.

2.1 Introduction.

In general, the application of external forces to a solid body produces complex internal forces which cause motion of the body, in the form of linear translation, rotation and deformation. The body is in a condition of stress and any changes in the shape or volume are then referred to as strain. In the case of an elastic body, after removal of the external forces, the material returns to its original unstressed condition. In the study of elasticity we only consider infinitesimal elastic deformations, where stress is linearly proportional to strain, as stated in Hooke's law. The parameters which connect stress and strain are the elastic constants and these can be determined experimentally by propagating ultrasonic elastic waves travel through a medium. The velocity of these waves and density of the sample can be used to determine the values of these elastic constants. To explain quantitatively the elastic behaviour of a solid body, under external stresses, for example temperature

and hydrostatic pressure, the concept of an elastic continuum is applied. Here crystalline (or noncrystalline materials) are assumed to behave like a homogeneous continuous medium. This continuum approximation is usually valid for elastic waves of wavelengths λ longer than 10^{-6} cm, i.e. frequencies below 10^{12} Hz, and ultrasonic waves fullfil this criterion.

In the folowing sections, a brief description of the theory of elasticity and the anharmonicity of solids, both crystal and noncrystalline (glass) systems, will be given. The propagation of elastic waves in crystals, including the thermodynamic definition of elastic constants, is discussed and the concept of anharmonicity is also outlined. General aspects of the effect of hydrostatic pressure and temperature on the elastic constants are also given. A comprehensive review of this field of study can be found in standard texts such as Nye (1957), Hearman (1961), Truel, Elbaum and Chick (1969) and Musgrave (1970).

2.2 Elasticity and Hooke's Law.

A component of the stress tensor σ_{ij} is defined as the force per unit area in the x_i direction on the area normal to the x_j direction. Hence σ_{ii} are the longitudinal components of stress, and σ_{ij} ($i \neq j$) are the shear components. As stated earlier, any deformations in

the shape or volume of a body are referred to as strain. To define a general expression for the strain, consider a point A in figure 2.1, in an undeformed initial state, which has coordinates (x_1, x_2, x_3) with respect to a system of Cartesian axes. After deformation this point will move to a new position A' with coordinates (x_1',x_2',x_3'). The displacement vector u_i is then defined as

$$u_i = (x_i' - x_i) \tag{2.1}$$

Now consider a second point B adjacent to point A with coordinates x_i+dx_i. After deformation the element AB becomes A'B' with a new position of B' in ($x_i'+dx_i'$). The displacement of B' is given by

$$u_i' = u_i + du_i \tag{2.2}$$

where du_i is a measure of the deformation of the element. The element of AB is said to be displaced without deformation if du_i is equal to zero. By using Taylor's theorem and neglecting higher order terms it can be shown that

$$u_i' = u_i + \epsilon_{ik}\, dx_k - \omega_{ik}\, dx_k \tag{2.3}$$

where

$$\epsilon_{ik} = \frac{1}{2}\left(\frac{\partial u_i}{\partial x_k} + \frac{\partial u_k}{\partial x_i}\right)$$

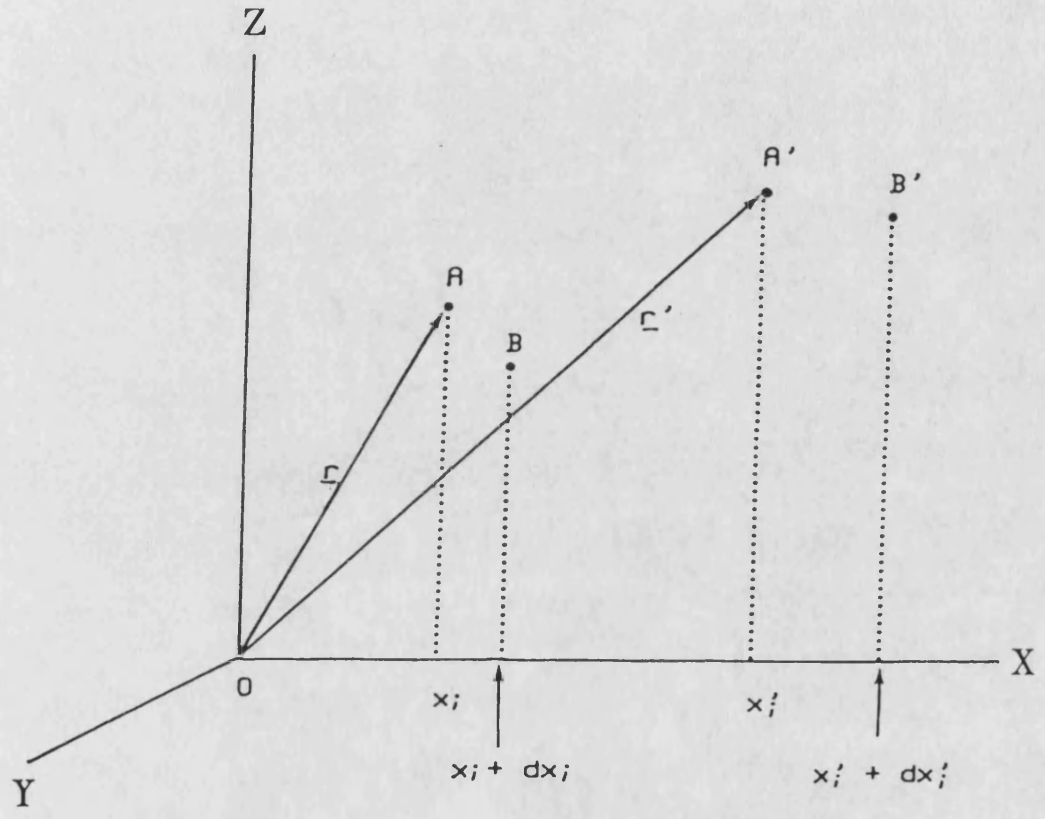

Figure 2.1 : General illustration of an element AB of an elastic body which under deformation becomes the element A'B'.

and

$$\omega_{ik} = \frac{1}{2}\left(\frac{\partial u_k}{\partial x_i} - \frac{\partial u_i}{\partial x_k}\right)$$

The last two equations are called second rank tensors of strain for symmetrical and rotational tensors of antisymmetry parts respectively (Nye 1960). Normal strains (ϵ_{ii}) for diagonal components are produced whenever the external stresses are perpendicular to the area of application whereas the nondiagonal components of ϵ_{ij} ($i \neq j$) are shear strains when the stresses are tangential to the surface of application. Figure 2.2 illustrates the stress and strain tensor for the cubic crystal system.

For sufficiently small deformations of the solid body, each component of stress is linearly related to each component of strain by Hooke's law which can be written in the form of

$$\sigma_{ij} = C_{ijkl}\epsilon_{kl} \qquad (i,j,k,l = 1,2,3) \qquad (2.4)$$

or conversely

$$\epsilon_{ij} = S_{ijkl}\sigma_{kl} \qquad (2.5)$$

Here C_{ijkl} and S_{ijkl} are fourth rank tensors called elastic stiffness or second order elastic constants (SOEC) and elastic compliance constants respectively. The

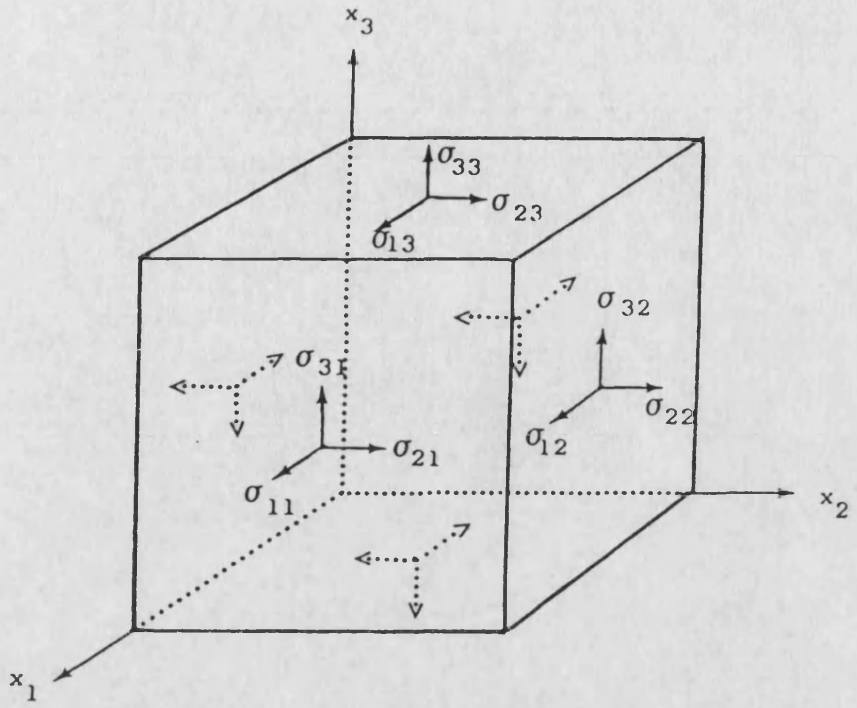

Figure 2.2 (a) : The six components of stress.

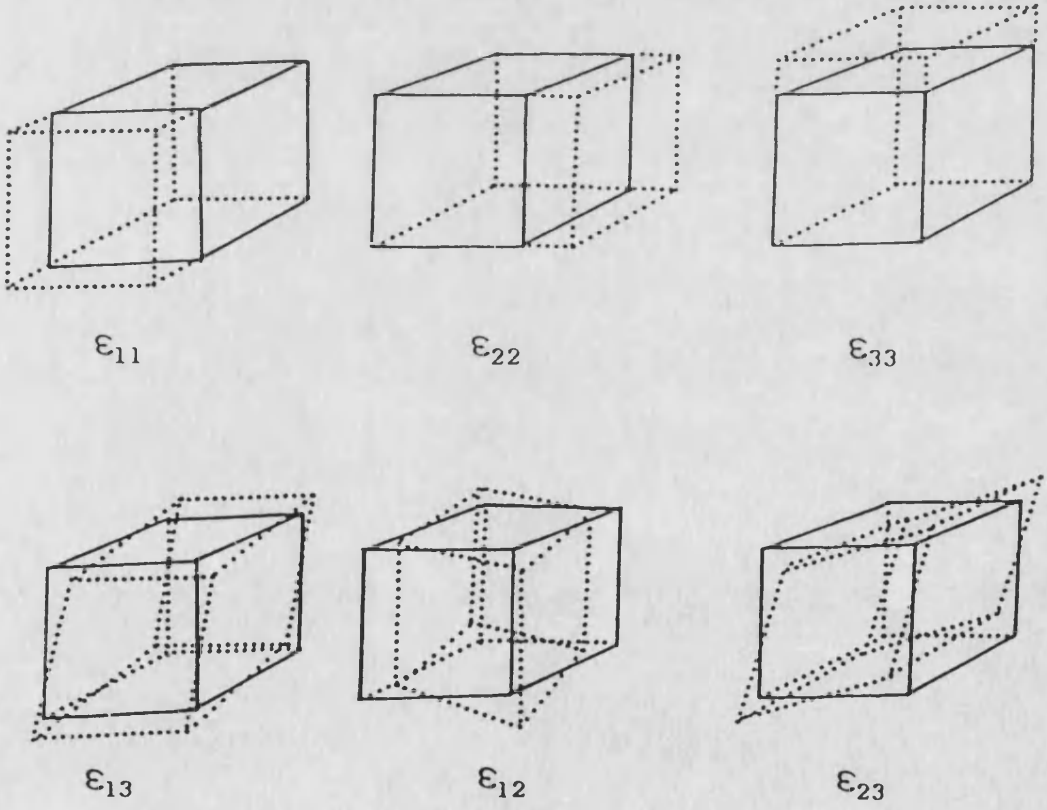

Figure 2.2 (b) : The six components of strain.

elastic constants have dimension of force per unit area (Nm^{-2}) or energy per unit volume (Jm^{-3}), whilst elastic compliances have reciprocal dimensions (m^2N^{-1}).

In general C_{ijkl} has 81 components. However this number reduces to 36 due to symmetry properties of stress (i.e. $\sigma_{ij} = \sigma_{ji}$) and strain ($\epsilon_{ij} = \epsilon_{ji}$) through rotational and translational equilibrium condition for an element of volume in the deformed state of a solid. Since the elastic potential is a function of thermodynamic state where a reversible thermodynamic process takes place under isothermal condition, this condition reduces the independent elastic constants to 21. Further reduction depends on symmetry properties of the material under consideration as Voigt's principle (Landau and Lifshitz 1970, Nye 1960) states that the symmetry of the physical process is dependent on the symmetry of the crystal; so the number of independent elastic constants is dramatically reduced as the degree of symmetry increases. For example a cubic crystal has only three independent elastic constants; there are seven for rhombohedral and six for tetragonal crystal systems. Details of the independent SOEC for all of the seven crystallographic systems are given by Brugger (1965a).

In practice, and for convenience, the elastic constants are written in the matrix notation (sometimes known as Voigt suffix notation) where the following scheme is applied:

Tensor notation	11	22	33	23,32	13,31	12,21
Matrix notation	1	2	3	4	5	6

For instance, C_{2233} is written as C_{23} and C_{1123} as C_{14}.

2.3 The Thermodynamic Definition of Elastic Constants.

Elastic constants can be also defined thermodynamically i.e. with respect to thermodynamic parameters, as was first introduced by Brugger (1964). In this definition the four main thermodynamic potentials can be involved, namely the internal energy U, the Helmholtz free energy F, the enthalpy H and the Gibbs free energy G. Each of these thermodynamic potentials is considered to be a function of entropy S, temperature T, thermodynamic tension components t_{ij} and reduced Lagrangian strain components η_{ij}/ρ_o, where ρ_o represents the density of the unstrained solid. The product of t_{ij} and η_{ij}/ρ_o is analogous referred to pressure and volume in the usual definition of thermodynamic potential in a fluid system. If the solid is not a piezeoelectric material and is free from magnetic and electric fields interactions, then the first and second laws of thermodynamics can be written in the following form

$$dU = Tds + (\frac{1}{\rho_o})t_{ij}d\eta_{ij} \qquad (2.6)$$

$$dF = -SdT + (\frac{1}{\rho_o})t_{ij}d\eta_{ij} \tag{2.7}$$

$$dH = TdS - (\frac{1}{\rho_o})\eta_{ij}dt_{ij} \tag{2.8}$$

$$dG = -SdT - (\frac{1}{\rho_o})\eta_{ij}dt_{ij} \tag{2.9}$$

The potentials and all other extensive variables are taken per unit mass and all the above are summed over repeated indices i and j, as is usual for tensor properties.

The thermodynamic tensions t_{ij} are given by

$$t_{ij} = \rho_o \left(\frac{\partial U}{\partial \eta_{ij}} \right)_{S,\eta'}$$

$$= \rho_o \left(\frac{\partial F}{\partial \eta_{ij}} \right)_{T,\eta'} \tag{2.10}$$

where η' indicates that all other components of η are held constant. From equations (2.6-2.9), the general definition of the elastic constants for any order n (n>2) is then given thermodynamically as the n^{th} partial derivative of the appropriate thermodynamic potential with respect to the Lagrangian strains, evaluated at zero strain, or with respect to the tensions, evaluated at zero tension. Therefore we have the following relations for adiabatic (isentropic) and isothermal elastic stiffness constants and compliance constants of n order, denoted by index S and T respectively in the form of

$$C^{S}_{ijkl\ldots} = \rho_o \left(\frac{\partial^n U}{\partial \eta_{ij}\, \partial \eta_{kl\ldots}} \right)_{S,\eta=0} \tag{2.11}$$

$$C^{T}_{ijkl\ldots} = \rho_o \left(\frac{\partial^n F}{\partial \eta_{ij}\, \partial \eta_{kl\ldots}} \right)_{T,\eta=0} \tag{2.12}$$

$$S^{S}_{ijkl\ldots} = -\rho_o \left(\frac{\partial^n H}{\partial t_{ij}\, \partial t_{kl\ldots}} \right)_{S,t=0} \tag{2.13}$$

$$S^{T}_{ijkl\ldots} = -\rho_o \left(\frac{\partial^n G}{\partial t_{ij}\, \partial t_{kl\ldots}} \right)_{T,t=0} \tag{2.14}$$

The energy density of the solid may then be written as

$$\rho_o U(\eta) = \left(\frac{1}{2}\right) C^{S}_{ijkl} \eta_{ij} \eta_{kl} + \left(\frac{1}{6}\right) C^{S}_{ijklmn} \eta_{ij}\, \eta_{kl}\, \eta_{mn} + \ldots \tag{2.15}$$

where

$$C^{S}_{ijkl} = \rho_o \left(\frac{\partial^2 U}{\partial \eta_{ij}\, \partial \eta_{kl}} \right)_{\eta=0}$$

and

$$C^{S}_{ijklmn} = \rho_o \left(\frac{\partial^3 U}{\partial \eta_{ij}\, \partial \eta_{kl}\, \partial \eta_{mn}} \right)_{\eta=0}$$

The first two terms in the above energy expansion are the second and third order contributions of the strain to the

elastic energy density. Since the form of this expansion is similar to the expansion of potential energy in terms of interatomic displacement, it is possible to relate the elastic stiffness constants to the interatomic forces in a solid.

The advantages of using these definition include generalisation of the accepted definition of the SOEC: the Voigt notation is still retained and the higher order of coefficients are identical with those derived from the anharmonic lattice theory. In this case, the higher order elastic stiffness constants such as third order elastic constant (TOEC) and fourth order elastic constant (FOEC) can be also derived using these thermodynamic definitions.

2.4 Propagation of Elastic Waves In Solid.

One way to determine the elastic properties of any solid is through a dynamic test in which elastic waves are propagated in the solid. The propagated waves are assumed to behave adiabatically: the entropy is conserved; their wavelengths are much greater than the interatomic spacing and the displacement of the atoms from their equilibrium position caused by these waves is small. These conditions ensure that the deformation is elastic and hence that Hooke's law is obeyed. Comprehensive descriptions on this area are well documented (for example, Kittel 1971, Auld 1973).

The equation of atomic motion in an elastic continuum medium can be obtained by equating the net force due to the internal stresses to the product of acceleration and mass per unit volume (de Launey 1956, Mason and McSkimin 1947, Thurston 1964 and Huntington 1947)

$$\rho_o \frac{\partial^2 u_i}{\partial t^2} = \frac{\partial \sigma_{ij}}{\partial x_j} \qquad (2.16)$$

where t and ρ_o represent time and the volume density of solid respectively. Here u_i is the displacement of an atom in the i-direction. By adopting Hooke's law and equation (2.3), eq. (2.16) can be rearranged in the form

of

$$\rho_o \frac{\partial^2 u_i}{\partial t^2} = \frac{1}{2} \frac{\partial}{\partial x_k} \left\{ C_{ijkl} \left(\frac{\partial u_i}{\partial x_j} + \frac{\partial u_j}{\partial x_i} \right) \right\} \qquad (2.17)$$

Since for an homogeneous medium the C_{ijkl} are independent of position, this equation reduces to

$$\rho_o \frac{\partial^2 u_i}{\partial t^2} = C_{ijkl} \frac{\partial^2 u_i}{\partial x_j \partial x_k} \qquad (2.18)$$

For any direction of wave propagation, a possible solution of this equation (2.18) is

$$\underline{U} = U_o \exp i\omega(t - \underline{N}.\frac{x}{v}) \qquad (2.19)$$

where $\underline{N}$ is a unit vector in the direction of propagation, U_o is the particle displacement amplitude, v is the magnitude of the phase wave velocity and ω is the angular frequency. By differentiating eq. (2.19) and substituting eq. (2.18), it can be shown that

$$\rho_o v^2 U_{oi} = C_{ijkl} U_{ol} N_k N_j \qquad (i,j,k,l = 1,2,3) \qquad (2.20)$$

where U is a unit vector in the direction of polarisation of the atom. This equation, known as Christoffel's equation, may be written in a more homogeneous form by putting $U_{oi} = U_{ol}\partial_{il}$ in eq. (2.20) and this will give

$$(\rho_o v^2 \partial_{il} - C_{ijkl} N_k N_j) U_{ol} = 0 \qquad (2.21)$$

where ∂_{ij} is a unit tensor.

For a specific combinations of $\underline{N}$ and $\underline{U}$, the equation of motion will provide only three solutions of wave velocities, one of which resembles a longitudinal and two shear waves. A pure longitudinal and shear plane waves are defined as waves which have the atomic motion in the direction of propagation ($\underline{U}x\underline{N} = 0$) and particle motion normal to the propagation direction ($\underline{U}.\underline{N} = 0$) respectively (Brugger 1965a). Waves which have particle motion most closely resembling pure modes referred to as quasi-longitudinal or quasi-shear modes. The number and propagation directions of pure modes are dependent on the crystal symmetry of a solid. In a cubic crystal pure modes propagate in three major types of directions, namely [100], [110] and [111] as illustrated in figure 2.3. Each is associated with one longitudinal and two transverse modes, although the latter may be degenerate in velocity. The expressions which relate the wave velocities and the elastic constants for cubic crystals are given in table 2.1. For rhombohedral and tetragonal crystal systems, the related expressions will be given in the chapter 8 and 9 respectively.

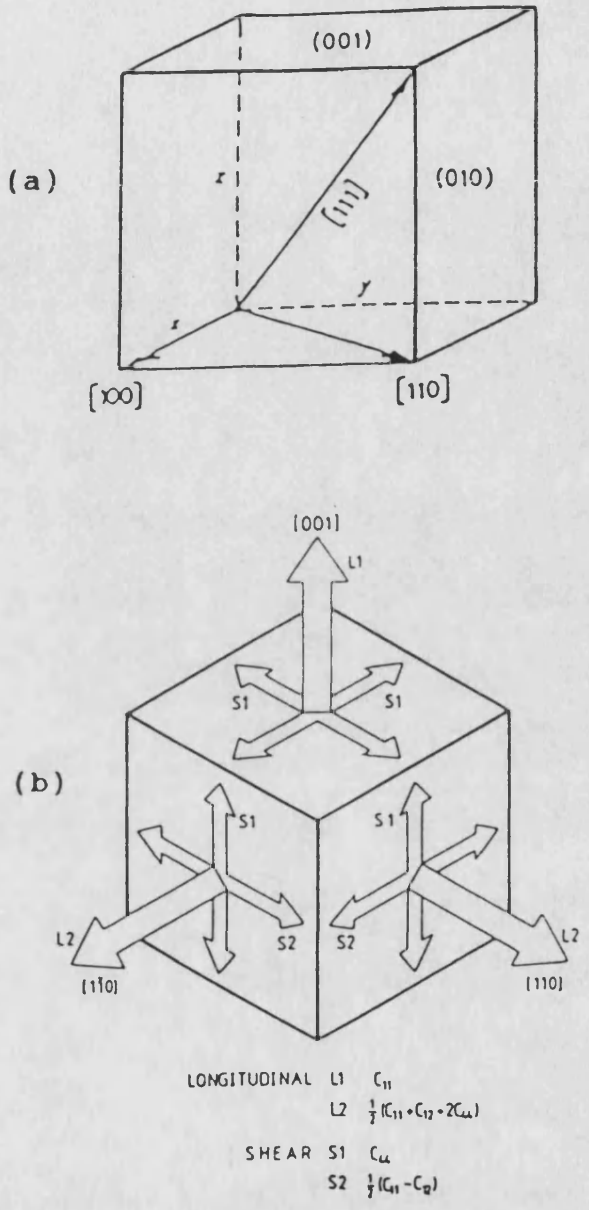

Figure 2.3 : (a) Major crystal directions in a cubic crystal system. (b) Pure mode directions for elastic waves propagating in a cubic crystal.

Table 2.1 : Ultrasonic wave velocity and elastic stiffness constant relationships for a cubic crystal.

Mode no.	Propagation direction $\underline{N}$	Polarisation direction $\underline{U}$	(ρV^2)
1.	[100]	[100]	C_{11}
2.	[100]	in (100) plane	C_{44}
3.	[110]	[110]	$(C_{11}+C_{12}+2C_{44})/2$
4.	[110]	[001]	C_{44}
5.	[110]	$[1\bar{1}0]$	$C'=(C_{11}-C_{12})/2$
6.	[111]	[111]	$(C_{11}+2C_{12}+4C_{44})/3$
7.	[111]	in (111) plane	$(C_{11}+C_{44}-C_{12})/3$

2.5 Atomic Vibrations in the Harmonic, Quasiharmonic and Anharmonic Approximations.

In the previous sections, the macroscopic concepts of elasticity were outlined. The experimental data usually refer to the macroscopic state and a connection to microscopic structure is needed. This section is concerned with the lattice dynamics through which the microscopic behaviour of atoms can be treated.

In a simple lattice dynamical model, the restoring forces between atoms and hence their potential energy are generally considered to be a function of the atomic displacement from equilibrium positions. If this expansion of atomic displacement is terminated in the quadratic term, only the harmonic force constant is retained, leading to a purely harmonic approximation (figure 2.4). In this approximation (sometimes known as the parabolic potential well) the vibrations of atoms are treated as a superposition of independent harmonic vibrations. The particular atoms in the solid execute small oscillations about their equilibrium position at any temperature. Here the atomic interaction with other degree of freedom of the system are not allowed. Among the consequences (see Ashcroft and Mermin 1976 for details) of this harmonic approximation are:

(a) there is no thermal expansion,

(b) the elastic constants are independent

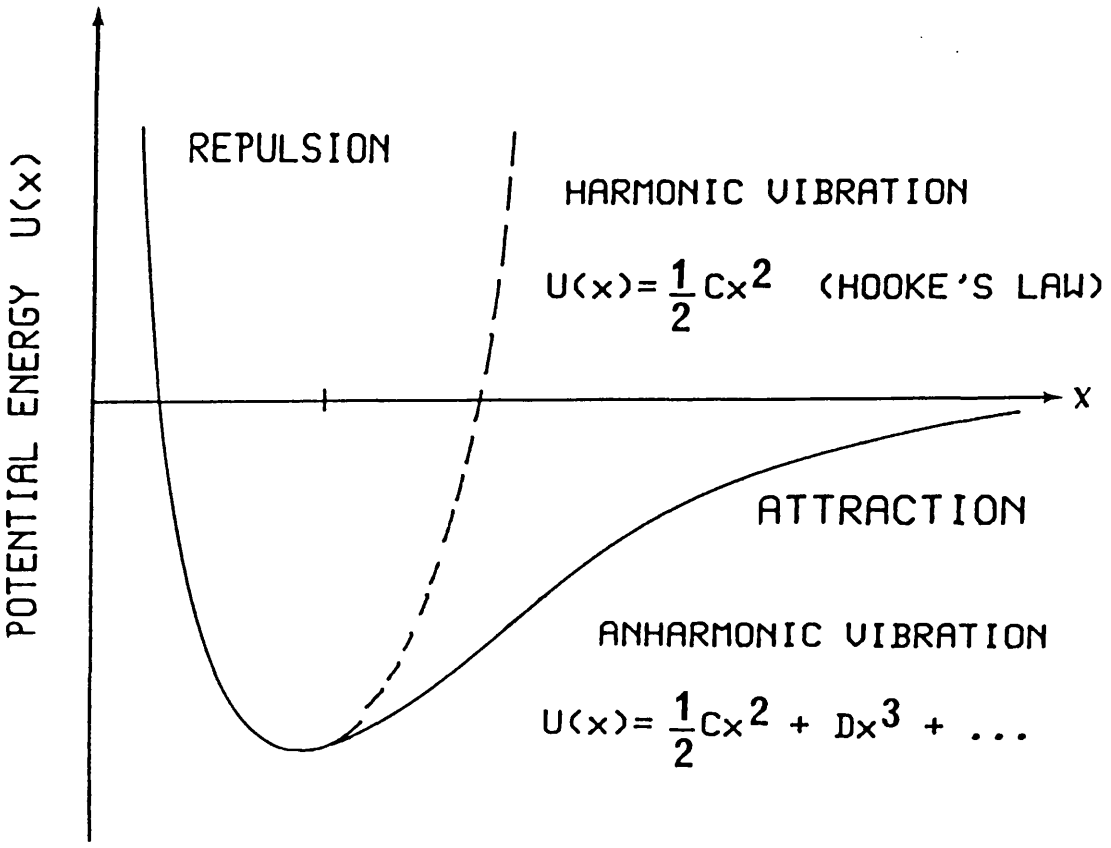

Figure 2.4 : Interatomic potential energy as a function of atomic displacement in the harmonic and anharmonic lattice vibration models for a solid.

of temperature and pressure,

(c) there is no difference between the adiabatic and isothermal elastic constants,

(d) the heat capacity becomes constant at high temperature,

(e) the specific heats measured at constant volume and pressure would be equal,

(f) the mean free path and life time of phonons would be infinite in a perfect crystal because there is no phonon-phonon interaction and this will result in an infinite thermal conductivity.

However in a real situation, this purely harmonic approximation is not sufficient to give even a qualitative description of many important thermodynamic properties of a solid. Even at zero Kelvin, this approximation is not correct, since anharmonicity still exists due to the zero point vibrations. At high temperature thermal fluctuations dominate the system. So it can be said that the nature of an atomic vibration itself is actually anharmonic. In order to get a correct model of the atomic vibrations in a solid, we have to take anharmonic effects into account.

The quasiharmonic approximation (Leibfried and Ludwig 1961) is rather more satisfactory than the harmonic one. As in the harmonic approximation the potential energy is also terminated in the quadratic term but the interatomic force constants are allowed to change with change in

interatomic distance, or in other words, the frequencies of atomic vibrations are volume dependent. Now the frequencies of the phonon modes are considered to depend indirectly on temperature via thermal expansion. This quasiharmonic approximation has been widely used in the interpretation and analysis of many experimental results. Even though the concept of the quasiharmonic approximation can explain the thermal behaviour of solid, but this approximation is not adequate for explaining many important thermodynamic properties. So a more realistic model must be considered.

As far as solids are concerned, their thermal behaviour is the result of the microscopic phenomena arising from the anharmonicity of lattice vibrations. This leads to a macroscopic nonlinearity. To achieve a description of anharmonicity, the potential energy U(x) should be expanded (see figure 2.4 for an illustration). The third and higher order terms of this expansion describe the asymmetry of the lattice potential energy; they are closely related to the higher order elastic constants in the defining expression of the lattice energy in terms of the elastic strain as written in eq. (2.15). The third order elastic constants (TOEC) themselves play an important role in accounting for the anharmonic and nonlinear properties of solids. Sometimes they alone suffice to describe the nonlinear behaviour of the solid in particular that associated with the long wavelength acoustic modes.

2.6 Variation of the SOEC with External Hydrostatic Pressure.

The change of SOEC with external pressure is one of the most important anharmonic effects, in which the influence of interatomic binding is exhibited most clearly. In general the normal behaviour of the SOEC versus pressure is to increase linearly with increasing pressure, which leads to a positive value of the pressure derivative of an elastic constant. Microscopically, the interatomic repulsive forces increase when the atoms are pushed closer together. However this effect may break down when the crystal is in a condition of lattice instability or in a vicinity of the phase transition; then the pressure derivatives of the SOEC can be negative. This behaviour implies a softening of acoustic vibrational modes: the nearest neighbour forces and hence the corresponding force constant decrease.

When the hydrostatic pressure is applied to a solid, it will effect the volume, length and density of solids. Both density and the velocity of sound waves are dependent on the state of strain of the solids. In principle the dimensions and density under pressure need to be found using the original values at ambient pressure (Seeger and Buck 1960). This difficulty has been solved by Thurston and Brugger (1964) by introducing the concept

of the "natural velocity" W_o which is defined as W_o (= $2l_o/t$). Here l_o is the unstressed length of sample and t is the experimentally measured transit time of the ultrasonic waves across the sample. To compare between the measured values of $(\rho W^2)'_{P=0}$ and the pressure derivatives of the effective SOEC $(\rho V^2)'$, the following relations has to be employed,

$$\frac{d(\rho V^2)}{dP} = 2\rho_o W_o \frac{dW}{dP} + \rho_o W_o^2 \frac{d(\rho/\rho_o)}{dP} + \rho_o W_o^2 \frac{d(V^2/W^2)}{dP} \qquad (2.22)$$

where

$$\frac{d(\rho/\rho_o)}{dP} = -2N_k N_m S_{kmii}$$

and

$$\frac{d(V^2/W^2)}{dP} = S_{11}+2S_{12}+2S_{13}+2S_{23}+S_{33}$$

The second and third terms in eq. (2.22) are actually the corrections for density and velocity respectively at that pressure. For convenience, this equation can be written in the following way

$$\frac{dC_{IJ}}{dP} = C_{IJ}^o \left(\frac{2}{f_o}\frac{df}{dP} + \beta^T - 2N_k N_m S_{kmii} \right) \qquad (2.23)$$

Here C_{IJ}^o represents the SOEC at ambient condition, df/dP is the gradient of measured frequency in the pulse echo

overlap experiment (see section 3.5) versus pressure, f_o is the overlap frequency and β^T and S_{kmii} are the isothermal volume compressibility and the elastic compliances respectively. The dC_{IJ}/dP measured and discussed throughout this thesis represent the pressure derivatives of the effective SOEC calculated at zero pressure whereas the B_{IJ} will refer to the pressure derivatives of the thermodynamic SOEC. The latter can be obtained from the measured values of dC_{IJ}/dP. The relations between those two parameters are given in table 2.2 for crystal of all Laue groups except those belonging to monoclinic and triclinic systems. Here S_1 (= S_{11} + S_{12} + S_{13}), S_2 (= S_{12} + S_{22} + S_{23}) and S_3 (= S_{13} + S_{23} + S_{33}).

Table 2.2 : Pressure derivatives of thermodynamic and effective elastic constants (after Salleh 1988).

$$B_{11} = \frac{\partial C_{11}}{\partial p} + 1 - (S_2 + S_3 - 3S_1)C_{11}$$

$$B_{12} = \frac{\partial C_{12}}{\partial p} - 1 - (S_3 - S_1 - S_2)C_{12}$$

$$B_{13} = \frac{\partial C_{11}}{\partial p} - 1 - (S_2 - S_1 - S_3)C_{13}$$

$$B_{14} = \frac{\partial C_{14}}{\partial p} - S_1 C_{14}$$

$$B_{15} = \frac{\partial C_{15}}{\partial p} - (S_2 - 2S_1)C_{15}$$

$$B_{16} = \frac{\partial C_{16}}{\partial p} - (S_3 - 2S_1)C_{16}$$

$$B_{22} = \frac{\partial C_{22}}{\partial p} + 1 - (S_3 + S_1 - 3S_2)C_{22}$$

$$B_{23} = \frac{\partial C_{23}}{\partial p} - 1 - (S_1 - S_2 - S_3)C_{23}$$

$$B_{24} = \frac{\partial C_{24}}{\partial p} - (S_1 - 2S_2)C_{24}$$

$$B_{25} = \frac{\partial C_{25}}{\partial p} + S_2 C_{25}$$

$$B_{26} = \frac{\partial C_{26}}{\partial p} - (S_3 - 2S_2)C_{26}$$

$$B_{33} = \frac{\partial C_{33}}{\partial p} + 1 - (S_1 + S_2 - 3S_3)C_{33}$$

$$B_{44} = \frac{\partial C_{44}}{\partial p} + 1 - (S_1 - S_2 - S_3)C_{44}$$

$$B_{45} = \frac{\partial C_{45}}{\partial p} + S_3 C_{45}$$

$$B_{46} = \frac{\partial C_{46}}{\partial p} + S_2 C_{46}$$

$$B_{55} = \frac{\partial C_{55}}{\partial p} + 1 - (S_2 - S_1 - S_3)C_{55}$$

$$B_{56} = \frac{\partial C_{56}}{\partial p} + S_1 C_{56}$$

$$B_{66} = \frac{\partial C_{66}}{\partial p} + 1 - (S_3 - S_1 - S_2)C_{66}$$

2.7 Estimation of the Compression of Solid at High Pressure.

Knowledge of the compression $V(P)/V_o$, the ratio of the volume V(P) at pressure P to that V_o at atmospheric pressure, is essential to an understanding of a solid material behaviour under pressure. The dependence of ultrasonic wave velocity upon pressure can be measured with high precision; however the pressure range is limited. The compression at pressure up to one or even two orders of magnitude higher than those available in ultrasonic experiments can be estimated from the elastic constants and their hydrostatic pressure derivatives by using an equation-of-state as proposed by Murnaghan (1944). This extrapolation works well up to very high pressure for many solids (Anderson 1966). For example measurements of the elastic constant of HgTe (Miller et al. 1981) have proved that the experimental data and calculated results of Murnaghan equation-of-state for a zinc-blende structure crystal up into pressure region of 20×10^8 Pa are in good agreement.

The physical basis for the equation-of-state rests upon the assumption that the bulk modulus B is linearly dependent upon pressure

$$B(P) = -V\left(\frac{\partial P}{\partial V}\right)_T = B_0 + P\left(\frac{\partial B}{\partial P}\right)_{P=0,T} \qquad (2.24)$$

By integrating eq. (2.24), Murnaghan (1944) obtained the equation-of-state

$$P=\frac{B_0}{B'_0}\left\{\left(\frac{V_0}{V(P)}\right)^{B'_0}-1\right\} \tag{2.25}$$

where $B'_0 = (\partial B/\partial P)_{P=0,T}$

which is more easily used in the logarithmic form

$$\ln\left(\frac{V_0}{V(P)}\right)=\frac{1}{B'_0}\ln\left[B'_0\left(\frac{P}{B_0}\right)+1\right]. \tag{2.26}$$

The measured ultrasonic wave velocities lead to adiabatic moduli, so to use this equation-of-state more accurately it is necessary to transform the data to isothermal moduli. The adiabatic and isothermal bulk moduli are related by

$$B_0^S=B_0^T(1+\alpha\gamma T) \tag{2.27}$$

and the isothermal hydrostatic pressure derivative $(\partial B^T/\partial P)$ $(= B_0'^T)$ has been shown to be (Overton 1962, Anderson 1966)

$$B_0'^T=B_0'^S+T\alpha\gamma\left(\frac{B_0^T}{B_0^S}\right)\left[1-\frac{2}{\alpha B_0^T}\left(\frac{\partial B_0^T}{\partial T}\right)_P-2B_0'^S\right]$$

$$+\left[T\alpha\gamma\left(\frac{B_0^T}{B_0^S}\right)\right]^2\left[B_0'^S-1-\frac{1}{\alpha^2}\left(\frac{\partial\alpha}{\partial T}\right)_P\right] \qquad (2.28)$$

where $(\partial B_0^T/\partial T)_P$ can be obtained from

$$\left(\frac{\partial B_0^T}{\partial T}\right)_P=\left(\frac{\partial B_0^S}{\partial T}\right)\Big/(1+T\alpha\gamma)-\frac{B_0^S}{T}\frac{T\alpha\gamma}{[1+T\alpha\gamma]^2}\left\{1+\frac{(\partial\alpha/\partial T)_P}{\alpha/T}\right\}. \qquad (2.29)$$

Here α and γ are linear thermal expansion and thermal Grüneisen parameter respectively. The compression up to the theoretical hydrostatic pressure of about 10 x 10^8 has been estimated for the materials studied in this work.

2.8 The Temperature Variations of the SOEC

The dependence of elastic constants upon temperature is another consequence of anharmonicity of the interatomic potential energy in solids. Early theoretical studies on this subject were done by Born and his co-workers (1939, 1943, 1954) and later by Leibfreid and Ludwig (1961). The normal behaviour of the thermal variations of the SOEC of most crystals, illustrated schematically in figure 2.5, is characterised by two general features; a linear increase with decreasing temperature and a zero slope in the region where the temperature approaches zero Kelvin. The linear dependence of elastic constants on temperature, especially above the Debye temperature θ_D, is due to the anharmonic nature of the lattice vibrations. The linearity of this dependence may break down in the vicinity of a phase transition. At sufficiently low temperatures it is expected that in most crystalline solids the slope of dC_{IJ}/dT would decrease i.e. $dC_{IJ}/dT \rightarrow 0$ as $T \rightarrow 0$ which is a direct consequence of the third law of thermodynamics. However in certain materials like glasses, this particular feature is not always observed; instead of showing a zero slope of dC_{IJ}/dT, the elastic constant increases to a maximum value at low temperature (~1K). This behaviour has been ascribed to interactions with two-level systems (Anderson et al. 1972, Phillips 1972). Since this effect only

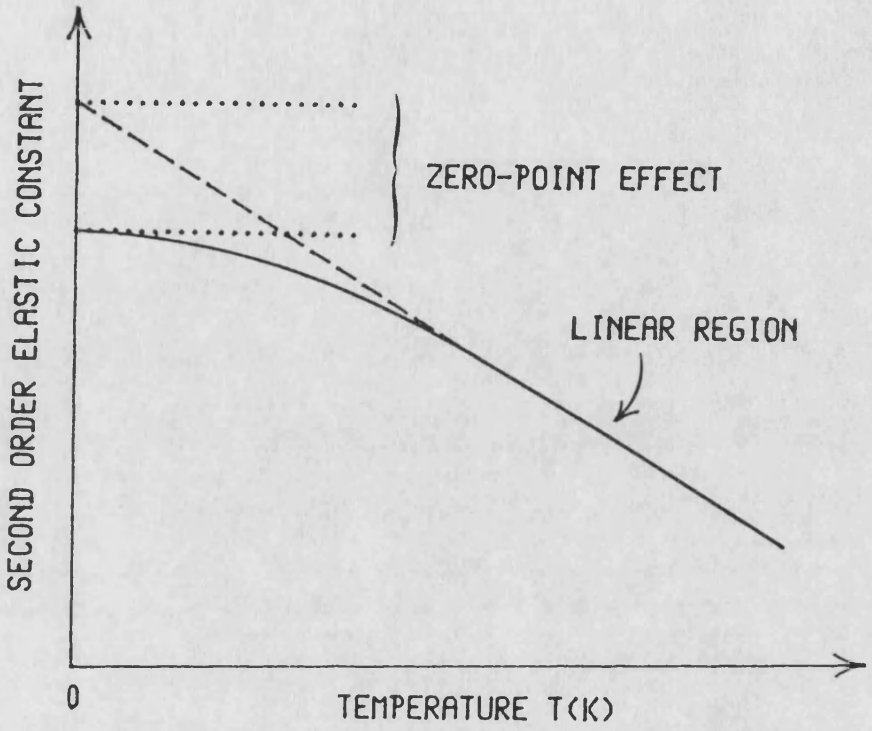

Figure 2.5 : Typical curve of second order elastic constant versus temperature (due to Garber and Granato 1975).

occurs in amorphous materials, this behaviour has been considered to be one of the universal properties of glass (an outline is given in chapter 4).

By assuming a linear chain, anharmonic oscillator model of a Debye solid, Lakkad (1971) has proposed a simple expression for the dependence of elastic constants on temperature, i.e.

$$C_{IJ} = C_o(1 - LF(T/\theta_D)) \qquad (2.30)$$

where C_o is the value of the elastic constant at zero Kelvin, θ_D is the Debye temperature, L is a constant and $F(T/\theta_D)$ is a mathematical function in the form of

$$F(T/\theta_D) = 3(T/\theta_D)^4 \int_0^{\theta_D/T} \left\{ x^3 \left[exp(x) - 1 \right] \right\} dx \qquad (2.31)$$

where x equals $h\nu/kT$. If two values of the elastic constants at two different temperatures and the Debye temperature of the material are known, then eq. (2.30) can predict (at least in theory) the behaviour of the elastic constant over the entire range of temperatures. Using this formula, the temperature dependences of the elastic constants of certain metals (Lakkad 1971) and some semiconductors (Cottam and Saunders 1973) have been calculated and the expression has been found to describe the experimentally observed temperature dependence. The bulk modulus can be treated in a similar manner.

The temperature derivatives of the SOEC (dC_{IJ}/dT) can

be derived mathematically through a quasiharmonic anisotropic continuum model, as discussed extensively by Garber and Granato (1975). The room temperature values of dC_{IJ}/dT for the cubic crystals and glasses studied here are calculated using the following equation (Thurston 1964)

$$\frac{dC_{IJ}}{dT} = C_{IJ}^{T}\left[\frac{2}{f_o}\left(\frac{df}{dT}\right) - \frac{\alpha_v}{3}\right] \qquad (2.32)$$

where α_v is the volume thermal expansion coefficient, f_o is the measured overlap frequency, C_{IJ}^{T} is the value of the SOEC evaluated at some fixed temperature T and at zero applied pressure. The temperature derivatives of the SOEC provide information which can be used to estimate of the magnitude of the fourth order elastic constants (FOEC) which are related to higher order repulsive interactions in solids. The FOEC for some glasses have been calculated using a combination of pressure and temperature dependences of ultrasonic wave velocities, and have been given in the paper by Brassington and Saunders (1981).

2.9 The Debye Temperature.

The concept of the Debye temperature θ_D is useful in describing the thermal behaviour of solids and it plays an important role in the theory of lattice vibrations. In brief this temperature is a measure of the separation of the low temperature quantum mechanical region, where the vibrational modes begin to be "frozen out", from the high temperature region where all modes begin to be excited according to classical theory. The Debye temperature θ_D can be obtained directly from heat capacity measurements, and it can be also derived from a set of the elastic constants. A solid in the Debye theory is assumed to behave like a non-dispersive continuum, so the phonons (the quanta of the lattice vibrations) are considered to travel with the same velocity whatever their wavelength and propagation vector. The maximum frequency of vibration ν_{max}, or the velocity of sound, can be related to a characteristic temperature θ_D. In practice the velocity is taken equal to the mean velocity of sound and can be computed by integration over the whole velocity surface (Anderson 1963). The relation between mean velocity and the characteristic Debye temperature is given by

$$\Theta_{\mathrm{D}}^{\mathrm{el}} = \left(\frac{9N}{4\pi V}\right)^{\frac{1}{3}} \left(\frac{h}{k}\right) \left[\int \left(\frac{1}{v_1^3} + \frac{1}{v_2^3} + \frac{1}{v_3^3}\right) \frac{\mathrm{d}\Omega}{\pi} \right]^{-\frac{1}{3}} \qquad (2.33)$$

where v_i is the ultrasonic wave velocity, h and k_B are the Plank and Boltzmann constants respectively. N/V is the number of atom per unit volume. This calculation involves a cubic equation and finding the average value of the three roots. This has been done by using a computer programme. In the case of non-isotropic materials, the ultrasonic velocities for each propagation direction $\underline{N}$, can be calculated from the Christoffel equation. In the programme the integral over solid angle is approximated as a sum taken at about 10288 point each subtending an equal solid angle Ω of 1.218×10^{-3} steradians.

For isotropic materials such as glass the mean velocity is written as

$$V_m = \left[\frac{1}{3}\left(\frac{1}{V_L^3} + \frac{2}{V_S^3}\right)\right]^{-1/3} \qquad (2.34)$$

where v_l $(=(C_{11}/\rho)^{1/2})$ and v_s $(=C_{44}/\rho)^{1/2})$ are longitudinal and shear ultrasonic wave velocities. The Debye temperature can then be calculated readily using the following equation

$$\Theta_D^{el} = \left(\frac{9N}{4\pi V}\right)^{\frac{1}{3}} \left(\frac{h}{k}\right) V_m \qquad (2.35)$$

2.10 Mode Grüneisen Parameters.

The mode Grüneisen parameter is an important tool for investigation of anharmonic effect in solid. One way to derive the Grüneisen parameter is by considering the entropy of the system in the quasiharmonic form (Barron 1955)

$$S=\sum_i S_i\left[\frac{\omega_i(V,T)}{T}\right] \tag{2.36}$$

where S_i is the contribution to the entropy of the mode i, with a frequency ω_i which is a function of both volume and temperature. The summation is over the measured frequency spectrum. Differentiation of $S_i\omega_i/T$ with respect to temperature and volume leads to

$$\left.\frac{\partial S_i}{\partial V}\right|_T = S'_i\left(\frac{\omega_i}{T}\right)\frac{1}{T}\left.\frac{\partial \omega_i}{\partial V}\right|_T \tag{2.37}$$

and

$$\left.\frac{\partial S_i}{\partial T}\right|_V = S'\left(\frac{\omega_i}{T}\right)\left[\frac{1}{T}\left.\frac{\partial \omega_i}{\partial T}\right|_V - \frac{\omega_i}{T^2}\right] \tag{2.38}$$

where $S_i'(x)=ds_i(x)/dx$.

The contribution to the heat capacity from mode i is, from (2.38),

$$C_i(T)=S'_i\left(\frac{\omega_i}{T}\right)\left|\left.\frac{\partial\omega_i}{\partial T}\right|_V-\frac{\omega_i}{T}\right| \qquad (2.39)$$

which, when combined with eq. (2.37) and (2.38) leads to

$$\left.\frac{\partial S}{\partial V}\right|_T=-\sum_i C_i(T)\frac{1}{T}\left.\frac{\partial\omega_i}{\partial V}\right|_T\left|\left.\frac{\partial\omega_i}{\partial T}\right|_V-\frac{\omega_i}{T}\right|^{-1}$$

$$=-\sum_i C_i(T)\frac{\partial\ln\omega_i}{\partial V}\left|1-\frac{\partial\ln\omega_i}{\partial\ln T}\right|^{-1} \qquad (2.40)$$

The factor in the bracket represents the first order anharmonic correction to the heat capacity. However this correction can be neglected in the calculation of thermal expansion. For instance in SiO_2, $d\ln\omega_i/d\ln T$ is about 0.01 (Gaskel 1966).

Now the Grüneisen parameter for an individual vibrational mode i is introduced as a measure of the volume dependence of the mode frequency ω_i and is defined as

$$\gamma_i=-\frac{d\ln\omega_i}{d\ln V} \qquad (2.41)$$

Insertion of this into eq. (2.40) without taking a correction yields

$$\left.\frac{\partial S}{\partial V}\right|_T=\frac{1}{V}\sum C_i(T)\gamma_i \qquad (2.42)$$

The derivation presented here treats the temperature and volume dependences of ω_i separately, eq. (2.40) shows that the explicit temperature dependence enters only as a small correction factor to the γ_i (or to the $C_i(T)$). The

anharmonic properties of solids are usually described in terms of an average thermal Grüneisen parameter γ^{th} which can be evaluated experimentally using

$$\gamma^{th} = \frac{\partial S}{\partial V}\Big|_T \frac{V}{C_V}$$
$$= \alpha V / \beta_v^S C_p = \alpha V / \beta_v^T C_v \qquad (2.43)$$

where α is the coefficient of volume thermal expansion, V is the volume, β_v^T and β_v^S is isothermal and adiabatic compressibility respectively and C_v and C_P are specific heats at constant volume and constant pressure respectively. By writing $C_v = \sum C_i(T)$ and substituting the last two equations

$$\gamma^{th} = \frac{\sum_i \gamma_i(T) C_i(T)}{\sum_i C_i(T)} \qquad (2.44)$$

which allows the experimental value of γ^{th} to be calculated from the individual mode Grüneisen parameter γ_i. The summation in eq. (2.44) is over all modes, so that in principle every γ_i must be measured. In a crystal this could be solved by measuring the phonon dispersion relations under pressure using neutron or Raman scattering method.

In the Debye approximation, only the acoustic modes are considered and their dispersion is ignored. Hence the volume dependence of the individual mode frequencies at the Brillouin zone centre (the ultrasonic limit) can be evaluated from a knowledge of the pressure dependences of

the elastic constants. This evaluation is straightforward for glasses. We now turn to discuss the way to do it for a crystal taking the cubic symmetry as an example.

2.10.1 Mode Grüneisen Parameter in a Cubic Crystal.

The expression for the mode Grüneisen parameters $\gamma(p,\underline{N})$ for a cubic crystal have been given by (Brugger and Fritz 1967)

$$\gamma(p,\underline{N}) = -(1/6w)\,(3B + 2w + k) \qquad (2.45)$$

where

$$w(p,\underline{N}) = C_{11}K_1 + C_{44}K_2 + C_{12}K_3$$

$$k(p,\underline{N}) = C_1K_1 + C_2K_2 + C_3K_3$$

with

$$K_1(p,\underline{N}) = N_1^2U_1^2 + N_2^2U_2^2 + N_3^2U_3^2$$

$$K_2(p,\underline{N}) = (N_2U_3 + N_3U_2)^2 + (N_3U_1 + N_1U_3)^2 + (N_1U_2 + N_2U_1)^2$$

$$K_3(p,\underline{N}) = 2(N_2N_3U_2U_3 + N_3N_1U_3U_1 + N_1N_2U_1U_2)$$

and

$$C_1 = C_{111} + 2C_{112}$$

$$C_2 = C_{144} + 2C_{166}$$

$$C_3 = C_{123} + 2C_{112}$$

Here N_i and U_i are the direction cosines for the direction of propagation and the direction of polarisation of the mode characterised by the index p.

Even though we have not measured a set of individual TOEC, the TOEC combinations C_1, C_2 and C_3 can be obtained from the pressure derivatives of the second order elastic constants

$$\frac{\partial C_{44}}{\partial P} = -\frac{(C_{11} + 2C_{12} + C_{44} + C_{144} + 2C_{166})}{(C_{11} + 2C_{12})} \qquad (2.46)$$

$$\frac{\partial C'}{\partial P} = -\frac{(3C_{11} + 3C_{12} + C_{111} - C_{123})}{2(C_{11} + 2C_{12})} \qquad (2.47)$$

$$\frac{\partial B}{\partial P} = -\frac{(C_{111} + 6C_{112} + 2C_{123})}{3(C_{11} + 2C_{12})}. \qquad (2.48)$$

The mode Grüneisen gammas for any chosen propagation direction $\underline{N}$ have been computed by solving the Christoffel equations in order to obtain the polarisation directions U_i and the mode velocities from the values of eigenvectors and eigenvalues respectively. The computer programme used to calculate the mode Grüneisen gamma for a cubic crystal is listed in appendix A.

The high and low temperature limits of the mean acoustic Grüneisen gammas can be obtained from the individual mode Grüneisen gammas. At low temperature each acoustic mode will be excited by an amount proportional to the specific heat $C(p,\underline{N})$ of that mode, which in turn is proportional to the inverse cube of the mode Debye temperature. Hence to obtain the low temperature acoustic Grüneisen parameter γ_o^{-1}, it is only necessary to weight $\gamma(p,\underline{N})$ by the inverse cube of the mode velocity $v(p,\underline{N})$

$$\bar{\gamma}_{\bullet}^{el} = \frac{\sum\int \gamma(p,\underline{N})\, v^{-3}(p,\underline{N})\, d\Omega}{\sum\int v^{-3}(p,\underline{N})\, d\Omega} \qquad (2.49)$$

where Ω is the solid angle. In the high temperature limit (i.e. $T > \theta_D$), all modes are excited classically. Then the weighted factors become equal to Boltzmann constant k, and the high temperature gamma $\bar{\gamma}^{\bullet l}$ can be calculated as an average of the $\gamma(p,\underline{N})$ over all directions

$$\bar{\gamma}^{el} = \frac{1}{3}\sum\int \gamma(p,\underline{N})\frac{d\Omega}{4\pi} \qquad (2.50)$$

The elastic mode Grüneisen parameter $\gamma^{\bullet l}$ is a measure only of the contribution of the zone-centre acoustic mode to the anharmonicity, whereas the thermal gamma γ^{th} (eq. 2.43) takes into account contribution from all modes on both acoustic and optic branches. At very low temperatures these two parameters can approach each other since only the low energy zone centre acoustic modes are excited.

2.10.2 The Mode Grüneisen Parameter in a Glass.

Glass itself can be treated as elastically isotropic solid. By writing the longitudinal and shear velocities of ultrasonic waves as v_l and v_s respectively and the vibration frequency ω_i as $q_i v_l$ (or $q_i v_s$) where q_i is the wave vector, the mode Grüneisen parameters of each modes can be defined as

$$\gamma_l = -\frac{dlnq_i v_l}{dlnV} \tag{2.51}$$

and

$$\gamma_s = -\frac{dlnq_i v_s}{dlnV} \tag{2.52}$$

If we assume that the wave vectors q_i scale as $V^{-1/3}$, then the γ's are independent of the index i and can be written as

$$\gamma_l = \frac{1}{3} + \frac{1}{\beta^T}\frac{dlnv_l}{dP} \tag{2.53}$$

and

$$\gamma_s = \frac{1}{3} + \frac{1}{\beta^T}\frac{dlnv_s}{dP} \tag{2.54}$$

where P is pressure. These equations can be rewritten in terms of the pressure derivatives of the effective SOEC

$$\gamma_l = \frac{-1}{3} + \frac{B^s}{2C_{11}} \frac{dC_{11}}{dP} \qquad (2.55)$$

$$\gamma_s = \frac{-1}{3} + \frac{B^s}{2C_{44}} \frac{dC_{44}}{dP} \qquad (2.56)$$

or in terms of the thermodynamic pressure derivatives of the SOEC

$$\gamma_l = \frac{-1}{6} + \frac{B^s}{2C_{11}} (B_{11} - 1) \qquad (2.57)$$

$$\gamma_s = \frac{-1}{6} + \frac{B^s}{2C_{44}} (B_{44} - 1) \qquad (2.58)$$

where B^s is the adiabatic bulk modulus. The mean value of the elastic Grüneisen parameter $\bar{\gamma}^{el}$ for glass system is obtained from

$$\bar{\gamma}^{el} = \frac{\left(\gamma_l + 2\gamma_s\right)}{3} \qquad (2.59)$$

These quantities are used to describe the anharmonicity of the long wavelength acoustic phonons in a glass in the quasiharmonic approximation.

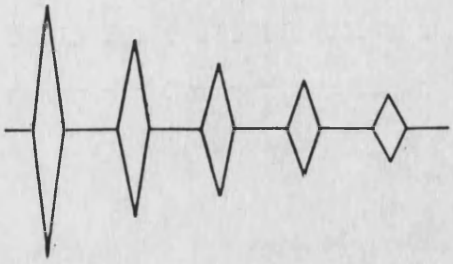

3

ULTRASONIC EXPERIMENTAL TECHNIQUES

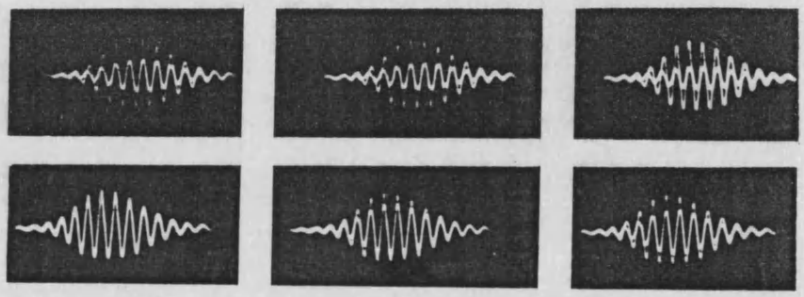

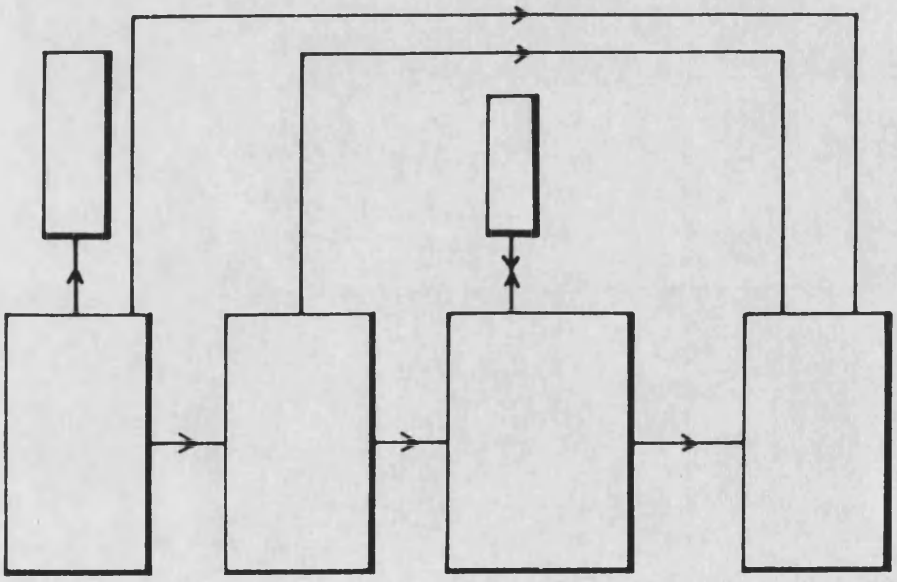

CHAPTER THREE

ULTRASONIC EXPERIMENTAL TECHNIQUES.

3.1 Introduction.

The concepts of the elasticity and anharmonicity were outlined in the previous chapter. In this chapter, the techniques by which these properties can be determined experimentally are given. Since the frequencies of the acoustic wavelength phonon modes are related to elastic constants of the solid body, measurement of the velocities of ultrasonic waves in solid enables the direct measurement of the second order elastic constants. Measurement of the transit time (t) of the waves leads to the propagation velocity v (=2l/t) where l is the thickness of sample under investigation.

In the simple pulse echo single ended configuration, illustrated in figure 3.1, the ultrasonic pulse is launched into a sample by means of a piezoelectric transducer bonded to it. The waves which travel in the sample are reflected at the opposite end of the sample and are detected on return by the same transducer. The pulse also undergoes another reflection; continuation of

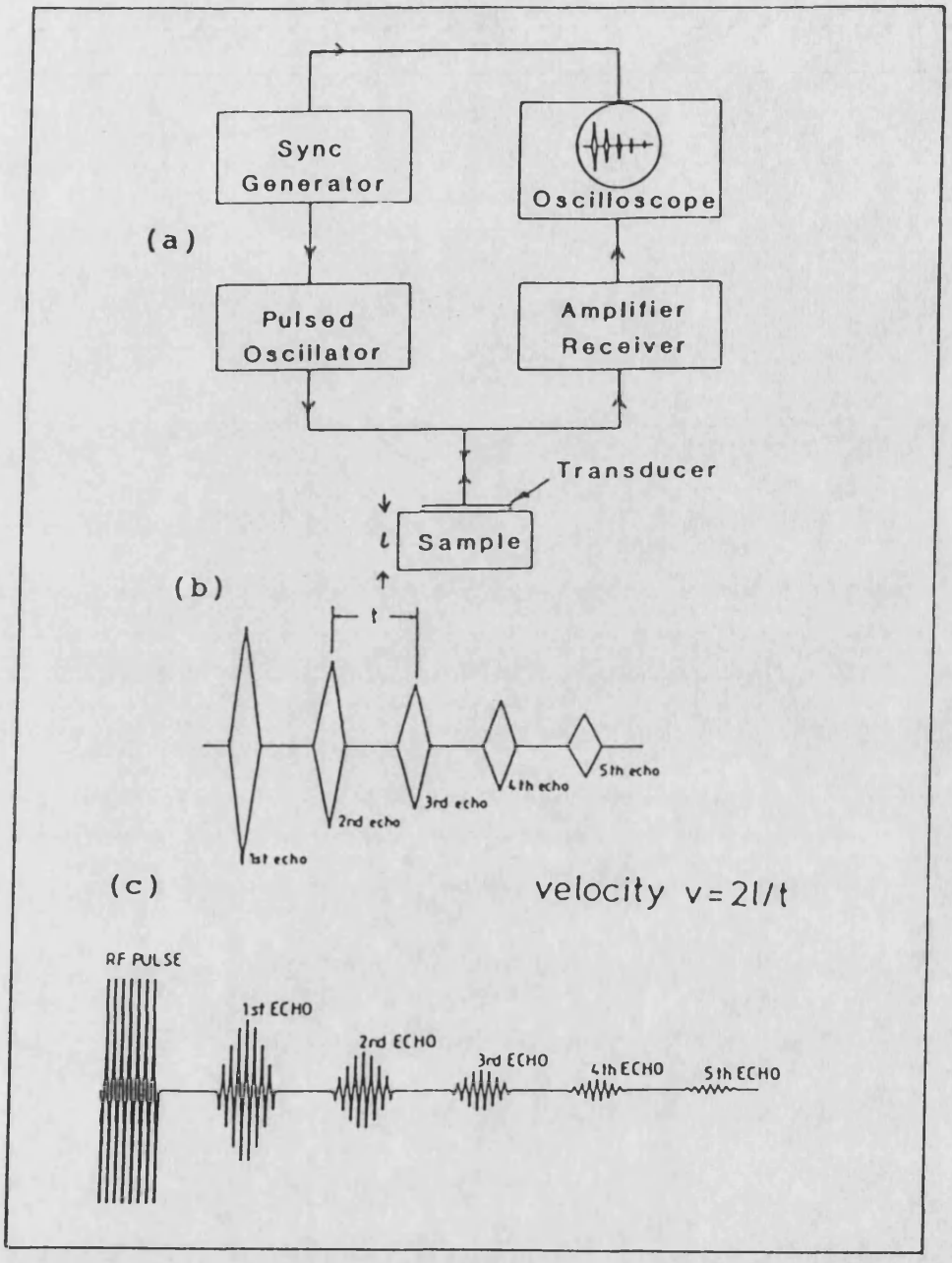

Figure 3.1 :

Schematic representation of (a) simple pulse ultrasonic system. (b) Envelope of pulse echo train and (c) detail of each echo as seen on oscilloscope display.

these processes will produce an echo train in which the echo heights decrease exponentially with time. This echo train, drawn schematically in figure 3.1, can be seen on the oscilloscope display. The distance between two succcessive echoes represents the transit time of propagation of the ultrasonic pulse in the sample. However this simple system is not sensitive enough to study the effect of temperature and pressure upon the elastic constants because the induced changes in transit time are relatively small (normally 1 part in 10^5). So another method must be employed to resolve accurately pressure and temperature changes induced in ultrasonic velocities. The pulse echo overlap method is used here (May 1958, Papadakis 1964, 1967). This versatile and accurate system enables one to measure ultrasonic velocity with high precision (see section 3.5). The basic requirements for this method, i.e. preparation of a sample and choice of a suitable transducer and bonding material are also outlined in this chapter. The dewar system used in the experiments to measure the temperature dependences of the SOEC is also briefly discussed (section 3.6). Section 3.7 relates to the hydrostatic pressure system.

3.2 Preparation of Ultrasonic Samples.

The first important thing to be considered when dealing with ultrasonic experiments is sample preparation. Details of this procedure are well documented (Brassington 1982, Lambson 1988). In brief the crystal was oriented by using the X-ray Laue back reflection method. Metallic crystal cutting and polishing were performed by a Servomet spark machine (Metals Research Ltd., Royston). For glass and insulating samples, the cutting and polishing processes were carried out using a diamond saw and a polishing machine (Logitech type PM2). Ultrasonic samples must have at least two end parallel faces, flat and smooth. Therefore most of the ultrasonic samples were prepared to have typical values of non-parallelism and misorientation of less than 10^{-4} radians and 0.5° respectively. If these faces of the sample were insufficiently parallel then the path of the waves moves away from the original direction after repeated reflections. This causes interference effects and distortion of the echo train as a result of the transducer receiving different phases of the wave across its diameter (Truell, Elbaum and Chick 1969). This becomes a serious problem especially at higher frequencies (30 MHz and above). So in general it can be said that the pulse echo overlap system itself can be

employed for rechecking the sample parallelism, by ensuring that the echo train is exponential.

In the case of crystals, where the specific crystallographic direction is needed, a substantial misorientation will cause the wave propagation in the crystal not to be pure mode in character. A diffraction effect can then occur and two or more waves of allowable polarizations might be created. This process is known as an acoustic mode conversion.

3.3 Quartz Piezoelectric Transducers.

The quartz transducer plays an important role in the field of ultrasonics where its piezoelectric properties allow the transduction between an electrical and mechanical energy, and vice versa at ultrasonic frequency. A transducer allows an electrical circuit to be used to drive a mechanical vibration. When an electric field is applied to such a crystal, it becomes strained by an amount directly proportional to the electric field strength: the electric polarisation produced when a mechanical stress is applied. Due to this phenomenon, the quartz transducer can be used as a transmitter and receiver in an ultrasonic system. When a radio frequency signal from ultrasonic equipment arrives at the transducer, it causes the quartz to vibrate at its fundamental resonance frequency (10 MHz) and this will

allow an ultrasonic plane wave to propagate into the sample. The reason for using quartz as transducer depends on the following characteristics (Mason 1950):

(a) a high electromechanical coupling factor,

(b) it shows a very small frequency dependence on temperature compared with other piezoelectric materials,

(c) a reasonable mechanical strength so that it can be thinly cut with high accuracy,

(d) it retains its piezoelectric properties up to 573°C where a transition to the β-phase occurs and

(e) it can act effectively as a phase sensitive device.

For the present work gold-plated quartz transducers, obtained commercially from Gooch and Housego Ltd. Ilminster, England, were used. They were of two types: X-cut (thickness of 0.29 $\pm$ 0.02 mm), Y-cut (thickness of 0.19 $\pm$ 0.02 mm). The first is used to generate and receive longitudinal waves; an X-cut transducer executes a piston-like action when excited by an electrical impulse. The Y-cut type was used for generating and receiving shear or transverse waves. To differentiate between these two, the Y-cut transducer is marked by a flat edge perpendicular to the polarisation direction. Figure 3.2 includes schematic illustrations of X- and Y-cut quartz transducers. The front face of each transducer has a central gold electrode spaced away from

Figure 3.2:

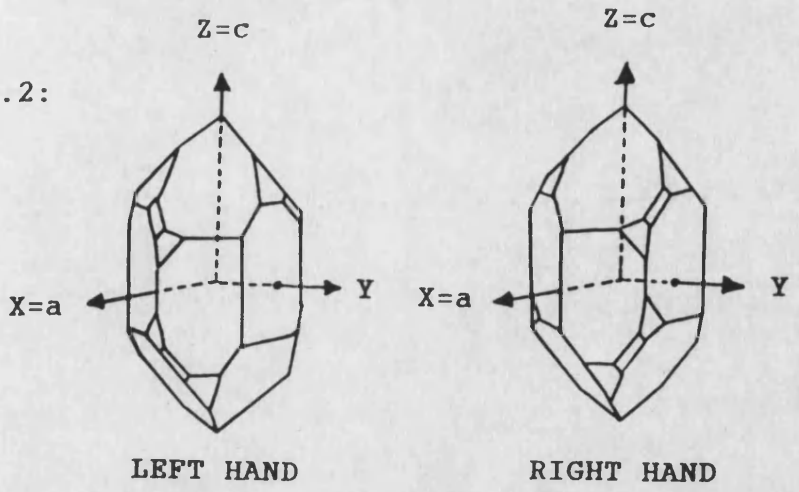

(i) The enantiomorphism in quartz.

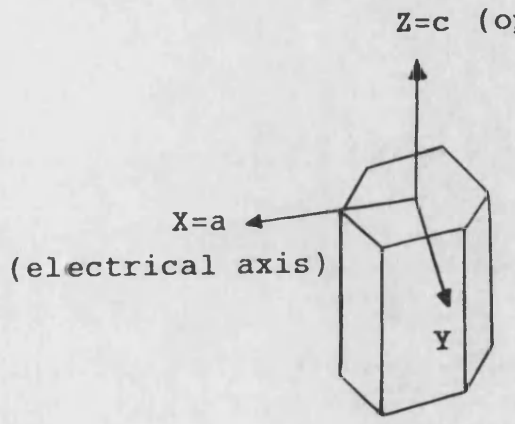

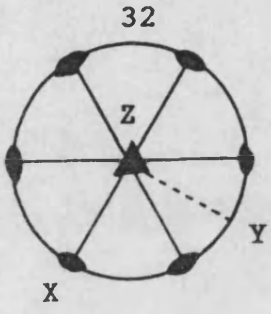

(ii) Point group symmetry element.

(iii) The orientation of the reference axes.

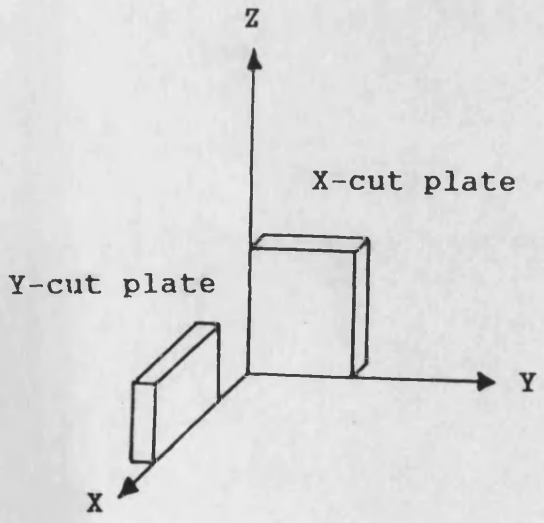

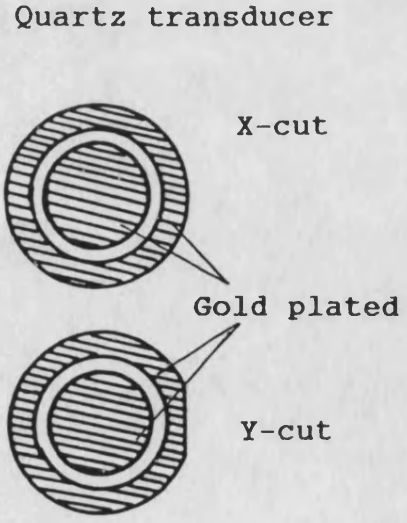

(iv) The arrangement of X- and Y-cut quartz transducers with respect to the crystallographic axes.

an outer ring of gold electrode. Elecrical contact was made to the central electrode. The outer electrode was used for earthing. The back part of the transducer was completely coated with a thin film of gold; it was directly connected to the outer ring of the frontal part by continuity of the gold coating round the edge. Throughout this work, transducers of diameter 6mm for X- and Y-cut have been used on account of the small surface areas of the samples.

3.4 Acoustic Bonding Materials.

The acoustic waves transmitted by the quartz transducer can only be launched successfully into the sample by physically bonding the transducer to one face of the sample with a specific bonding material as illustrated in figure 3.3. A good bonding material should not damage or react with either the sample surface or the quartz transducer, and should provide the appropriate type of wave over the specific range of temperature and pressure where the experiment is to be carried out. For instance, in the case of hydrostatic pressure experiments, the chosen bonding agent should be stable and resist erosion when immersed in castor oil or a similar pressure transmitting medium.

The basic requirement for good bonding is that there should be a minimum loss of the acoustic energy. This is

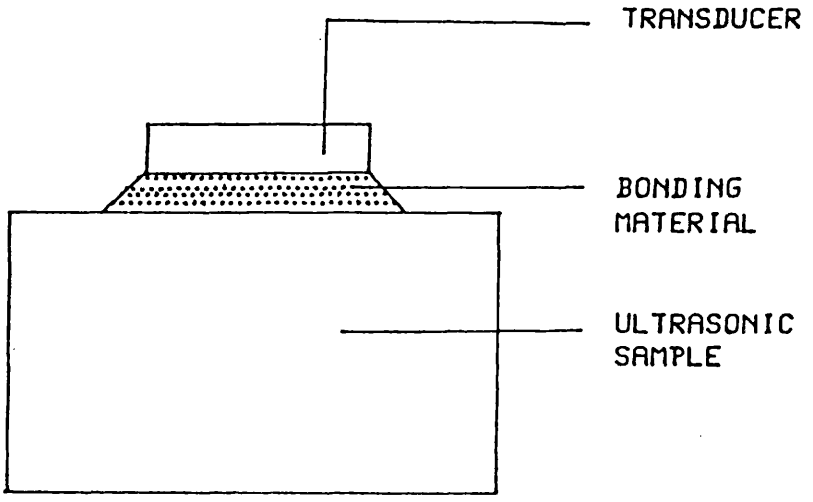

Figure 3.3 :

Schematic representation of a quartz transducer bonded to an ultrasonic sample.

normally achieved by using a suitable type of bonding material as a relatively thin and uniform layer between the two surfaces of the sample and transducer. Before making a bond, it is an essential that both surfaces are free from dirt or dust. To achieve this, both surfaces have to be cleaned with an acetone. Usually a small amount of bonding material is placed on the sample face, the transducer is then over placed this and gently pressed and rotated. This will produce a uniform and thin bond approximately 3 μm thick.

The following three types of bonding materials have been mainly employed in this work:

(i) A viscoelectric resin, Dow Resin 276-V9 (Dow-Corning Corp.) is best used for experiments carried out at room temperature. A thin bond of this resin enables the transmission of ultrasonic shear waves as well as longitudinal waves. This bonding material is also useful for measuring the temperature dependence of the hydrostatic pressure derivatives of the SOEC measurement to -20°C for both modes.

(ii) For low temperature measurements, i.e. below room temperature and down to 4.2K, Nonaq Stopcock grease (Fisher Scientific Co.) has been used. To decrease the probability of bond breaking especially at low temperature, this bonding material must be always kept in a dessicator to reduce the absorption of moisture.

(iii) High temperature coupling paste Du Pont Thick Film Conductor Composition 9770 (Du Pont UK Ltd.) has

been recognized as being suitable for high temperature work (in excess of 450°C). Unlike of other bonding materials, dry bonding of Du Pont is required through a heat treatment process (see Salleh 1988 for details) to ensure that both type of waves are successfully propagated into the sample.

3.5 Pulse Echo Overlap System.

The pulse echo overlap system used in our work extends the simple pulse echo single ended system by means of overlapping any two selected visually intensified echoes on the oscilloscope. The block diagram of the pulse echo overlap system and the associated waveforms are illustrated in figure 3.4 and figure 3.5 respectively.

A pulse of 10 MHz radio frequency is generated by the pulse modulator and receiver unit (Matec 6600). A high resolution oscillator set (Matec 110) itself generates a synchroniser square wave which is used to power the decade divider and dual delay set (Matec 122A). The frequency of this square wave is similar to that of the sine wave produced by a pulse modulator and receiver unit (Matec 6600). This frequency is then reduced in the decade divider and dual delay set (Matec 122A) by dividing it with a factor of 10 in order to trigger the pulse modulator and receiver (Matec 6600). Each triggered pulse creates a radio frequency burst which is in turn

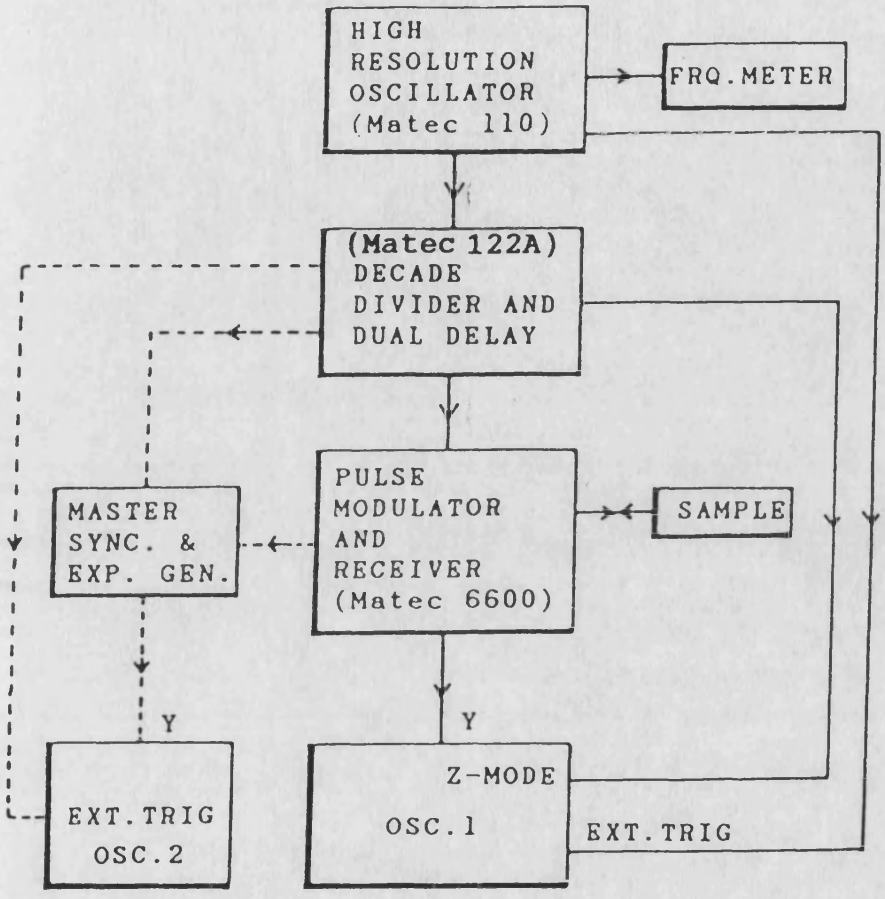

Figure 3.4 :

Block diagram of the pulse echo overlap system.

(1) Signal Generator.

(2) Master Sync. from High Resolution Oscillator.

(3) Divided Sync. (÷10)

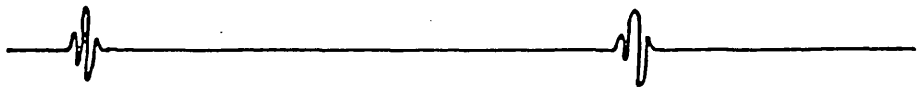

(4) Radio Frequency (r.f.) Pulses to Sample.

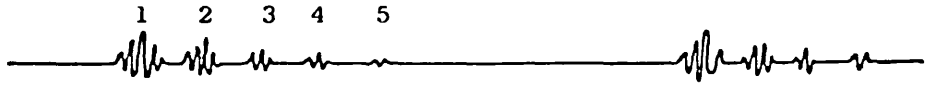

(5) Radio Frequency Echoes.

(6) Z modulation - Intensification of Echoes 1 and 2

(7) Video Out.

(8) Overlap of Echoes 1 and 2.

Figure 3.5 :

Schematic of the pulse echo overlap waveforms.

transformed by the quartz transducer into a mechanical vibration within the crystal. The successive reflections are then detected by the transducer and amplified by a receiver (Matec 6600) set. The r.f. signals produced by this process are displayed on the oscilloscope as illustrated in figure 3.1.

For each echo train, the decade divider and dual delay set (Matec 122A) produces a pair of square wave pulses which are channelled to the Z-mode of an oscilloscope. By decreasing the oscilloscope brightness, only two intensified echoes are observed on the screen. When the time base of the oscilloscope is roughly set to the value of the echo width, the two intensified echoes will be overlapped on top of each other as seen on the display. To ensure that this overlap image remains stationary, the oscilloscope has to be triggered by a high resolution oscillator (Matec 110) with a rate equivalent to the delay between the chosen echoes. Critical adjustment of this equipment can then be used to produce cycle-to-cycle matching within the echoes. The transit time measurements have to be consistent and systematic in order to reduce the experimental errors i.e. mismatch of overlapped echoes. In practice a cycle near to the centre of the first echo is chosen and overlapped over the equivalent cycle of the second echo. The echo transit time is given by the reciprocal of the oscillator frequency which is read digitally from the frequency meter. In essence, the transit time of

ultrasonic waves is measured by matching the phase of the 10MHz signal within the overlapped echoes, rather than merely matching the envelope of the echo. The acoustic attenuation measurement of any sample may also be performed simultaneously using this pulse echo overlap system, by connecting an electronically generated exponential curve from the master synchroniser and exponential generator to a second oscilloscope as illustrated by dotted line in figure 3.4. The equipment used to construct this system has been supplied by Matec Company, USA.

3.6 The Low Temperature Dewar System.

The low temperature dewar set consists essentially of inner and outer dewars as illustrated in figure 3.6. The inner dewar is supported by a stiff spring and connected to the cryostat by a rubber sleeve. The space in the inner dewar can be evacuated by a rotary pump and monitored by a Pirani gauge (Edwards Type M6A head). The sample holder with its signal input leads and a thermocouple is located in the inner dewar. The outer dewar is suspended from a frame. Careful alignment of the non-silvered strips down the inner and outer dewar makes it possible to see the level of the refrigerants in the dewars. To reduce any heat conduction to the environment, both dewars are silver plated.

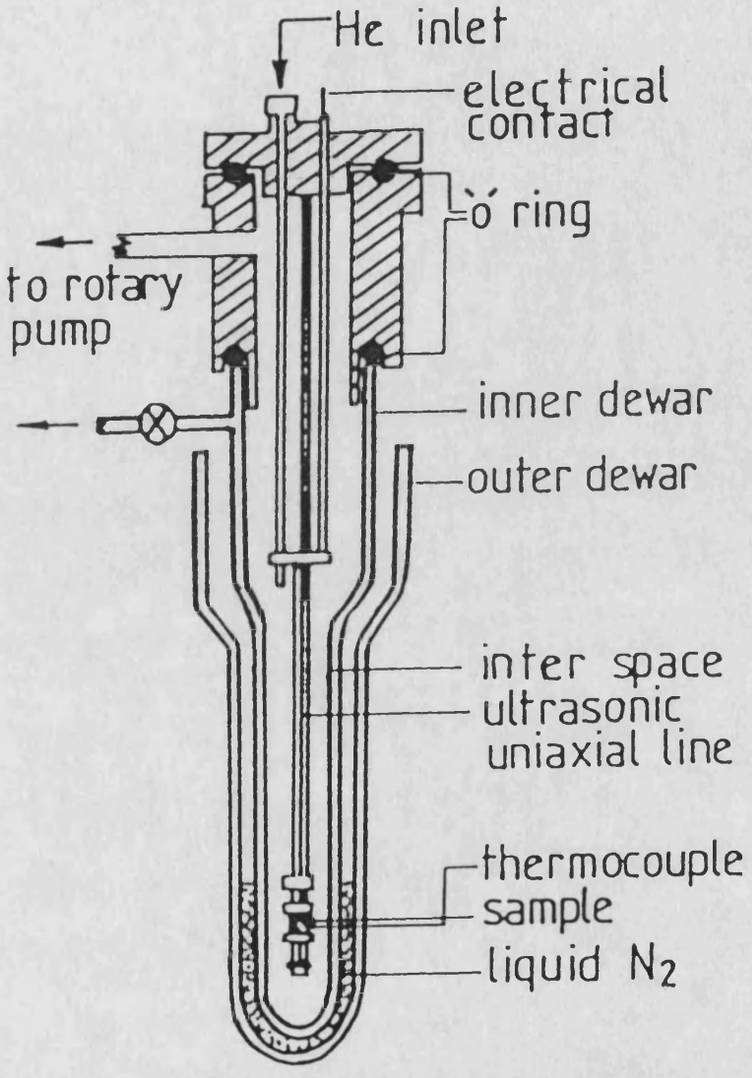

Figure 3.6(a) :

Diagram of low temperature dewar system.

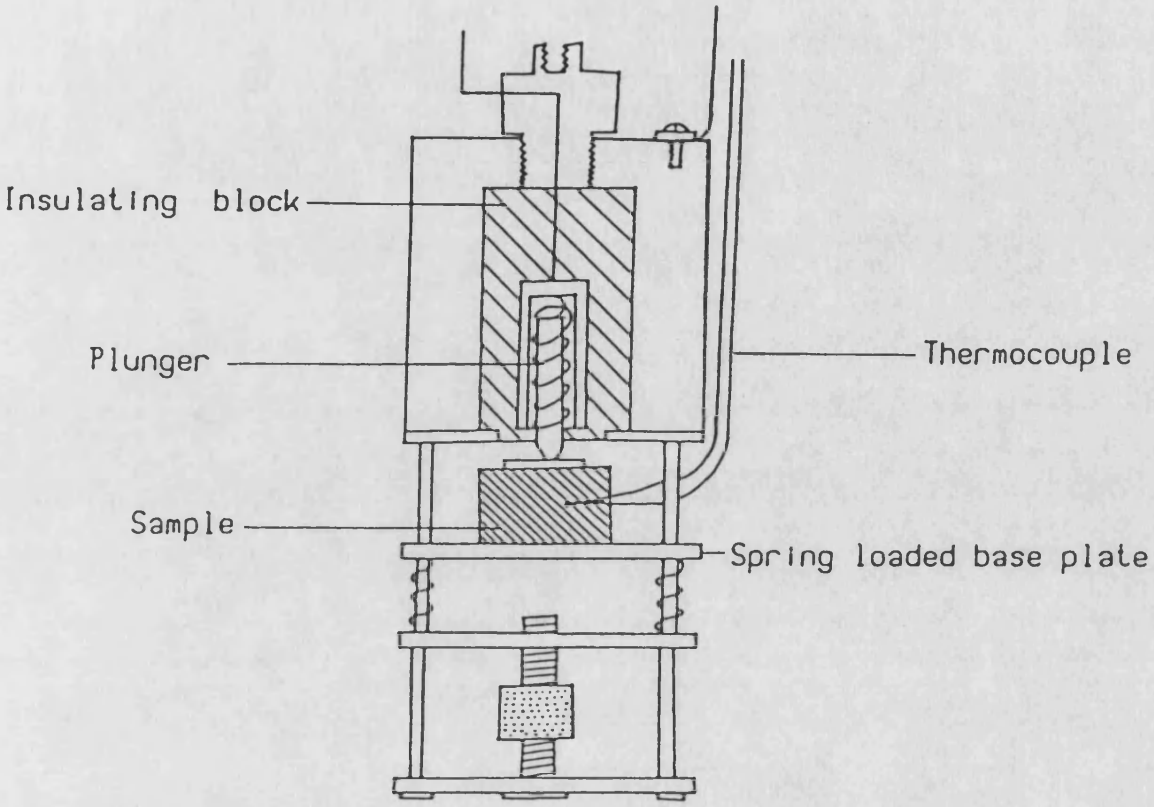

Figure 3.6(b) :

Schematic of low temperature sample holder.

To measure the temperature, a gold 1% iron-chromel and copper-constantan thermocouple junction is contacted onto the surface of the sample. The temperature determined to an accuracy of $\pm$ 0.1K is displayed digitally on an electronic thermometer (Thor Cryogenics 7010). Before starting any measurement, the interspace between the double walls of the inner dewar has to be evacuated to approximately 0.05 torr and then sealed off by a ground glass tap. When the sample holder is in position, the inside of the inner dewar is then vacuum pumped. By filling the outer dewar with liquid nitrogen, the ultrasonic sample can be cooled down towards 77K with a reasonable cooling rate of 0.5K per minute. To achieve liquid helium temperature (4.2K), the outlet of the head of cryostat is connected to a liquid helium container through a transfer tube which takes liquid helium into the inner dewar. In measuring the ultrasonic wave velocities as a function of temperature, the data is taken on both cooling and warming cycles, in order to check the validity and reproducibility of the measurements.

3.7 Hydrostatic Pressure System

This section gives a brief description of the design and operation of the hydrostatic pressure system which is used to study the effect of hydrostatic pressure upon the SOEC. The specification of pressure systems is well documented and discussed extensively by various workers such as Bridgman (1958), Wentorf (1962) and Bradley (1969).

The hydrostatic pressure system employed in this work (Brassington 1982) is a simple piston-and-cylinder arrangement as drawn schematically in figure 3.7, capable of generating pressure up to 10 kbar. This equipment consists of two pistons which are inserted into opposite sides of the bore of a steel cylinder. The upper piston is pushed downward using 50 tons hydraulic press which is operated by a hand pump (Bishop Lifting Services, Bristol, England) to the fixed lower piston in order to create hydrostatic pressure on the sample within the pressure cell.

The sample holder itself (figure 3.7) is constructed onto the upper piston where the manganin coil gauge (see the following section), thermocouple and the signal input leads are also mounted. A safety alarm device is also included in this system to prevent sample holder crushing, in case the upper piston is being pushed too close to the lower piston. Seals between the pistons and

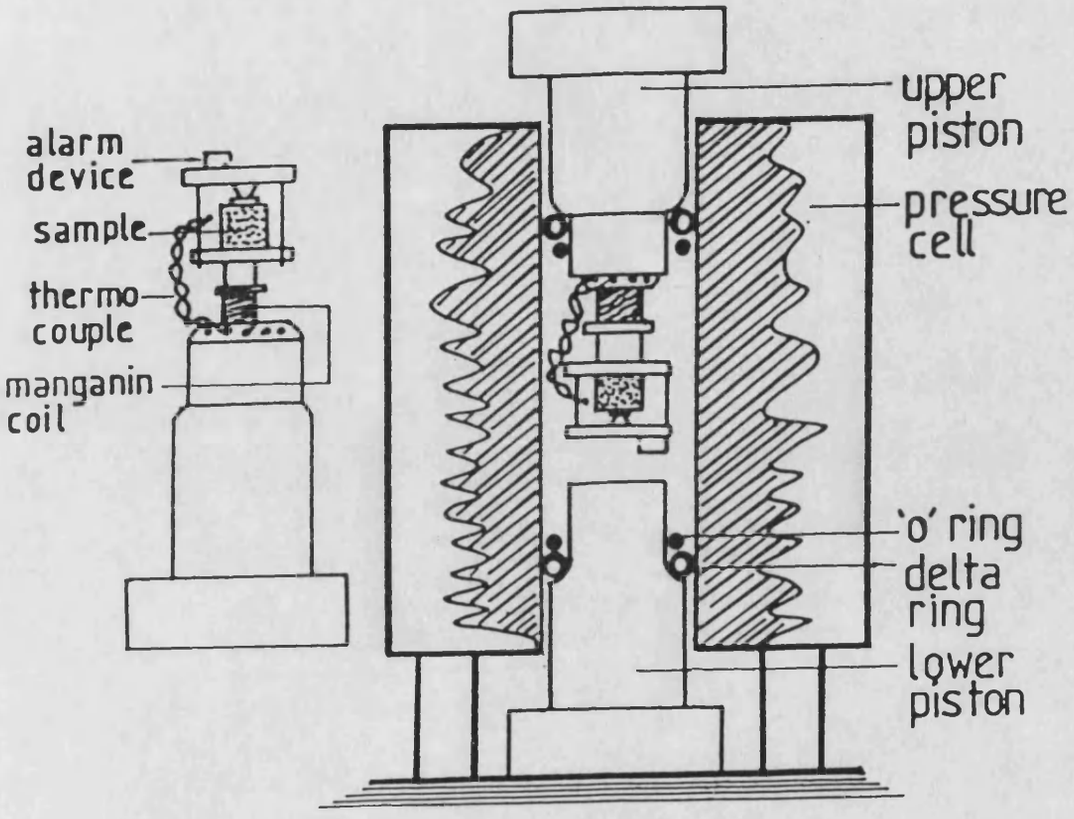

Figure 3.7 :

Diagram of hydrostatic pressure cell and sample holder.

the internal cylinder wall are formed by a rubber O-ring and a p.t.f.e or beryllium copper delta ring attached to the leading section of each piston. The cavity between these two pistons is filled with fluid which serves as a pressure transmitting medium. Several types of fluids have been identified depending on the range of pressure needed:

i) for pressures less than 3 kbar, castor oil is normally employed,

ii) Plexol-244 oil for higher pressures up to 10 kbar,

iii) Silicone fluid (Dow Corning 200/1000 CS) for combination of higher pressures and temperatures.

For safety purposes, the pressure cell is enclosed in a steel cabinet, the door of which is always locked shut during the experiment.

Before taking any data, usually the pressure of the system is increased to a maximum value and held there for about 30 minutes, in order to stabilize the transducer-sample bond and to ensure no leakage in the system throughout the experiment. The pressure is then released and the system is left for another 30 minutes to regain its thermal equilibrium. Then the pressure inside the cavity is increased in steps of about 0.1 kbar and the variation of the echo transit time under hydrostatic pressure is measured after about 15 minutes, to allow for the thermal equilibrium to be reached once more.

3.8 Manganin Coil as a Pressure Gauge.

In high pressure experiments up to about 100 kbar, a manganin coil (Cu-Mn-Ni alloy) can be used as a pressure gauge (Samara and Giardini 1964) due to the fact that its electrical resistivity is sensitive to changes in pressure. The resistance of manganin wire is nearly linearly dependent upon pressure (Bridgman 1958). As a result, this gauge is widely used in piston-cylinder, multi-anvil and other high pressure systems. The pressure coefficient of resistance of manganin wire is 2.4×10^{-3} $kbar^{-1}$ (for calibration, see Samara and Giardini 1964). The pressure inside the hydrostatic pressure cell (section 3.7) has been calculated using:

$$P = (\Delta R/R_{atm})/2.4 \times 10^{-3} \text{ kbar}$$

Here ΔR denotes $(R_P - R_{atm})$ where R_P is the coil resistance at pressure P and R_{atm} is the coil resistance at atmospheric pressure. The resistance is measured using a digital multimeter. The value of the applied hydrostatic pressure is determined to within 1%. The temperature coefficient of resistance of manganin wire is very small 10×10^{-6} $^{o}C^{-1}$ (Wang 1967), and since the experiment is carried out isothermally, this has only a small effect upon the hydrostatic pressure measurement.

3.9 Experimental Errors and Corrections.

Throughout this ultrasonic work several possible sources of experimental errors which affect the overall accuracy of elastic constants and their temperature and pressure derivatives have been recognized. These sources will now be discussed individually.

(i) Measurements of Sample Dimensions.

The dimensions (thickness) of each ultrasonic sample were measured by using a digital micrometer having a resolution of $\pm$0.002 mm. Several measurements were made at different points on the relevant face of each sample and the average values of these measurements was taken as a sample thickness. The standard deviations of these measurements were normally of the order of 0.02%. This typical error contributes directly to the derived velocity and leads to an error of about 0.04% in the resultant SOEC.

(ii) Measurements of Sample Density.

The room temperature densities of all ultrasonic samples were measured by Archimedes' principle. Each value was calculated using

$$\rho_s = W_a \rho_f / (W_a - W_f)$$

where ρ_s is the density of the sample, ρ_f is the density of the floatation medium used; W_a and W_f are the weight of the sample in air and when immersed in the floatation medium respectively. Samples were weighed using an analytical balance which had a resolution of 0.1 mg. This procedure enabled the densities to be determined to within 0.1%. From the equation C_{IJ} (= ρv^2), it can be seen that the error in the density measurement contributes an error directly to the calculated SOEC. To obtain a good value of the SOEC at any temperature, both the dimensions and density of each sample must be known. This can be solved by calculating the dimensional changes from the thermal expansion data (American Institute of Physics Handbook). However this may not be known for a new material; then the room temperature density of each ultrasonic sample has to be used as a reasonable approximation in determination of the temperature dependences of the SOEC. The corresponding error in density and dimensional measurement contributes to a maximum error of about 1% to the SOEC.

(iii) Transit Time Errors.

The largest component of systematic error in the determination of the SOEC is due to the delays included in transit time measurements from multiple internal reflection within the transducer and the sample. Acoustic impedance (the product of density and sound velocity) of both the transducer and the sample are the characteristics that determine the relative contributions of reflections and transmissions of the ultrasonic wave at the sample-transducer interface. Since the physical properties of both media are different, there is an acoustic impedance mismatch between the transducer and the sample. Thus when an ultrasonic wave reaches the transducer and sample interface, part will be reflected and the rest is transmitted. Each portion will undergo multiple reflections in the transducer and sample respectively. As a result the received echoes will be delayed by a certain amount of time and hence the error of a measured transit time was enhanced. In this connection Kittinger (1977) has provided a procedure to correct the measured transit times. In brief his mathematical computations relates the estimated echo delay δt (in units of the reciprocal fundamental transducer frequency) to the acoustic reflection coefficient. From such calculations the real transit time of an ultrasonic wave can be obtained. In our work, these

have been achieved through a computer programme of "TRANS-CORR" (Brassington 1982) which is based on Kittinger's work. Corrections in practice are in the order of 2 to 5% and lead to an increase in the ultrasonic wave velocity. It is important to note that these corrections take no account of the presence of the gold plated electrode and the acoustic bond material between the transducer and the specimen. However according to Kittinger, those contributions to the apparent echo delay are small.

(iv) Diffraction and Non-Parallelism.

The propagation of ultrasonic waves is essentially assumed to be plane wave in nature because the beamwidth is large compared with the wavelength. Here the piezoelectric transducer is regarded as a piston source of these waves. However in a real situation, some radiated energy may still be lost from the sides of the cylindrical region of acoustic flux because the transducer is finite in extent and has a diffraction field. When a small transducer has to be used, the errors in transit time measurement due to these diffraction effects can be significant. This effect has been studied by Truell et al. (1969) and they concluded that when ultrasonic waves are propagated along two- or four-fold symmetry axes, the transit time error due to diffraction is of order 0.01%, providing the crystal orientation is

accurate to within 0.5° and the area of the transducer is smaller than that of the sample.

As mentioned in section 3.2, for a sample which is not perfectly parallel the transducer will receive different phases of the wave across its surface. However this error can be reduced to negligible proportions by ensuring the faces of each ultrasonic sample are parallel to better than 10^{-3} radians, which they are here.

(v) Pressure dependences of the SOEC.

The errors in dC_{IJ}/dP at zero pressure can be determined from the error in the gradients of the plot of the change in natural velocity with applied pressure where the corresponding error can be obtained through a least mean square fit computer programme. The hydrostatic pressure itself can be measured within an accuracy of 0.25%. For the longitudinal mode the typical error in dC_{IJ}/dP is about 2%. Since the relative changes of shear ultrasonic wave velocity under hydrostatic pressure are usually considerably smaller than those for the longitudinal mode, the errors introduced are rather larger (~5%).

4

SOME ASPECTS OF THE NATURE OF GLASS.

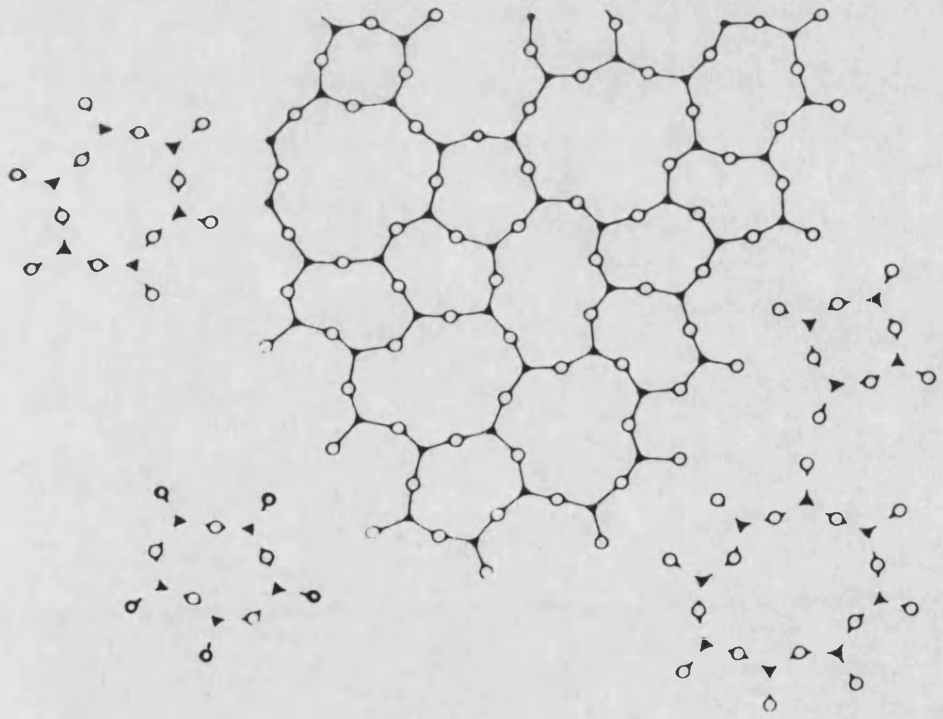

CHAPTER FOUR

SOME ASPECTS OF THE NATURE OF GLASS.

4.1 Definition of Glass.

Glass as defined by the American Society for Testing Materials (1945) is an inorganic product of fusion which has been cooled to a rigid condition without crystallizing. However glass can also be produced in other ways; for instance by the direct condensation of vapour or compressing a liquid (Mackenzie 1960) or through electron beam irradiation (Wong and Angell 1976). In this case Mackenzie (1960) defined glass as any isotropic material, whether inorganic or organic, which lacks three dimensional atomic periodicity and has a viscosity greater than about 10^{14} poise. A more general definition has been proposed by Wong and Angell (1976) that a glass is an X-ray amorphous material which exhibits a glass transition. The terms glass, or vitreous, or more generally amorphous have been used interchangeably by many workers and this practice is followed in this thesis. It is not our aims to review the physics of glass extensively since the definitive descriptions have been well documented and available elsewhere (for examples see Mackenzie 1960, Elliott 1984).

4.2 Formation of Glass.

In general glass is obtained by allowing a liquid to cool through its freezing point without developing any crystallisation phase. The process of glass formation can be indicated by considering the variation of a physical property such as the volume with temperature (Mackenzie 1960) as illustrated in figure 4.1.

On cooling a glass forming liquid, the volume does not show an abrupt change as it does when crystallisation occurs but decreases steadily until in a specific temperature region, the rate of change of volume with temperature decreases. This narrow temperature interval is known as the glass transition temperature T_g. At T_g the coefficient of thermal expansion and the heat capacity of the liquid change rapidly to values near to those for the corresponding crystal. Even though there is no essential change in liquid structure at this point, the rigidity of both liquid and glass are obviously different. It seems that both belong structurally and thermodynamically to the same phase (Turnbull and Cohen 1960). Slow cooling gives more time for structural adjustment to take place and thus leads to a lower value of T_g than that obtained from rapid cooling. To form a crystal the liquid must be cooled very slowly (often requiring in addition a nucleating centre). At the melting point T_m an abrupt change of volume occurs.

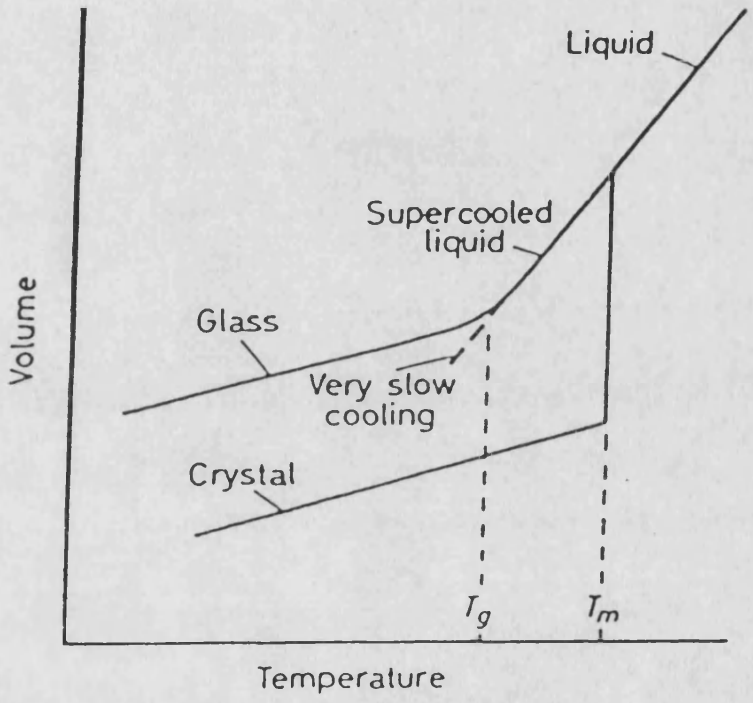

Figure 4.1 : Volume-temperature relation between glassy, liquid and crystalline states.

4.3 Microscopic Structure of Glass.

By definition, glass is amorphous , i.e. it is one of a group of non-crystalline materials which has isotropic macroscopic physical properties and reveals no grain structure when viewed under an optical microscope. Knowledge of glass structure is important because it relates to various physical properties such as density, thermal expansion, viscosity, surface tension and also miscellaneous mechanical (including elastic), chemical and electrical properties of glass. Reviews of the main hyphotheses concerning the microscopic structure of glass are many, for instance see Porai-Koshits (1985). In short, glass structure studies were inspired by Mendelev in 1860. However the experimental side did not commence until 1921 when Lebedev who used his results to introduce a crystallite hyphothesis of glass structure, that is that inorganic glasses possess a partly ordered structure. However this hyphothesis was challenged by Zachariasen (1932) who suggested with particular reference to some oxide glasses that a glass could be modelled by a random network of atoms with near-perfect short range order.

4.3.1 The Random Network Theory.

In developing the random network theory, Zachariasen (1932) made certain assumptions including those below.

(a) The strength of the interatomic binding forces in a glass must be similar to those of corresponding crystal with the same chemical composition.

(b) The three dimensional atomic network still exists in a glass; however it lacks periodicity. This will lead to the macroscopically isotropic physical properties. The network cannot be entirely random because the interatomic distances must not fall below a given minimum value. As a consequence all interatomic distances are not equal; this has been proved by X-ray diffraction studies.

(c) The disordered character of the glass structure due to lack of long-range order produces an internal energy surplus over that of the corresponding crystal structure. However, this difference in internal energy cannot be too high, otherwise devitrification would take place very rapidly. In order to fullfil this condition, Zachariasen proposed that the basic structural units in glass and its corresponding crystal must be assumed to be the same i.e. like oxide crystals, oxide glasses are composed of networks of polyhedra around cations as illustrated in figure 4.2a. Disorder without any important increase in internal energy can develop if the

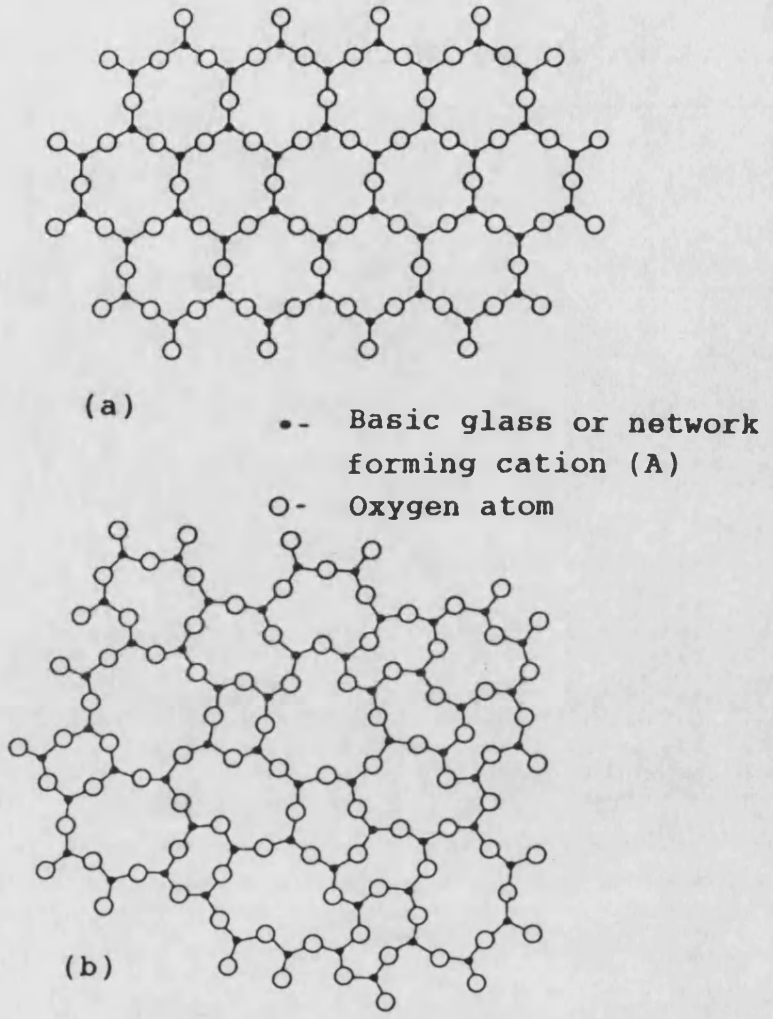

Figure 4.2 : Schematic two-dimensional representation of (a) an oxide crystal and (b) a glass of the same chemical composition (A_2O_3) due to Zachariasen (1932).

relative orientation of polyhedra in a glass is different from that in the crystal. The disorder can occur if the angle, formed by a bond joining two polyhedra or cations, can vary over a wide range, from point to point in glass, about the fixed values obtaining in the crystal. Hence, whereas in a crystal the atomic rings (i.e. the shortest closed circuits of network bonds) are of identical shape with identical numbers of atoms, in the glass a variety of ring sizes will be present (compare figures 4.2a and 4.2b), although the average number of atoms per ring will be approximately the same as in the crystal. There must be some rings in glass larger than the crystal ring size to explain the fact that the density of a glass is always lower than that of corresponding crystal structure.

(d) Almost all atoms in a glass are structurally inequivalent. Therefore, the energy required to detach an atom from the network will be different for each individual atom. In other words, the energy required to break one of the chemical bonds (links between cation and anion) which hold the structural units together, thereby forming the network, will be different for each individual link (crosslink or bridge), though, of course, for the majority of bonds of the same type, this energy value will not be much different from a certain average value. As a consequence, there will be a gradual melting of a glass with increasing temperature; there will be a continuous break down of the network with increasing temperature as compared with the definitive melting point

of crystals.

The investigation of the structure of simple glasses through an X-ray diffraction method by Warren (1934) substantially confirmed Zachariasen's concepts i.e. the absence of the periodicity and symmetry in a glassy network. Since then this model has become widely known as the random network theory.

4.3.2 Network Formers and Network Modifiers.

Zachariasen (1932) has also proposed the rules to determine the glass forming ability of different oxides, which in general illustrate the characteristics of the oxygen atom and its polyhedra in a glass structure. In brief, to form a single oxide glass, one oxygen must be bonded to not more than two cations and the coordination number of oxygen must be three or four. In other words the number of oxygen atoms which surround a cation must be low. The oxygen polyhedra must be bonded to one another at their vertices and not at their edges or surfaces and additionally, if the network is required to be three dimensional, at least three of the polyhedron vertices must be bonded to other polyhedra.

According to these rules, the simple oxides of the types AO and A_2O, where A is cation should not show any potential to form glasses by themselves. On the other hand oxides of types A_2O_3, AO_2 and A_2O_5 can form glasses

which have a three dimensional random network structure composed of AO_3 triangles or AO_4 tetrahedra with shared vertices. Thus, the following pure oxides of B_2O_3, SiO_2, GeO_2, P_2O_5, As_2O_3, P_2O_3, As_2O_5, Sb_2O_3, V_2O_5, Sb_2O_5 and Ta_2O_5 should be capable of forming single oxide glasses. These types of oxide groups are called the glass formers or network formers and the corresponding cations are known as basic glass formers or basic network formers. Some of these pure oxides, for instance B_2O_3 (borate), SiO_2 (silicate), GeO_2 (germanate), P_2O_5 (phosphate) and As_2O_3 (arsenate) have been confirmed to form pure glasses by their own on melting by themselves. A multicomponent glass can also be produced by cooling the melt of more than one type of glass former oxide. Normally the glass formers are highly resistant to chemical attack and have a high melting point for example B_2O_3 (723K), P_2O_5 (853K), As_2O_3 (586K) and SiO_2 (1883K) (Bridge, Patel and Waters 1983). This is because their continuous three dimensional random network is rigidly held together by the strong M-O bonds where M is the cation.

On the other side, some oxides do not have any ability to share in bulding up of a three dimensional network, because they do not fulfill the previous rules. However these oxides can behave as glass or network modifiers. In principle, the cations of such oxides can induce in breaking of some crosslinking or bridging bonds between the tetrahedra vertices of the network former (figure 4.3) in order to develop several holes in which

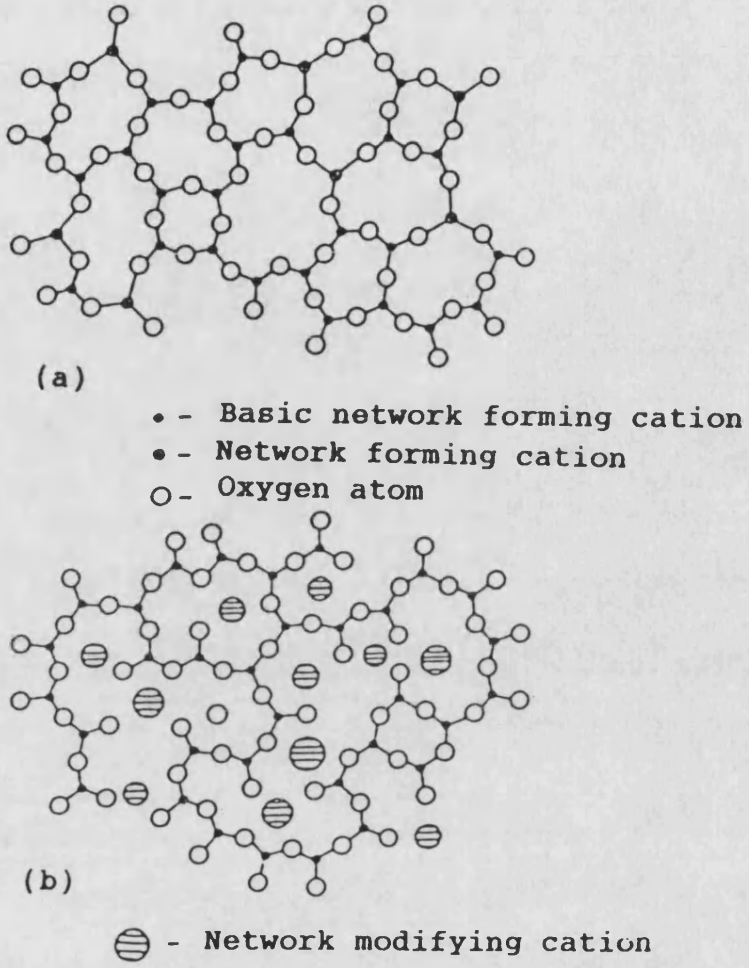

Figure 4.3 : Schematic two-dimensional representation of the microscopic structure of binary oxide glass; (a) composed of basic glass former and glass former; (b) showing the effect of network modifying cations on the network of the glass former.

modifying cations can be settled and scattered at random i.e. the cations reside interstitially. These cations link with the non-bridging oxygen; however the bond strength between and the network is much less than that between network formers and oxygen. The rules of the network modifiers in a glass structure have also been treated by Zachariasen (1935) where:

(a) A condition for cations residing interstitially in a glass, whose network forming cation carries charges 3, 4 or 5, is that the modifying cations should not cause a great increase of the potential energy.

(b) The requirement of minimal change in the potential energy requires a small repulsion between network forming cations A and interstitial cation B and this is turn means that the charge on cation B must be small, and distances between cations large.

(c) The holes in the network are filled gradually as the network is being formed, the dimensions of the holes are of the same order as the size of the interstitial cations.

So from (b) and (c) it has been concluded that the modifying cations B must be large and carry a small charge. Such oxides as Ag_2O, Na_2O, Li_2O, K_2O, CaO, BaO and PbO are categorized as network or glass modifiers. Physically the network modifiers play an important part when they are added into the network formers. For example some oxides i.e. Na_2O, K_2O behave as fluxes which can lower the melting temperature of a pure glass by

decreasing its viscosity. The chemical durability of pure glasses can be improved (Ermolenko 1966) through an addition of certain oxides known as glass stabilisers (such as CaO, MgO and Al_2O_3) into the system.

4.3.3 Structure of Binary Borate Glass.

Early studies on B_2O_3 glass structure by means of X-ray diffraction method (Warren 1941) indicated that the pure glass is composed of a random network in which each boron atom is triangularly bonded to three oxygen and each oxygen is bonded to two boron atoms. Other workers such as Fajan and Barker (1952) have considered a pure B_2O_3 glass as a molecular solid composed of $(B_2O_3)_2$ molecules. Nuclear magnetic resonance (NMR) experiments have confirmed that glassy B_2O_3 consists of some planar BO_3 units which are randomly arranged in a three-dimensional network by sharing all three oxygen atom with adjacent BO_3 units (Bray and O'Keefe 1963, Bray 1985). The planar BO_3 unit presumably involves sp^2 hybridization, with the third p orbital being vacant and extending in a direction perpendicular to the BO_3 plane. This vacant orbital accepts electron density from the unpaired electrons of the oxygen atoms, forming a partial double bond as evidenced by a shortening of the B-O bond from a normal single bond value of approximately 1.50Å to about 1.35Å.

An addition of an ionic oxide M_2O (i.e M = Ag, Li, Na, K) into a pure borate (B_2O_3) glass in order to obtain B_2O_3-xM_2O glass where x is a molar fraction of M_2O produces the following network modifications (Mackenzie 1960).

(i) The B-O-B bond may be broken by oxygen anions in order to form non-bridging terminal oxygen atoms (figure 4.3b).

(ii) A filled orbital of an oxygen anion may overlap with an empty p orbital on a boron atom, resulting in a change of hybridization of the boron atom to the sp^3 tetrahedral configuration. As a consequence, a BO_4 tetrahedron with three bridging and one terminal oxygen atoms is formed.

(iii) An oxygen atom may contribute electron pairs to two BO_3 units which causes the change in coordination of two borons from sp^2 to sp^3 hybridization and no terminal oxygen atom is observed.

In fact all these possible processes are believed to occur depending on the concentration of ionic oxide M_2O present in the borate glass system. It has been reported that a successive addition of ionic oxides into the pure borate glass result in changes of the average coordination of boron atom; this is normally known as the "borate anomaly". That such an anomaly occurs has been supported by means of NMR, X-ray diffraction and also ultrasonic experiments. In general in the range from pure B_2O_3 to 30 mole percent of M_2O, all oxide ions are involved in the process of increasing the coordination number of boron atoms from 3 to 4. Between 30 and 50 mole percent the proportion of tetrahedra and planar triangles remains relatively constant and above 50 mole percent the process reverses and the planar triangle of BO_3 rapidly

become favored until at 70 mole percent of M_2O all boron atoms again have the coordination number of 3. Bray (1985) has shown that an increment of ionic oxide M_2O causes a progressive change of the boron coordination number resulting in the network formation of various structural group units as illustrated in figure 4.4. These structural groupings are composed of BO_3 and BO_4 polyhedra as found in crystalline borate. The concentration of these groups depend on the mole percent of M_2O introduced into the borate glass system.

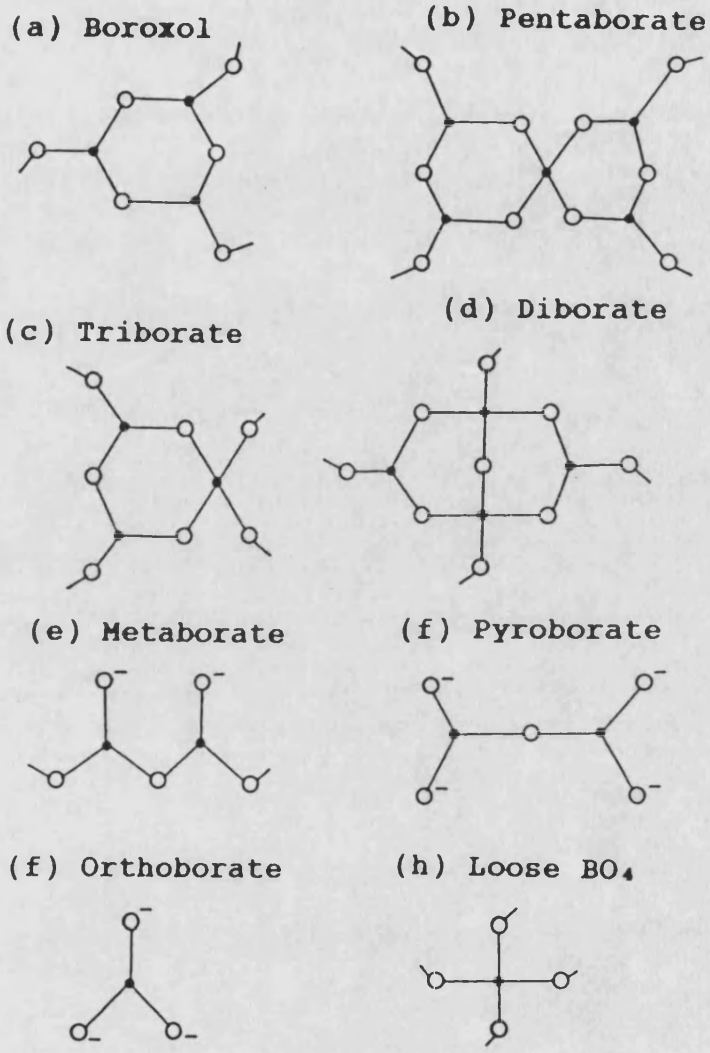

Figure 4.4 : Some structural groupings in borate glasses as indicated from nuclear magnetic resonance experiments (Bray 1985). Small solid circles represent boron atoms, open circles oxygen atoms and an open circle with negative sign indicates a non-bridging oxygen.

4.3.5 Structure of Binary Phosphate Glass.

The concepts involved in the structure of phosphate crystals and glasses have been discussed in detail by numerous workers (for example van Wazer et al. 1958, Westman 1960 and Wignal et al. 1977). Briefly at room temperature, the thermodynamically stable P_2O_5 crystal consists of discrete P_4O_{10} molecules, in which each phosphorus atom is surrounded by three bridging and one terminal oxygen atom. The P-O bond is covalent in nature and the terminal P-O bonds (1.39Å) are significantly shorter than the bridging bonds (1.62Å) (deDecker and MacGillavry 1941).

The basic structural unit in pure P_2O_5 and binary phosphate glasses is a tetrahedral PO_4 group similar to those of binary silicate glasses. This has been confirmed by low-angle X-ray and neutron scattering experiments (Biscoe et al. 1941, Wignal et al. 1977). In this structural unit, the phosphorus atom is covalently bonded to four oxygen atoms which lie at the corners of a tetrahedron. In the case of calcium metaphosphate glass, the P-O-P bond angle is approximately 140° (Biscoe et al. 1941). The PO_4 tetrahedra are linked together to form the three dimensional network of the glass structure. The total number of oxygen atoms in a phosphate glass is always greater than twice the number of phosphorus atoms, and therefore for all compositions there is an

appreciable number of oxygen atoms which are bonded only to one phosphorus as well as those that are bonded to two phosphorus atoms.

General speaking van Wazer (1958) has suggested that possible microscopic structure of the binary glasses in the composition range between highly P_2O_5 and 50 mole% metal oxide is essentially a random network of the type described by Zachariasen (1932). Within the range of 50 to 60 mole% of metal oxides, mixtures of small rings and chains of varying lengths in relative amounts dependent on the composition are present in a phosphate glass. From 60 to 70 mole% metal oxides, only chains occur. So in brief increasing concentration of modifying oxide results in an increasing number of singly bonded oxygen atoms.

4.4 Vibrations in Crystals and Glasses.

The subject of atomic vibrations in a solid has been discussed at length, furnished with mathematical functions in a number standard texts (Kittel 1956, Elliott 1984, Burns 1985). In this section, only that small part of whole subject will be treated which is related directly to our present studies of crystalline and glassy solids. In general, for a solid which is composed of N atoms the lattice vibrations may be considered as the superposition of 3N independent normal modes. In a crystal, which exhibits periodicity of the lattice, these normal modes are plane wave excitations, whose quantized states are called phonons and are characterized by a wavevector $\underline{k}$, an angular frequency ω ($=2\pi\nu$) and a polarisation vector. This quantized energy of the lattice waves can take values E as $(2n+1)\hbar\omega/2$. The frequency of a particular normal mode depends upon its wavevector, and this may be conveniently represented by a phonon-dispersion curve which is a plot of ω versus $\underline{k}$ for specified crystal directions. The maximum value of $\underline{k}$ is determined by the shortest wavelength λ_{min} that can be propagated through the crystal. For a monoatomic chain the λ_{min} would be 2a where a is a lattice parameter of a crystal, hence k_{max} is π/a. The range between $-\pi/a$ and

π/a is called the first Brillouin zone. The number of atoms in the unit cell then determines the number of branches in the Brillouin zone. A schematic $\omega(\underline{k})$ plots for a given crystal direction, for the case of two atoms per unit cell is shown in figure 4.5. When there are C atoms in the unit cell of a crystal, there will be 3 acoustic branches and 3C-3 optical branches in the phonon spectrum. Thus for each $\underline{k}$ there will be 3C modes. To distinguish the type of vibrations in a given branch, it is useful to observe the behaviour of $\omega(\underline{k})$ as $\underline{k}$ approaches the zone centre (k=0). In the case of the acoustic branches, their frequencies go to zero as $\underline{k}$ tends to zero; at the zone centre the atoms in each unit cell vibrate in the same direction (infinite wavelength). However the frequencies of optical branches have a finite value as $\underline{k}$ tends to zero; at the zone centre the atoms vibrate against each other. Along certain symmetry axes of the optical and acoustic branches for specific crystal directions may be degenerate over part or all of the allowed range of $\underline{k}$. The branches can be subclassified into longitudinal or transverse (shear) modes, depending on the direction of particle polarisation with respect to wavevector $\underline{k}$. This is only strictly true for pure mode directions. However at a general value of $\underline{k}$, the lattice vibrations are not strictly longitudinal or transverse, nor are acoustic branch vibrations completely in phase or optic branch modes completely out of phase.

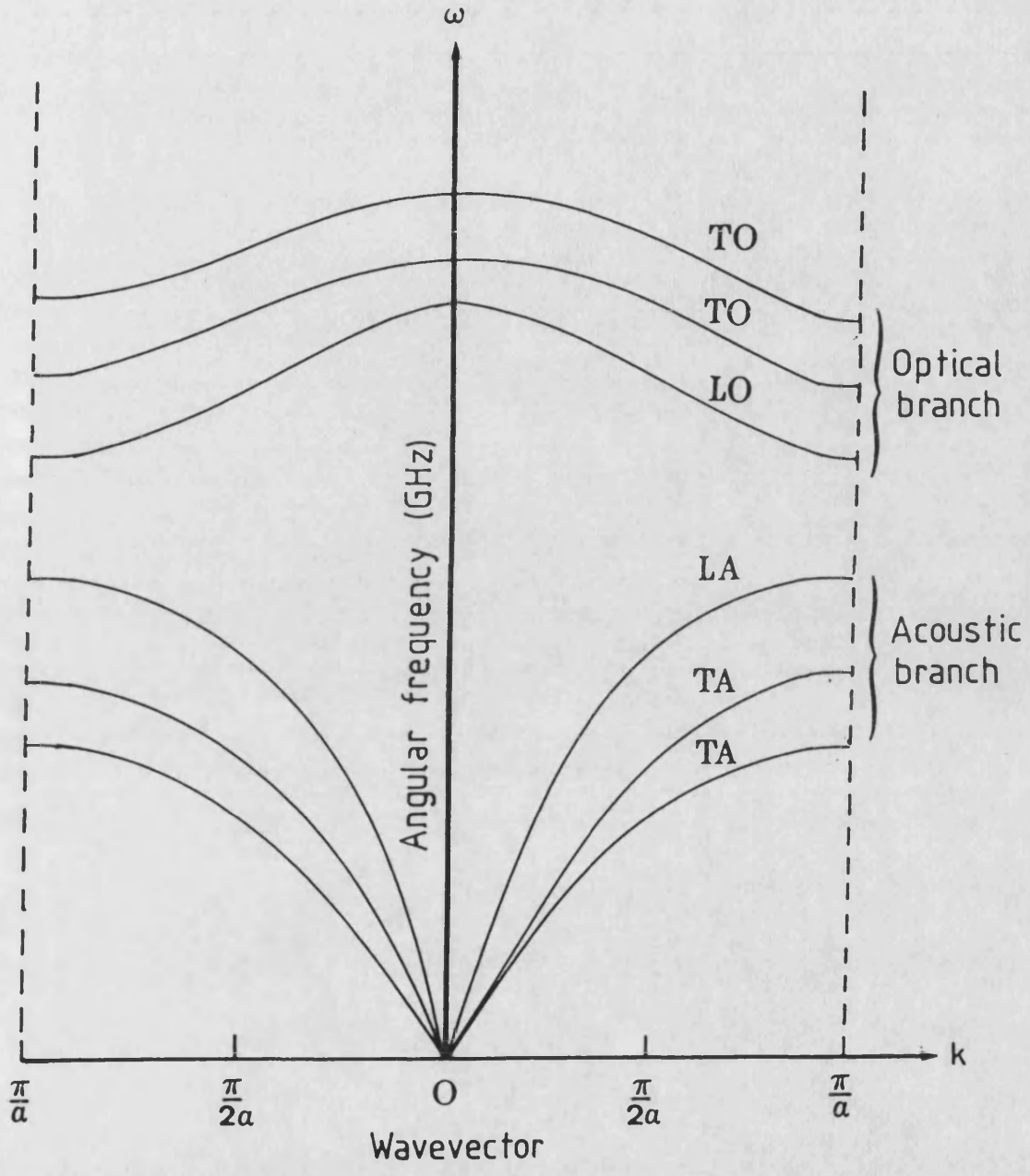

Figure 4.5 : Schematic illustration of a phonon dispersion curve for an arbitrary crystal direction with two atom per unit cell. LO and TO designate longitudinal and transverse optical modes respectively. LA and TA represent longitudinal and transverse acoustic modes respectively.

At the low frequency limit, near to the Brillouin zone centre i.e. in the ultrasonic range of frequencies, where the wavelength λ ($=2\pi/k$) is large compared with the interatomic spacing, the lattice waves behave as waves in an elastic continuum. Here the phase velocity ω/k is almost identical to the group velocity $d\omega/dk$ and is equal to the sound velocity for waves of given polarisation in a specified crystal direction. The maximum values of the acoustic mode velocities occur near to the Brillouin zone centre. As the wavelength of the acoustic waves becomes of the order of the interatomic spacing, their velocities decrease and at the zone boundary the group velocity is always zero. This final point is because that acoustic wave behaves as a standing wave carrying no energy, developing as a consequence of periodical symmetry in a crystal. At low temperatures, only the very low frequency acoustic modes are excited to any appreciable extent; the solid then behaves as an elastic continuum. The measured acoustic wave velocities at low temperatures then can be used to estimate the elastic Debye temperature.

Glass has no long-range order and hence no periodic symmetry. In the harmonic approximation its atomic vibration can still be resolved into normal modes, but these are no longer plane waves. One immediate consequence of nonperiodicity in glass is that at high frequency, when the wavelength becomes comparable with the interatomic spacing, the simplicity of the dispersion

curve will be lost (Dean 1964, Anderson 1965). Thus the curve is smeared out more and more with increasing wave vector. The phonons become extremely complex, and impossible to define acoustic and optical branches (Elliott 1984). A phonon in the original sense does not exist. At very short wavelength the concept of a wave vector becomes of doubtful physical significance. So at this high frequencies, the main difference in atomic vibrations in a crystal and a glass appears; the selection rules which are based on the long range order are not obeyed in glass (Anderson 1965). As a result, many effects which show sharp features in crystals are considerably broadened in a glass. However, in low frequency regime (the long wavelength limit), where the detailed atomic structure is not so important, a glass like other solids behaves as an elastic continuum and the normal modes will be the elastic waves as in the continuum medium. Near k=0 well defined dispersion relation still exists, and both longitudinal and transverse sound waves can be directly observed in glasses via the ultrasonic experiment and up to frequencies of at least about 40GHz by Brillouin scattering (Hunklinger 1982). The long wavelength features of the glass will be nondirectional since it is macroscopically isotropic. Most of the information on the vibrational properties of glass has been obtained at wavevectors close to the origin of the Brillouin zone and the effects of pressure on these modes is a main concern

of the present work.

4.5 Universal Properties of Glass.

At low temperatures glasses show some striking thermal and acoustic behaviour which are markedly different from those of corresponding crystals. These unusual properties can be viewed as being specific properties to the glassy state. Among of these universal properties of glasses include an excess of specific heat capacity, thermal conductivity, relaxation processes and the dependences of the sound wave velocity upon temperature. An extensive review of the subject can be obtained elsewhere, for instance Hunklinger and Arnold (1976), Elliott (1984), Phillips (1987) and Rivier (1987). Numerous models have been suggested; however only one model has the potential to explain adequately these low temperature acoustic and thermal anomalies of glasses. This model is termed as the tunnelling model or sometimes the two-level system model where these words being used interchangeably in the literature; they arise from proposals by Anderson et al. (1972) and Phillips (1972) independently. Only an outline of the concepts involved which are relevant to part of our studies in a glasses (chapter 6) need be presented here.

4.5.1 The Theoretical Model of Two-Level Systems.

In 1971 Zeller and Pohl discovered that silica glass shows some thermal anomalies at low temperatures. For example, below 1K, the specific heat of this glass is much higher than that for crystalline silica (α-quartz) and exhibits a linear dependence with respect to temperature rather than T^3. They suggested that this anomaly is intrinsic due to the nature of randomness of the amorphous network itself. Their findings indicated that amorphous materials contain, in addition to phonons, low energy excitations, which usually do not exist in crystalline solids.

The central hypothesis of the two-level system model proposed by Anderson et al. (1972) and Phillips (1972) rests on an assumption that groups of atoms of low energy excitations in the amorphous network are capable of tunnelling or movement between double well potentials with almost equal energies. This means such groups of atoms can occupy one of two local equilibrium positions which are separated by a barrier a height potential barrier V. A schematic illustration of this two-level system (TLS) model (Anderson et al. 1972) is given in figure 4.6.

At very low temperatures where only ground states have to be considered, the groups of atoms are still able to tunnel through a barrier. This gives rise to an energy splitting of the ground state for this two-level system

given by

$$E = \sqrt{\Delta^2 + \Delta_0^2} \qquad (4.1)$$

where $\Delta_0 = \hbar\omega_0 \exp(-\lambda)$

$$\lambda = d\sqrt{2mV/\hbar^2}$$

The parameter Δ designates the asymmetry of two-level potential, Δ_o represents the tunneling energy and λ is a tunnelling parameter describing the overlap of the wavefunctions of two states in a quantum mechanical theory (Phillips 1981). The parameter ω_o is the frequency of oscillation in an individual well. Furthermore, it is assumed that the parameters Δ and λ are independent of each other and both have a uniform distribution in energy splitting given by $P(\Delta,\lambda)d\Delta d\lambda$ ($= \bar{P}d\Delta d\lambda$), where $\bar{P}$ has a constant value. In fact this condition is not really true for the parameter λ (eq. 4.1) which is determined by Plank constant h, the height of the potential barrier V, the distance d between two well minima and the mass m of the tunneling particles. However this basic assumption does give reasonable agreement with experimental results; for instance in explaining a linear dependence of the specific heat of vitreous silica upon temperature in the very low temperature region (Pohl 1981).

In amorphous materials the low energy excitations are spatially localized (Hunklinger 1977) and hence can be considered as oscillators as illustrated in figure 4.7.

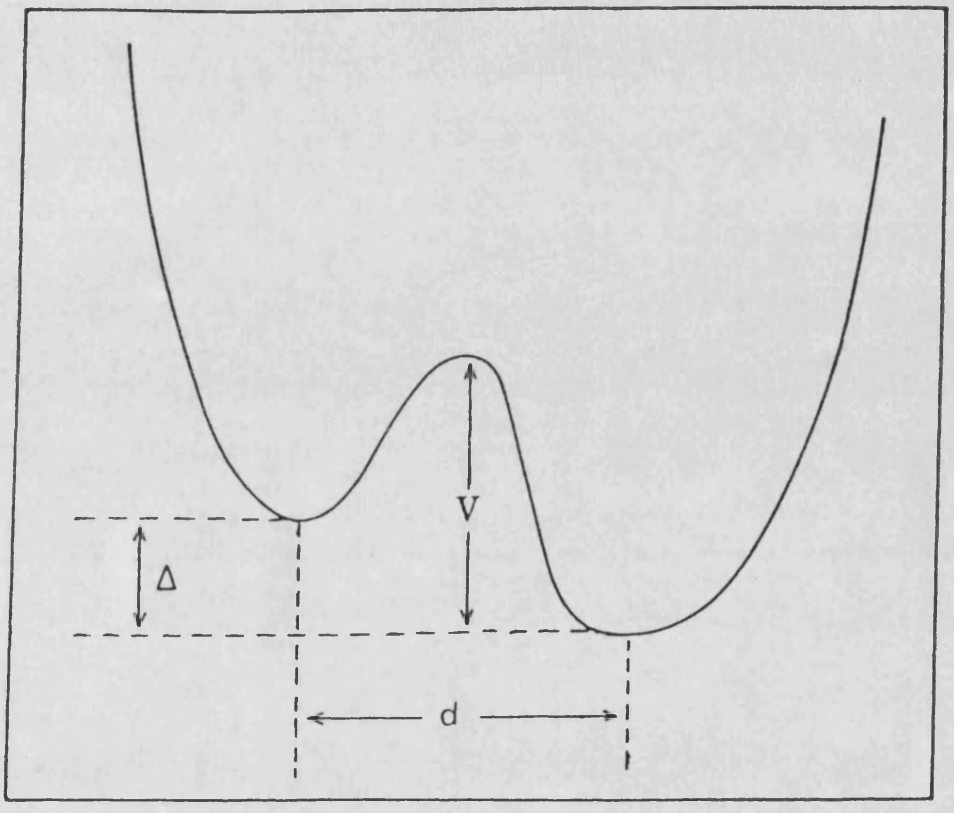

Figure 4.6 : Schematic representation of a double well potential, sometimes known as the two level system, characterized by a barrier V, asymmetry energy Δ and distance d.

At very low temperatures the most likely interaction between such an oscillator and a phonon is the direct process. The phonon will be resonantly absorbed if its energy coincides with the level splitting E of the oscillator. Since the distribution of energy splittings of the low energy excitations is broad, a resonant absorption of each phonon can occur. The observed saturation immediately shows that these oscillators can not have equally spaced levels like harmonic oscillators (see figure 4.7a). Obviously they must have non-equally spaced levels like strongly anharmonic oscillators (figure 4.7b). A more careful analysis of the experimental data by Hunklinger (1977) has suggested that under most experimental conditions it is sufficient to consider only two levels. The most convincing experiment for the validity of the two-level system model has been reported by Hunklinger and his co-workers (1972): the frequency dependence of the resonant absorption of phonons in glass system. Briefly, at low frequency the temperature dependence of the resonant absorption is simply given by the fact that the upper level of these two-level system becomes more and more thermally populated at higher temperatures (Anderson et al (1972).

At very low temperatures the resonant interaction of two level system with phonons of a frequency ω (= E/$\hbar$) is a dominant process, and the phonon absorption of this process is given by Anderson et al. (1972) and Phillips (1972) as

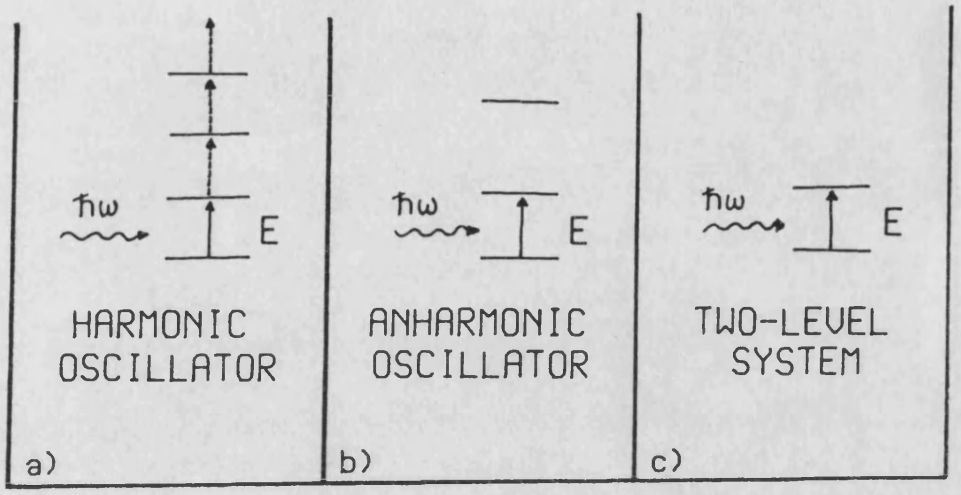

Figure 4.7 : Schematic representation of the resonant interaction between phonons and different types of oscillators. The dashed arrows in (a) indicate the increasing excitation of the harmonic oscillator by absorption of several phonons (Hunklinger 1977).

$$\alpha_{res} = \frac{\pi\omega}{\rho v^3} \bar{P}\gamma^2 \tanh\frac{\hbar\omega}{2kT} \qquad (4.2)$$

where ρ is the mass density, v is the ultrasonic wave velocity, $\bar{P}$ the density of states of the tunneling system and γ the deformation potential of the tunneling system for the interaction with phonons. The factor $\tanh(\hbar\omega/2kT)$ expresses the population of the two states. By using the Debye spectrum for the thermal phonons and the elementary transport theory, it can be shown that resonant interaction of phonons with low energy exitations describes an anomalous behaviour of the thermal conductivity κ in a variety of glasses (Zeller and Pohl 1971), that is that κ directly proportional to T^2 in the low temperature region (Hunklinger and Arnold, 1976). So far this theoretical model has been successful in describing the low temperature thermal and acoustic properties of many amorphous solids, however there is no agreed explanation concerning the microscopic origin of this system.

4.5.2 The Effect of Two-Level System to the Behaviour of the Ultrasonic Wave Velocities in the Low Temperature Region.

Interestingly, the influence of these low energy excitations on the elastic wave propagation can be

studied in detail through ultrasonic experiments. The sound wave velocity and attenuation as a function of temperature have been investigated in various types of glasses by many workers (Hunklinger and Arnold 1976, Hunklinger and Schickfus 1981, Phillips 1981). When the ultrasonic waves are propagated in a glass, their behaviour in the low temperature regime is determined predominantly by three processes; in addition to the anharmonic effects, there is the resonant interaction of phonons with tunneling system and also a relaxation process due to the perturbation of the population out of equilibrium by elastic strains. A strong and temperature dependent resonant absorption of sound waves in most amorphous materials is reflected by a strong temperature dependence of the ultrasonic wave velocity. An increase of sound wave velocity v with respect to temperature occurs at low temperatures which can be written in the logarithmic form (Piche et al. 1974)

$$\left(\frac{\Delta v}{v}\right)_{res} = C_{res} \ln \frac{T}{T_0} \qquad (4.3)$$

where

$$C_{res} = \frac{\bar{P}\gamma^2}{\rho v^2}$$

Here Δv (= $v(T) - v(T_o)$ where T_o is an arbitrary reference temperature. The gradient of the $\frac{\Delta v}{v}$ versus $\ln(T/T_o)$ plot at this temperature range determines the strength of interaction between phonons and the two-level system, which then can be used to estimate the magnitude

of the resonant absorption (eq. 4.2) of the ultrasonic waves. Due to this mechanism the sound wave velocity increases (figure 4.8) up to a maximum point at temperature T_{max} (~1K).

As the temperature is increased, the thermal equilibrium population of the two levels is disturbed. Beyond T_{max}, a resonant absorption begins to decrease and so equation (4.2) no longer holds. Now the relaxation process, within the ensemble of tunneling systems, takes over and causes the sound wave velocity (figure 4.8) to decrease. The relaxation process itself arises due to the fact that the strain field associated with the sound waves influences the energy splitting of the two level system and disturbs the equilibrium occupation. For insulating glasses, a logarithmic decrease of sound wave velocity with temperature occurs due to this relaxation process and leads to a negative slope with a magnitude is about half that of the value for the case of resonant interactions (eq. 4.3), i.e.

$$\left(\frac{\Delta v}{v}\right)_{rel} = -\frac{1}{2}\left(\frac{\Delta v}{v}\right)_{res}$$

$$= -\frac{1}{2} C_{rel} \ln \frac{T}{T_0} \qquad (4.4)$$

In our experimental work the ultrasonic wave velocities have been measured for two types of glasses as a function of temperature down to 4.2K. The ultrasonic wave velocity in each glass increases steadily at lower temperatures rather than having a zero slope like that

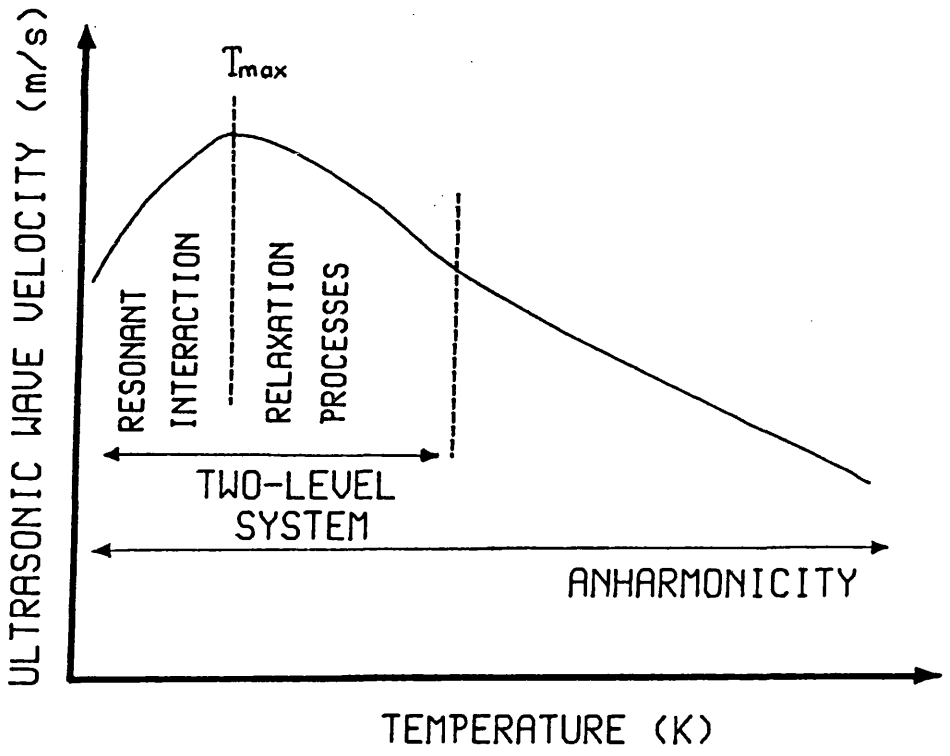

Figure 4.8 : Schematic diagram (not to scale) of the general variation of ultrasonic wave velocity with temperature in most amorphous materials.

found for crystalline solids when the temperature is decreased towards 4.2K which indicates that the relaxation phenomena caused by the interaction of an ultrasonic wave with the two-level system takes place. Due to the lack of very low temperature cryogenic equipment the measurements could not be made down below 4.2K, so that the resonant interaction of phonons with two-level system cannot be observed in our experiment. However a number of reported experiments (Piché et al. 1974, Hunklinger and Schickfus 1981, Weiss et al. 1982, Raychaudhuri and Hunklinger 1983-1984, Neckel et al. 1986) have shown that the mechanisms of resonant absorption, relaxation process and anharmonicity are responsible for governing the behaviour of the ultrasonic wave velocity in most amorphous materials at low temperature region. In the following two chapters, the hydrostatic pressure and temperature dependences of the ultrasonic wave velocities for some interesting glassy materials are now presented.

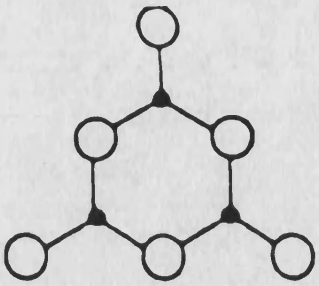

5

ELASTIC BEHAVIOUR UNDER PRESSURE OF SUPERIONIC GLASSES

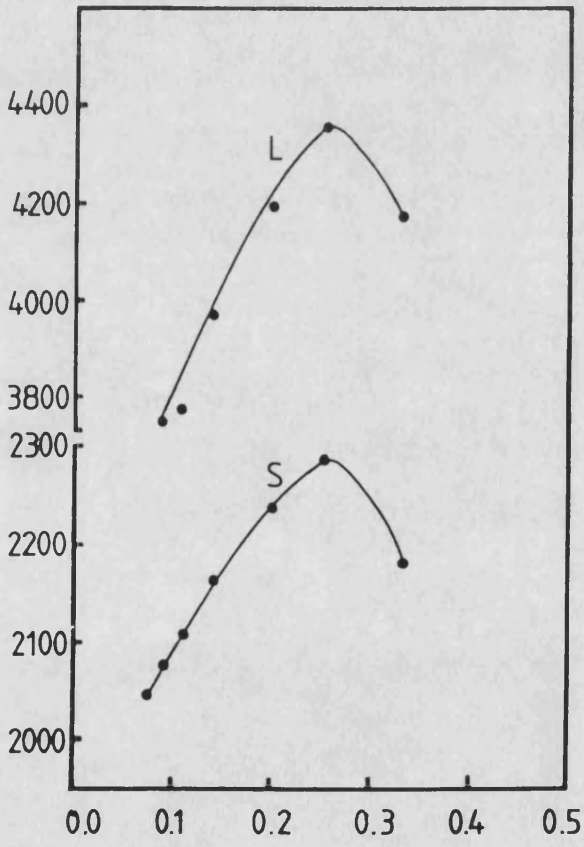

CHAPTER FIVE

ELASTIC BEHAVIOUR UNDER PRESSURE OF SUPERIONIC GLASSES.

5.1 Introduction.

Superionic materials are substances which exhibit high values of ionic conductivity at relatively low temperatures. Several superionic materials at room temperature have been reported and amongst these is a glass-like ionic system. This type of glass is synthesized by combining AgI with other inorganic materials (Takahashi et al. 1972). AgI itself is a crystalline substance. In this chapter an ultrasonic study of the effects of pressure on the elastic properties of a series of superionic glass system in the form of ($AgI.Ag_2O.B_2O_3$) is reported. X-ray diffraction experiments by Schiraldi (1978) have shown that the mechanism of conductivity of this glass is completely ionic with silver ions moving through extended tunnels. Hence the vibrational properties of such superionic glasses are strongly influenced by the presence of mobile ions. Therefore ultrasonic techniques have proved particularly useful in investigating the nature of the

fast ionic dynamics of these glasses (Chiodelli et al. 1982, Minami et al. 1982, Carini et al. 1983, Carini et al. 1984a-b).

The main objective of this present work is to acquire the first information about the anharmonicity of the long-wavelength acoustic modes in these glasses. To achieve this, the hydrostatic pressure derivatives of the elastic constants have been determined experimentally in a number of glasses belonging to the binary $(Ag_2O)_y(B_2O_3)_{1-y}$ and ternary $(AgI)_x[(Ag_2O)_y(B_2O_3)_{1-y}]_{1-x}$ systems. Their elastic properties as well as the pressure effects will be discussed. The discussion of acoustic vibrational anharmonicity is based upon the Grüneisen parameter approach as was introduced earlier in chapter 2.

5.2 Synthesis of Superionic Glass Samples.

Cylindically shaped (diameter, about 10mm; height, about 10mm) samples belonging to the binary and ternary glass systems have been kindly supplied by Dr. G. Chiodelli and Dr. A. Magistris of the University of Pavia, Italy. Since the properties of most glasses depend on their thermal history, it is useful to know the technique for synthesising of the glass. Details of the preparation of superionic glass are available elsewhere (Chiodelli et al. 1982, Carini et al. 1984a) and only a brief

description need be given.

The raw materials are Merk certified reagent grade AgI, $AgNO_3$ and boric acid. The composition of the batches are planned by assuming a complete expulsion of NO_2 from $AgNO_3$ and of H_2O from the boric acid, so that the composition of the glasses obtained are referred to the fixed ratio Ag_2O/B_2O_3 equal to unity. The batch materials are carefully ground, mixed, heated and melted in open alumina crucibles maintained at 700°C and the melt is kept at this temperature, while being repeatedly stirred to ensure the complete removal of vapour. Finally they were quenched by pouring them into an internally Teflon coated metallic mould which is immersed in liquid nitrogen. Homogeneous glass cylinders are obtained. The glass is transparent to light. The colour changes with increasing AgI content from ruby red to pale yellow. Each ultrasonic glass sample is prepared to have flat and mutually parallel faces. In order to avoid any light induced decomposition the specimens are always kept in darkened dessicator.

5.3 Experimental Results.

The experimental data for superionic glasses obtained from the ultrasonic work described in chapter 3 will now be presented.

5.3.1 Density Measurement.

The density of each superionic glass sample has been measured at room temperature (300K) using Archimedes' principle (see section 3.9(ii)) with acetone as the floatation fluid of previously determined density (0.792 gcm^{-3}). The choice of acetone is made for two reasons: it is not absorbed by and does not react with the hygroscopic glass compositions, its low surface tension discourages bubbles of air from adhering to the sample during immersion. Results of the density meaurements are shown in table 5.1 to 5.2 and plotted in figure 5.1 as a function of chemical composition for binary and ternary silver borate glasses respectively. The average error in the present measurement is estimated about $\pm$ 0.010 gcm^{-3}.

5.3.2 Ultrasonic Waves Velocities and the SOEC.

The velocities of longitudinal and shear ultrasonic waves propagated through the glasses were determined at room temperature by the pulse echo overlap system as

Table 5.1 : Experimental values at room temperature of the density ρ, sound velocities of longitudinal (V_l) and transverse (V_s) waves of silver borate glasses $(Ag_2O)_y(B_2O_3)_{1-y}$: a) present work b) Carini et al. (1985).

y	ρ	V_l	V_s	V_l	V_s
	(kgm^{-3})	(ms^{-1})		(ms^{-1})	
		a	a	b	b
0.09	2520	3753	2074	3885	2043
0.11	2590	3761	2105	3973	2083
0.14	2850	3973	2167	4101	2147
0.20	3280	4191	2236	4253	2249
0.25	3560	-	-	4353	2289
0.33	4030	4232	2181	4271	2250

Table 5.2 : Densities and velocities of sound in silver borate glasses $(AgI)_x[(Ag_2O)_y(B_2O_3)_{1-y}]_{1-x}$: a) present work b) Carini et al. (1984).

x	ρ	V_l	V_s	V_l	V_s
	(kgm^{-3})	(ms^{-1})		(ms^{-1})	
		a	a	b	b
y=0.20					
0.20	3360	3911	2141	4060	2165
0.30	3350	-	-	3868	2045
0.40	3650	-	-	3640	1925
y=0.33					
0.10	4270	4079	2078	4106	2144
0.20	4380	3895	2049	3967	2069
0.40	4660	-	-	3509	1819
0.50	4780	-	-	3238	1679
0.60	4840	3011	1603	3013	1547
y=0.50					
0.30	5420	-	-	3367	1606
0.40	5550	-	-	3147	1524
0.50	5680	-	-	2843	1314
0.60	5760	-	-	2545	1168
0.70	5820	2276	1030	2277	1029

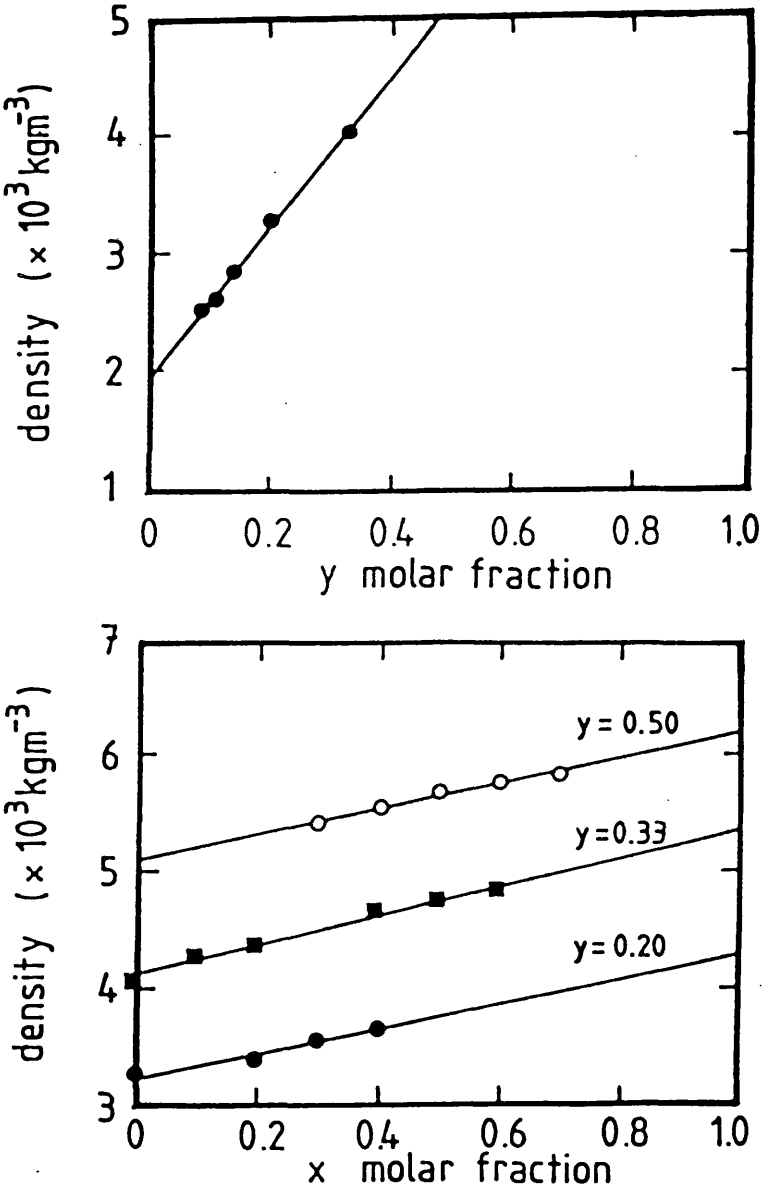

Figure 5.1 : Variation of the density versus composition in the (a) $(Ag_2O)_y(B_2O_3)_{1-y}$ and (b) $(AgI)_x[(Ag_2O)_y(B_2O_3)_{1-y}]_{1-x}$ glass systems.

previously described in chapter 3. The results for glasses in the binary and ternary series are given in tables 5.1 and 5.2 respectively. Figure 5.2 illustrates the compositional dependences of the ultrasonic wave velocities of glasses belonging to the binary series. The elastic stiffnesses and other elastic properties of both binary and ternary superionic glasses are shown in tables 5.3 and 5.4 respectively. The measured velocities and the elastic stiffnesses of these glasses (see tables 5.2 and 5.3) are in reasonable agreement with the data of Carini, Cutroni, Federico and Tripodo (1985). The elastic stiffnesses measured here are those used in the analysis of the effects of hydrostatic pressure on the elastic properties.

5.3.3 Effects of Hydrostatic Pressure and Temperature Upon the Second Order Elastic Constants.

Experimental results obtained for the dependence of the natural velocity (W) waves upon hydrostatic pressure are given in figure 5.3 and 5.4 for both types of glasses. The relative changes in natural velocity obtained for both series of silver borate glasses were found to be linearly dependent upon hydrostatic pressure. The values of the derivatives $[(\rho V^2)']_{P=0}$ were used to obtain the pressure derivatives $(dC_{IJ}/dP)_{P=0}$ of the elastic constants given for binary glasses in table 5.3 and for those containing AgI as a component in table 5.4.

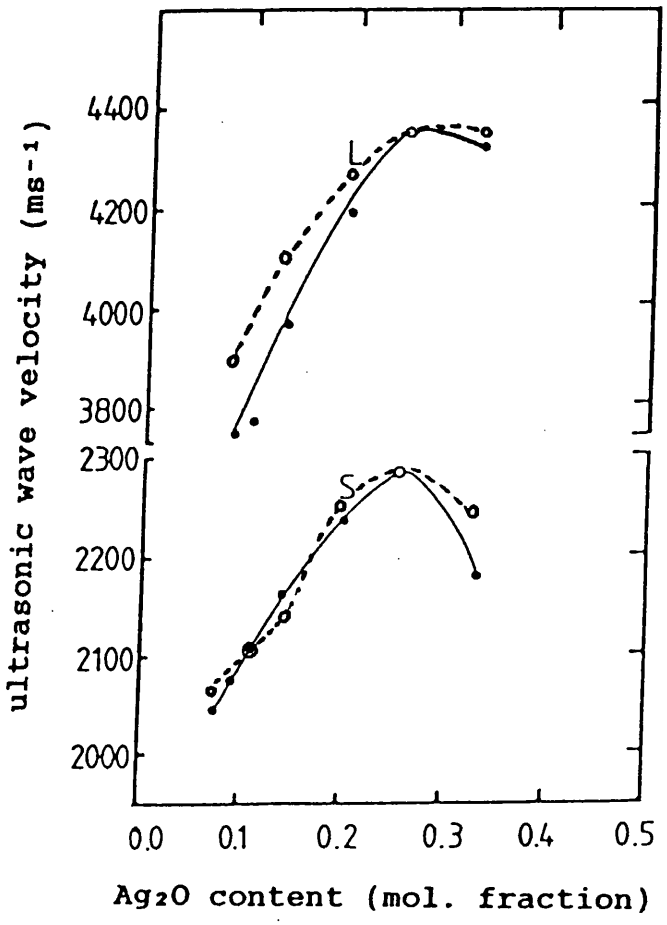

Figure 5.2 : The ultrasonic wave velocity as a function of Ag_2 content in binary silver borate glasses for longitudinal (L) and shear (S) modes. The velocity values labelled (o) have been obtained from Carini et al. (1985).

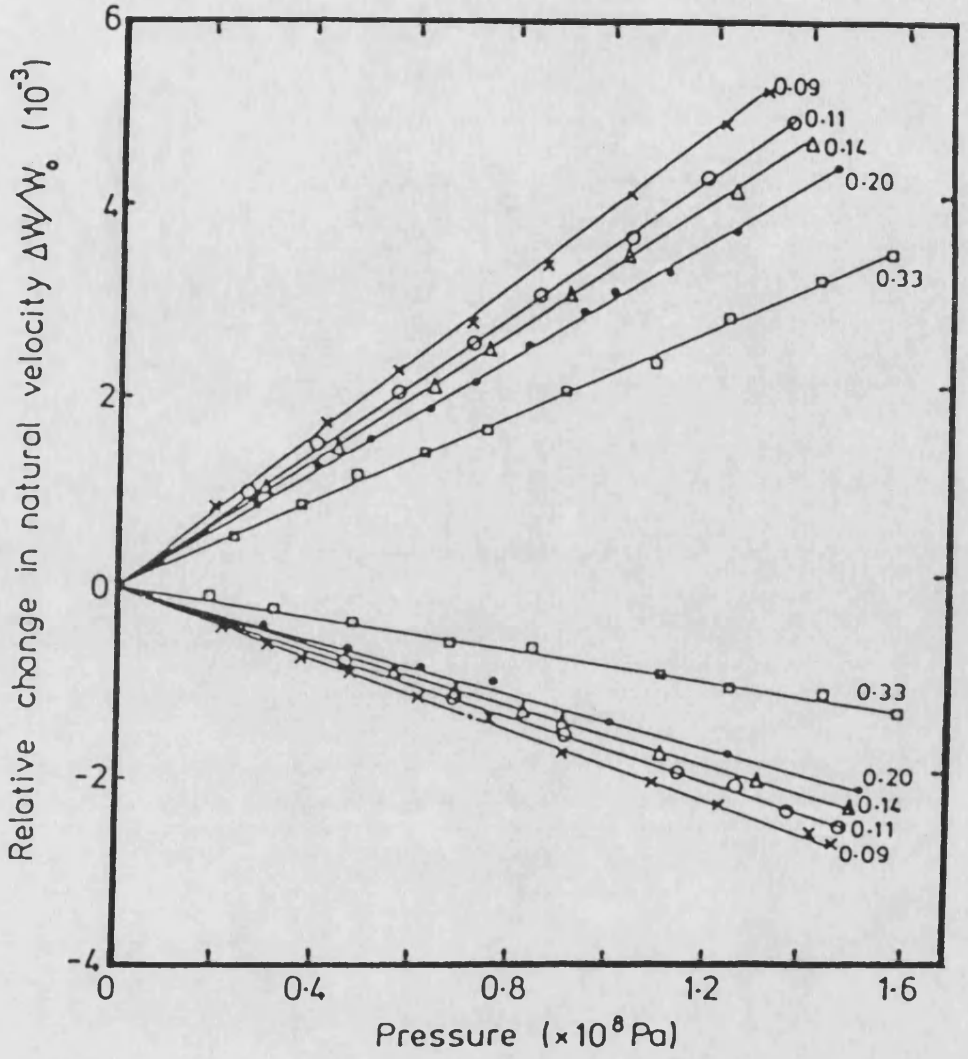

Figure 5.3 : Relative change in the natural wave velocity of longitudinal (the upper set of positive - going lines) and shear (the lower set of negative-going lines) modes induced by application of hydrostatic pressure to silver borate glasses of composition $(Ag_2O)_y(B_2O_3)_{1-y}$. The molar proportions of Ag_2O are the numbers adjacent to the lines. The temperature is 16°C.

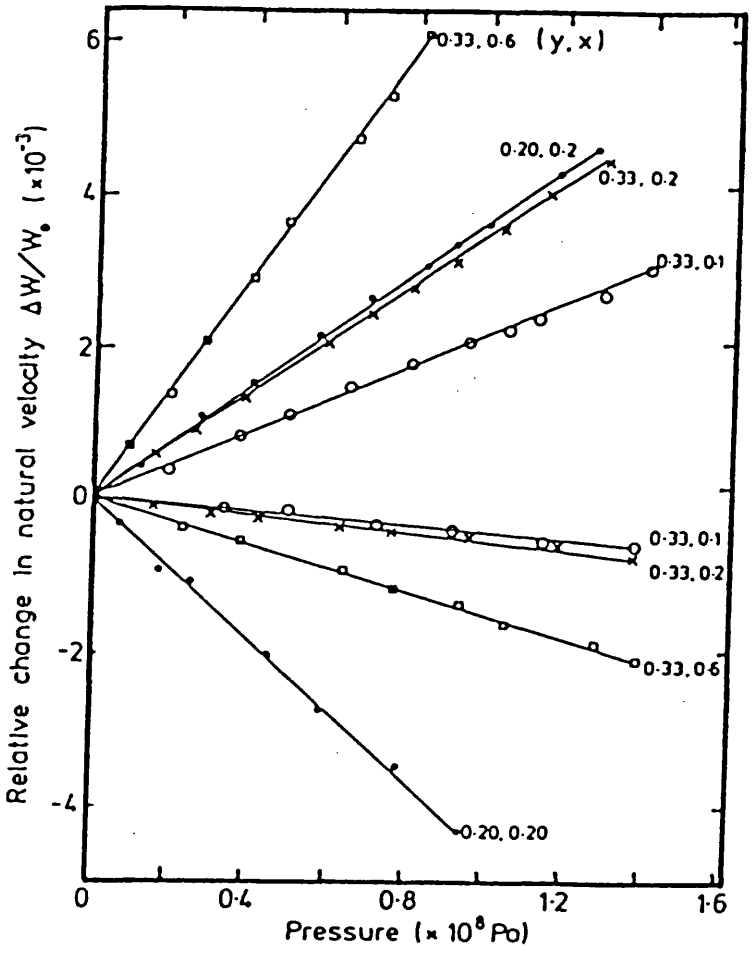

Figure 5.4 : Relative change in the natural wave velocity of longitudinal (the upper set of positive - going lines) and shear (the lower set of negative-going lines) modes induced by application of hydrostatic pressure to silver borate glasses of composition $(AgI)_x[(Ag_2O)_y(B_2O_3)_{1-y}]_{1-x}$. The values of y and x are appended to each line. The temperature is 16°C.

Table 5.3 : The second order elastic constants (unit 10^{10} Nm^{-2}), hydrostatic pressure derivatives dC_{ij}/dP, Grüneisen parameters and the initial slope $[(\rho V^2)'_{P=0}$ $(10^{-3})]$ of the hydrostatic pressure dependence of the modulus for silver borate glasses $(Ag_2O)_y(B_2O_3)_{1-y}$.

y	0.09	0.11	0.14	0.20	0.33
Elastic stiffness constants					
C_{11}	3.55	3.66	4.42	5.76	7.22
C_{12}	1.38	1.37	1.74	2.48	3.38
C_{44}	1.08	1.15	1.34	1.64	1.92
B^S	2.10	2.13	2.63	3.58	4.66
Hydrostatic pressure derivatives					
dC_{11}/dP	3.41	3.28	3.60	4.06	3.88
dC_{12}/dP	3.82	3.64	4.03	4.65	4.17
dC_{44}/dP	-0.21	-0.19	-0.22	-0.29	-0.15
dB^S/dP	3.68	3.51	3.89	4.45	4.08
B_{11}	4.97	4.83	5.16	5.60	5.40
B_{12}	3.04	2.85	3.25	3.88	3.42
B_{44}	1.00	0.99	0.95	0.86	0.99
Grüneisen parameter γ_L	0.84	0.80	0.91	1.10	1.09
Grüneisen parameter γ_S	-0.37	-0.34	-0.38	-0.49	-0.34
Grüneisen parameter $\bar{\gamma}_{el}$	0.04	0.03	0.05	0.04	0.10
$(\rho v_1^2)'$	4.01	3.66	3.44	3.06	2.33
$(\rho v_s^2)'$	-1.74	-1.61	-1.44	-1.36	-0.74

Table 5.4 : The second order elastic constants (unit 10^{10} Nm^{-2}), hydrostatic pressure derivatives $\partial C_{IJ}/\partial P$, Grüneisen parameter and the initial slope $[(\rho v^2)'$ $(10^{-3})]$ of the hydrostatic pressure dependence of the modulus for silver borate glasses $(AgI)_x[(Ag_2O)_y(B_2O_3)_{1-y}]_{1-x}$.

y	0.20	0.33	0.33	0.33	0.50
x	0.20	0.10	0.20	0.60	0.70
Elastic stiffness constants					
C_{11}	5.14	7.10	6.65	4.39	3.01
C_{12}	2.06	3.42	2.97	1.90	1.78
C_{44}	1.54	1.843	1.84	1.24	0.62
B^S	3.05	4.65	4.19	2.728	2.19
Pressure derivatives					
dC_{11}/dP	4.30	3.41	5.10	6.90	8.11
dC_{12}/dP	6.80	3.443	5.27	7.32	7.52
dC_{44}/dP	-1.25	-0.02	-0.047	-0.22	0.29
dB^S/dP	5.96	3.43	5.24	7.18	7.72
B_{11}	5.85	4.91	6.71	8.43	9.57
B_{12}	6.02	2.69	4.51	6.56	6.79
B_{44}	-0.08	1.11	1.10	0.94	1.39
Grüneisen parameter γ_L	1.16	0.95	1.47	1.98	2.78
Grüneisen parameter γ_S	-1.42	-0.19	-0.22	-0.40	0.35
Grüneisen parameter $\bar{\gamma}_{el}$	-0.57	0.19	0.34	0.39	1.16
$(\rho v_1^2)'$	3.64	2.04	3.50	7.24	12.69
$(\rho V_s^2)'$	-4.60	-0.41	-0.52	-1.48	1.62

The temperature dependences of the elastic stiffnesses have been determined for a number of these glasses between liquid helium and room temperature; as an example the results obtained for $(AgI)_{0.2}[(Ag_2O)_{0.2}(B_2O_3)_{0.8})]_{0.8}$ are given figure 5.5. The increases in C_{11} and C_{44} at low temperature are considered to result from interactions with two-level-type systems as outlined in chapter 4. Similar findings have been reported in vitreous silica (Raychaudhuri and Hunklinger 1984), TeO_2 glass (Benbattouche, Saunders and Sidek 1989) and samarium phosphate glass (see the following chapter). Hence the temperature dependences of the second order elastic constants for $(AgI)_{0.2}[(Ag_2O)_{0.2}\ (B_2O_3)_{0.8})]_{0.8}$ glass will be treated in a similar manner to that for samarium phosphate glass. Further discussion of this subject including its application to the $(AgI)_{0.2}[(Ag_2O)_{0.2}\ (B_2O_3)_{0.8})]_{0.8}$ glass will be given in chapter 6. In brief the dependence of ultrasonic wave velocity and hence elastic constant upon temperature can be accounted for by two contributions which are difficult to separate; the thermally activated relaxation processes and anharmonic effects.

The effects of pressure upon the elastic properties are expected to assist in developing an understanding of the nature of fast ionic conductivity in these glasses which require knowledge of the effect of pressure on properties such as bulk modulus and volume. The compression has been calculated using eq. (2.26) for

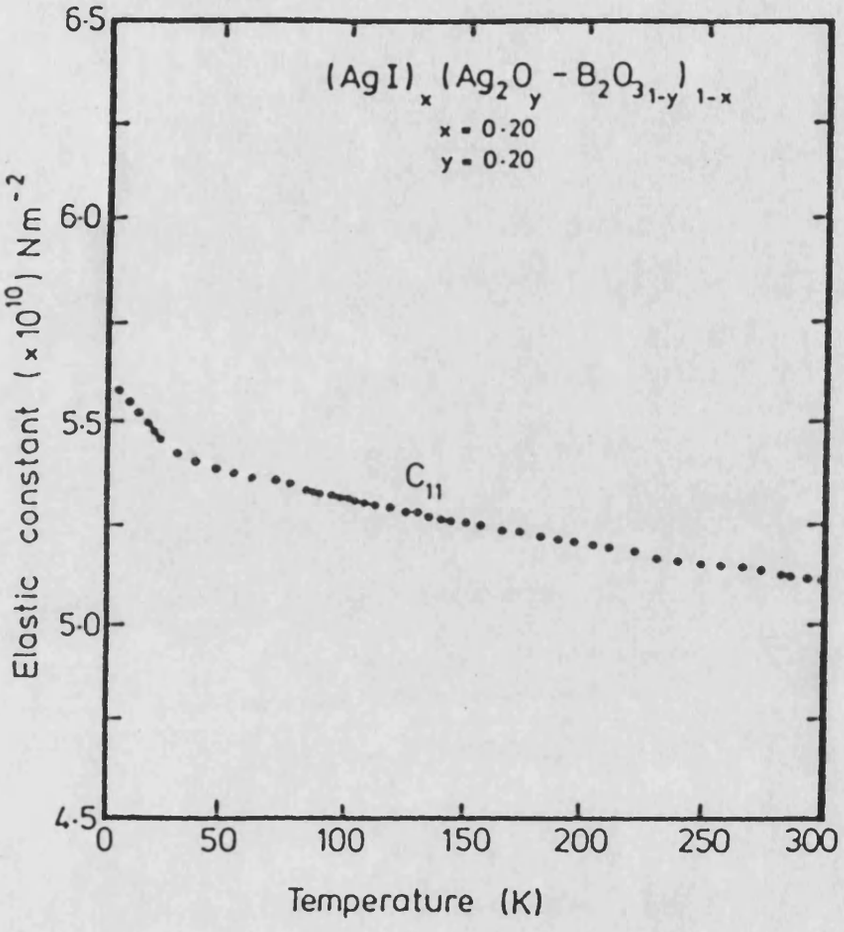

Figure 5.5 : (a) Temperature dependences of C_{11} for $(AgI)_{0.2}[(Ag_2O)_{0.2}(B_2O_3)_{0.8}]_{0.8}$ glass.

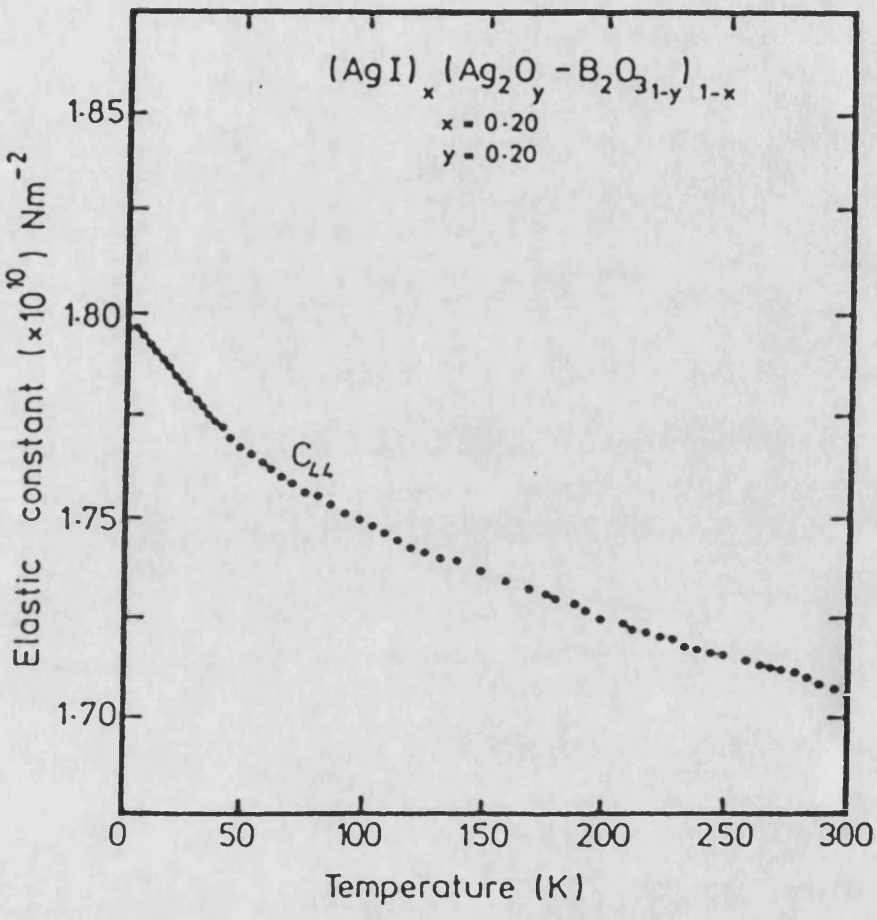

Figure 5.5 : (b) Temperature dependences of C_{44} for $(AgI)_{0.2}[(Ag_2O)_{0.2}(B_2O_3)_{0.8}]_{0.8}$ glass.

$(Ag_2O)_{0.33}(B_2O_3)_{0.67}$ (figure 5.6) for which the thermal Grüneisen parameter γ^{th} (= 0.18) and the linear thermal expansion α (= 8.15 x 10^{-6} K^{-1}) needed in addition to the bulk modulus are available. The isothermal bulk modulus B^T obtained as 4.66 x 10^{10} Nm^{-2} from the adiabatic value B^S measured at atmospheric pressure (denoted by the zero suffix) by using eq. (2.27). The hydrostatic pressure derivative B'^T of isothermal bulk modulus at zero pressure has been calculated as 4.06 using eq. (2.28) with dB^T/dT has been obtained as 7.3×10^6 $Nm^{-2}K^{-1}$. For this binary glass the adiabatic and isothermal bulk moduli are very similar and so too are their respective pressure derivatives; in consequence, determination of the compression using the adiabatic B^S and B'^S would have resulted in a negligible difference from that obtained using the isothermal properties. However in the absence of the thermodynamic data necessary to convert the measured adiabatic quantities to isothermal properties, estimation of the compression for the ternary galsses from the adiabatic B^S and B'^S should be adequate, and has been carried out for the glass with y = 0.33 and x = 0.6 (figure 5.6). The ternary glass has a rather larger compression than the binary material.

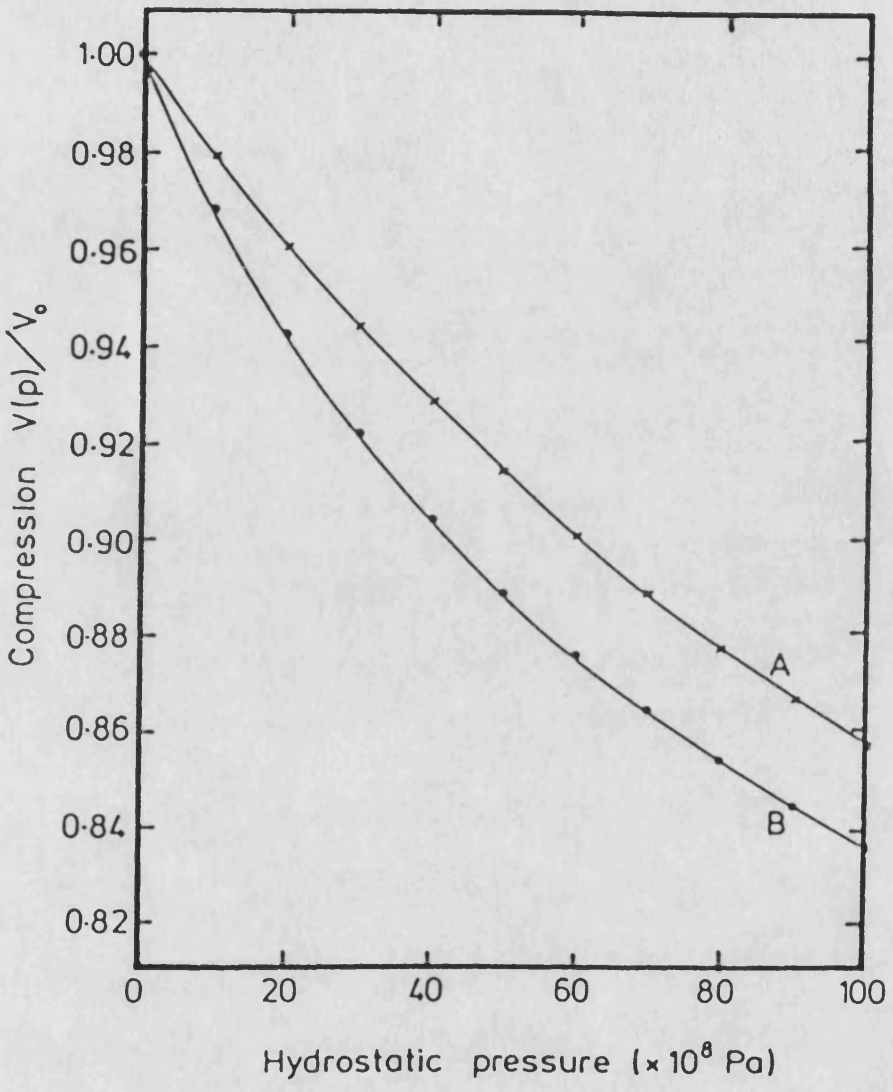

Figure 5.6 : The compression V(P)/Vo of the silver borate glass of composition $(Ag_2O)_{0.33}(B_2O_3)_{0.67}$ (curve A) and the ternary glass $(AgI)_{0.6}[(Ag_2O)_{0.33}(B_2O_3)_{0.67}]_{0.4}$ (curve B) estimated by use of the Murnaghan (1944) equation-of-state.

5.4 Discussion

5.4.1 Compositional Dependences of Ultrasonic Wave Velocity and the SOEC in Glasses Belonging to the Binary and Ternary Systems.

Much useful information about the nature of these glasses can be gained through the compositional dependences of ultrasonic wave velocity and also elastic stiffnesses. For the binary glasses it is found that the ultrasonic wave velocities (figure 5.1) and elastic stiffness (figure 5.7) increase as the Ag_2O content is raised up to a y value of about 0.25. Both shear and longitudinal velocities reach a maximum at y = 0.25 and then decrease as the Ag_2O content is increased further. This unusual behaviour is also found in sodium borate glasses (Na_2O-B_2O_3), so it can be said the role of silver atom in the glassy network is quite similar to sodium atom (Carini et al. 1985). Since the density increases with increasing Ag_2O concentration the elastic stiffnesses $C_{11}(=\rho V^2)$ and $C_{44}(=\rho V^2)$ continue to rise in glass with a y value beyond 0.25. Both these stiffnesses approximately double over the Ag_2O concentration range up to y equal to 0.33.

On the basis of the random network theory, as was introduced in chapter 4, the vitreous B_2O_3 is built up on planar triangles BO_3 (Bray and O'Keefe 1963). The

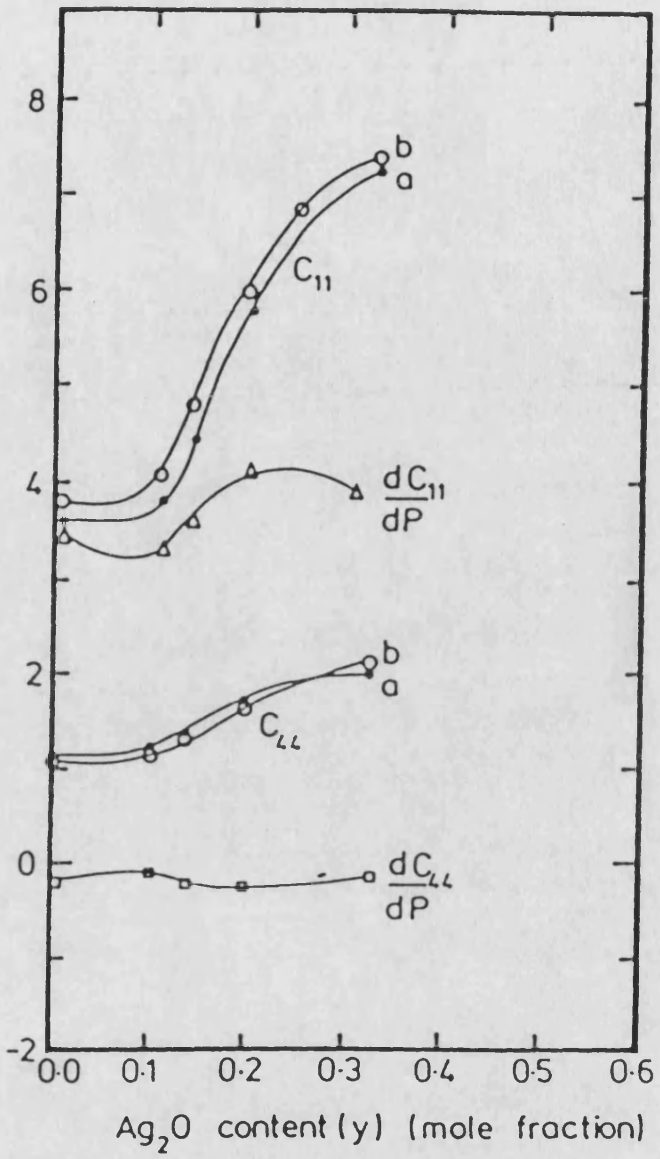

Figure 5.7 : The elastic constants (in units of 10^{10} Nm^{-2}) and their hydrostatic pressure derivatives of binary $(Ag_2O)_y(B_2O_3)_{1-y}$ glasses. The elastic constant values labelled (o) have been obtained from Carini et al. (1985). The values of the pressure derivatives dC_{IJ}/dP correspond directly to the numbers on the vertical axis.

addition of Ag_2O will strengthen the structure by producing fourfold coordinated boron. Analysis of Raman spectra shows these fourfold coordinated boron assisting the formation of BO_4 tetrahedral group with crosslinkage between the same planar units and this group is increasing up to a critical concentration of about 0.25 molar fraction. Further addition of Ag_2O weakens the network by producing singly bonded oxygen ions (non-bridging oxygen). The same oxygen ions that originally bridge between two structural units are substituted by two oxygen ions, bonded only to a single unit; this is substantiated by the appearance of a peak in the internal friction curve, for $y > 0.25$ binary glass (Boulus 1971).

Structural studies of the glasses in the binary system using ^{11}B nuclear magnetic resonance (Kim and Bray 1974) have established that the fraction of boron atoms existing as BO_4 tetrahedral units increases as $y/(100-y)$ up to 30 mol.% Ag_2O. Each Ag_2O unit added results in the production of two BO_4 groups. Therefore, Carini et al (1984a) have suggested that the enhancement of the moduli with increasing molar concentration y of Ag_2O results from a stiffening of the structure as the four-fold coordination of boron (as BO_4 units) rises, with consequent increased cross-linking between planar BO_3 triangular groups. Experimental evidence for such a structural effect with increase in Ag_2O content is provided by an increase in the Raman band at 770 cm^{-1},

confirming the network-modifying action of Ag_2O, while the band at 800 cm^{-1}, characteristic of B_2O_3 glass itself, decreases in intensity (Carini et al. 1984b).

The sound velocity behaviour of the ternary glasses as a function of AgI content have been measured by Carini et al. (1984a). They reported that the ultrasonic velocity in the ternary glasses decreases continuously with AgI concentration. Their findings are confirmed by our present measurements on a series of ternary glasses (table 5.2). Physically this implies progressive softening of the network by introducing the new species (AgI). For example, the elastic stiffness constants for ternary glasses y=0.33 (table 5.4) decrease as the molar fraction of AgI is increased.

5.4.2 Hydrostatic Pressure Derivatives.

The effects of pressure on the elastic constants of binary glasses are consistent with this structural picture. Both dC_{11}/dP and dB/dP have normal positive values as shown in table 5.3. The pattern of enhancement of the material stiffness with increasing Ag_2O content extends to these pressure derivatives, both of which increase with increasing Ag_2O content y (up to y equal to 0.2). The small reductions in dC_{11}/dP and dC_{44}/dP when y is increased to 0.33 are consistent with the observation of Kim and Bray (1974) that, when the Ag_2O

content is increased beyond 30 mol.%, the fraction of boron atoms existing in BO_4 unit begins to decrease. dC_{44}/dP is slightly negative for the binary glasses (figure 5.7). This anomalous feature also occurs in a number of other oxide glasses and is usually ascribed to bond bending motions of bridging oxygen atoms (Sato and Anderson 1980). The gradient of the pressure induced changes in the natural velocity of shear waves decreases steadily with increasing Ag_2O content (figure 5.3); the implication here is that the silver ions tend to impede bond bending.

The effects induced by incrementing the silver concentration by AgI have the opposite sense to those due to Ag_2O. This finding is illustrated by the gradients of natural velocity with pressure measured in the series of ternary glasses having the constant y value of 0.33 (figure 5.4). When the AgI content is increased, there is a large increase in dC_{11}/dP and a smaller increase in the (negative) value of dC_{44}/dP. This is opposite to the effect of increasing the concentration of Ag_2O in the binary glass (figure 5.3).

Now, ultrasonic (Carini et al 1983), Raman (Malughani and Mercier 1984, Carini et al. 1984b), optical and extended X-ray absorption fine structure (Dalba, Fontana, Fornasini, Mariotto, Masullo and Rocca 1983) studies of the ternary glasses suggest that the AgI exists in microdomains and may not markedly change the glass matrix. There are close similarities between the

low-frequency regions of the Raman spectra of the ternary glasses and AgI, which are consistent with the formation of microdomains which may resemble crystalline AgI at a local level (Carini et al. 1984b). This view is supported by the observation that electrical property measurements extrapolate to the corresponding values of pure α-AgI (Dalba et al. 1983). Elastic moduli, determined by Brillouin scattering for glasses in the series, also extrapolate to corresponding data for α-AgI (Borjesson and Torrell 1985). Certainly the structural sites occupied by silver ions, which have been introduced as AgI, are not the same as they are for Ag_2O. The opposite sense of the effects of AgI (figure 5.4) on the dC_{IJ}/dP to those of Ag_2O (figure 5.3) is in accord with the quite different structural effects induced by adding AgI or Ag_2O.

5.5 Vibrational Anharmonicity of the Long Wavelength Acoustic Modes in Silver Borate Glasses.

In section 2.10, the mode Grüneisen parameters for crystalline and glass (amorphous) were defined. Properties such as thermal expansion and the lattice thermal conductivity depend upon the anharmonic nature of interatomic forces and are often discussed simply in terms of the Grüneisen constant γ^{th}, a single phenomenological parameter taken as an average measure of the anharmonicity. In order to quantify further the vibrational anharmonicity of a series of silver borate glasses, the mode Grüneisen parameters γ have been numerically calculated (see section 2.10.2 for details). For the silver borate glass of composition $(Ag_2O)_{0.33}(B_2O_3)_{0.67}$ at room temperature the linear coefficient of thermal expansion is 8.15 x 10^{-6} K^{-1}, the specific heat C_p at constant pressure is 196.74 J K^{-1} $mole^{-1}$ (Avogadro et al. 1983), the isotropic bulk modulus B^S is 4.66 x 10^{10} Nm^{-2} and the molar volume is 30.55 x 10^{-6} m^3. These data lead to rather small value of 0.18 for γ^{th}. In a crystal the modes which contribute to γ^{th} are characterized by a frequency, a wavevector and a polarization vector; the anharmonic effects lead to coupling between the modes to give a finite lifetime. For an amorphous solid at higher frequencies the modes are no longer plane waves as were mentioned earlier in chapter

4. The wavevector $\underline{q}$ is no longer a good quantum number and cannot be used to classify the vibrational states. However, in the long-wavelength limit, the regime of ultrasonic waves, an amorphous solid appears iotropic and behaves as an elastic medium. These vibrational excitations are more heavily damped, i.e. they have a shorter lifetime, than those in a crystalline solid.

As stressed in chapter 2, measurements of the pressure dependences of the elastic stiffnesses can be used to quantify the anharmonicity of these low-frequency modes by determining the acoustic-mode Grüneisen parameters by the following equations (Lambson, Saunders, Bridge and El-Mallawany 1984) in the form of

$$\gamma_L = -\frac{B}{6C_{11}}\left(3 - \frac{2C_{12}}{B} - \frac{3dB}{dP} - \frac{4dC_{44}}{dP}\right),$$

$$\gamma_S = -\frac{1}{6C_{44}}\left(2C_{44} - 3B\frac{dC_{44}}{dP} - \frac{3}{2}B + \frac{3}{2}C_{12}\right).$$

In general the mean acoustic-mode Grüneisen parameter $\bar{\gamma}_{\bullet 1}$ in the long-wavelength limit must be obtained from γ_L and γ_S by use of complex weighting functions but at high enough temperature ($T>\theta_D$) to ensure excitation of all the vibrational modes, the expression reduces to the mean of two shear modes and one longitudinal mode as written in eq. (2.59). This is a reasonable approximation at room temperature for these glasses. The Debye temperatures

estimated from the room temperature elastic constants using eq. (2.35) for binary and ternary glasses are given in table 5.5. The longitudinal γ_L and shear γ_S and mean acoustic-mode Grüneisen parameter for a series of binary and ternary glasses are given in tables 5.3 and 5.4 respectively. For each material the positive values of γ_L show that the application of hydrostatic pressure causes the longitudinal acoustic modes to stiffen. This is normal behaviour in the sense that it means physically that the energies of these modes are raised when the glass is squeezed volumetrically. In contrast the negative values found for γ_S confirm that the shear acoustic modes soften under pressure.

For vitreous silica and Pyrex both the longitudinal and the shear acoustic modes Grüneisen parameters are negative (table 5.6), an unusual feature which can be ascribed to their low coordination number and ease of bending vibrations (Sato and Anderson 1980). Silica glasses consist of four-fold coordinated cations based on SiO_4 tetrahedra. The negative pressure dependences (and corresponding positive temperature dependences) of their elastic stiffnesses stem from this open structure which allows bending vibrations of the bridging oxygen ions. The negative γ_S values found here for silver borate glasses provide some indication that bond bending is not completely inhibited in these materials.

The determination of γ^{th} (= 0.18) for $(Ag_2O)_{0.33}(B_2O_3)_{0.67}$ glass now enables a direct comparison

Table 5.5 : The elastic Debye temperature of binary and ternary silver borate glasses.

Composition parameters x	y	Density (kgm^{-3})	Number of atoms per volume N/V ($x10^{28}$ atoms m^{-3})	θ_D (K)
0.0	0.09	2520	8.687	296
0.0	0.11	2590	8.526	298
0.0	0.14	2850	8.776	310
0.0	0.25	3560	8.760	329
0.0	0.20	3280	8.905	322
0.2	0.20	3360	6.421	276
0.3	0.20	3550	5.758	255
0.4	0.20	3650	5.045	230
0.0	0.33	4030	8.556	311
0.1	0.33	4270	7.864	288
0.2	0.33	4380	7.023	273
0.4	0.33	4660	5.694	227
0.5	0.33	4750	5.068	201
0.6	0.33	4840	4.502	184
0.3	0.50	5420	6.310	208
0.4	0.50	5550	5.803	192
0.5	0.50	5680	5.325	161
0.6	0.50	5760	4.830	139
0.7	0.50	5820	4.349	118

Table 5.6 : Comparison for a number of the hydrostatic pressure derivatives of the elastic constants and the long-wavelength acoustic mode Grüneisen parameters. References can be found in the paper by Lambson et al. (1984) with exception of the $Pd_{40}Ni_{40}P_{20}$ metallic glass (Lambson, McDonald, Gibbs and Saunders 1986).

Material	$(\partial B/\partial P)_{P=0}$	$(\partial C_{44}/\partial P)_{P=0}$	γ_L	γ_S	$\bar{\gamma}_{el}$	α ($\times 10^{6}°C^{-1}$)
$(Ag_2O)_{0.2}(B_2O_3)_{0.8}$	+4·45	−0·29	+1·09	−0·49	+0·04	
$(Fe_2O_3)_{0.38}(P_2O_5)_{0.62}$	+4·73	−0·16	+1·1	−0·3	+0·70	
Amorphous As	+6·42	+1·73	+2·34	+1·45	+1·75	+8 to +10·3
Amorphous As_2S_3	+6·52	+1·87	+2·61	+2·49	+2·53	+22·4
$Pd_{40}Ni_{40}P_{20}$ (Metglas)	+6·4	+1·8	+2·34	+1·45	+1·75	
Pyrex	−4·72	−2·39	−1·74	−1·50	−1·58	+3·2
Fused silica	−6.3	−4·1	−2·8	−2·36	−2.5	+0.45

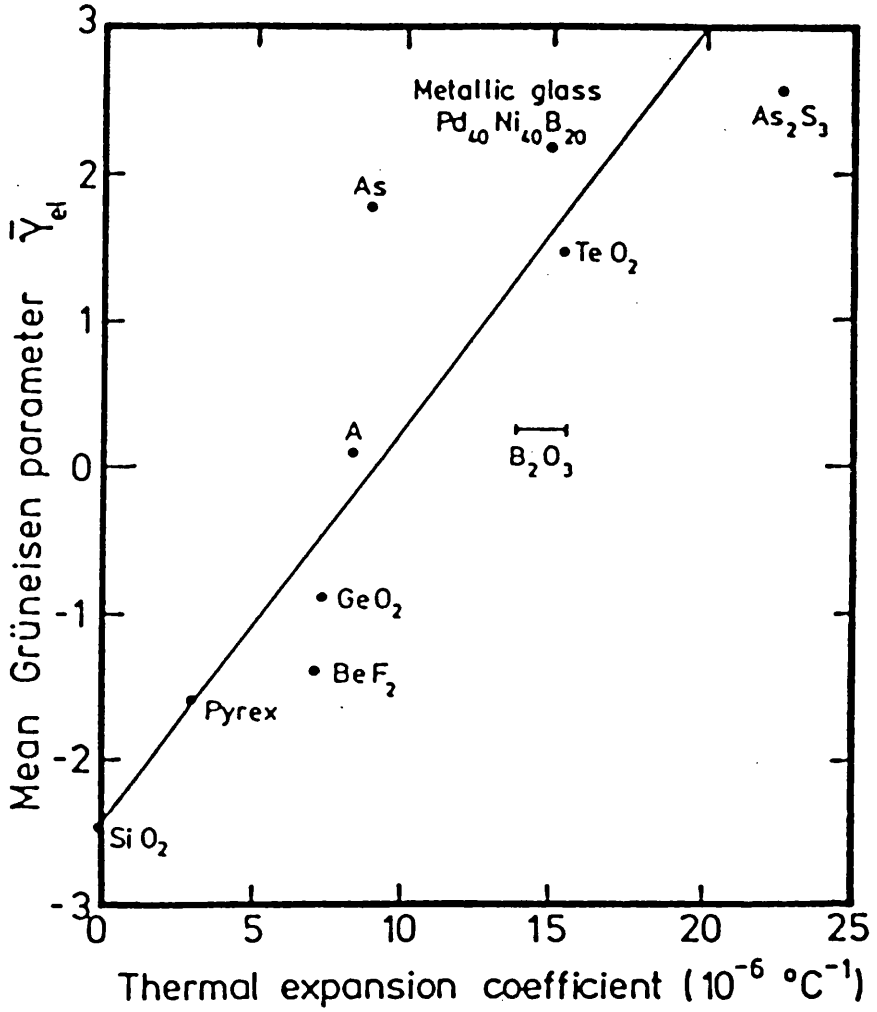

Figure 5.8 : Correlation between the mean long wavelength acoustic mode Grüneisen parameter $\bar{\gamma}_{el}$ and the linear coefficient of thermal expansion for a number of glasses. The point labelled A corresponds to the binary $(Ag_2O)_{0.33}(B_2O_3)_{0.67}$ glass.

between γ^{th} and $\bar{\gamma}_{el}$ (= 0.13) for a silver borate glass. The closeness of γ^{th} and $\bar{\gamma}_{el}$ implies that either the other modes have similar Grüneisen parameters to the long-wavelength acoustic phonons or the latter modes contribute substantially to the thermal properties. These situations are not mutually exclusive. The fact that the long-wavelength acoustic modes do contribute substantially to the collective summations over the modes in amorphous materials is indicated by the strong correlation found (Lambson et al. 1984) between the room temperature thermal expansion and $\bar{\gamma}_{el}$. The silver borate glass $(Ag_2O)_{0.33}(B_2O_3)_{0.67}$ conforms well with this correlation (figure 5.8) being positioned in the region of small but positive $\bar{\gamma}_{el}$ and a moderate thermal expansion.

6

THE ELASTIC BEHAVIOUR WITH TEMPERATURE AND PRESSURE OF SAMARIUM PHOSPHATE GLASSES

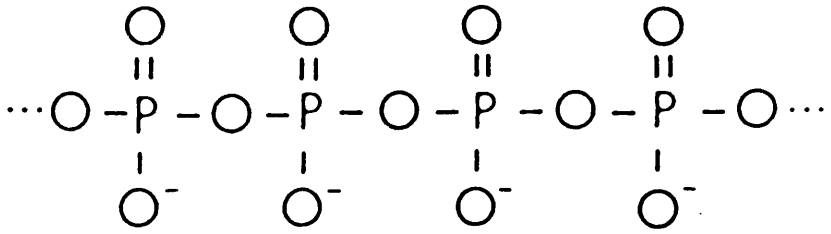

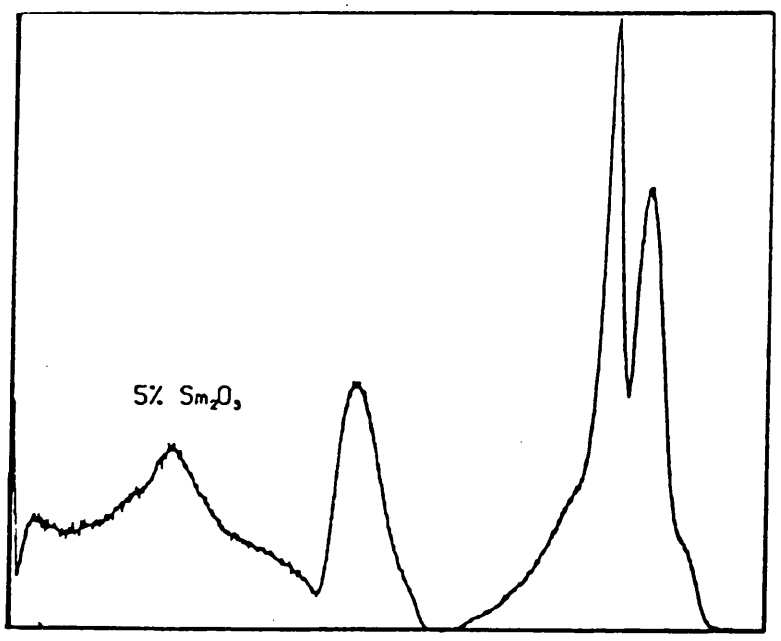

CHAPTER SIX

THE ELASTIC BEHAVIOUR WITH TEMPERATURE AND PRESSURE OF SAMARIUM PHOSPHATE GLASSES.

6.1 Introduction

Glasses containing rare earth ions in high concentration have considerable potential for applications in optical data transmission, detection, sensing and laser technology. For example neodymium phosphate glasses have been widely used in lasers. In rare earth systems the energy of the $4f^{n+1} \rightarrow 4f^{n}d^{1}$ transition governs the systematics of the cohesive energy changes and determines the rare earth ion valence. The lanthanide element samarium has a marked tendency to exhibit valence instability in many of its crystalline compounds. Application of hydrostatic pressure can induce a transition from the divalent (semiconducting) state to an intermediate valence (metallic) state in which samarium compounds exhibit extraordinary behaviour. The transition from the divalent state involves a sharp reduction of the ionic radius in the intermediate valence state. Anomalous elastic behaviour is associated with this valence instability: application of pressure induces a marked decrease in the bulk and longitudinal moduli.

The objective of this part of the study of the effect of temperature and hydrostatic pressure on the elastic behaviour of materials is to find out whether samarium ions in a glassy matrix show any unusual elastic behaviour which might be commensurate either with valence fluctuation in an intermediate valence state or with mixed valence. Phosphate glasses are characterised by low viscosity at the melting temperature which facilitates manufacture and so are useful hosts for studies of the properties of rare earth ions in a glassy matrix. Their microscopic structures are quite well-known and their Raman spectra having been characterised in terms of the vibrations of simple structural components (Hall, Brawer and Weber 1982). In addition the behaviour of the elastic properties under hydrostatic pressure of iron (Brassington et al. 1981) and molybdenum (Comins et al. 1987) phosphates are available for comparison and so help assess how samarium ions in a glassy matrix behave as a function of temperature and hydrostatic pressure.

6.2. Production of The Glass Samples

The samarium phosphate glass samples for ultrasonic works were obtained from Dr. B. Bridge of the Department of Physics at Brunel University, Middlesex, United Kingdom. Considerable technical difficulties have had to be overcome in the preparation of glasses belonging to the Sm_2O_3-P_2O_5 system. Samarium phosphate glasses have been prepared containing up to 25mole% Sm_2O_3, which corresponds to the metaphosphate composition $M(PO_3)_x$, where M represents the metal modifier cation and x its oxidation state. High purity dry Sm_2O_3 and P_2O_5 were mixed in preweighed proportions in alumina crucibles of 100cc capacity. Melting was carried out in an electrical furnace. Below about 1380°C the melts were too viscous for pouring. Melts prepared above this temperature were poured into a split, steel mould preheated to 500°C.

It was not possible to make glasses from starting products containing more than about 25mole% Sm_2O_3 because such melts were too viscous at the highest temperature (1500°C) which could be reached in the furnace. The samples containing up to 25mole% Sm_2O_3 were clear, pale yellow and good optical quality glasses. The specimen made starting from 30mole% Sm_2O_3 material was opaque and not homogeneous. However its elastic behaviour was determined and the results are included here for

completeness. After preparation, samples were stored in plastic containers in a dessicator. Electron micrographs of carbon replicas were examined for any distinctive features which would indicate phase separation or microcrystallinity but did not show such features (Saunders, private communication). The compositions of the glass samples quoted in this chapter, given in table 6.1 are nominal, referring to that of the starting materials. The density of each glass sample, which was determined by Archimedes' principle using toluene as the immersant, is also given in table 6.1

6.3 The Microscopic Structure of Samarium Phosphate Glasses.

Raman spectroscopic studies of these samarium-modified glasses have been carried out by Mierzejewski and his co-workers (1988). Figure 6.1 shows their results of the Raman spectra of the samarium phosphate glasses containing 5 mole%, 15 mole% and 25 mole% Sm_2O_3. Their observations have provided useful evidence that the basic structural features of these samarium glasses are essentially similar those of other phosphate glasses. They have concluded that any unusual features in the physical behaviour of these glasses are likely to accrue from the samarium ion. The Raman spectra show that these materials are built up from phosphorus-oxygen tetrahedral

Table 6.1 : Compositions and physical properties of a series of samarium phosphate glasses $(Sm_2O_3)_x(P_2O_5)_{1-x}$. A6 is a ceramic rather than a glass.

Sample Notation	Sm_2O_3 x%	P_2O_5 (1-x)%	Density (gcm^{-3})	N/V ($x10^{31}$) atom/m^3	Molar Volume (cm^3)
A1	0.05	0.95	3.217	8.78	47.34
A2	0.10	0.90	3.263	8.22	49.84
A3	0.15	0.85	3.280	7.65	52.73
A4	0.20	0.80	3.326	7.21	55.11
A5	0.25	0.75	3.516	7.11	55.07
A6	0.30	0.70	3.731	7.05	54.67

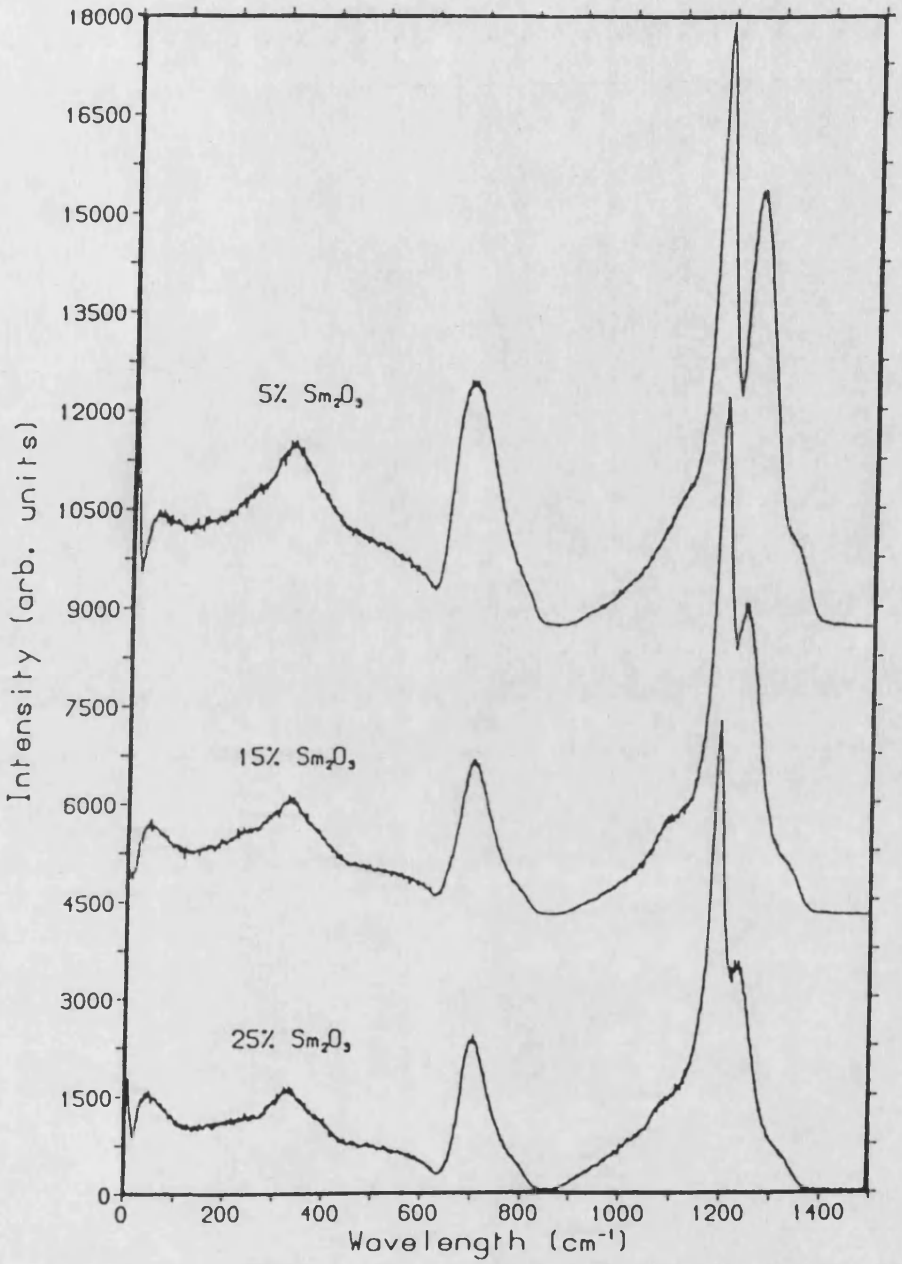

Figure 6.1 : The Raman spectra at room temperature of samarium phosphate glasses (after Mierzejewski et al. 1988).

units. Covalent bonding dominates within and between the PO_4 tetrahedra. One of the four oxygen atoms in a tetrahedron is doubly bonded to the phosphorus and does not contribute to the coherence of the network. Pairs of PO_4 tetrahedra can only share one corner. Vitreous P_2O_5 itself is considered to be a three-dimensional disordered network of PO_4 tetrahedra, most of which are linked at three corners.

Addition of metal oxide results in reduction of the number of cross-linking P-O-P bonds between pairs of tetrahedra. Oxygen introduced by the modifier oxide compensates for the deficit of oxygen caused by this reduction of bonds between tetrahedra. Increase of modifier content leads to a tendency towards inclusion of chains of PO_4 tetrahedra in the structure: glasses having the metaphosphate composition are considered to consist of long chains of PO_4 tetrahedra (van Wazer and Campanella 1950). A polymeric $(PO_2\text{-}O\text{-})_n$ chain is made up of PO_4 adjacent tetrahedra connected at two corners, so that there are two non-bridging oxygen atoms on each tetrahedron. Evidence that such chains are probably present in vitreous metaphosphate $NaPO_3$ (Fawcett, Long and Taylor 1976) comes from its resemblance of the Raman spectrum to that of crystalline Maddrell's salt $NaPO_3$-II which contains $(PO_2\text{-}O\text{-})_n$ chains of infinite length. The infrared spectra of vitreous metaphosphates are consistent with the number of modes available for a zig-zag chain rather than for a straight one (Shih and Su

1965). The modifier cations occupy sites between the non-bridging oxygen atoms and provide weaker ionic bonds between the strong covalently bound chains.

6.4 Experimental Results and Discussion

The data for samarium phosphate glasses obtained from the ultrasonic wave velocity measurements as a function of temperature and hydrostatic pressure will now be presented. The SOEC together with their temperature and hydrostatic pressure derivatives have then been calculated and compared with other phosphate glass systems. The 20 mole% Sm_2O_3 glass has been chosen to find out whether there is any indication of the effects of two-level system in this type of glass.

6.4.1 Compositional Dependences of the Ultrasonic Wave Velocities and Elastic Constants.

The compositional dependence of the velocities of ultrasonic waves propagated in samarium phosphate glasses is shown in figure 6.2 and tabulated in table 6.2. An interesting feature is the minimum in the velocity of the longitudinal mode at the composition 20 mole% Sm_2O_3. The elastic stiffnesses of the samarium phosphate glasses are given in table 6.3. Comparison of these elastic properties with those of molybdenum phosphate glasses (Patel and Bridge 1983, Comins et al. 1987) reveals a rather surprising fact. The glasses modified with

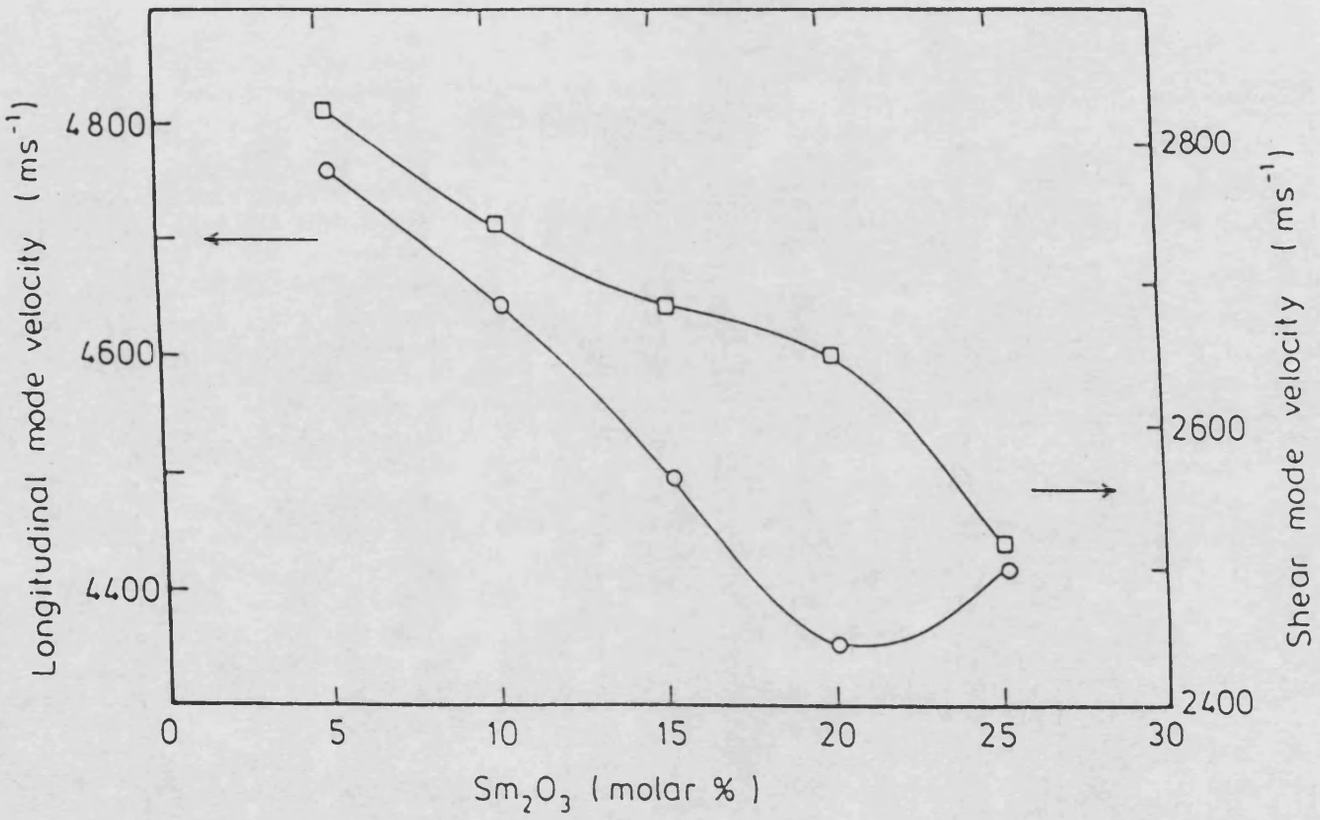

Figure 6.2 : The velocities of longitudinal and shear ultrasonic waves as a function of samarium phosphate glass composition.

Table 6.2 : The ultrasonic wave velocities, initial slope of hydrostatic pressure works and elastic Debye temperature of samarium phosphate glasses at room temperature.

Sample	A1	A2	A3	A4	A5
Thickness (mm)					
l	7.275	6.882	8.257	5.674	6.436
Ultrasonic wave velocity (ms^{-1})					
V_l	4755	4642	4500	4357	4421
V_s	2824	2742	2684	2655	2512
Initial slope of pressure work ($x10^{-3}$)					
$(\rho V_l^2)'$	-0.947	-1.068	-1.296	-1.629	-0.825
$(\rho V_s^2)'$	-1.438	-1.855	-1.996	-2.158	-1.492
Debye temperature (K)					
θ_D	265	280	253	245	232

Table 6.3 : The second order elastic stiffness constants (unit 10^{10} Nm^{-2}), elastic compliance and volume compressibility (unit 10^{-11} m^2N^{-1}) and Poisson's ratio of samarium phosphate glasses $(Sm_2O_3)_x(P_2O_5)_{1-x}$ at 291K.

Sample	A1	A2	A3	A4	A5
Elastic stiffness constants					
C_{11}	7.27	7.03	6.64	6.31	6.87
C_{12}	2.14	2.12	1.92	1.62	2.44
C_{44}	2.56	2.45	2.36	2.34	2.22
B^S	3.85	3.76	3.49	3.19	3.92
Elastic compliance constants					
S_{11}	1.59	1.65	1.73	1.77	1.79
S_{12}	-0.36	-0.38	-0.39	-0.36	-0.47
S_{44}	3.90	4.07	4.23	4.26	4.51
Volume compressibility					
β_V	2.60	2.66	2.86	3.14	2.55
Poisson's ratio					
σ	0.22	0.23	0.22	0.20	0.26

samarium are much stiffer than those with molybdenum, although directional d-electron contributions to the interatomic binding are expected in the molybdenum phosphates. As an example, the measured moduli for a phosphate glass containing 35 mole% MoO_3 are:

$$C_{11} = 4.0 \times 10^{10}\ Nm^{-2}$$

$$C_{44} = 1.2 \times 10^{10}\ Nm^{-2}$$

$$B^S = 2.2 \times 10^{10}\ Nm^{-2}$$

which can be seen to be much smaller than those of the glass containing 30 mole% Sm_2O_3 (table 6.3). The elastic moduli of P_2O_5 (Patel, Bridge and Waters 1983) glass itself are:

$$C_{11} = 4.8 \times 10^{10}\ Nm^{-2}$$

$$C_{44} = 1.21 \times 10^{10}\ Nm^{-2}$$

$$B^S = 2.5 \times 10^{10}\ Nm^{-2}$$

Comparison of these data with those of the samarium phosphate glasses shows that inclusion of only 5 mole% Sm_2O_3 as a modifier induces a large stiffening effect in the glass.

The effects of increase of Sm_2O_3 content on the elastic stiffness bear an interesting relationship to the glass structures inferred from the Raman spectra. When the Sm_2O_3 content is raised from 5 mole% to 20 mole%, C_{11}, C_{44} and the bulk modulus each decrease substantially (table 6.3) as plotted in figure 6.3. The Poisson's ratio (figure 6.4) also shows a similar effect.

As the structure changes from the three-dimensional network to the chain structure typical (van Wazer and

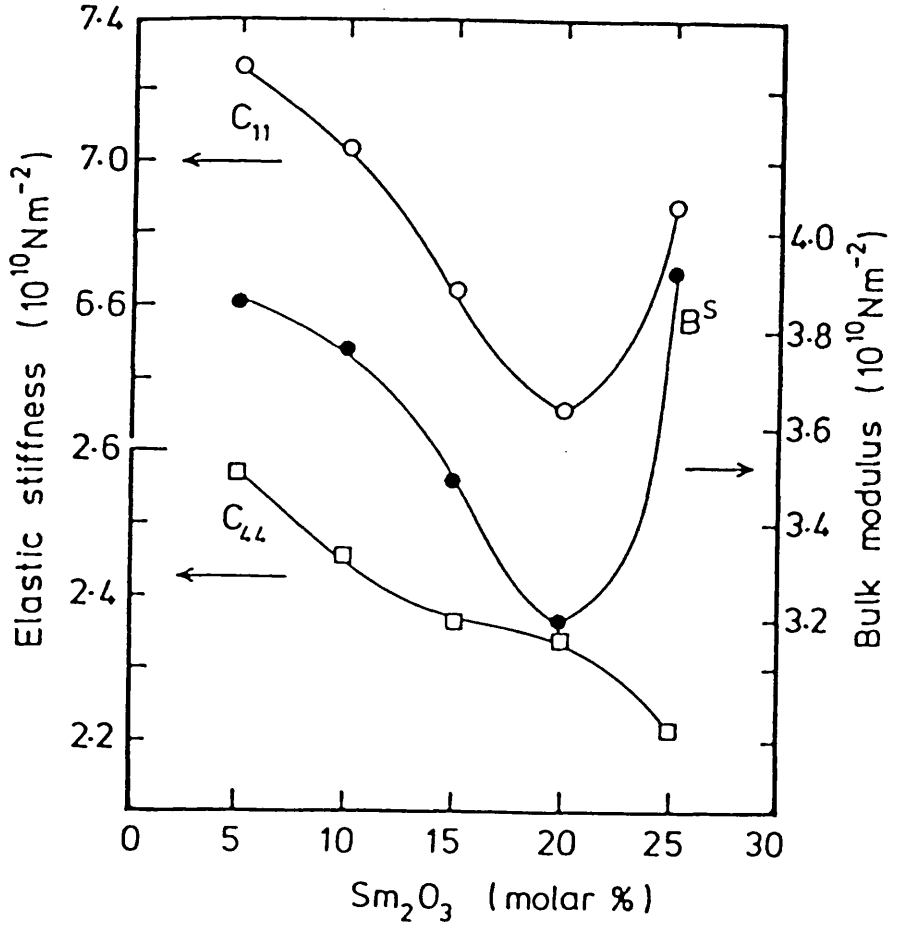

Figure 6.3 : The elastic stiffnesses C_{11}, C_{44} and bulk moduli of samarium phosphate glasses.

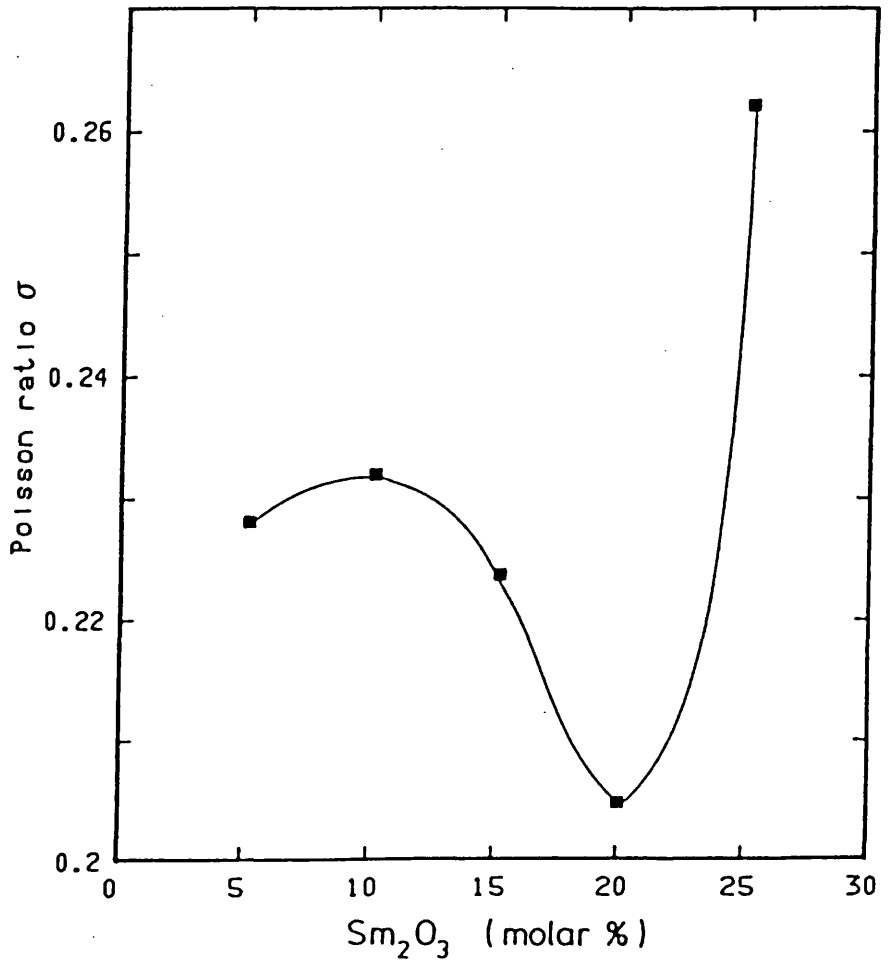

Figure 6.4 : Poisson's ratio as a function of samarium phosphate glass composition.

Campanella 1950) of the metaphosphate composition the rigidities towards shear and hydrostatic stress decrease. When the content of Sm_2O_3 is increased beyond 20 mole% into the metaphosphate range, the longitudinal stiffness C_{11} and the bulk modulus B^S commence to increase while C_{44} flattens out (table 6.3 and figure 6.3). The compositional dependence of the elastic moduli of the samarium phosphate glasses (figure 6.3) is entirely different from that of molybdenum phosphate glasses over similar ranges of molecular concentration. For the latter materials both C_{11} and C_{44} increase considerably as the proportion of MoO_3 is increased from 10 mole% to 50 mole%. Here an increase of MoO_3 results in stiffening of both longitudinal and shear moduli (Patel and Bridge 1983, Comins et al. 1987). The cobalt phosphate glasses also show similar behaviour (Bridge and Higazy 1986). In contrast the elastic stiffness C_{11} decreases to a minimum in the vicinity of the metaphosphate composition in the samarium glass system.

6.4.2 The Effect of Temperature on the Ultrasonic Wave Velocities and the SOECs.

The ultrasonic wave velocities for a series of samarium phosphate glasses have been measured as a function of temperature. The relative change of ultrasonic wave velocity in each glasses with temperature is plotted in figure 6.5. To provide a comparison with these glasses, the temperature dependences of the longitudinal and shear mode velocities have also been measured for the 15 mole% La_2O_3 phosphate glass and the result is plotted in figure 6.6. A slight dip occurs in the longitudinal mode velocity-temperature plot for each samarium phosphate glass (figure 6.5a): this mode has a positive gradient from about 200K upwards. For shear mode velocity (figure 6.5b), this pattern is only observed in the 5 mole% Sm_2O_3 phosphate glass. However both shear and longitudinal wave velocities in these glasses show unusual behaviour with temperature: the ultrasonic wave velocities increase nonlinearly when the temperature is decreased down to 100K. This behaviour is not observed in the structurally similar 15 mole% lanthanum phosphate glass (figure 6.6) in which the ultrasonic wave velocities increase linearly as the temperature is decreased.

The ultrasonic wave velocity dependence upon

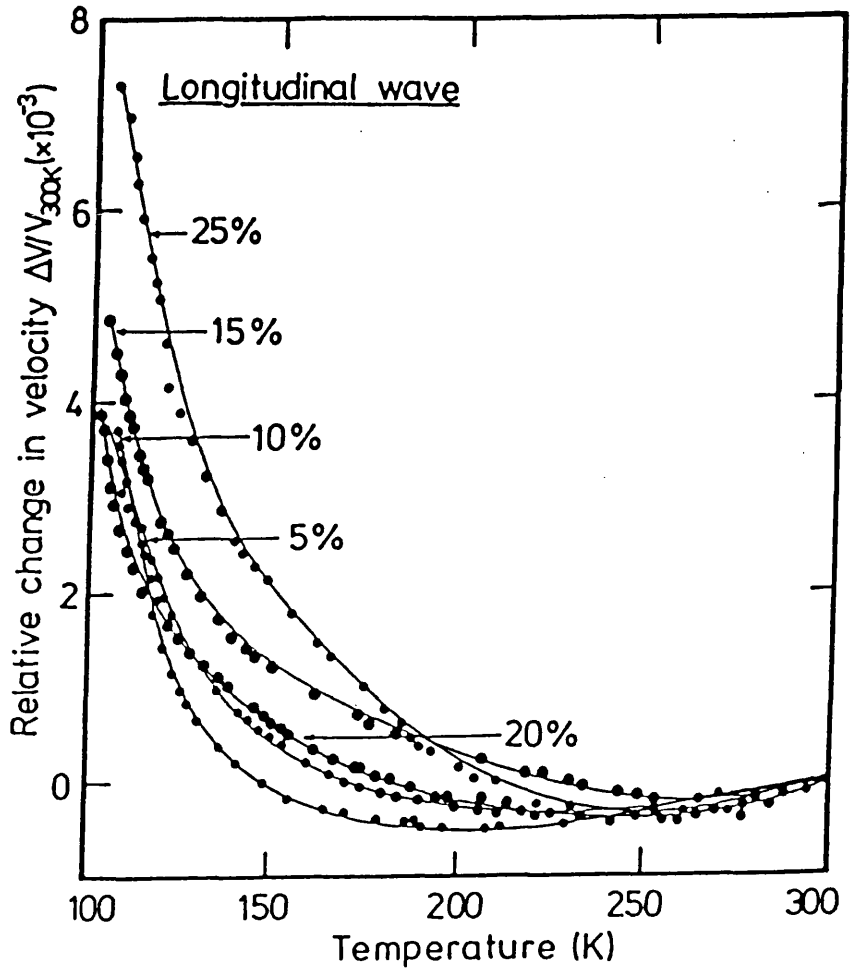

Figure 6.5a : Relative variation of longitudinal mode velocities of samarium phosphate glasses. The numbers on each curves correspond the percentage of Sm_2O_3 in phosphate glasses. The curves are solely drawn as a visual guide.

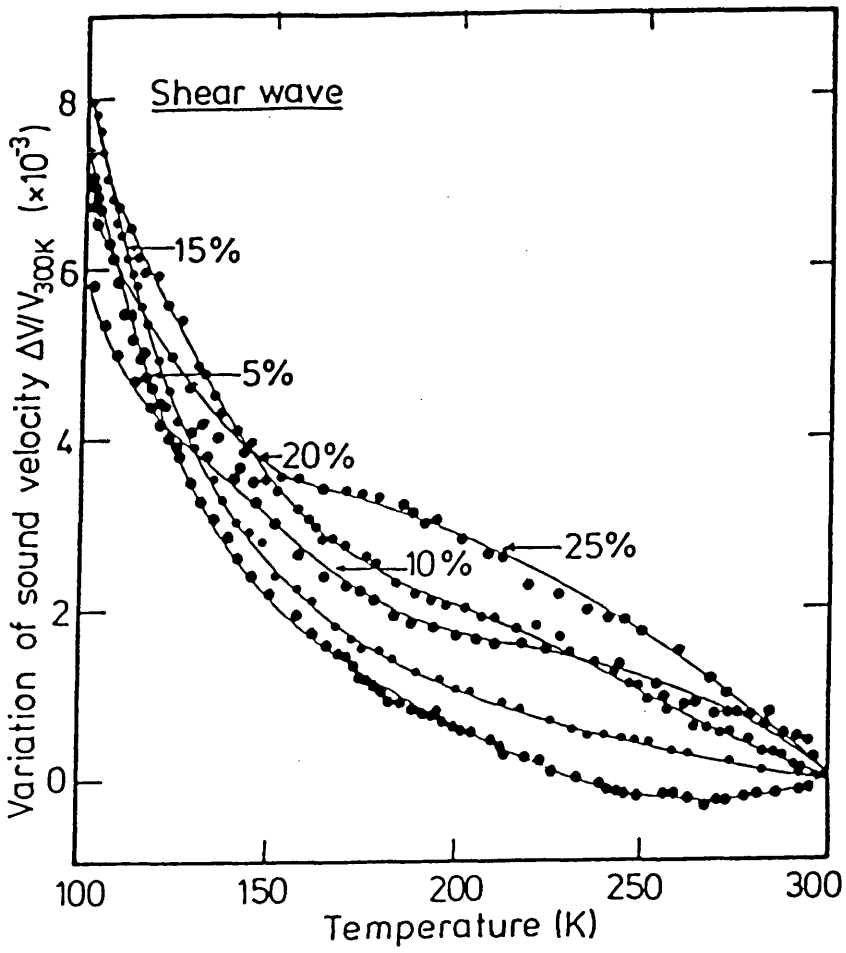

Figure 6.5b : Relative variation of shear mode velocities of samarium phosphate glasses. The numbers on each curves correspond the percentage of Sm_2O_3 in phosphate glasses. The curves are solely drawn as a visual guide.

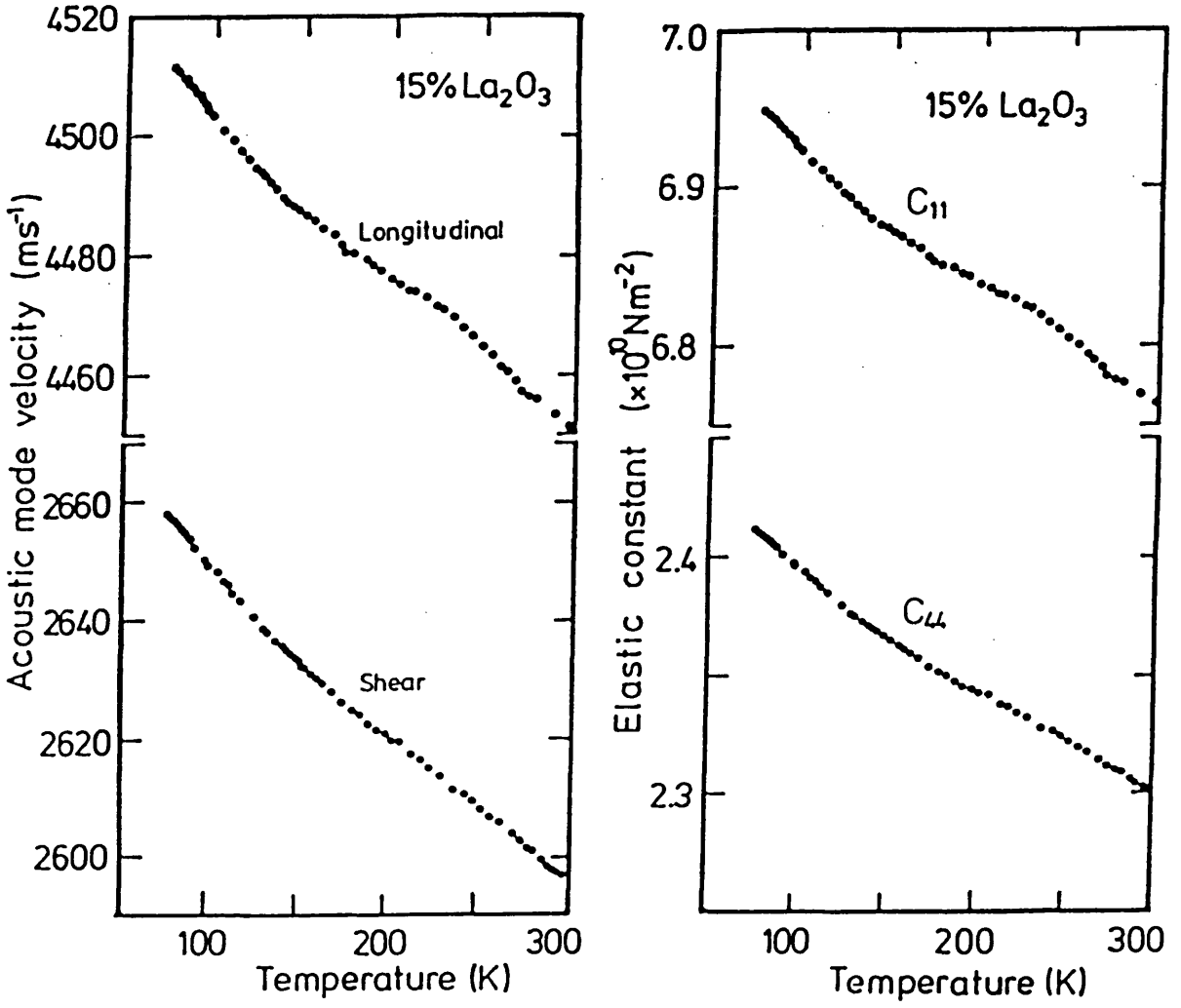

Figure 6.6 : The temperature dependence of the sound velocities and elastic stiffnesses C_{11} and C_{44} of 15 mole% La_2O_3 phosphate glass.

temperature in samarium glasses resembles that of the sound velocities of cubic $Sm_{0.58}Y_{0.42}S$ single crystals (Yogurtcu et al. 1985). In that crystalline material, the temperature induced softening is most pronounced for the longitudinal mode propagated in the [001] direction with the transverse [001] acoustic phonon showing a much smaller effect. This is consistent with a change in valence altering the samarium ion radius, which is a volume rather than a shear effect and so influences longitudinal rather than transverse modes. In the samarium phosphate glasses the effect of temperature on the longitudinal wave velocity is noticeably larger than that on the shear wave velocity.

The temperature variations of the elastic constants for all samples are shown in figure 6.7. A computer program was used to fit polynomials to these data. The coefficients of these polynomials were then used to calculate the values of C_{11} and C_{44} at selected temperature of 300K, 200K and 100K as given in table 6.4. In this table values of C_{12}, bulk modulus B^S, Young's modulus and Poisson ratio have also been included. In general within the temperature range of 100K to 300K, the elastic constants C_{11} and C_{44} decrease by less than 2%. This quite a small change and can be considered to be typical of this type of glass. It is important to mention that, in the calculation of the temperature variations of the elastic constants of these glasses, the thermal expansion corrections to the lengths and densities have

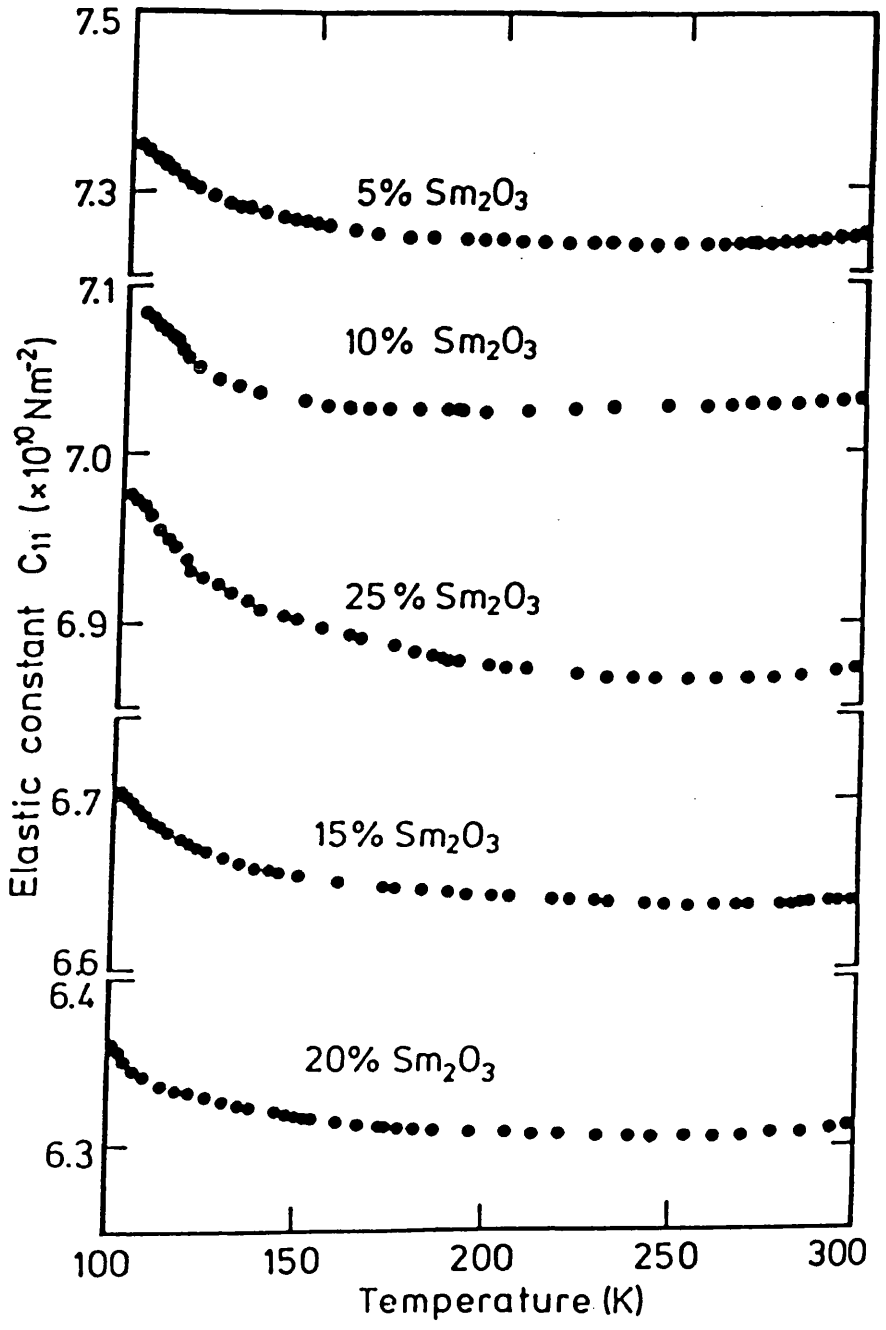

Figure 6.7a : The temperature dependence of elastic stiffness C_{11} of samarium phosphate glasses.

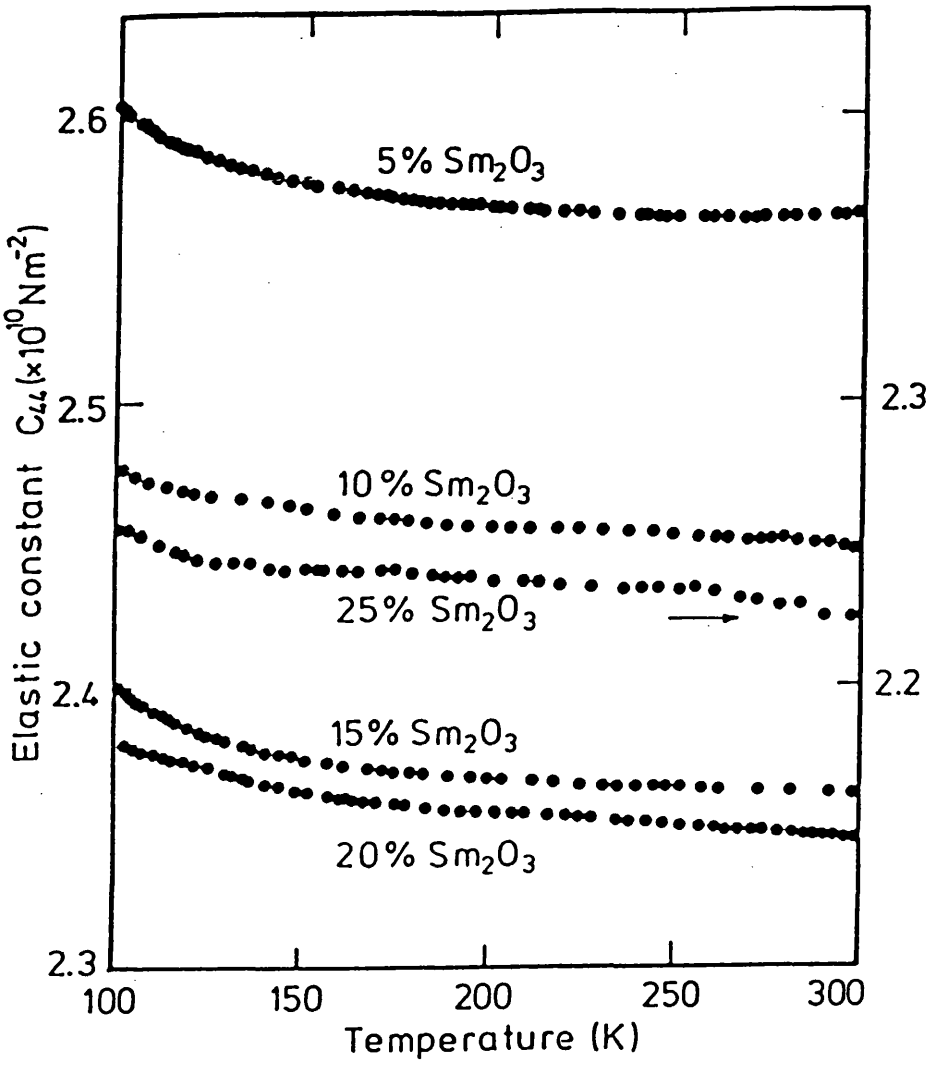

Figure 6.7b : The temperature dependence of elastic stiffness C_{44} of samarium phosphate glasses.

Table 6.4 : Elastic properties of samarium phosphate glasses at three different temperatures; in each case 300K (top), 200K (middle) and 100K (bottom). Elastic constants, bulk modulus and Young's modulus have units of 10^{10} Nm^{-2}.

Sample	A1	A2	A3	A4	A5
Long. vel (m/s)					
	4755	4642	4500	4356	4421
	4754	4640	4501	4355	4422
	4772	4659	4521	4373	4454
Shear vel (m/s)					
	2824	2739	2684	2656	2516
	2825	2744	2686	2661	2522
	2846	2755	2706	2675	2590
Elastic stiffness					
C_{11}	7.273	7.031	6.641	6.311	6.873
	7.270	7.024	6.645	6.309	6.875
	7.327	7.083	6.705	6.360	6.975
C_{44}	2.565	2.448	2.362	2.346	2.225
	2.568	2.456	2.367	2.355	2.237
	2.605	2.477	2.401	2.380	2.258
C_{12}	2.143	2.135	1.917	1.619	2.423
	2.134	2.112	1.911	1.599	2.401
	2.117	2.129	1.903	1.600	2.459
Bulk modulus B^S					
	3.853	3.767	3.492	3.183	3.906
	3.846	3.749	3.489	3.169	3.892
	3.854	3.780	3.504	3.187	3.964
Young's modulus					
	6.298	6.036	5.782	5.650	5.610
	6.301	6.048	5.791	5.662	5.632
	6.378	6.099	5.864	5.717	5.693
Poisson's ratio σ					
	0.228	0.233	0.224	0.204	0.261
	0.227	0.231	0.223	0.202	0.259
	0.224	0.231	0.221	0.201	0.260

not been applied. This is because of the lack of thermal expansion data for these glasses in the temperature range 4.2K to 300K. However it is possible to estimate the magnitude of the expected corrections by employing the thermal expansion data of other phosphate glasses arguing that the microscopic structure of phosphate glasses is similar (Mierzejewski et al. 1988). Comins et al. (1987) have reported the coefficient of thermal expansion for a number of MoO_3 phosphate glasses. For 26 mole% MoO_3 phosphate glass, the room temperature of these coefficient is 7.5×10^{-6} K^{-1}. From this data it has been estimated that the elastic constants data of the 25 mole% Sm_2O_3 phosphate glass in the present study will be too large by 0.15% at 100K and by slightly more at 4.2K.

Table 6.5 shows that the temperature derivatives of C_{11} and of the bulk modulus of samarium phosphate glasses have anomalously positive values at 300K. To date, such positive values of temperature dependences of the SOEC have only been found in vitreous silica and some other tetrahedral glasses and have been attributed to their low coordination number and ease of bond bending vibrations (Sato and Anderson 1980). However it should be noted that dC_{44}/dT remains negative for samarium phosphate glasses in the whole temperature range (table 6.5).

Table 6.5 : Temperature derivatives of the second order elastic stiffness constants and the bulk modulus of samarium and lanthanum phosphate glasses. B3 is the 15 mole% La_2O_3 phosphate glass sample.

Sample	T(K)	dC_{11}/dT	dC_{12}/dT	dC_{44}/dT	dB^s/dT
		(10^6 $Nm^{-2}K^{-1}$)			
A1	300	2.10	1.09	0.51	1.43
	100	-17.30	3.05	-10.20	-3.72
A2	300	1.50	5.02	-1.76	3.84
	100	-19.7	-7.32	-6.2	-11.5
A3	300	0.92	1.34	-0.21	1.20
	100	-22.1	-4.75	-8.6	-10.5
A4	300	1.32	1.85	-1.01	1.67
	100	-22.5	-1.11	-5.5	-14.9
A5	300	2.27	5.35	-1.54	4.32
	100	-26.8	-12.4	-7.2	-17.2
B3	300	-6.15	2.69	-4.42	-12.04
	100	-10.0	3.72	-6.86	-19.15

6.4.3 The Relaxation Effect in the 20 mole% Sm_2O_3 Phosphate Glass.

To establish the elastic behaviour of a samarium phosphate glass below 100K, ultrasonic wave velocity measurements of both longitudinal and shear modes of the 20 mole% Sm_2O_3 have been carried out down to 4.2K. The experimental results are plotted in figure 6.8. The variations of the elastic constants of C_{11} and C_{44} with temperature of this glass are shown in figure 6.9. Usually, as stressed in section 2.8, the variation of ultrasonic wave velocity and hence elastic constant with temperature is due to the anharmonicity of the vibrational modes. In this connection, the observed linear temperature dependence of the ultrasonic wave velocities over a wide range of temperature beyond 150K can be understood in terms of the quasiharmonic atomic oscillator model (Liebfried and Ludwig 1956). This model predicts that an elastic modulus of a material should approach 0K with a zero slope and should be almost linear with temperature at high temperatures. At low temperatures the elastic constants of 20 mole% Sm_2O_3 phosphate glass do not conform with this predicted behaviour but rise steeply as the temperature is decreased. There is a marked resemblance here to the temperature dependence of the velocity of longitudinal

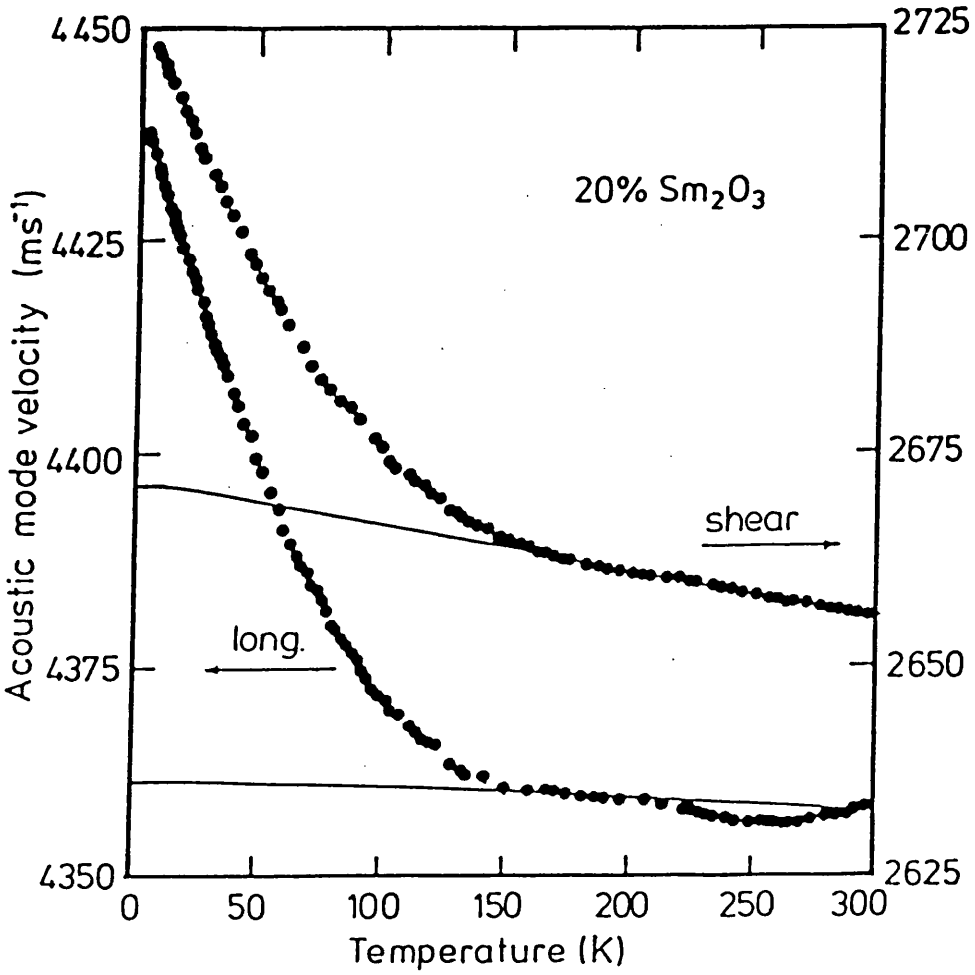

Figure 6.8 : The temperature dependences of longitudinal and transverse mode velocities of 20 mole% Sm_2O_3 phosphate glass. The solid lines represent the predicted temperature dependences of these velocities of the anharmonic oscillator model. The departure of the measured velocities at low temperatures from the predictions of this model point to a contribution from two-level systems to the elastic properties of this glass.

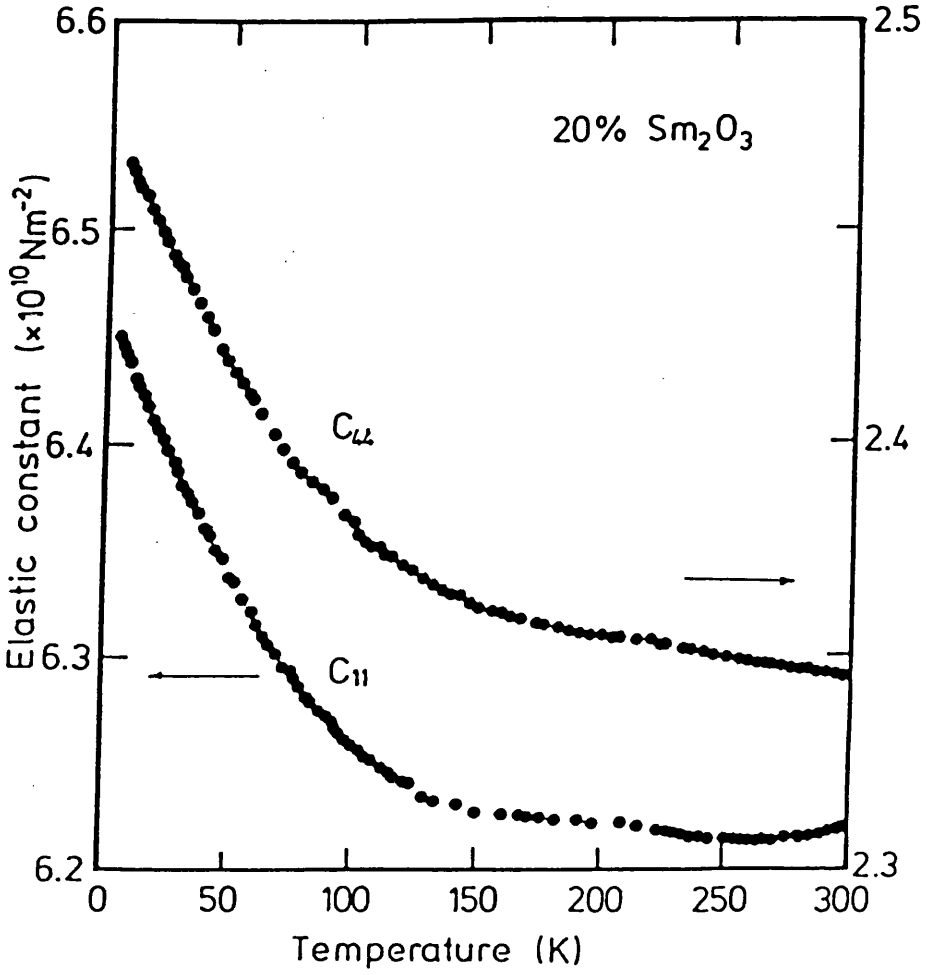

Figure 6.9 : The temperature dependences of elastic stiffness constants C_{11} and C_{44} of 20 mole% Sm_2O_3 phosphate glass.

ultrasonic waves propagated in vitreous silica (Piché et al. 1974, Hunklinger 1982, Raychaudhuri and Hunklinger 1984), vitreous TeO_2 (Benbattouche, Saunders and Sidek 1989) and $(AgI)_{0.2}[(Ag_2O)_{0.2}(B_2O_3)_{0.8}]_{0.8}$ glass (see previous chapter) at low temperatures in which the velocity increases as the temperature is lowered due to a relaxation process with two-level systems (TLS). In vitreous silica the velocity reaches a maximum at temperature T_{max} and then decreases. This decrease in the ultrasonic velocity at very low temperatures (below T_{max}) is due to a resonant interaction. This means phonons are resonantly absorbed if their energy $\hbar\omega$ coincides with the energy splitting of the resonators (chapter 4). The relaxation effect arises because the strain field associated with the ultrasonic wave influences the energy splitting of the two-level systems. Since the measurements of ultrasonic wave velocity have been made in 20 mole% Sm_2O_3 phosphate glass only down to 4.2K, the results obtained should correspond to the relaxation interaction regime above T_{max}.

The next step is to assess the magnitude of the extra contribution to the ultrasonic wave velocities and to find out if its order of magnitude is consistent with it being due to the relaxation effect. To do this, the elastic constants and their temperature dependences which might be expected from the more usual anharmonic effects must first be found. This has been estimated on the basis of a model of an anharmonic oscillator coupled with the

Debye vibrational spectrum; in this case the temperature dependence of an elastic constant can be calculated through equation (2.30). The elastic Debye temperature θ_D for this glass has been obtained from low temperature ultrasonic velocity data and is 251K. Expressions (2.30) have been fitted to the higher temperature data for ultrasonic wave velocities in order to obtain the solid lines shown in figure 6.8 which correspond to the background velocities in the absence of any contributions from relaxation effects. The relaxation interaction produces an increase in the ultrasonic wave velocity as the temperature is reduced. Raychaudhuri and Hunklinger (1984) have suggested that the relaxation contribution should take a logarithmic, frequency independent form. This can be written

$$\Delta V/V = -A_{rel} \ln [T/T_o] \qquad (6.1)$$

where T_o is an arbitrary and A_{rel} is a constant. In their work Raychaudhuri and Hunklinger (1984) use a constant C whose value is deduced from the resonant interaction. However in our experiment we cannot reach the low temperatures required to go below T_{max} into the region where the resonant contribution becomes important. Nevertheless it is useful to compare the magnitudes of the relaxation contributions to the ultrasonic wave velocities in 20 mole% Sm_2O_3 phosphate glass, vitreous silica, TeO_2 glass and $(AgI)_{0.2}[(Ag_2O)_{0.2}(B_2O_3)_{0.8}]_{0.8}$.

For 20 mole% Sm_2O_3 phosphate glass T_o (198K for longitudinal and 187K for shear waves) has been taken as the temperature at which the measured velocity departs from that calculated from the anharmonic model (i.e. the solid lines in figure 6.8). The contribution $\Delta V/V$ to the ultrasonic velocity due to the relaxation interaction has then been obtained from the difference ΔV between the measured velocity and that computed (V) on the basis of the anharmonic model; results for $\Delta V/V$ for the longitudinal and shear waves as a function of $\ln(T/T_o)$ are plotted in figure 6.10a. A similar treatment has also been carried out on the ultrasonic wave velocities measured in $(AgI)_{0.2}[(Ag_2O)_{0.2}(B_2O_3)_{0.8}]_{0.8}$ glass and the result is given in figure 6.10b. These plots are used to find out how well a logarithmic dependence of velocity upon temperature expressed in equation (6.1) fits the data. For both longitudinal and shear waves $\Delta V/V$ is approximately linearly dependent upon $\ln(T/T_o)$ at temperatures above about 10K. The calculated values of A_{rel} are compared with those for other glasses in table 6.6. For Suprasil W, A_{rel} is estimated from the experimental results obtained by Raychaudhuri and Hunklinger (1984) in the temperature range above T_{max} where the relaxation interaction is operative at low frequency (3170 Hz).

The general behaviour of the ultrasonic wave velocities in 20 mole% Sm_2O_3 phosphate glass as well as in the superionic glass is consistent with the anomalous

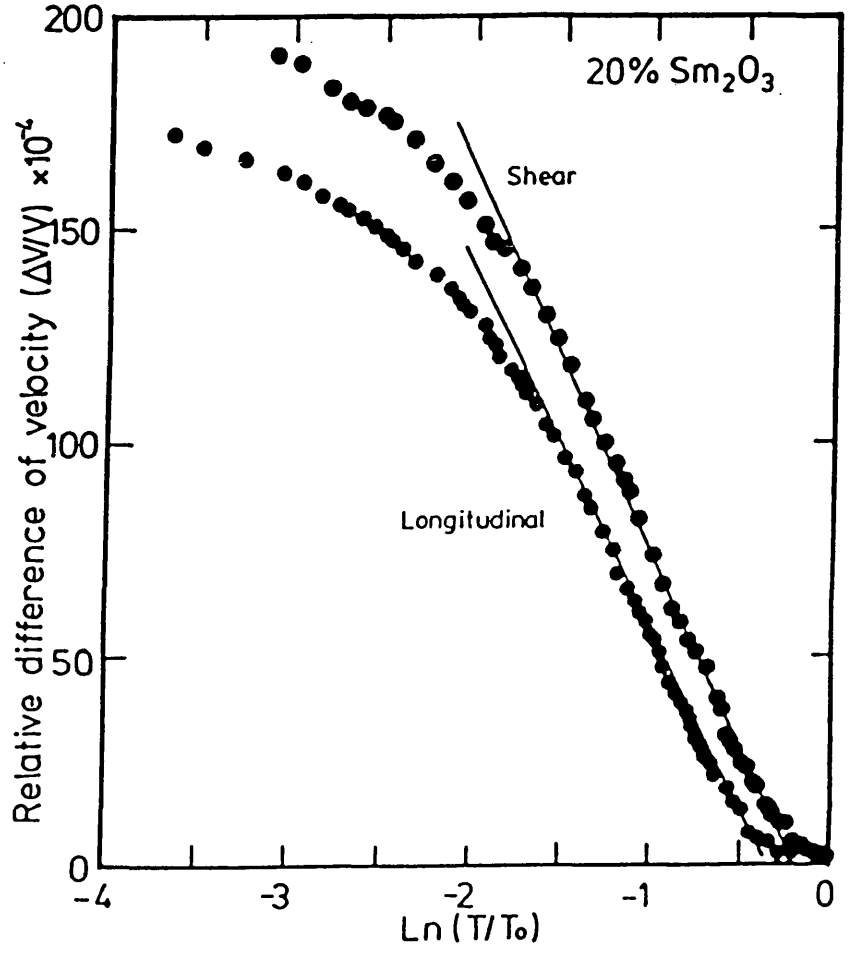

Figure 6.10a : The relative difference $\Delta V/V$ between the measured velocities and the background velocities estimated from the anharmonic model plotted against $\ln(T/T_o)$, (a) for longitudinal waves T_o is 198K and (b) for shear ultrasonic waves T_o is 187K.

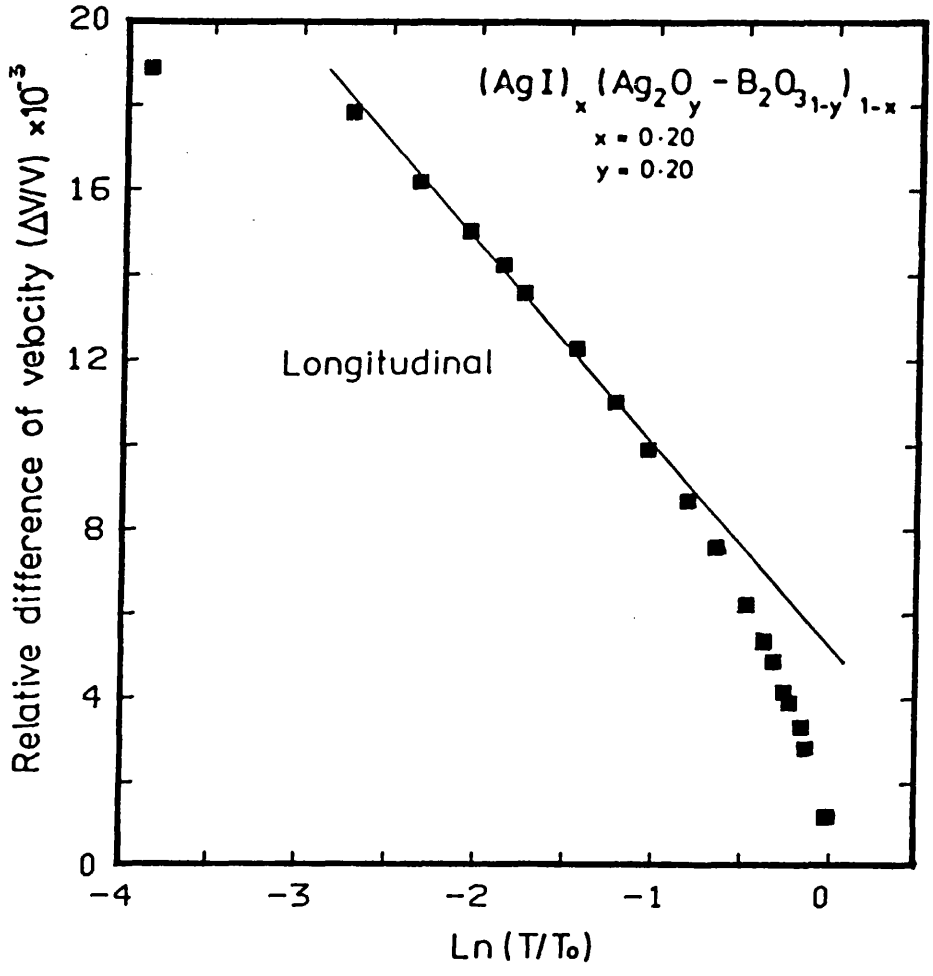

Figure 6.10b : The relative difference $\Delta V/V$ versus $\ln(T/T_o)$ of a superionic glass for longitudinal ultrasonic waves. T_o is taken as 124K.

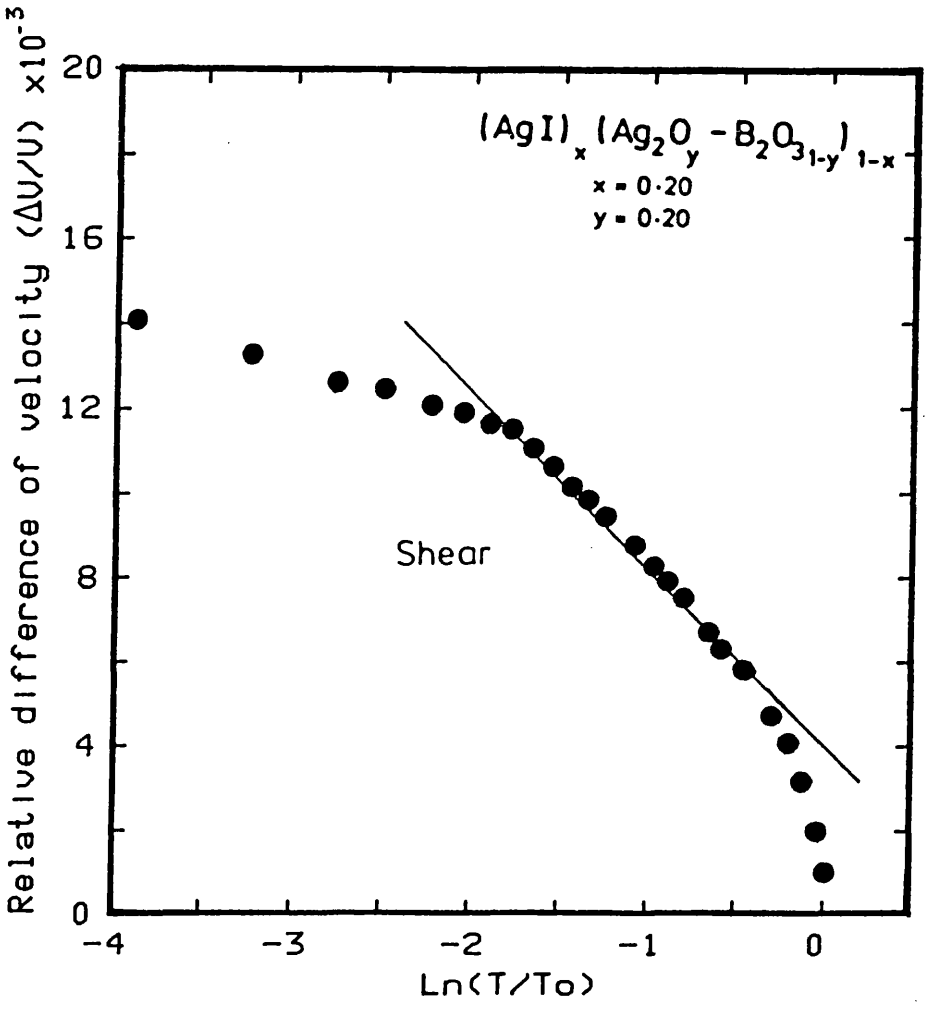

Figure 6.10b : The relative difference $\Delta V/V$ versus $\ln(T/T_o)$ of a superionic glass for shear ultrasonic waves. T_o is taken as 123K.

Table 6.6: Collection of values of A_{rel} for longitudinal and shear mode ultrasonic waves velocities and the second order elastic constants of Suprasil W (Raychaudhuri and Hunklinger 1984), pure TeO_2 glass (Benbattouche, Saunders and Sidek 1989), $(AgI)_{0.2}[(Ag_2O)_{0.2}(B_2O_3)_{0.8}]_{0.8}$ glass and 20 mole% Sm_2O_3 phosphate glass.

Glass	A_{rel} (10^{-4})		C_{IJ} (10^{10} Nm^{-2})	
	long.	shear	C_{11}	C_{44}
Suprasil W	10	-	8.5	-
TeO_2	30	28	5.6	2.0
20 mole% Sm_2O_3	84	92	6.3	2.4
$(AgI)_{0.2}[(Ag_2O)_{0.2}(B_2O_3)_{0.8}]_{0.8}$	39	21	5.1	1.5

increase at low temperatures being due to a contribution to elastic stiffening by a relaxation process with two level systems. Plausibly the turnover below about 10K observed for the 20 mole% Sm_2O_3 glass corresponds to the onset of the resonant interaction contribution to velocity expected at very low temperatures and which in the case of vitreous SiO_2 together with the relaxation effect and anharmonicity is responsible for the the occurrence of a maximum in the ultrasonic wave velocity at T_{max}.

6.5 The Effect of Hydrostatic Pressure upon the SOEC

The relative changes induced by application of hydrostatic pressure on the natural wave velocity in samarium phosphate glasses have been found to be linearly dependent upon pressure. The effects of pressure were completely reversible, the velocity following the same pressure dependence when the pressure was decreased as it had when increasing pressure was applied. After each pressure cycle the elastic moduli reverted to their original values. X-ray studies show that the samples remain amorphous after being subjected to pressures up to 10^9 Pascal (Saunders, private communication). Figure 6.11 shows the unusual feature that the ultrasonic wave velocity decreases with pressure. The usual behaviour of solids is for the velocity to increase with pressure.

Amorphous materials can be divided into two groups according to their elastic behaviour under pressure. Many glasses, including amorphous arsenic (Brassington et al. 1980), As_2S_3 (Brassington et al. 1981a), chalcogenide (Thompson and Bailey 1978) and fluorozirconate glass (Brassington et al. 1981b) behave normally in that their bulk and shear moduli increase under hydrostatic pressure. A complete set of dC_{IJ}/dP and B_{IJ} data for samarium phosphate glasses is given in table 6.7. The

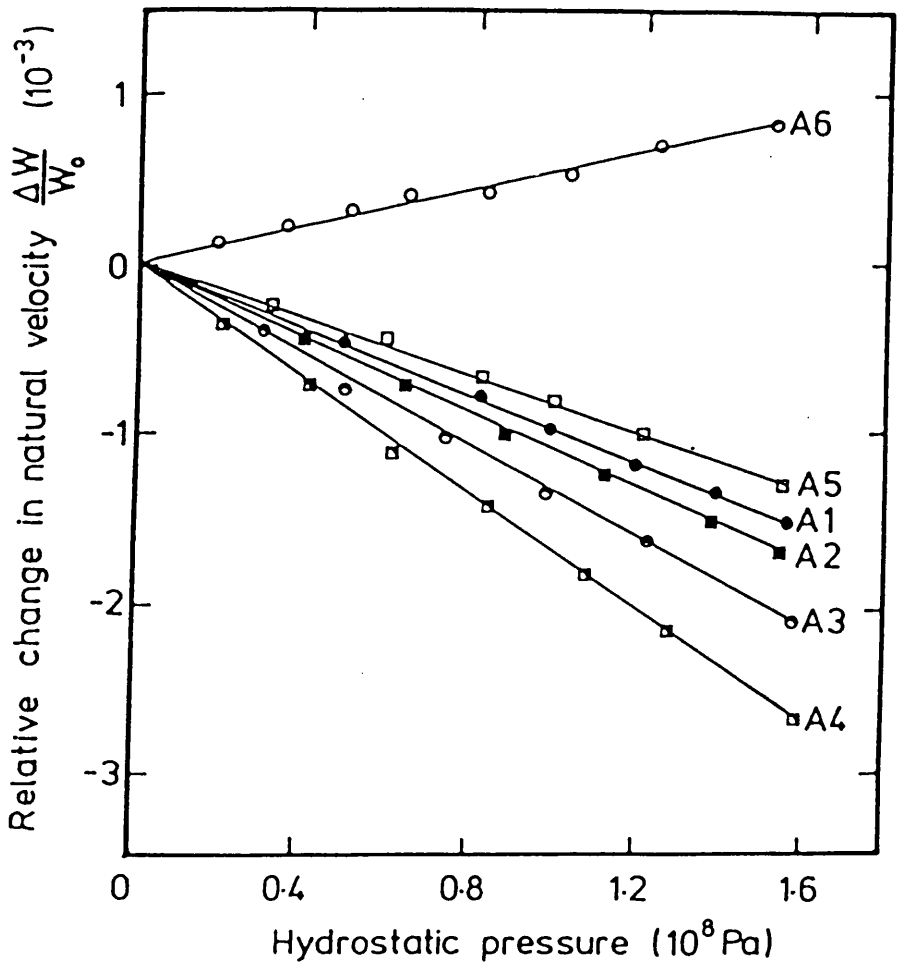

Figure 6.11a : The hydrostatic pressure dependences of the "natural" wave velocities of the longitudinal mode propagated in samarium phosphate glasses. The compositions of the glasses are those corresponding to the nomenclature given in table 6.1.

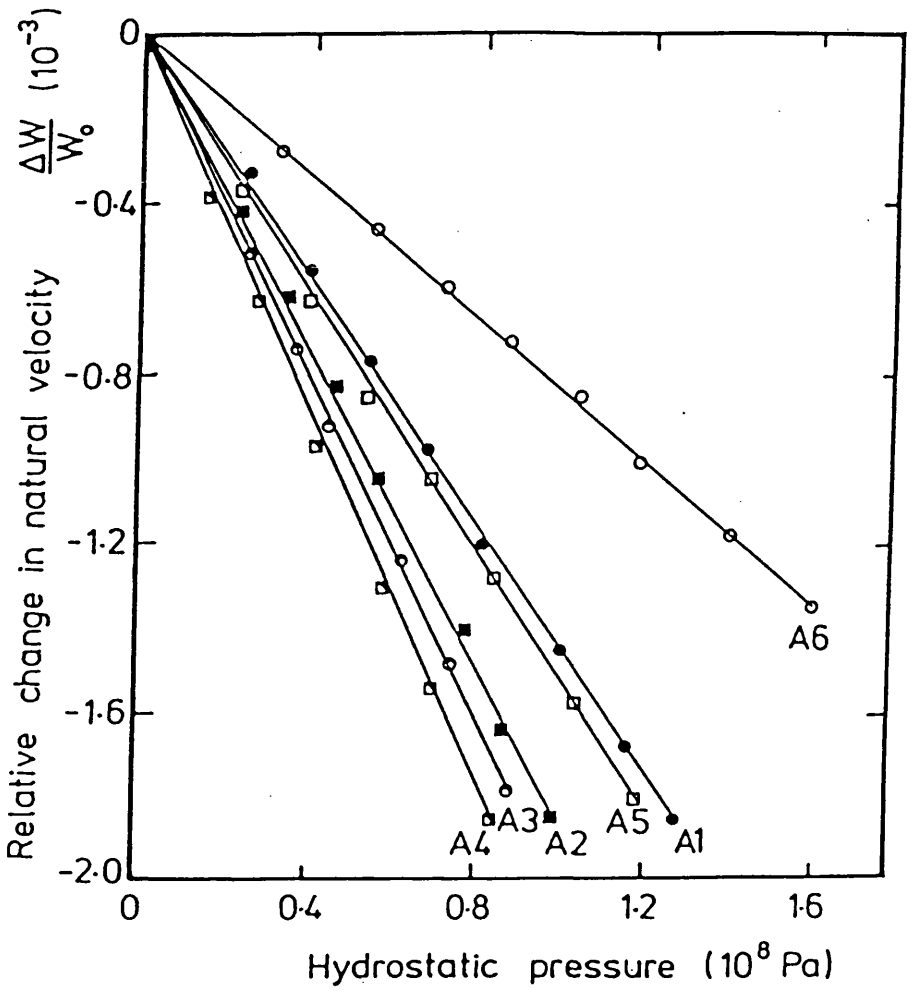

Figure 6.11b : The hydrostatic pressure dependences of the "natural" wave velocities of the shear mode propagated in samarium phosphate glasses. The compositions of the glasses are those corresponding to the nomenclature given in table 6.1.

Table 6.7 : The effective (dC_{IJ}/dP) and thermodynamic (B_{IJ}) pressure derivatives of the SOEC of a series of samarium phosphate glasses.

Sample	A1	A2	A3	A4	A5
dC_{11}/dP	-0.75	-0.88	-1.09	-1.40	-0.55
dC_{12}/dP	0.28	0.51	0.35	0.14	0.40
dC_{44}/dP	-0.52	-0.69	-0.72	-0.77	-0.47
dB^{S}/dP	-0.06	0.05	-0.13	-0.37	0.08
B_{11}	0.88	0.74	0.55	0.26	1.04
B_{12}	-0.53	-0.30	-0.47	-0.69	-0.40
B_{44}	0.71	0.52	0.51	0.48	0.72

nonlinear acoustic properties of the these glasses are anomalous in that the pressure derivatives of the bulk and shear moduli as well as longitudinal moduli are negative. Although uncommon, such behaviour has been recognised in vitreous silica and high silica content glasses (Bogardus 1965, Hughes and Kelly 1953). It is really extraordinary: when subjected to pressure, these materials become easier to compress! In the silica-based glasses such negative pressure dependences have been attributed to the open, four-fold coordinated structure which facilitates bending vibrations of the bridging oxygen ions. If such an explanation based on $P\text{-}O_{bridging}\text{-}P$ bond bending were to be applicable to the anomalous elastic behaviour of samarium phosphate glasses under pressure, then the elastic constants of other phosphate glasses would also be expected to show negative values of dB^S/dP and dC_{44}/dP. But that is not observed. For the molybdenum phosphate glasses (in the composition range 35 mole% MoO_3 to 76 mole% MoO_3, substantially higher concentrations than in these samarium glasses) the pressure derivatives of the elastic constants are positive (Comins et al. 1987). Although dC_{44}/dP (= -0.16) is slightly negative for an iron phosphate glass of composition $(Fe_2O_3)_{0.38}(P_2O_5)_{0.62}$, the pressure derivative dB^S/dP shows a positive value (= +4.73). Thus the negative pressure derivatives dB^S/dP, dC_{11}/dP and dC_{44}/dP with $dC_{11}/dP > dC_{44}/dP$, seem to be characteristic of the samarium ion in the phosphate

network.

A recent experimental study of the elastic properties of samarium tellurite glasses shows that these have the normal positive signs for the hydrostatic pressure derivatives of the elastic stiffness constants (El-Mallawany and Saunders, 1988). Hence the unusual elastic behaviour under pressure is restricted to the samarium phosphate glasses. This first study shows that there is much to learn about the behaviour of samarium ions under pressure in a glassy matrix.

As the similarity of their Raman spectra indicates a close structural affinity between samarium and lanthanum phosphate glasses, a powerful test of this suggestion would be to determine the pressure dependences of the elastic stiffnesses of a lanthanum phosphate glass. This has been done. The elastic stiffnesses at 291K of a 15 mole% La_2O_3 phosphate glass have been measured giving elastic constant and their hydrostatic pressure derivatives as

$$C_{11} = 6.76 \times 10^{10}\ Nm^{-2}$$

$$C_{44} = 2.31 \times 10^{10}\ Nm^{-2}$$

$$dC_{11}/dP = +3.56$$

$$dC_{44}/dP = +0.13.$$

A full set of the elastic data of lanthanum phosphate glasses is given in Appendix C. The relevant point here is that the hydrostatic pressure derivatives of the elastic moduli of this lanthanum phosphate glass are positive. Now in contrast to samarium, lanthanum does not

usually show any other valence state than three. Since the prime difference between lanthanum and samarium phosphate glasses is the ability of samarium to undergo a pressure induced transformation from divalent to an intermediate valence state between two and three, the indications are that such an effect is responsible for the anomalous decrease in elastic stiffnesses under pressure found in the samarium phosphate glasses. In this respect the elastic behaviour of these glasses resembles that found in crystalline SmS (Tu Hailing, Saunders and Bach 1984) and $Sm_{1-x}Y_xS$ (Yogurtcu et al. 1984). At atmospheric pressure SmS is an ionic semiconductor with the rocksalt structure. Samarium has an outer electonic configuration $4f^6 5s^2 5p^6 5d^0 6s^2$. In rare-earth chalcogenides the d levels are broadened into a band, hybridized with the 6s band while the 4f electrons essentially retain their atomic form. When hydrostatic pressure is applied to SmS, the f-level and the d-band lower edge cross. A semiconductor-metal transition takes place at about 6.5 x 10^8 Pa involving delocalisation of a 4f electron from the samarium ion ($4f^6 5d^0$ - $4f^5 5d^1$) and the valence increases from 2+ into an intermediate value between 2 and 3. Now Sm^{2+} ($4f^6$) has an almost 20% larger ionic radius than Sm^{3+} ($4f^5$) so that at the isostructural transition there is a large decrease in volume. The elastic behaviour and interatomic binding forces in SmS are strongly influenced by these valence effects. Both the bulk modulus and C_{11} decrease when a pressure

exceeding 3 x 10^8 Pa is applied while the shear modulus $(C_{11}-C_{12})/2$ increases almost linearly with pressure in the normal way (Tu Hailing, Saunders and Bach 1984). Due to the substantially smaller size of the Sm^{3+} ion than that of the Sm^{2+} ion, longitudinal acoustic modes, which alter the unit cell volume, are strongly affected by the valence instability and so C_{11} and in turn the bulk modulus $(C_{11}+2C_{12})/3$ decrease under pressure. Transverse phonons which involve volume conserving shears are much less influenced by the incipient valence transition at 6.5 x 10^8 Pa. As pressure is increased towards that at which the transition takes place in SmS, dB^S/dP and dC_{11}/dP become large and negative showing that the balance between the attractive and repulsive contributions to the interatomic binding alters completely. These attractive forces dominate the higher order elastic constants, the reverse of the more normal situation of dominance by the repulsive interactions. The transition occurs when the nearest-neighbour repulsive forces become reduced to such an extent that the crystal volume can decrease sharply. The marked softening of the elastic moduli of the samarium phosphate glasses under pressure (figure 6.12) indicates that the samarium ions in the glassy matrix shows the same tendency to a valence transition under pressure as they do in the crystalline state.

The negative value of dB^S/dP indicates instability, and cannot continue indefinitely with increasing

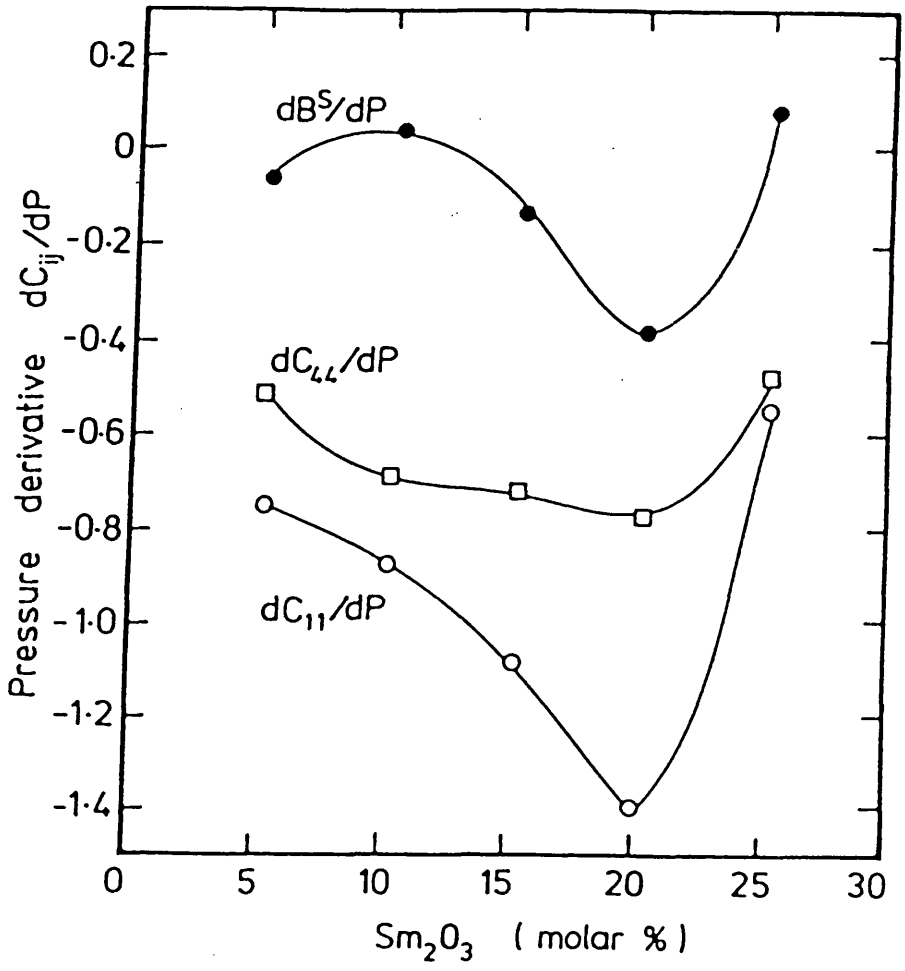

Figure 6.12 : The compositional dependence of the hydrostatic pressure derivatives dC_{11}/dP, dC_{44}/dP and dB^S/dP of the elastic stiffnesses of samarium phosphate glasses.

pressure. To test whether the softening of the long wavelength acoustic modes in these glasses might lead to some form of phase instability, specimens of the 25 mole% Sm_2O_3 glass have been subjected to pressures in a diamond cell and examined visually up to 100 kbar (Saunders, private communication). No marked visual changes which might be indicative of a phase change (such as densification, phase separation or crystallisation) were observed as the pressure was exerted.

6.6 Vibrational Anharmonicity of Samarium Phosphate Glasses.

The elastic mode Grüneisen parameters in the long wavelength limit, which quantify the vibrational anharmonicity of the acoustic modes, have been determined by using equations (2.55-.58). Table 6.8 shows that the longitudinal γ_L and shear γ_S mode Grüneisen parameters of these phosphate glasses are negative (with the exception of γ_L for the ceramic material of composition 30 mole% Sm_2O_3). This most unusual property means that the application of hydrostatic pressure causes the long wavelength acoustic mode frequencies and the energies associated with these modes to decrease. The mean Grüneisen parameter $\bar{\gamma}_{el}$ has been obtained from γ_L and γ_S using equation (2.59). The plot of mode Grüneisen parameter against glass composition (figure 6.13) has a

Table 6.8 : Compositional dependences of the three combinations of the third order elastic constants (unit 10^{11} Nm^{-2}) and acoustic mode Grüneisen parameters of samarium phosphate glasses.

Sample	A1	A2	A3	A4	A5
$C_{111} + 2C_{112}$	-1.02	-0.84	-0.57	-0.25	-1.22
$C_{144} + 2C_{166}$	-0.82	-0.59	-0.53	-0.46	-0.84
$C_{123} + 2C_{112}$	-0.61	0.34	0.49	0.66	0.46
γ_l	-0.36	-0.40	-0.45	-0.52	-0.32
γ_s	-0.55	-0.70	-0.70	-0.69	-0.58
$(\gamma_l+2\gamma_s)$	-0.49	-0.60	-0.62	-0.63	-0.50

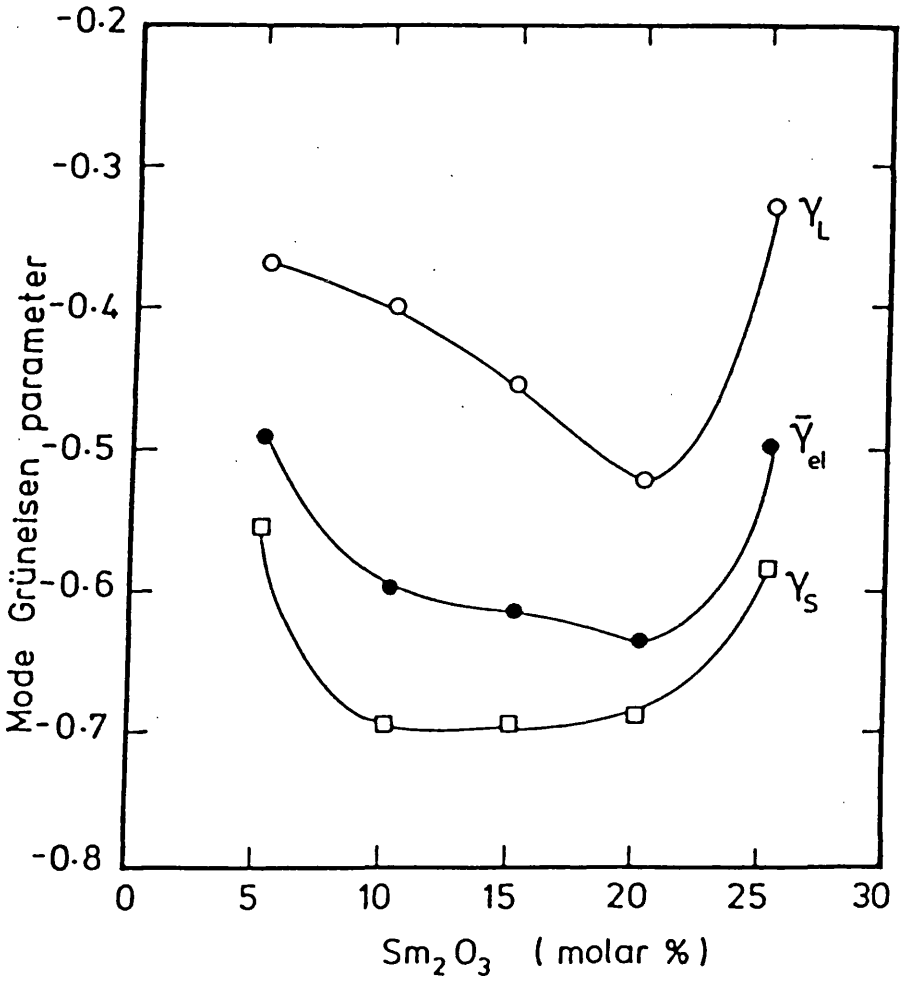

Figure 6.13 : The mean acoustic mode Grüneisen parameters γ_L, γ_S and $\bar{\gamma}_{el}$ in the long wavelength limit for samarium phosphate glasses.

minimum at a composition of 25 mole% Sm_2O_3. In general this extremum at this composition in the elastic properties is a characteristic feature of the samarium phosphate glasses. Acoustic mode softening and anomalous vibrational anharmonicity are greatest in those glasses having the long chain metaphosphate structure.

The ultrasonic behaviour found here as a function of temperature and pressure has established acoustic mode softening in the samarium phosphate glasses. This mode softening is probably related either to valence instability or pressure-variable mixed valence of the samarium ions in these glasses.

7

ELASTIC PROPERTIES OF LANTHANIDE CHALCOGENIDE Ce_3S_4 SINGLE CRYSTAL

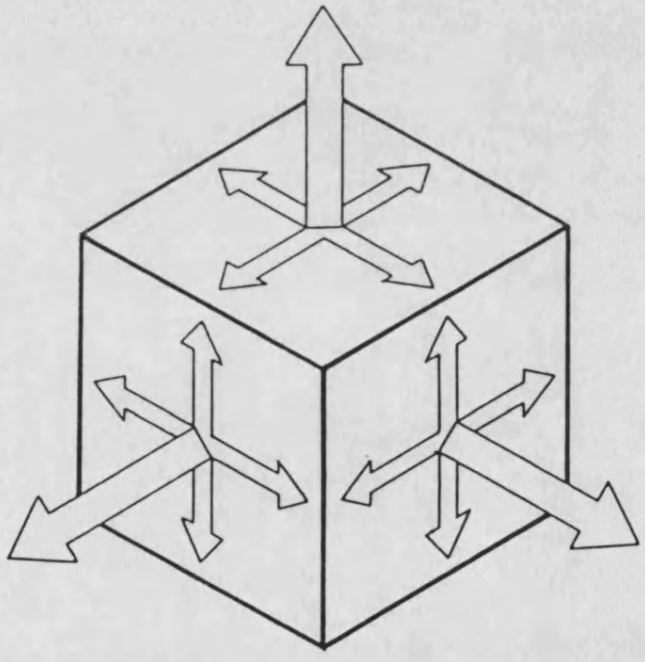

CHAPTER SEVEN

ELASTIC PROPERTIES OF LANTHANIDE CHALCOGENIDE Ce_3S_4 SINGLE CRYSTAL.

7.1 Introduction.

Rare earth chalcogenides are new perspective materials which are attracting much attention from physicists. Compounds of this class are characterized by a wide range of interesting properties; some are metals, some semiconductors and some insulators. Generally they have relatively high melting points, good thermal stability, interesting magnetic, optical, electrical, elastic and thermal properties. It is believed that these materials might be useful in the future as among other things a high-temperature thermoelectric materials, magnetic elements, high-temperature thermistors and laser materials (Methfessel 1965). However, there is not a great deal of knowledge of the physical properties of rare-earth chalcogenides at present.

One of these chalcogenide compounds has been chosen for our ultrasonic studies, namely cerium sulphide (Ce_3S_4). Its elastic properties will be compared with La_3S_4 which has a similar chemical structure. Interestingly La_3S_4 undergoes a structural phase transformation at 103K where a cubic to tetragonal

transformation takes place (Ford et al. 1980, Wruk et al. 1985, Futterer et al. 1986). This transition has been associated with acoustic phonon mode softening because the elastic stiffnesses $(C_{11} - C_{12})/2$ and C_{11} were found to decrease as the temperature was lowered into the transition region. Recently Futterer et al. (1988) have reported that a similar phase transition was not observed in Ce_3S_4 single crystal.

The application of hydrostatic pressure can have pronounced effects on the elastic properties of crystals which undergo phonon-mode softening and hence can provide useful information concerning lattice stability. Therefore as part of the broad study of mode-softening and its relationship to the phase stability of Th_3P_4 structure compounds, the effects of hydrostatic pressure on the velocity of ultrasonic waves propagated in monocrystalline Ce_3S_4 have been measured here. Additionally the temperature dependences of the SOEC of this crystal obtained from Futterer et al. (1988) are now also available for discussion. The central object of this chapter is to compare the dependences of the elastic stiffnesses upon temperature (Futterer et al. 1988) and hydrostatic pressure of this Th_3P_4 structure compound with those in La_3S_4 which is known to undergo a structural phase transition associated with mode-softening.

7.2 The crystal structure of Ce_3S_4.

The phase diagram of cerium sulphide has not yet been completely determined. In brief cerium monosulphide (CeS) crystal has the rock-salt structure like NaCl, whereas Ce_2S_3 and Ce_3S_4 crystals have the thorium phosphide (Th_3P_4) structure with a space group of $I\bar{4}3d$ (T^6_d) (Zachariasen 1949). The thorium phosphide structure itself, illustrated in figure 7.1, is a body centred cubic (bcc) with 28 atoms per unit cell. In such a structure it is possible to allocate cations and anions in a wide range of stoichiometry with the extremal compositions Ce_2S_3 and Ce_3S_4. The first has the defect thorium phosphide structure with 28 atom per unit cell and 10-2/3 cerium atoms distributed at random over 12 equivalent sites. This leaves on average every ninth cerium site vacant or in other words in the Ce_2S_3 compound the metal sublattice only contains vacancies. As cerium is added to Ce_2S_3 these sites are gradually filled until the composition Ce_3S_4 is achieved, corresponding to complete occupation of all sites. In this compound both sublattices of cerium and sulphur are filled and each cerium atom is surrounded by eight sulphur atoms and eight next-nearest neighbour cerium atoms. Based on wet chemical analysis by Morke et al. (1985), the lattice spacing of each composition is given as follows

Ce_4S_4 ; (CeS) : 5.772 Å

$Ce_{2.996}S_4$; (Ce_3S_4) : 8.622 Å

$Ce_{2.717}S_4$; (Ce_2S_3) : 8.625 Å

Optical and transport measurements of Ce_3S_4 and Ce_2S_3 crystals (Kurnick et al. 1964) indicate that the former is a metal whereas the latter is a semiconductor. A large fraction of ionic bond is observed in Ce_2S_3 whilst Ce_3S_4 is predominantly metallic (Zachariasen 1949). Ryan et al. (1962) have reported that no phase transformation was indicated by the thermoelastic properties of Ce_3S_4 and Ce_2S_3 crystals between 4K to 1300K.

7.3 Crystal Growth of Ce_3S_4 Monocrystal.

The Ce_3S_4 samples studied here have been prepared by Dr. Futterer and his co-workers at Institut für Experimentalphysik VI, Ruhr-Universitat Bochum, Federation Republic of German. A brief description of the crystal growth is presented here for reference purposes.

Crystalline sulphur and cerium sponge with purity of 5N and 4N respectively, were mixed in stoichiometric quantities in a quartz ampoule. This was slowly raised in temperature over a period of three days up to 400°C to complete the reaction. Then the temperature was again slowly increased from 400°C to 700°C over a further three day period to homogenise the compound. The resulting large grained powder was compressed into tablets. These were then placed inside a degassed molybdenum crucible and sealed under a pressure of about 250mbar of argon. To

homogenise the charge further, the crucible was heated for one hour at 1900°C using a radio-frequency generator. Then to grow crystals by the Bridgman-Stockbarger method the crucible was lowered out through the temperature gradient at a speed of 1.5 mmh^{-1}. The colour of Ce_3S_4 is similar to that of the lanthanum sulphide La_3S_4 i.e. black-gray.

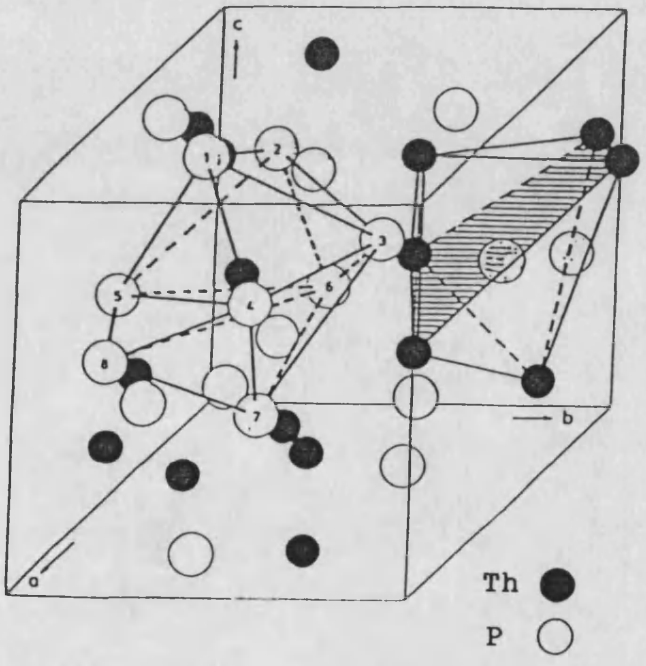

Figure 7.1 : Crystal structure of Th_3P_4 (after Zachariasen 1949).

7.4 Experimental Result and Discussion.

The single crystal of Ce_3S_4 was oriented along the required crystallographic axes to within $\pm$ 0.5° by the X-ray Laue back reflection technique. The [100] and [110] faces were then polished flat and parallel to within about 10^{-4} radian; these samples were sufficient for evaluation of a full set of elastic constants in this cubic crystal. The ultrasonic velocities in the [100] and [110] directions (see table 2.1) together with hydrostatic pressure derivatives were measured as described in chapter 3.

7.4.1 The Ultrasonic Waves Velocities and the SOEC.

The elastic properties of Ce_3S_4 obtained from our experiment at room temperature are compared with those of La_3S_4 in table 7.1. The elastic stiffness of Ce_3S_4 crystal is somewhat larger compared with La_3S_4 crystal. This is consistent with the finding that the latter crystal undergoes the soft mode transition to the tetragonal form at 103K while the first one did not change structure in the temperature region above 80K (Futterer et al. 1988). Hence at room temperature stoichiometric La_3S_4 is closer to transition and, as acoustic mode softening is associated with the structural

Table 7.1 : The elastic properties of Ce_3S_4 and La_3S_4 at room temperature (291K). La_3S_4 data are taken from Ford et al. (1980).

	Ce_3S_4	La_3S_4
Density (kgm^{-3})	5671	5450
Elastic stiffnesses (x 10^{10} Nm^{-2})		
C_{11}	17.74	10.7
C_{12}	5.27	5.7
C_{44}	3.14	3.1
$C'=(C_{11}-C_{12})/2$	3.24	2.5
Bulk modulus B^S	7.43	7.37
Anisotropy ratio C_{44}/C'	0.972	1.24
C'/B	0.44	0.34
C_{44}/B	0.42	0.42
Elastic compliances (x 10^{-10} m^2N^{-1})		
S_{11}	0.118	0.148
S_{12}	-0.037	-0.052
S_{44}	0.318	0.322
Volume compressibility	0.135	0.136
Debye temperature θ_D^{el} (K)	275	-

change, is less stiff elastically. The larger anisotropy ratio C_{44}/C' (=1.24) of the stoichiometric La_3S_4 crystal is also in accord with this viewpoint; C' (= C_{11} - $C_{12})/2$) softens dramatically (so that C_{44}/C' enlarges) in La_3S_4 as the transition is approached.

An interesting feature of Ce_3S_4 is an almost isotropic elastic behaviour at room temperature. This is usefully visualised by the dependence of acoustic mode velocity upon propagation direction obtained as the eigenvalues of the Christoffel equations and plotted in figure 7.2 and compared with figure 7.3 of La_3S_4 (Ford et al. 1980). However, this elastic isotropic behaviour is not retained at low temperatures. The measurements of the elastic stiffness constants of Ce_3S_4 made down to low temperatures by Futterer et al. (1988) are shown in figures 7.4 to 7.6 and table 7.2. The temperature dependences of the elastic constants of La_3S_4 have also been reported (Ford et al. 1980, Wruk et al 1985) and are reproduced here in figure 7.7 as a comparison with the data for Ce_3S_4.

In general the elastic behaviours of both crystals show certain similarities as the temperature is reduced in that the shear stiffness (C_{11} - $C_{12})/2$ decreases dramatically, C_{11} shows an anomalous decrease but not so substantial as that of (C_{11} -$C_{12})/2$, and C_{44} increases in the normal way. However, La_3S_4 undergoes the cubic to tetragonal transformation (Wruk et al. 1985) at 103K where abrupt changes occur in the ultrasonic wave

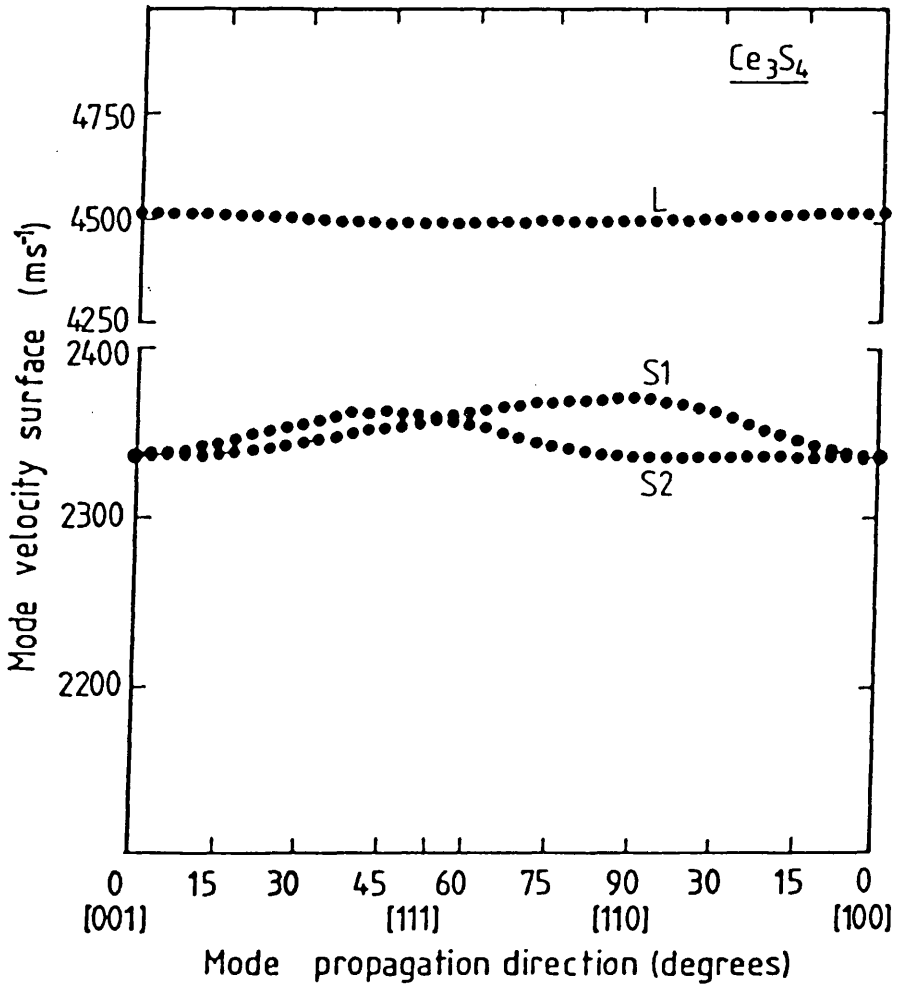

Figure 7.2 : Dependence of the velocity of ultrasonic waves upon propagation direction in Ce_3S_4 single crystal.

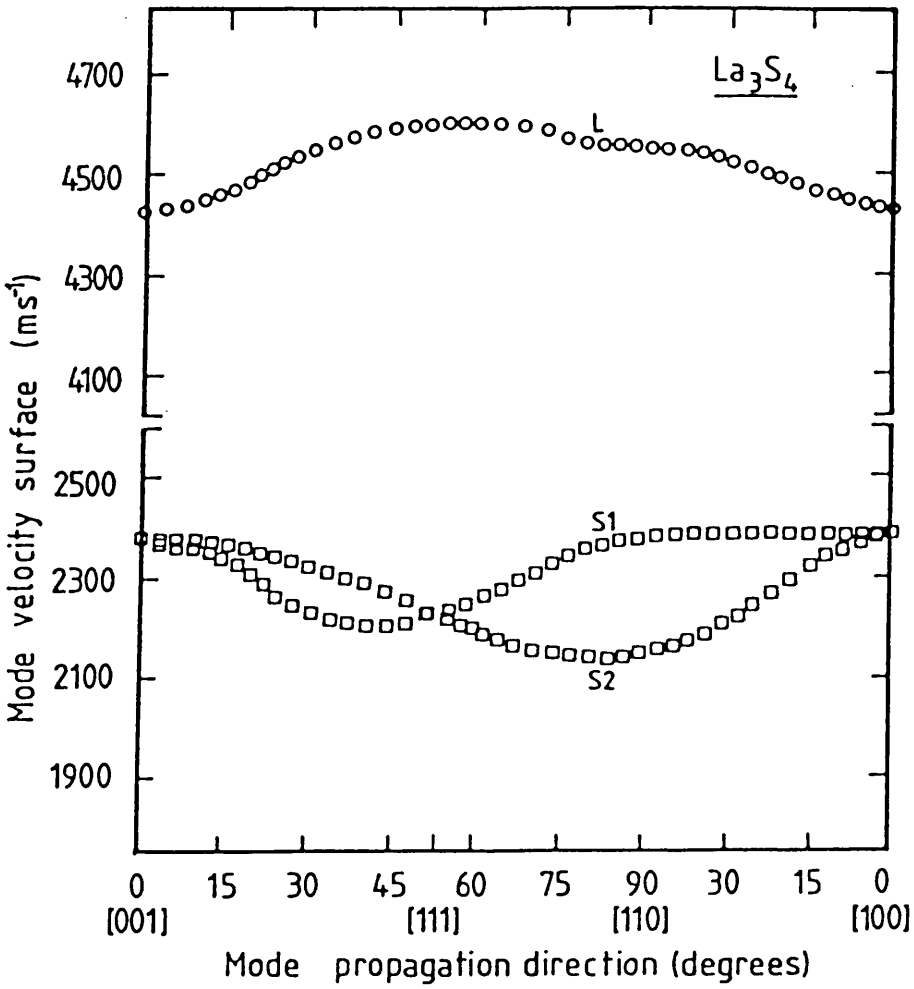

Figure 7.3 : Dependence of the velocity of ultrasonic waves upon propagation direction in La_3S_4 single crystal. Basic data used in the computation are taken from Ford et al. (1980).

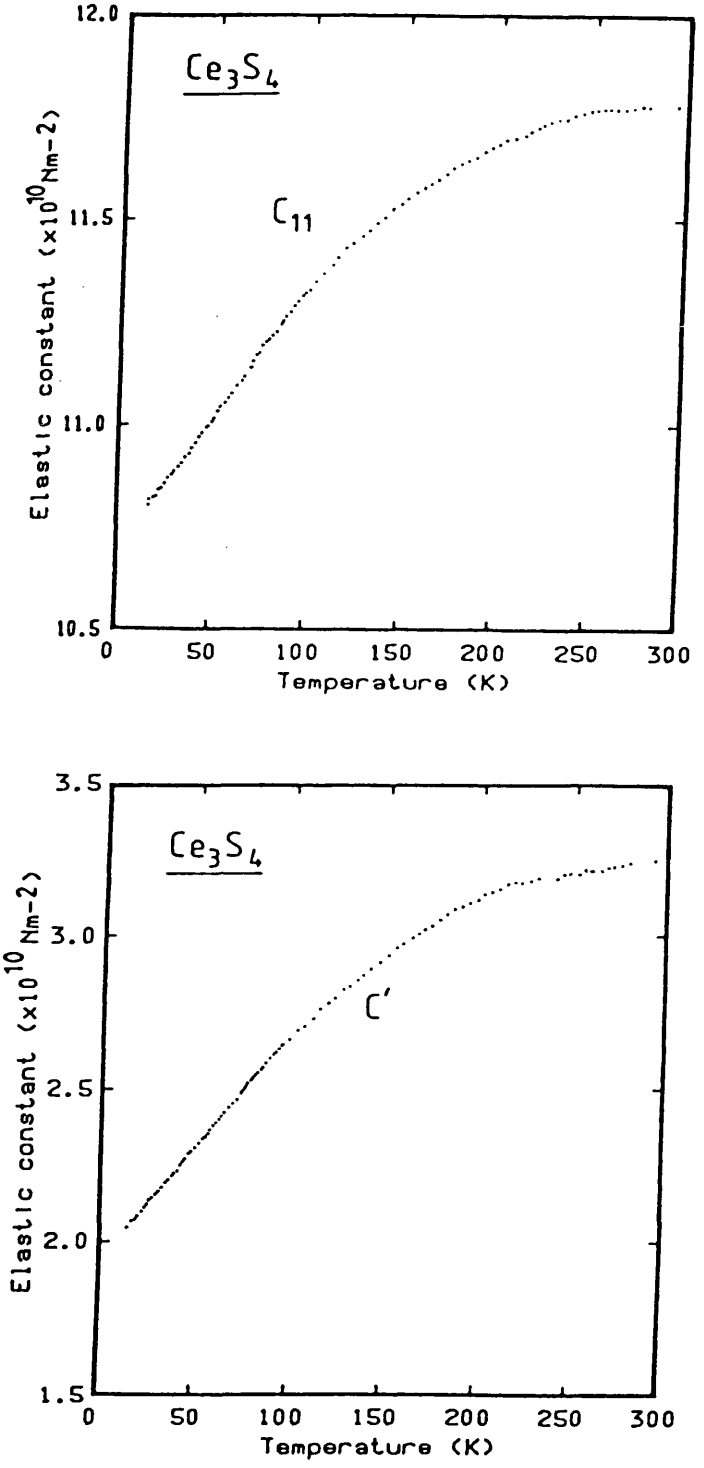

Figure 7.4 : The temperature dependences of the elastic stiffnesses (a) C_{11} and (b) $(C_{11} - C_{12})/2$ of Ce_3S_4 (after Futterer et al. 1988).

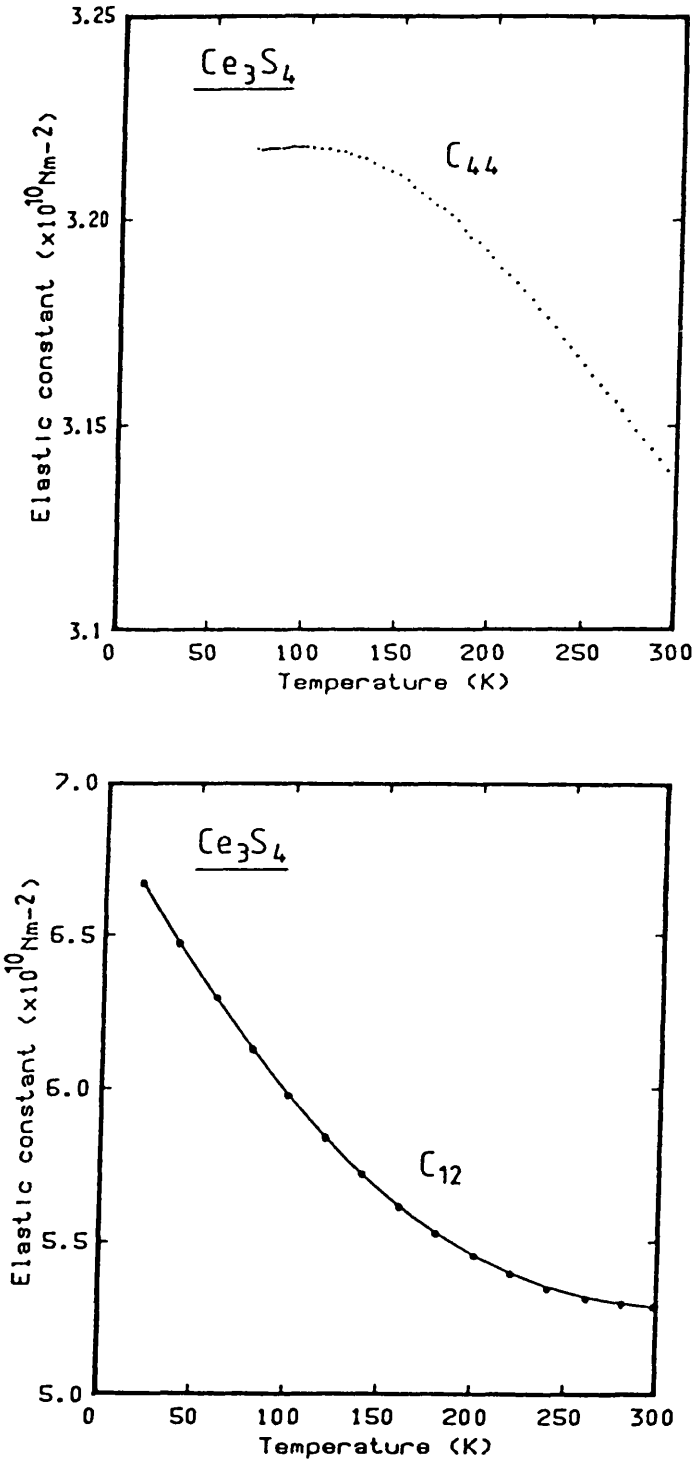

Figure 7.5 : The temperature dependences of the elastic stiffnesses C_{44} and C_{12} of Ce_3S_4 (after Futterer et al. 1988).

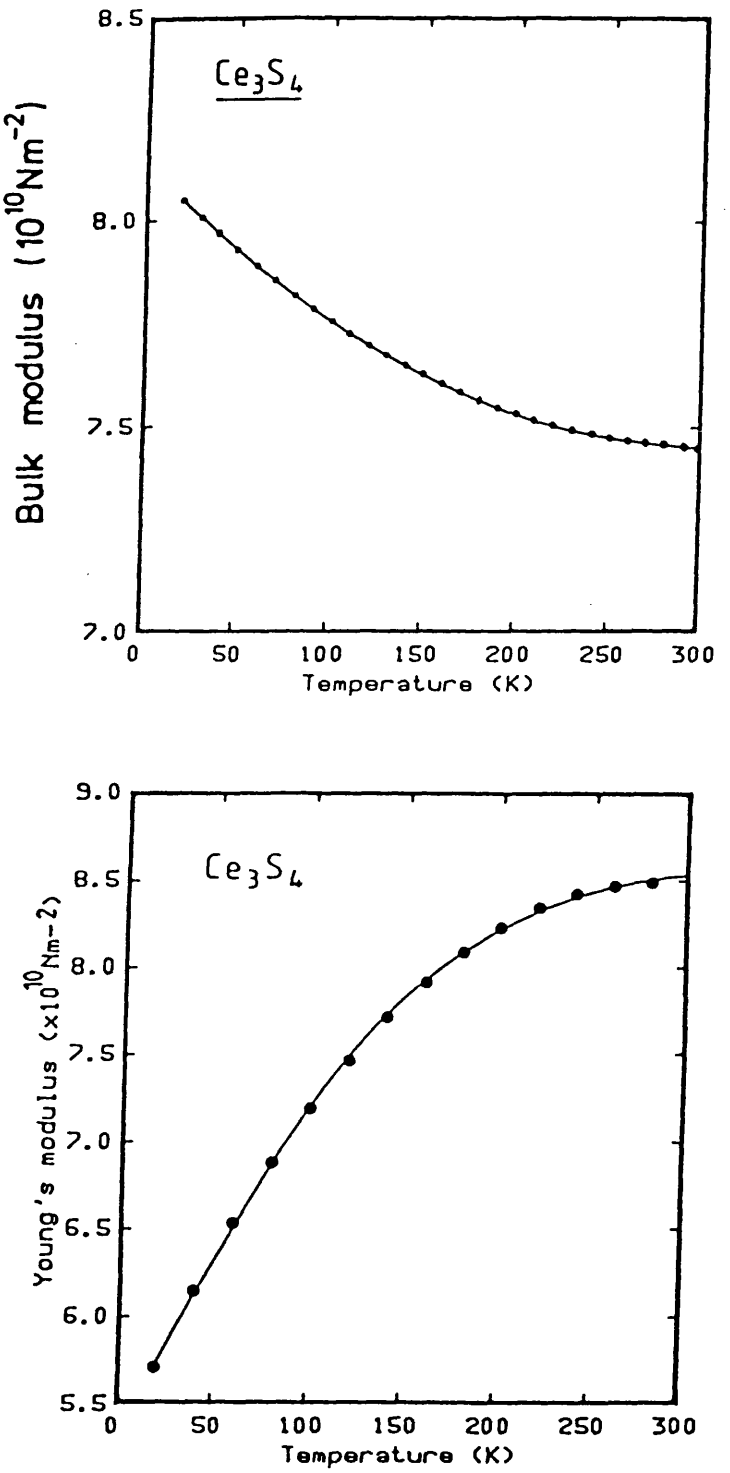

Figure 7.6 : The temperature dependences of the (a) bulk modulus and (b) Young's modulus in the XY plane of Ce_3S_4. Data used in the computation are taken from Futterer et al. (1988).

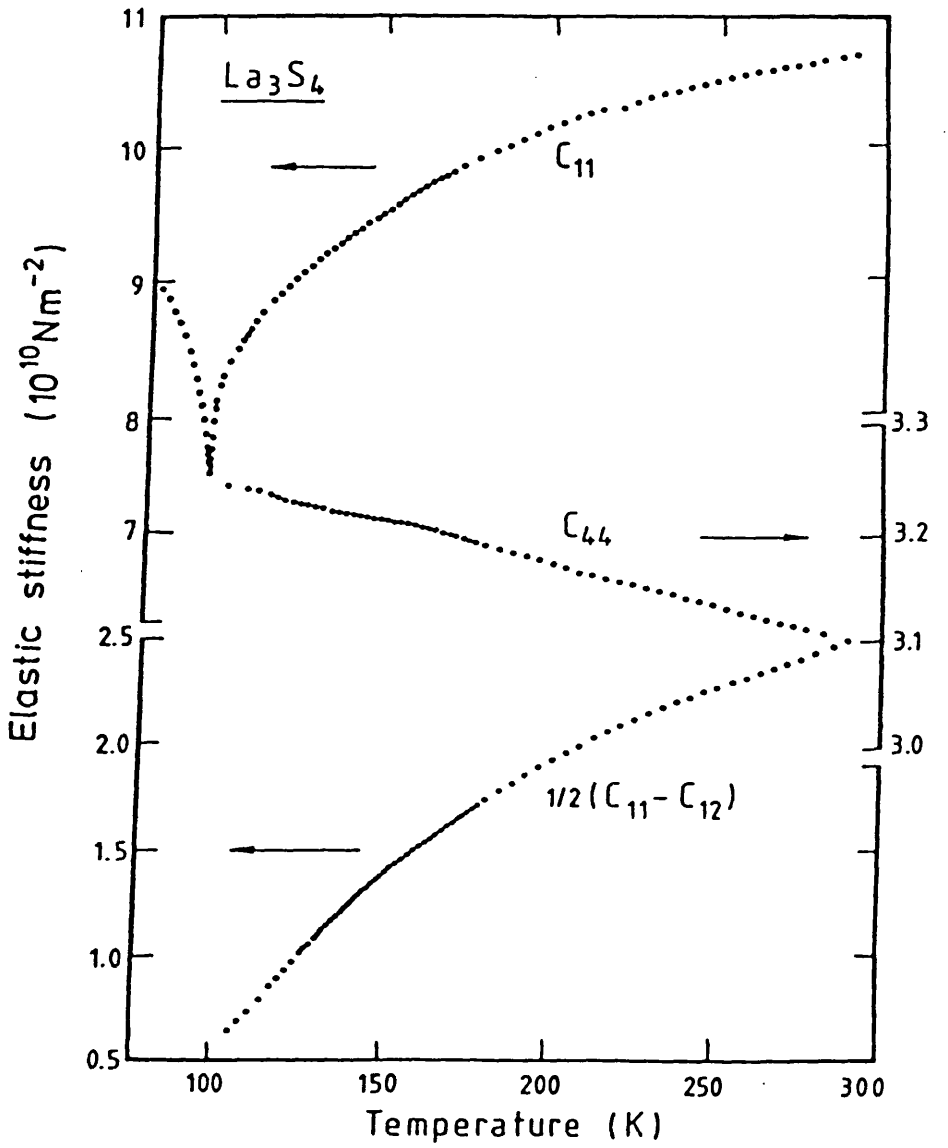

Figure 7.7 : The temperature dependences of the elastic stiffnesses C_{11}, C_{44} and $(C_{11} - C_{12})/2$ of La_3S_4 (after Ford et al. (1980)).

velocity temperature dependences. In contrast, for Ce_3S_4 the anomalous decreases of C_{11} and $(C_{11} - C_{12})/2$ (see figure 7.4) with reducing temperature continues down to the lowest temperature (16K) at which measurements have been made. Here lattice instability develops in Ce_3S_4 as the temperature is reduced. However there is no sign of phase transition being induced by this acoustic phonon mode softening in this crystal above 16K. Since La_3S_4 shows acoustic-mode softening which is associated with the onset of a phase change, and that in Ce_3S_4 is similar, it seems probable that Ce_3S_4 may undergo a structural transformation at even lower temperature than has been reached. Figure 7.5 shows that the elastic stiffness C_{44} of Ce_3S_4 behaves normally, increasing as the temperature is reduced and becomes almost invariant with temperature below about 100K. Hence the most interesting feature of the elastic behaviour of Ce_3S_4 with temperature is a marked softening of the zone centre acoustic phonons propagating down a [110] direction and polarised $[1\bar{1}0]$. This softening is not so pronounced as that in La_3S_4. The longitudinal modes propagated down the [001] axes also soften as the temperature is reduced as shown by the behaviour of C_{11}. Table 7.2 shows that the shear anisotropy ratio C_{44}/C' of Ce_3S_4, increases to 1.27 at 80K and continues to rise as the temperature is reduced further. La_3S_4 has the unusual property of becoming more compressible as the temperature is reduced: $(dB^S/dT)_{300K}$ is about $+5 \times 10^7$ $Nm^{-2}K^{-1}$. Ce_3S_4 shows the

Table 7.2 : The second order elastic constants and the adiabatic bulk modulus B^S of Ce_3S_4 single crystal at temperature range 80K to 300K. The data for the calculation are extracted from Futterer et al. (1988).

	Elastic stiffness constants (x 10^{10} Nm^{-2})					
T(K)	C_{11}	C_{12}	C_{44}	C'	B^S	C_{44}/C'
80	11.21	6.13	3.22	2.54	7.82	1.27
90	11.27	6.05	3.22	2.61	7.79	1.23
100	11.32	5.98	3.22	2.67	7.76	1.20
110	11.37	5.91	3.22	2.73	7.73	1.18
120	11.42	5.84	3.22	2.79	7.70	1.15
130	11.46	5.78	3.21	2.84	7.67	1.13
140	11.50	5.72	3.21	2.89	7.65	1.11
150	11.54	5.67	3.21	2.94	7.63	1.09
160	11.58	5.62	3.21	2.98	7.60	1.08
170	11.61	5.57	3.20	3.02	7.58	1.06
180	11.64	5.53	3.20	3.06	7.56	1.05
190	11.67	5.49	3.20	3.09	7.55	1.03
200	11.69	5.45	3.19	3.12	7.53	1.02
210	11.71	5.42	3.19	3.15	7.52	1.01
220	11.73	5.39	3.18	3.17	7.50	1.00
230	11.74	5.36	3.18	3.19	7.49	1.00
240	11.76	5.34	3.17	3.21	7.48	0.99
250	11.76	5.33	3.16	3.22	7.47	0.98
260	11.77	5.31	3.16	3.23	7.46	0.98
270	11.77	5.30	3.15	3.24	7.46	0.97
280	11.77	5.30	3.15	3.24	7.45	0.97
290	11.77	5.29	3.14	3.24	7.45	0.97
300	11.76	5.29	3.14	3.23	7.45	0.97

more usual increase of bulk modulus as the temperature is reduced but the effect is marginal, (dB^S/dT) at 300K being only -0.7×10^7 $Nm^{-2}K^{-1}$. The acoustic mode softening indicates incipient instability in this compound as the temperature is reduced.

7.4.2 The Elastic Behaviour under Pressure and the Grüneisen Parameters.

The effect of hydrostatic pressure on the "natural" wave velocity W (Thurston and Brugger 1964) in Ce_3S_4, plotted in figure 7.8, is linear and the gradients for each of the five modes studied are positive. The implication is that all the acoustic modes stiffen in the normal manner under pressure. The gradients $[d(\rho_o W^2)/dP]_{P=0}$ have been used to obtain the pressure derivatives (dC_{IJ}/dP) given in table 7.3. The hydrostatic pressure derivatives of the stoichiometric La_3S_4 (Ford et al. 1980) are also included in this table. It is interesting to note that while both materials soften elastically as the temperature is reduced, they stiffen under hydrostatic pressure.

Knowledge of the compression V(P)/Vo introduced in chapter 2 is prerequisite in interpretation of the effects of hydrostatic pressure on the physical properties of materials. To evaluate this property, the Murnaghan (1944) equation-of-state has been employed (see section 2.7). Since the thermodynamic data such as the

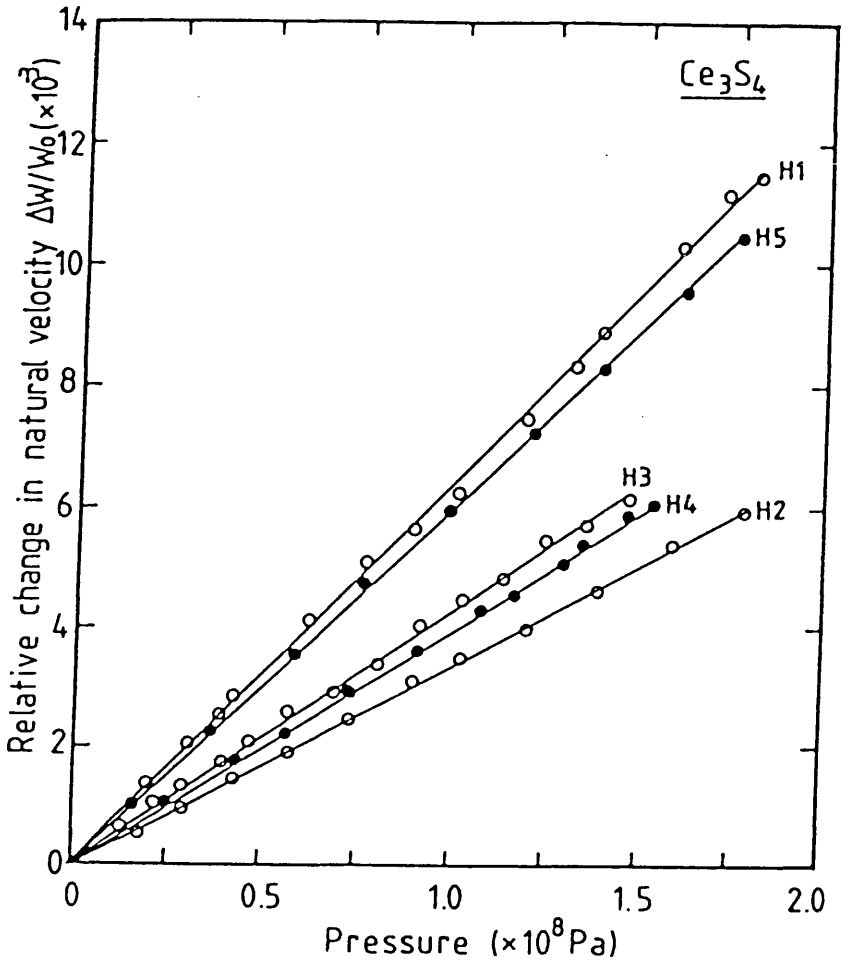

Figure 7.8 : Relative change in natural velocity of ultrasonic waves propagated along [001] and [110] axes in Ce_3S_4 at room temperature. The modes are H1:$\underline{N}$[001]$\underline{U}$[001], H2:$\underline{N}$[001]$\underline{U}$ in (001) plane, H3:$\underline{N}$[110]$\underline{U}$[110], H4:$\underline{N}$[110]$\underline{U}$[001], H5:$\underline{N}$[110]$\underline{U}$[1$\bar{1}$0] where $\underline{N}$ and $\underline{U}$ are the propagation and polarization vectors, respectively.

Table 7.3 : The effective pressure derivatives dC_{IJ}/dP and the pressure derivatives B_{IJ} of the thermodynamic second order elastic constants, third order elastic constant combinations and the mean acoustic mode Grüneisen parameter $\bar{\gamma}^{el}$ for Ce_3S_4 and La_3S_4 single crystals at room temperature (291K). La_3S_4 data are taken from Ford et al. (1980).

	Ce_3S_4	La_3S_4
Hydrostatic pressure derivatives of elastic stiffnesses		
dC_{11}/dP	12.1	9.0
dC_{12}/dP	4.0	5.7
dC_{44}/dP	2.1	3.1
dC'/dP	4.0	1.6
dB^s/dP	6.7	6.8
Thermodynamic pressure derivatives		
B_{11}	13.6	10.5
B_{12}	3.3	4.9
B_{44}	3.3	4.2
Third order elastic constant combination (x 10^{11} Nm^{-2})		
$C_{111} + 2C_{112}$	-30.3	-23.2
$C_{144} + 2C_{166}$	-7.3	-9.3
$C_{123} + 2C_{112}$	-7.3	-10.8
Mean acoustic mode Grüneisen parameter $\bar{\gamma}^{el}$	3.15	2.85

specific heat and the linear thermal expansion of Ce_3S_4 are not yet available, it is not possible to determine the thermal Grüneisen parameter γ^{th}; therefore the mean elastic Grüneisen parameter $\bar{\gamma}^{el}$ has been used to calculate the isothermal bulk modulus and its pressure derivatives from the measured adiabatic quantities. The adiabatic and isothermal properties of Ce_3S_4 and La_3S_4 at 291K are given in table 7.4. However since the corrections are not large, the error introduced into the compressibility is probably smaller than the experimental error. In the absence of thermal expansion data for Ce_3S_4 that for La_3S_4 has been used. The compressions of these two isotypic crystals, given in table 7.5, are found to be the same within experimental error.

In general the elastic stiffnesses and their hydrostatic pressure derivatives are quite similar for Ce_3S_4 and La_3S_4. This is the usual pattern found for crystals having the same structure. The pressure derivatives dC_{IJ}/dP of these two lanthanide chalcogenides follow the normal trend of a rocksalt-structural crystal, where $dC_{11}/dP > dC_{12}/dP > dC_{44}/dP$. Ce_3S_4 shows the common behaviour that dC_{11}/dP is the largest pressure derivative. This is because the longitudinal compression along an axis causes of shortening interatomic distances of atoms and their nearest neighbours, so that their repulsive forces are increased. In contrast dC'/dP and dC_{44}/dP are small and positive because repulsive forces do not contribute to them. Furthermore the shear moduli

Table 7.4 : Adiabatic (S) and isothermal (T) properties of Ce_3S_4 and La_3S_4 (Ford et al. 1980) at room temperature (291K).

	Ce_3S_4	La_3S_4
Bulk modulus (x 10^{10} Nm^{-2})		
Bo^S	7.43	7.37
Bo^T	7.1	7.13
Pressure derivatives		
$(dBo^S/dP)_{P=0}$	6.7	6.8
$(dBo^T/dP)_{P=0}$	6.5	5.3
Temperature derivatives (x 10^{10} $Nm^{-2}K^{-1}$)		
(dBo^S/dT)	-0.7	+5.0
(dBo^T/dT)	-0.68	+4.8
Volume thermal expansion (x 10^{-5} K^{-1})		
α_v	-	+4.0

Table 7.5 : The compression V(P)/Vo of Ce_3S_4 and La_3S_4 at 291K calculated based on Murnaghan (1944) equation-of-state.

Pressure (x 10^9 Pa)	Ce_3S_4	La_3S_4
1	0.9868	0.9866
2	0.9748	0.9742
3	0.9638	0.9627
4	0.9536	0.9521
5	0.9442	0.9421
6	0.9355	0.9328
7	0.9273	0.9240
8	0.9197	0.9157
9	0.9125	0.9079
10	0.9057	0.9004

are associated to the volume conserving of a crystal. Our observations for Ce_3S_4 shows that this crystal is stable against shear stresses. However dC'/dP is much smaller for La_3S_4 than it is for Ce_3S_4 (table 7.3). This reflects the observation that the shear stiffness C' softens so markedly in La_3S_4 as the transition is approached and is softer than that of Ce_3S_4 even at room temperature.

As usual the hydrostatic pressure derivatives have been used to obtained the acoustic mode Grüneisen parameters $\gamma(p,\underline{N})$ in the long wavelength limit using equation (2.45) and plotted as a function of the wave propagation direction for Ce_3S_4 in figure 7.9 and La_3S_4 in figure 7.10. The $\gamma(p,\underline{N})$ are positive for all modes in both crystals. Application of pressure to Ce_3S_4 (as for La_3S_4) leads to an increase in mode frequency (or energy) in the normal way. The non-linear acoustic behaviour of this crystal is normal in this sense, even though the elastic softening with temperature is so pronounced. The high mean acoustic gamma $\bar{\gamma}^{el}$ is calculated using equation (2.50) which should hold reasonably well for Ce_3S_4 and La_3S_4 which have Debye temperatures rather below room temperature. The θ_D value given for Ce_3S_4 in table 7.1 should be used with some caution as, when long wavelength acoustic mode softening occurs in a crystal the soft mode contribution to the integral over velocity space and hence to θ_D is overestimated. Since the acoustic mode softening with temperature is so dramatic for La_3S_4, it is not possible to estimate the elastic Debye

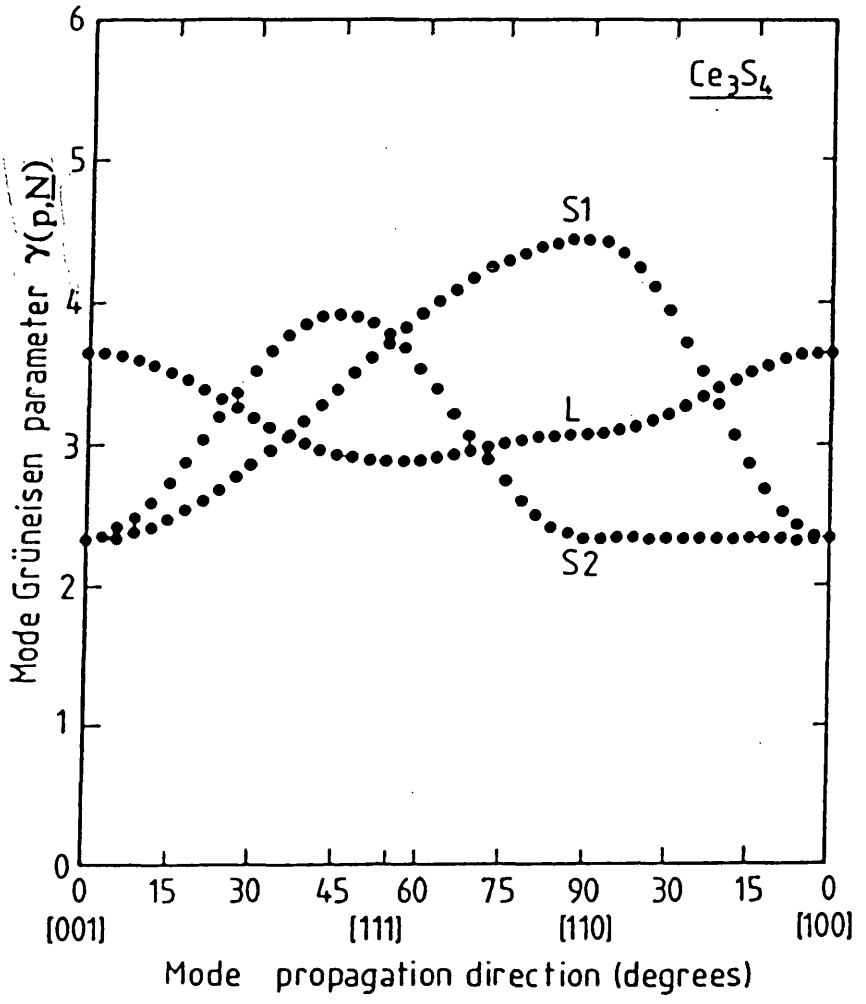

Figure 7.9 : The orientation dependences of the acoustic-mode Grüneisen parameters $\gamma(p,\underline{N})$ in the long-wavelength limit for Ce_3S_4.

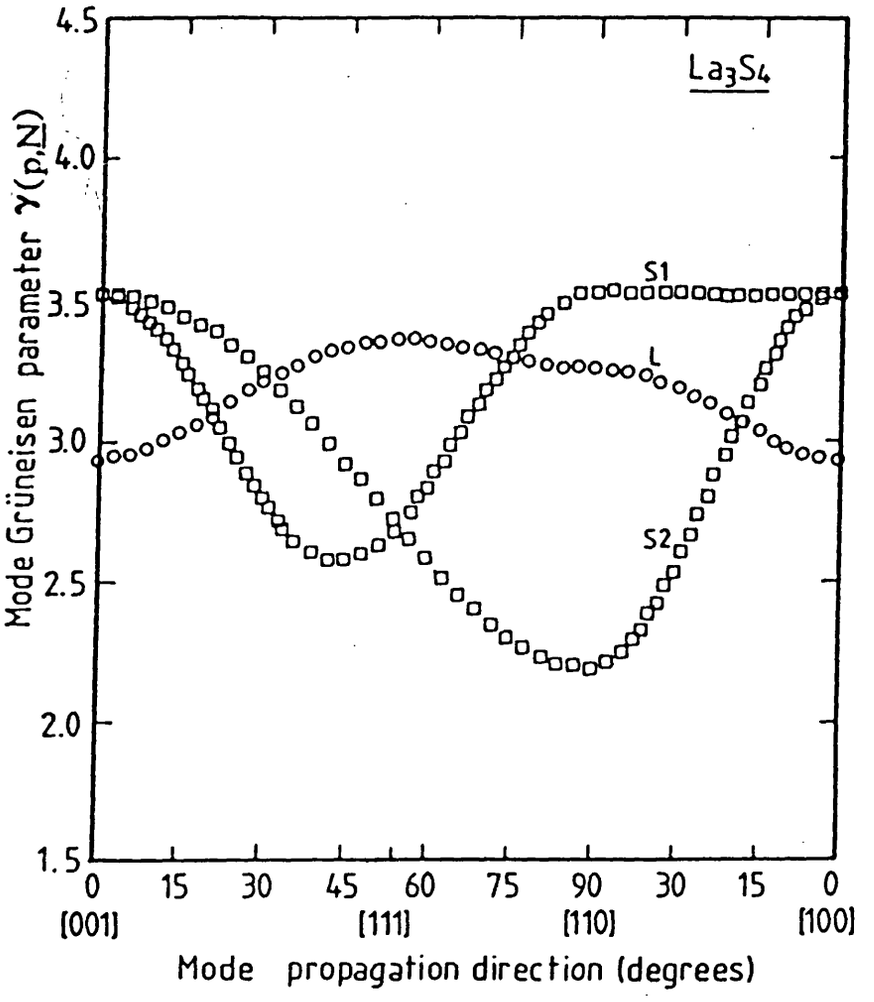

Figure 7.10 : The orientation dependences of the acoustic-mode Grüneisen parameters $\gamma(p,\underline{N})$ in the long-wavelength limit for La_3S_4. Data used in the computation are taken from Ford et al. (1980).

temperature, and so the Debye temperature for this compound is best determined from specific heat measurements (244K: Westerholt et al. 1979). As mentioned in section 2.10.1 $\bar{\gamma}^{el}$ is a measure only of the contribution of the zone-centre acoustic modes to the vibrational anharmonicity. Optic modes are expected to play a significant role in the thermal Grüneisen parameter γ^{th} of both these crystals at room temperature but comparison with the $\bar{\gamma}^{el}$ obtained here cannot be made yet as the thermodynamic quantities required to calculate γ^{th} are not yet available.

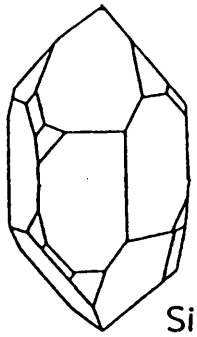

8

ACOUSTIC MODE VIBRATIONAL ANHARMONICITY OF THE RHOMBOHEDRAL SINGLE CRYSTAL BERLINITE

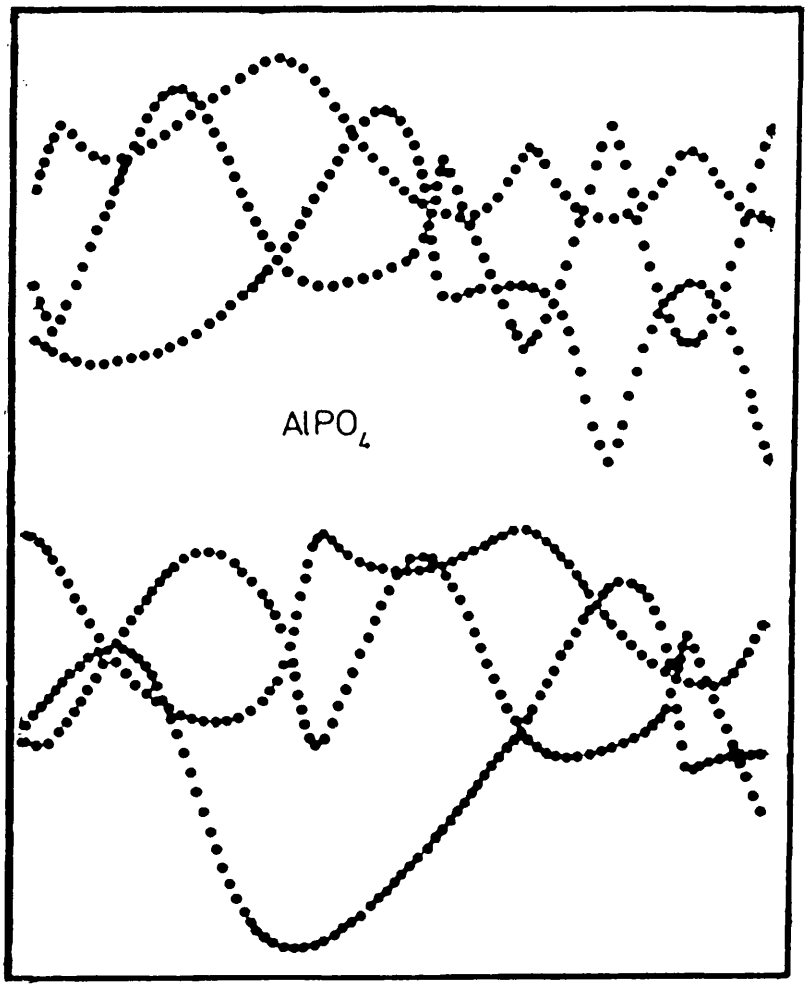

CHAPTER EIGHT

ACOUSTIC MODE VIBRATIONAL ANHARMONICITY OF THE RHOMBOHEDRAL SINGLE CRYSTAL BERLINITE

8.1 Introduction.

Several oxides with the composition $A^{III}B^{V}O_4$ exist in structures which can be considered as a derivative of isoelectronic quartz SiO_2, constructed by replacing half the Si atoms by A^{III} and the other half by B^{V} (Buerger 1948). Aluminium phosphate ($AlPO_4$) in its rhombohedral modification berlinite belongs to the same point group (32) in the trigonal R1 crystal system as quartz and so is noncentrosymmetric and piezoelectric. The structural relationship between the two materials is close (Thong and Schwarzenbach 1979) and many similarities between their physical properties have been pointed out: elastic properties (Chang and Barsch 1976, Bailey et al. 1982, Wang Hong et al. 1986), piezoelectric properties (Wang Hong et al. 1986), surface acoustic wave (SAW) velocities (O'Connell and Carr 1977). Berlinite also resembles quartz in many of its other low- and high-temperature properties such as density, hardness and refractive indices (Schwarzenbach 1966). Quartz is used in many

electronic devices based on bulk acoustic, surface acoustic and surface-skimming bulk wave technologies. Berlinite has larger piezoelectric coupling coefficient than quartz: there is considerable interest in its potential for technological applications. Device design will rely upon knowledge of fundamental physical properties including the elastic constants and their behaviour with pressure.

The second order elastic constants of berlinite have been measured previously using several different techniques, including ultrasonic pulse superposition (Bailey et al. 1982), ultrasonic pulse echo overlap (Chang and Barsch 1976) and the resonance method (Mason 1950, Wang Hong et al. 1986). Considerable differences occur between the various data sets. Temperature dependence measurements of the SOEC's as illustrated in figure 8.1 (Chang and Barsch 1976) show that the elastic constants, except C_{66} and C_{14}, decrease in the normal way with increasing temperature. The unusual behaviour of C_{66} and C_{14} resembles that in quartz, although the temperature derivatives of the SOEC's of berlinite are less than half those of quartz.

As far as berlinite is concerned, no information has been published yet on the effects of hydrostatic pressure on the lattice-dynamical behaviour for this crystal. So for the first time the elastic behaviour of berlinite under pressure is carried out here, in order to quantify the acoustic-mode vibrational anharmonicity which is

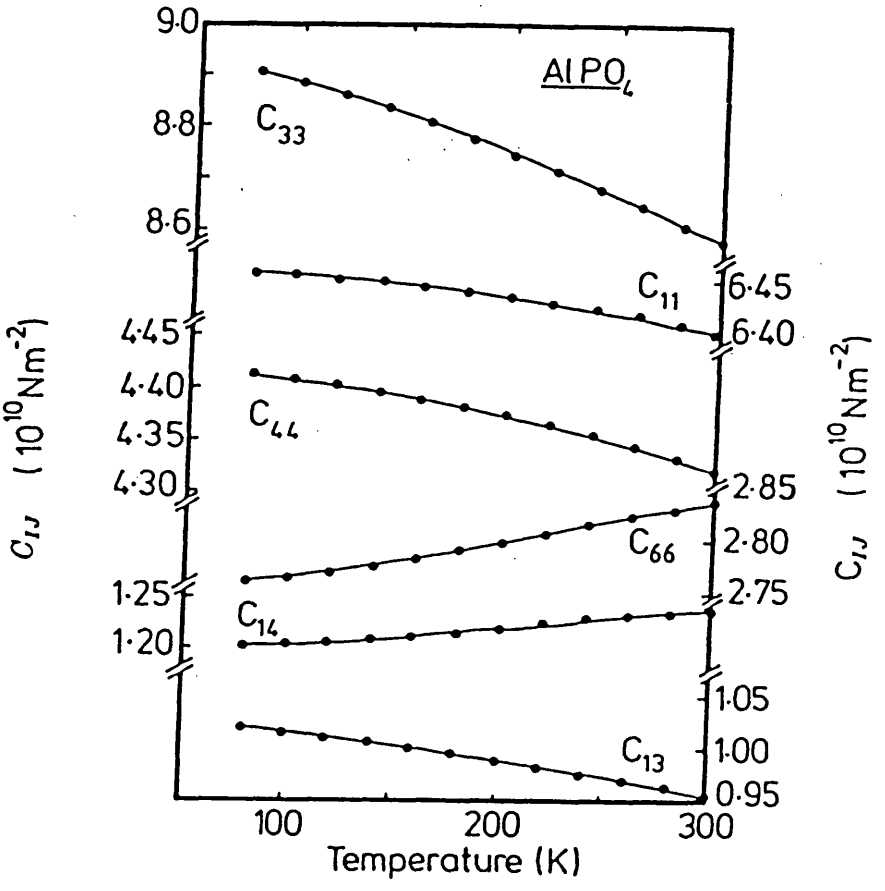

Figure 8.1 : Zero-field elastic stiffness constants of berlinite as a function of temperature (after Chang and Barsch 1976).

approached here by reference to the mode Grüneisen parameters.

8.2 Experimental Procedure and Evaluation of Elastic Parameters.

8.2.1 Sample preparation.

Good optical-quality single crystals of berlinite ($AlPO_4$) obtained from Institute of Crystal Materials, Shandong University, Jinan Shandong, People's Republic of China, were grown using a slow-heating technique in an autoclave using methods described elsewhere (Detaint, Poignant and Toudic 1980). The defects in these crystals have been characterized by optical and scanning electron microscopy and by their effects on electrical properties (Wang Hong et al. 1986).

To determine the crystal orientation needed for ultrasonic-wave propagation, the Laue x-ray back reflection method has been employed. To specify the elastic moduli without ambiguity and relate them to other physical properties, in particular the phonon dispersion curves, it is necessary to define the crystallographic axial set with respect to the atomic arrangement in the crystal in which the measurements are made. This has been achieved by following the Institute Radio Engineering (IRE) standards on piezoelectric crystals (Proc. IRE 1949

and 1958); the Z axis parallel to the optic axis, the X axis parallel to one of the three binary axes (normal to the Z axis), and the Y axis completes the right-handed orthogonal axial set.

Several specimens with pairs of faces parallel to better than 10^{-4} radians were cut and polished. The cuts prepared include X, Y, Z cuts and one off-axis (see table 8.1 for directions selected for ultrasonic wave propagation).

The density of berlinite was determined using the liquid-immersion technique as 2.652 ± 0.020 gcm^{-3}. This is in reasonable agreement with results of other workers 2.620 gcm^{-3} using the same technique, 2.618 gcm^{-3} by the X-ray powder method (Swanson et al. 1960); the density reported by Mason (1950) was 2.566 gcm^{-3}.

8.2.2 The SOEC and their Hydrostatic Pressure Dependences

To obtain the ultrasonic-wave velocities (table 8.2), the transit time of a 10MHz ultrasonic pulse was measured by the pulse echo overlap technique (Papadakis 1967) as explained in chapter 3. X- and Y-cut quartz transducers were attached to the specimen with Dow Resin 276-V9. The six independent elastic constants (tables 8.3 and 8.4) have been obtained from measurements made on six modes (2, 3, 7, 8, 9, 10) which do not involve a piezoelectric contribution, and so are referred to as unstiffened

Table 8.1 : The effective second order elastic constant [C_{IJ}] of berlinite. Y'/+45° designates a propagation direction in the +Y+Z plane at an angle of 45° to the +Y axis. e is the piezoelectric tensor and ϵ is the effective dielectric tensor.

No.	N	U	Mode	[ρV^2]
1	X	X	L	$C_{11} + e_{11}^2/\epsilon_{11}$
2	X	~Y	FS	$(C_{66} + C_{44})/2 + [(C_{66} - C_{44})2 + 4C_{14}^2]^{1/2}/2$
3	X	~Z	SS	$(C_{66} + C_{44})/2 - [(C_{66} - C_{44})^2 + 4C_{14}^2]^{1/2}/2$
4	Y	Y	QL	$(C_{44} + C_{11})/2 + [(C_{44} - C_{11})^2 + 4C_{14}^2]^{1/2}/2$
5	Y	~Z	QS	$(C_{44} + C_{11})/2 - [(C_{44} - C_{11})^2 + 4C_{14}^2]^{1/2}/2$
6	Y	X	S	$C_{66} + e_{11}^2/\epsilon_{11}$
7	Z	Z	L	C_{33}
8	Z	Y	S	C_{44}
9	Y'/+45°	Y'	QL	$(C_{11} + C_{33} + 2C_{44} - 2C_{14})/4 + [(C_{11} - C_{33} - 2C_{14})^2/4 + (C_{44} + C_{13} - C_{14})^2]^{1/2}/2$
10	Y'/+45°	Z'	QS	$(C_{11} + C_{33} + 2C_{44} - 2C_{14})/4 - [(C_{11} - C_{33} - 2C_{14})^2/4 + (C_{44} + C_{13} - C_{14})^2]^{1/2}/2$
11	Y'/+45°	X	S	$(C_{44} + C_{66} + 2C_{14})/2 + (e_{26}')^2/\epsilon_{22}'$
12	Y'/-45°	Y'	QL	$(C_{11} + C_{33} + 2C_{44} - 2C_{14})/4 + [(C_{11} - C_{33} - 2C_{14})^2/4 + (C_{44} + C_{13} - C_{14})^2]^{1/2}/2$
13	Y'/-45°	Z'	QS	$(C_{11} + C_{33} + 2C_{44} - 2C_{14})/4 - [(C_{11} - C_{33} - 2C_{14})^2/4 + (C_{44} + C_{13} - C_{14})^2]^{1/2}/2$
14	Y'/-45°	X	S	$(C_{44} + C_{66} - 2C_{14})/2 + (e_{26}'')^2/\epsilon_{22}'$

$e_{26}' = -(e_{11} + e_{14})/2$
$e_{26}'' = -(e_{11} - e_{14})/2$
$\epsilon_{22}' = (\epsilon_{11}^S + \epsilon_{33}^S)/2$

L = Longitudinal
FS = Fast Shear
SS = Slow Shear
S = Shear

QL = Quasi - Longitudinal
QS = Quasi - Shear
$C_{ij} = C_{ij}^E$
$\epsilon_{ij} = \epsilon_{ij}^S$

Table 8.2 : Natural wave velocity W (units ms^{-1}), the initial slope $(\rho_o W^2)'$ of the hydrostatic pressure dependence, and the elastic modulus $(\rho_o W^2)$ (units 10^{10} Nm^{-2}) for each ultrasonic mode (nomenclature given in Table 8.1) propagated in berlinite at 298K.

Mode	W	$(\rho_o W^2)'$	$(\rho_o W^2)$
1	4501	3.704	5.373
2	2827	1.573	2.119
3	4337	-1.663	4.988
7	5732	6.312	8.714
8	4032	1.221	4.312
9	5416	3.683	7.780
10	3306	3.377	2.900
11	3089	-2.812	2.531

Table 8.3 : The second order adiabatic elastic stiffness constants and isothermal compliance constants of berlinite at room temperature (298K). Units of stiffness 10^{10} Nm^{-2}, compliance 10^{-11} m^2N^{-1}.

C_{11}	C_{12}	C_{13}	C_{14}	C_{33}	C_{44}	C_{66}	Reference
6.488	0.898	1.460	-1.217	8.714	4.312	2.795	This work
6.344	0.232	5.810	-1.214	5.581	4.315	3.056	Wang et al. (1986)
6.931	1.051	1.349	-1.299	8.862	4.302	2.940	Bailey et al. (1982)
6.401	0.724	0.957	-1.235	8.576	4.317	2.838	Chang et al. (1976)
10.500	2.93	6.930	-1.270	13.35	2.310	3.790	Mason (1957)

S_{11}	S_{12}	S_{13}	S_{14}	S_{33}	S_{44}	S_{66}	Reference
1.745	-0.295	-0.243	0.576	1.229	2.644	4.079	This work
1.695	-1.470	-0.154	0.519	1.749	2.609	3.685	Wang et al. (1986)
1.642	-0.321	-0.201	0.593	1.190	2.682	3.925	Bailey et al. (1982)
1.731	-0.282	-0.162	0.578	1.202	2.649	4.026	Chang et al. (1976)
1.610	-0.100	-0.890	0.890	1.610	5.300	3.220	Mason (1957)

Table 8.4 : Comparison of the elastic data of berlinite at 298K with that of other rhombohedral crystals. The units of the elastic stiffness and compliance constants are 10^{10} Nm^{-2} and 10^{-11} m^2N^{-1} respectively.

	Berlinite	Quartz[a]	Calcite[b]	Bismuth[c]	Antimony[d]
C_{11}	6.488	8.68	14.52	6.33	10.13
C_{12}	0.898	0.70	5.50	2.45	3.45
C_{13}	1.460	1.91	5.25	2.50	2.92
C_{14}	-1.217	-1.80	-2.03	0.74	2.09
C_{33}	8.714	10.58	8.43	3.80	4.50
C_{44}	4.312	5.82	3.90	1.10	3.93
C_{66}	2.795	3.99	4.52	1.94	3.34
S_{11}	1.745	1.30	1.09	2.61	1.63
S_{12}	-0.296	-0.15	-0.35	-0.80	-0.61
S_{13}	-0.243	-0.30	-0.46	-1.20	-0.66
S_{14}	0.576	0.45	0.75	-2.16	-1.19
S_{33}	1.229	1.02	1.76	4.21	3.09
S_{44}	2.644	2.00	3.35	11.52	3.81
S_{66}	4.079	2.91	2.90	6.79	4.47

References:

(a) McSkimin, Andreath and Thurston (1965).
(b) Kaga (1968)
(c) Tu Hailing and Saunders (1983)
(d) Saunders and Yogurtcu (1984)

modes.

There are considerable discrepancies between published sets of elastic constants for berlinite (table 8.3). Hence it was considered necessary to make an extensive series of measurements to assist in resolving this problem. The mean elastic constants obtained are compared with those of other workers in table 8.3. The results lie close to the data sets given by Chang and Barsch 1976, and Bailey et al. 1982) and can be considered as providing confirmation of those two groups of workers. There is substantial scatter in the values of C_{13}; our own value of C_{13} being a little larger than that given in their papers. The source of much of the difference between the elastic constant sets probably stems from the fact that the crystals employed by different groups have different defect structures. Now the mean values a set of elastic constants (in units of $10^{10}Nm^{-2}$) can be calculated as follows

$C_{11} = 6.5$ $C_{12} = 0.90$

$C_{13} = 1.24$ $C_{14} = -1.24$

$C_{33} = 8.72$ $C_{44} = 4.31$

$C_{66} = 2.86$

from a combination of data given by Chang and Barsch (1976), Bailey et al. (1982) and our present data.

However, the present aim of measurement of the hydrostatic pressure derivatives of the elastic constants necessitates use of the actual ultrasonic-pulse transit times obtained on our own crystals to provide a basis for

determining the relative effects on wave velocity induced by hydrostatic pressure, and this has been done. Hydrostatic-pressure dependences (figure 8.2) up to 3 X 10^8 Pa were made in a piston and cylinder apparatus (see chapter 3 for details) using Plexol 201 as the pressure-transmitting medium. The calculated pressure derivatives dC_{IJ}/dP (chapter 2) for the berlinite are compared with those of other rhombohedral crystals in table 8.5. The pressure derivatives of the effective bulk modulus for a uniaxial crystal can be written (Saunders and Yogurtcu 1984a, 1984b) as follows:

$$\partial B/\partial P = -2B^2((1/B)+(1/A^2)\{A(L-6+Q+R) - S[T(C_{11}+C_{12}) + U - V]\})$$

where

$$B = 1/(2S_1+S_3)$$

$$A = C_{33}(C_{11}+C_{12})-2C_{13}(C_{33})$$

$$L = B_{11}+B_{12}-4B_{13}+2B_{33}$$

$$Q = (S_2-2S_1)(C_{11}+C_{12})$$

$$R = 2(2S_1-3S_3)C_{33}+4S_3C_{13}$$

$$S = (C_{11}+C_{12}-4C_{13}+2C_{33})$$

$$T = B_{33}-1+(2S_1-3S_3)C_{33}$$

$$U = C_{33}[B_{11}+B_{12}+(S_3-2S_1)(C_{11}+C_{12})]$$

$$V = 4C_{13}(B_{13}+1-S_3S_{13})$$

$$S_1 = S_{11}+S_{12}+S_{13}$$

$$S_3 = 2S_{13}+S_{33}$$

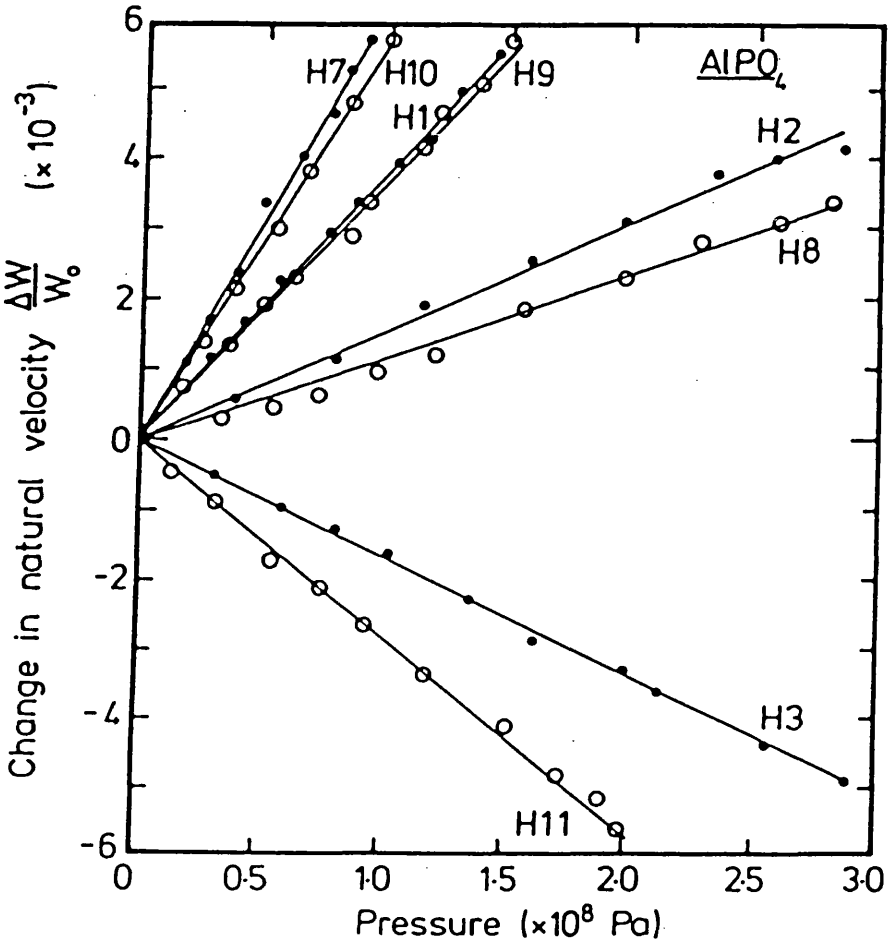

Figure 8.2 : The relative changes in the natural wave velocity induced by application of hydrostatic pressure to $AlPO_4$. The labelling of the modes is the same as that in table 8.1.

To express the data in a thermodynamic form suitable for ease of calculating the mode Grüneisen parameter, the hydrostatic pressure derivatives B_{IJ} (table 8.5) have been obtained using

$$B_{11}=\partial C_{11}/\partial P-1-(S_3-2S_1)C_{11}$$
$$B_{12}=\partial C_{12}/\partial P-1+(S_1)C_{12}$$
$$B_{13}=\partial C_{13}/\partial P-1+(S_1)C_{13}$$
$$B_{14}=\partial C_{14}/\partial P-(S_1)C_{14}$$
$$B_{33}=\partial C_{33}/\partial P+1-(S_1-2S_3)C_{33}$$
$$B_{44}=\partial C_{44}/\partial P+1+(S_1-2S_3)C_{44}$$
$$B_{66}=\partial C_{66}/\partial P+1+(S_1)C_{66}$$

8.2.3 Compression of Berlinite at High Pressure.

The compression V(P)/Vo of berlinite has been obtained by using the Murnaghan equation-of-state described in chapter 2. This parameter is usefully used to estimate the volume dependence of this crystal upon pressures of much greater magnitudes than directly available in ultrasonic experiments. The relative compressions of berlinite and quartz is illustrated in figure 8.3 taking as input data the pressure derivatives of bulk moduli equal to 7.41 and 6.33 and isothermal bulk moduli equal to 3.02 x 10^{10} Nm^{-2} and 4.72 x 10^{10} Nm^{-2} for berlinite and quartz, respectively, in each case. The volume change

Table 8.5 : The hydrostatic pressure derivatives at 298K of the effective SOEC [dC_{IJ}/dP] and thermodynamic SOEC [B_{IJ}] of berlinite crystal and other rhombohedral crystals.

	Berlinite present work	Quartz (a)	Calcite (b)	Bismuth (c)	Antimony (d)
dC_{11}/dP	8.792	3.28	3.02	6.38	10.8
dC_{12}/dP	12.958	8.66	2.05	2.38	2.9
dC_{13}/dP	3.338	5.97	3.19	4.69	6.7
dC_{14}/dP	2.196	1.93	-1.25	1.70	2.7
dC_{33}/dP	12.235	10.84	2.80	6.62	8.0
dC_{44}/dP	1.663	2.66	0.92	3.37	5.71
dC_{66}/dP	-2.083	-2.69	0.49	2.00	3.90
B_{11}	9.429	5.36	3.59	6.98	11.14
B_{12}	11.908	7.74	0.88	1.44	1.64
B_{13}	2.602	5.05	2.64	4.14	5.80
B_{14}	2.272	1.73	-1.31	1.84	2.67
B_{33}	16.877	12.08	5.47	9.20	10.74
B_{44}	3.443	4.08	2.20	4.58	6.91
B_{66}	-1.240	-1.19	1.35	2.80	4.70

References:

(a) McSkimin, Andreath and Thurston (1965).
(b) Kaga (1968)
(c) Tu Hailing and Saunders (1983)
(d) Saunders and Yogurtcu (1984)

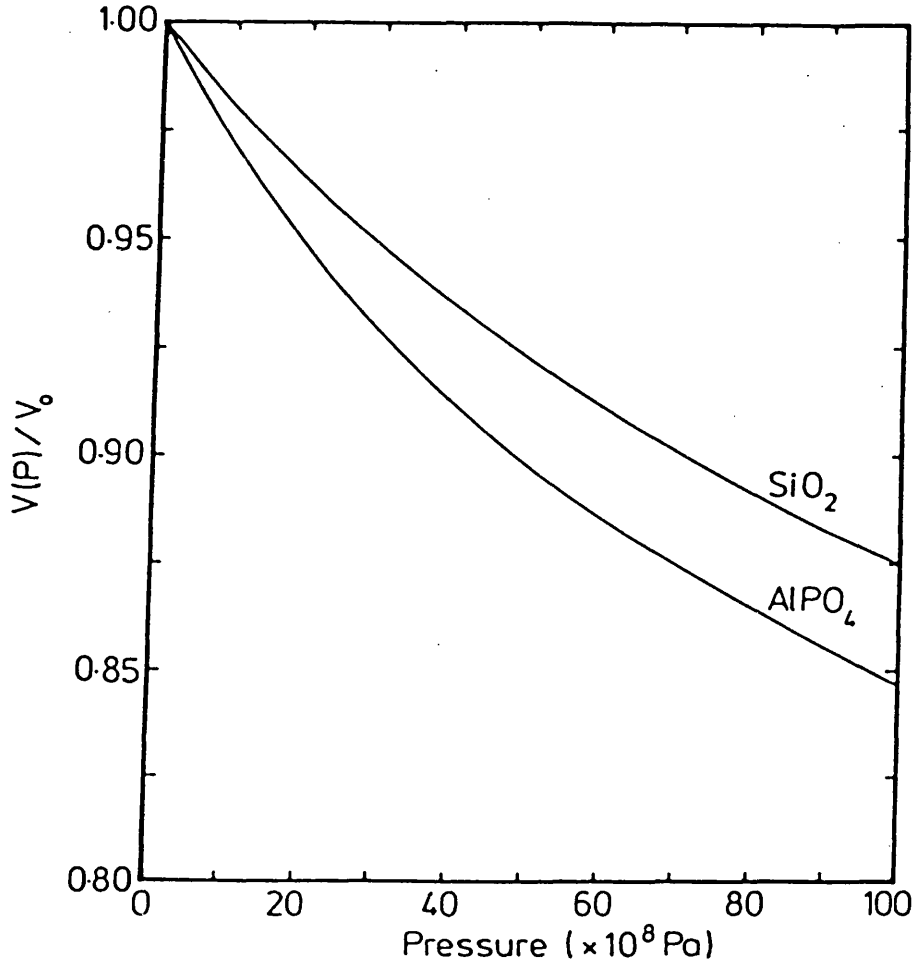

Figure 8.3 : The compressions of berlinite and quartz, extrapolated to high pressure using the Murnaghan equation-of-state.

induced by the application of a given pressure is much larger for berlinite than for quartz - the former material has much less resistance to the volumetric stress.

8.3 Discussion.

8.3.1 Structural Aspects of $AlPO_4$.

In general the atomic structural arrangement of a material and the strength of its interatomic binding forces determine the elastic behaviour of a crystal. Buerger (1948) considered the berlinite form of $AlPO_4$ to be derivative of quartz, which for comparison can be written as $SiSiO_4$, in which half the Si^{4+} sites are occupied by Al^{3+} and the other half by P^{5+} ions. The space group is $P3_121$ and the point group 32 (Sharan and Dutta 1964). The two crystals have the common feature of containing tetrahedra of oxygen atoms linked together at all the corners with equivalent species, either silicon or aluminium and phosphorus, at the tetrahedron centres. The lattice parameters (nm) are similar, being at 20°C (Knolmayer 1980);

	a	c	c/a
Quartz	0.49129	0.54046	1.100
Berlinite	0.49428	1.09737	2x1.110

The main difference between the two structures is the

doubled c-axis dimension of berlinite due to the different atomic species, aluminium and phosphorus. The bonding is mixed ionic and covalent in character. Using an electric field calculation in a charge-density refinement Thong and Schwarzenbach (1979) obtained atomic charges of +1.4 for Al, +1.0 for P, and -0.6 for O. The P-O bond is somewhat more covalent than the Al-O bond.

8.3.2 Room Temperature Elasticity of Berlinite.

As might be anticipated from the structural similarity of the two materials, the elastic moduli of berlinite bear a close formal resemblance to those of quartz (table 8.4). In general its smaller elastic constants show that berlinite is significantly less elastically stiff than quartz, a feature which is consistent with reduced covalent and enhanced ionic contribution to the interatomic binding as compared with quartz. Unlike many other crystals having a uniaxial crystal structure such as arsenic, antimony, or bismuth and consistent with its three-dimensional, oxygen tetrahedral framework, berlinite shows no tendency towards layerlike behaviour (for example, C_{11} is less than C_{33}).

The linear compressibility β, which is a measure of the reduction in the length of a line when a crystal is subjected to hydrostatic pressure, is a useful quantity to consider in relation to elastic anisotropy for a

uniaxial crystal. The linear compressibility in the XY plane β_{XY} (= $S_{11} + S_{12} + S_{13}$) (1.21 for berlinite and 0.85 for quartz) is larger than that β_Z (= $S_{33} + 2S_{13}$) along the Z axis (which is 0.743 and 0.420 respectively for these two materials). Thus both crystals have a markedly anisotropic response to hydrostatic pressure, a line in the XY plane contracting about one and one half times more than one in the Z direction for a given pressure. Hence the effect of hydrostatic pressure is to decrease the a spacing more than the c spacing, driving the c/a ratio further away from 2 for berlinite and from unity for quartz. For crystals with a certain layerlike character, such as the group-V semimetals arsenic, antimony or bismuth, $\beta_Z > \beta_{XY}$. This character is also reflected in the anisotropy of the linear thermal expansion (Bunton and Weintraub 1967, Pace and Saunders 1971, and White 1972) which can be very anisotropic in a layerlike crystal so that the Z-direction component α_{33} is substantially larger than α_{11}. In contrast to the layerlike materials, for berlinite (and quartz), α_{11} is greater than α_{33} (Austin, Salni and Pierce 1940) which is consistent with $\beta_Z < \beta_{XY}$ and $C_{11} < C_{33}$. The excitation of lattice vibrations is easier in the softer directions in the XY plane than along the stiffer Z direction, hence the larger value of S_{11} than S_{33}. This finding is emphasized by the occurrence of negative values of transverse-mode Grüneisen parameters in the XY plane.

8.3.3 The Elastic Mode Grüneisen Parameters.

As discussed earlier in chapter 2, the knowledge of the hydrostatic pressure dependences of the elastic constants (table 8.5) permits an assessment of the anharmonicity of acoustic modes in the long-wavelength limit. A physical description of this vibrational anharmonicity is best sought in terms of the Grüneisen parameters in the anisotropic continiuum model. Expressions for the zone-centre acoustic-mode Grüneisen $\gamma(p,\underline{N})$ of rhombohedral crystals in terms of thermodynamic pressure derivatives (Tu Hailing and Saunders 1983) have been used to compute these parameters for berlinite

$$\begin{aligned}\gamma(p,\underline{N}) = &-(2\omega\beta^T)^{-1}\\ &\times\{1+2\omega[S_1(U_1^2+U_2^2)+S_3U_3^2]-B_{11}(N_1U_1+N_2U_2)^2\\ &-B_{66}(N_1N_2-N_2U_1)^2-B_{33}N_3^2U_3^2\\ &-B_{44}[(N_2U_3+N_3U_2)^2+(N_3U_1+N_1U_3)^2]\\ &-2B_{13}(N_1N_3U_1U_3+N_2N_3U_2U_3)\\ &-2B_{14}(N_1^2U_2U_3+2N_2N_3U_1U_3+2N_1N_3U_1U_2\\ &-N_2^2U_2U_3+N_2N_3U_1^2-N_2N_3U_2^2)\}\,,\end{aligned}$$

where

$$\begin{aligned}\omega = &C_{11}(N_1U_1+N_2U_2)^2+C_{66}(N_1U_2-N_2U_1)^2+C_{33}N_3^2U_3^2\\ &+C_{44}[(N_2U_3+N_3U_2)^2+(N_3U_1+N_1U_3)^2]\\ &+2C_{13}(N_1N_3U_1U_3+N_2N_3U_2U_3)\\ &+2C_{14}(N_1^2U_2U_3+2N_1N_2U_1U_3+2N_1N_3U_1U_2\\ &-N_2^2U_2U_3+N_2N_3U_1^2-N_2N_3U_2^2)\,.\end{aligned}$$

Essentially as consequence of the negative pressure derivative dC_{66}/dP (table 8.5), the Grüneisen parameter γ for shear modes are negative over quite a large range of propagation directions (figure 8.4). Usually elastic constants and lattice vibrational frequencies increase under hydrostatic pressure so that the mode Grüneisen parameters are positive. All the longitudinal and quasilongitudinal modes show this normal behaviour with the Grüneisen parameters ranging between 0.624 and 2.65, the largest value being associated with the pure longitudinal mode propagating along the Z axis, the direction of strongest bonding.

Aluminium phosphate undergoes an α-β displacive transformation (figure 8.5) which closely resembles that quartz. At T_o equal to about 853K inclusion of 180° rotational symmetry about the Z axis takes the trigonal α form berlinite (point group 32) to the hexagonal β form (point group 622) (Arnold 1965). Raman spectra studies (Scott 1970, 1971) show that as the temperature is increased towards T_o an optic-phonon mode softens at the Γ point from its room-temperature wave number ($\sim$220 cm^{-1}); at high temperature a one-phonon anharmonic coupling ensues by Fermi resonance with a state at 158 cm^{-1}. In the context of Landau theory (Landau and Lipshitz 1958) the α–β structural change involves a symmetry breaking which is consistent with a second-order transition. For quartz the tilt angle of the SiO_4

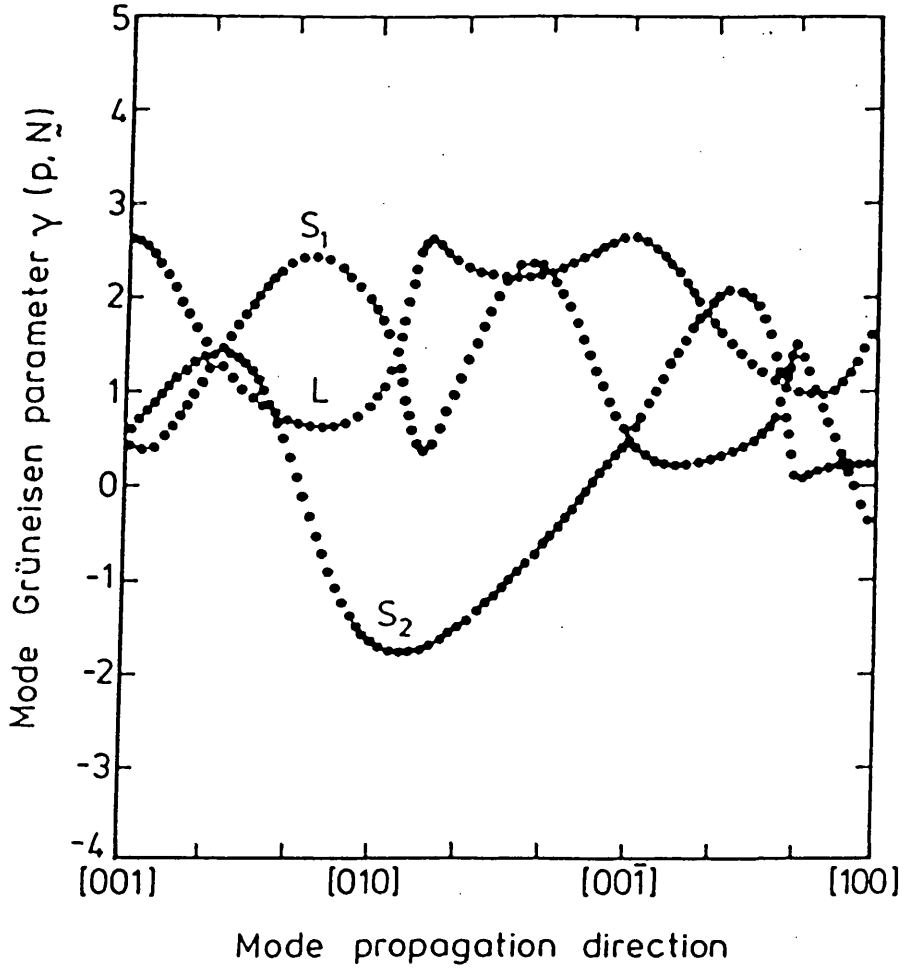

Figure 8.4 : (a) The Brillouin-zone centre, acoustic mode Grüneisen parameters of berlinite as a function of mode propagation direction.

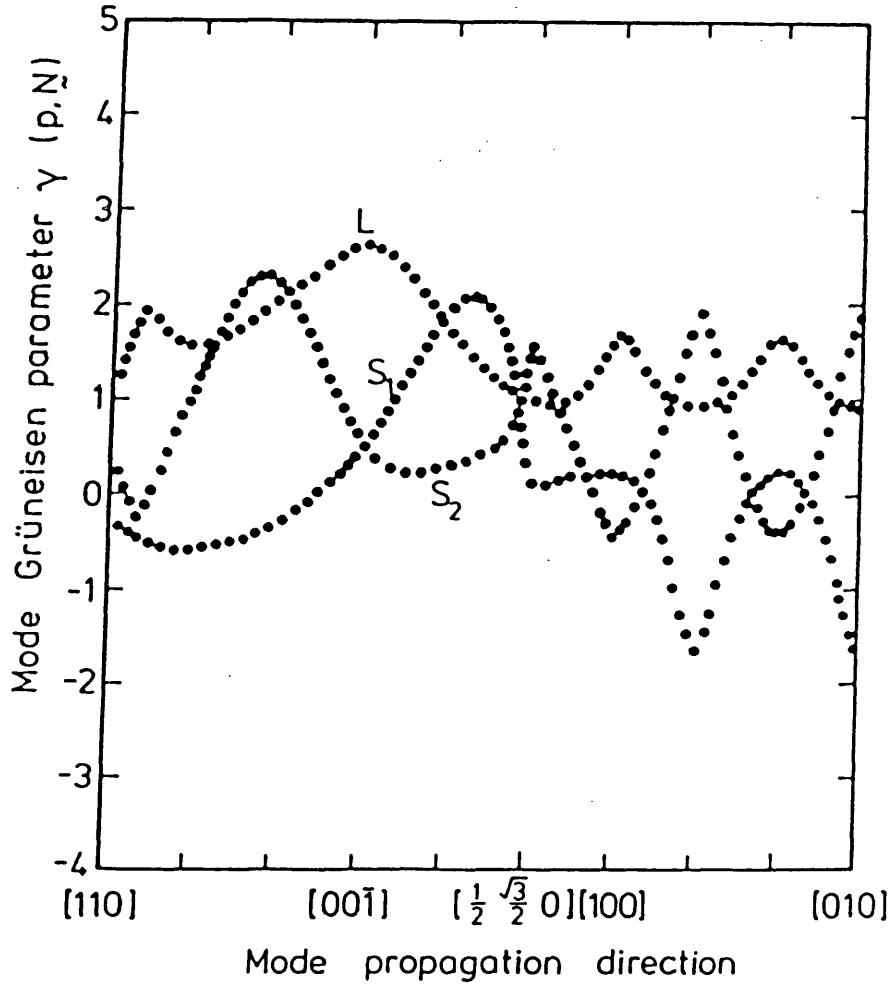

Figure 8.4 : (b) The Brillouin-zone centre, acoustic mode Grüneisen parameters of berlinite as a function of mode propagation direction.

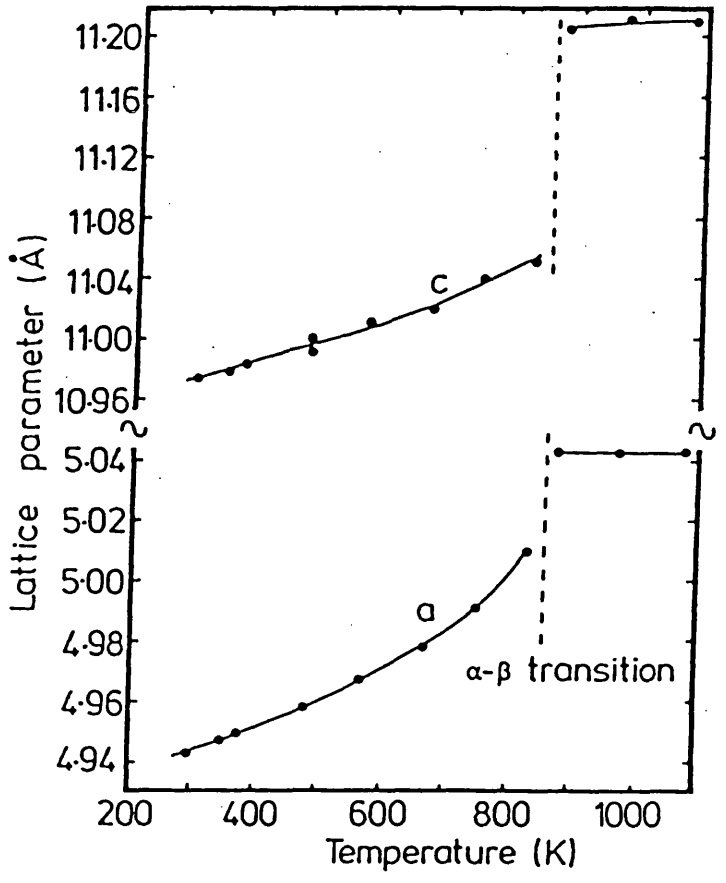

Figure 8.5 : Lattice parameters of berlinite versus temperature as measured by Chang and Barsch (1976).

tetrahedra about their twofold axis can be taken as the order parameter (Grimm and Dorner 1975). For berlinite the measured changes in atomic positions with increasing temperature indicate that as the transition is approached the PO_4 and AlO_4 tetrahedra rotate around a binary axes and that there is also a relative translation along this axis (Ng and Calvo 1976, and Lang et al. 1977). The tilt of the tetrahedra about their binary axes reverses in a sense at about 40K below T_o before changing continously to the β-phase orientation. The tilt angle by itself is not an acceptable order parameter (Lang et al. 1977). In spite of this unresolved difficulty it is clear that optic-phonon mode softening constitutes the driving mechanism of the transition.

8.3.4 The Effect of Soft Optic Phonon Mode to the Elasticity.

To proceed to find out how the optic-phonon mode softening might influence elastic stiffness, it is useful to return to consider the situation in quartz, which is better understood. The transition in quartz is nearly second in character and is driven by a zone centre soft optic phonon with an energy of 25.8 meV (207 cm^{-1}) at room-temperature (Axe and Shirane 1970). Above the transtition inelastic scattering shows the critical behaviour expected for a soft-phonon mode. The eigenvactors for this soft mode correspond closely to the

atomic displacements appropriate to the structural change.

Crystallographic and neutron scattering studies for quartz have been made in the hexagonal-system reference frame, while all the elastic-constant work (including the study of berlinite) has been referred to the IRE standard (1949, 1958) which is the X, Y, Z axial set in the trigonal system. The phonons which are central to discussion of mode softening have wave vectors parallel to $[\zeta 00]$ (Bauer et al. 1971) in the hexagonal reference frame and will be denoted $[\zeta 00]_H$; their direction of propagation corresponds to the Y direction in the trigonal system which is used to define the ultrasonic-mode propagation directions and elastic stiffness relationships of table 8.1. X-ray measurements (Arnold 1965 and Comes et al 1970) show strong diffuse scattering along the $[\zeta 00]_H$ direction of α quartz. Now neutron elastic scattering studies have shown that softening of the optic-phonons occurs predominantly in the $[\zeta 00]_H$ direction (Bauer et al. 1971) and is the origin of the strong x-ray diffuse scattering along this direction. In the quartz structure there is only one irreducible representation for phonons with wave-vector $\underline{q}$ along the $[\zeta 00]_H$ direction; one phonon branch cannot cross another so as the optic branch softens it depresses the transverse-acoustic branch in this direction. In the long-wavelength limit the slope of the depressed acoustic branch is given by $\omega/q(=(C_{66}/\rho)^{1/2})$.

The measured value of C_{66} for quartz is consistent with the calculated depression of this acoustic branch for wave vector $\underline{q}$ close to the zone center (Bauer et al. 1971); C_{66} shows an anomalous increase with temperature and dC_{66}/dP is anomalously negative value (table 8.5) which is often indicative of acoustic-mode softening. Since the α-β transition in berlinite has close structural affinity with that in quartz, it can be anticipated that anharmonic coupling of the soft optic mode to the transverse acoustic mode should also occur and that the behaviour of C_{66} should reflect this. It does. C_{66} increases with temperature (figure 8.1) and dC_{66}/dP is anomalously negative (table 8.5). In both materials the transverse-acoustic branch having modes propagating normal to the three-fold rotational axis show unusual behaviour of decrease of the elastic constant C_{66} with pressure which is consistent with pressure induced mode softening at the long-wavelength limit. Negative mode Grüneisen parameters, which imply a decrease in the energy of the mode under pressure, are indicative of incipient lattice instability (Chang and Barsch 1973).

The long wavelength acoustic shear mode Grüneisen parameters of berlinite are negative for certain crystallographic directions most markedly in a core of directions centered on the Y ([010]) direction (figure

8.4). This is consistent with the predictions of the soft mode theory and suggests that even far below the phase transition temperature there could already be a degree of anharmonic coupling between the strain and the order parameter.

8.3.5 Thermal Grüneisen Parameter γ^{th}.

As pointed out earlier the anharmonicity of the lattice vibrations is responsible for thermal expansion α of a material, as well as the nonlinear acoustic behaviour under a finite stress. The thermal Grüneisen parameter γ^{th} as stressed in chapter 2 (see table 8.6) is a thermodynamic quantity often used to describe anharmonicity. For a noncubic crystal γ^{th} is a second rank tensor property, and for a rhombohedral crystal its two independent components are given by

$$\gamma_{XY}^{th}=[(C_{11}+C_{12})\alpha_{11}+C_{13}\alpha_{33}]V/C_P$$

$$\gamma_{Z}^{th}=(2C_{13}\alpha_{11}+C_{33}\alpha_{33})V/C_P$$

where C_P is the specific heat at constant pressure (= 93.222 $Jmol^{-1}K^{-1}$) (Wagman et al. 1968). γ_{XY}^{th} has been determined to be 0.649 and γ_{Z}^{th} is equal to 0.646 in the high temperature limit $T(>\theta_D)$. The mean long wavelength acoustic mode Grüneisen parameters γ^{el}_{XY} (= 0.487) and

Table 8.6 : A summary of Grüneisen parameters and thermal expansion (in unit of 10^{-5} K^{-1}) data for rhombohedral crystals in the high temperature limit ($T > \theta_D$). Data are extracted from various tables given by Tu Hailing and Saunders (1983). The thermal expansion data for $AlPO_4$ are taken from Austin et al. (1940).

	$\gamma_{\parallel}^{el}$	$\gamma_{\perp}^{el}$	$\gamma_{\parallel}^{th}$	$\gamma_{\perp}^{th}$	α_{33}	α_{11}
Quartz	-0.16	0.26	0.96	1.18	0.80	1.30
Calcite	0.87	-0.13	-	-	2.51	-0.49
Bismuth	1.90	0.20	1.10	1.32	1.7	1.14
Al_2O_3	0.54	0.39	0.48	0.43	0.57	0.50
$LiNbO_3$	-0.31	0.05	-	-	0.75	1.54
$AlPO_4$	-	-	0.646	0.649	1.59	0.97

γ^{el}_z (= 1.227) are quite different. In the high temperature limit the thermal Grüneisen parameters include contributions from all branches of the phonon spectrum and all wave vectors throughout the acoustic and optic branches which should account for the differences between the components of γ^{el} and γ^{th}.

$$\partial C_{11}/\partial P - B_{11} = -1 + (S_2 + S_3 - 3S_1)C_{11}$$
$$\partial C_{12}/\partial P - B_{12} = 1 + (S_3 - S_1 - S_2)C_{12}$$
$$\partial C_{13}/\partial P - B_{13} = 1 + (S_2 - S_1 - S_3)C_{13}$$
$$\partial C_{33}/\partial P - B_{33} = -1 + (S_1 + S_2 - 3S_3)C_{33}$$
$$\partial C_{44}/\partial P - B_{44} = -1 + (S_1 - S_2 - S_3)C_{44}$$
$$\partial C_{66}/\partial P - B_{66} = -1 + (S_3 - S_1 - S_2)C_{66}$$

9

ELASTIC PROPERTIES OF LITHIUM TETRABORATE

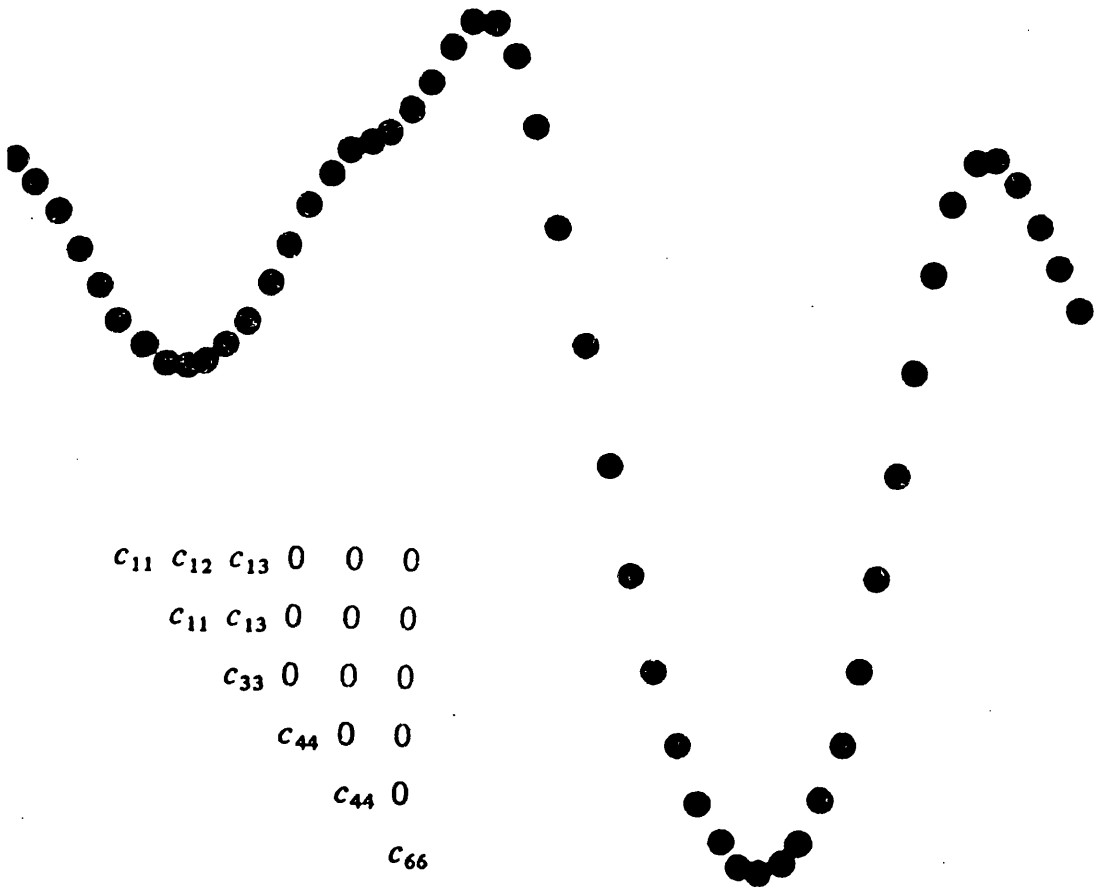

$$\begin{matrix} c_{11} & c_{12} & c_{13} & 0 & 0 & 0 \\ & c_{11} & c_{13} & 0 & 0 & 0 \\ & & c_{33} & 0 & 0 & 0 \\ & & & c_{44} & 0 & 0 \\ & & & & c_{44} & 0 \\ & & & & & c_{66} \end{matrix}$$

CHAPTER NINE

ELASTIC PROPERTIES OF LITHIUM TETRABORATE

9.1 Introduction.

The new piezoelectric material lithium tetraborate ($Li_2B_4O_7$) has attracted much attention as a promising candidate as a surface acoustic wave (SAW) substrate and for bulk acoustic wave (BAW) devices, which require a combination of high electromechanical coupling factor and good temperature stability (Whatmore et al. 1981, Adachi et al. 1983, Peach et al. 1983). Its coupling factor is approximately four times greater than that of berlinite and ten times that of quartz. The phase diagram of the Li_2O-B_2O_3 system reported by Sastry and Hummel (1959) shows that lithium tetraborate does not undergo a phase transition on cooling from the melting point (917°C) to room temperature. There has been a substantial effort to grow single crystals of lithium tetraborate and now high quality crystal are available (Nagel et al. 1977, Robertson and Young 1982). Numerous investigations of lithium tetraborate have been reported which include of infrared transmission (Garrett, Iyer and Greedan 1977) elastic, piezoelectric and dielectric properties (Fukuta et al. 1983, Shiosaki et al. 1984). A complete set of

independent elastic stiffness constants and their temperature dependences (for a limited range of temperature) of this crystal have already been determined (Shorrocks et al. 1981, Adachi et al. 1985). In order to establish its elastic behaviour below room temperature and to find out if it shows any indication of lattice instability, the elastic constants have been measured here down to 4.2K by using the experimental techniques presented in chapter 3.

Values of the hydrostatic pressure derivatives of the elastic constants are usually needed as design parameters to assess the non-linear acoustic contributions to resonators and acoustic devices made from lithium tetraborate. No experimental results have been published on the effects of hydrostatic pressure of the elastic stiffness constants of lithium tetraborate. Hence a central objective of the present work has been to measure the effects of hydrostatic pressure on the elastic constants to quantify the acoustic mode vibrational anharmonicity. Lattice parameter measurements as a function of temperature and hence the linear thermal expansion of lithium tetraborate have also been made here using X-ray diffraction. The available elastic and thermal data then enables us to assess the thermal Grüneisen parameters and thus to make a comparison with the elastic Grüneisen parameters. The relations between elastic anisotropy, acoustic anharmonicity, and thermal expansivity in this non-cubic crystal will be discussed.

9.2 General Description of Crystalline Structure of Lithium Tetraborate.

$Li_2B_4O_7$ belongs to the tetragonal symmetry TI crystal system (space group $I4_1cd$, point group 4mm) with a polar axis along the fourfold crystallographic Z axis (Krogh-Moe 1962). An analysis by Krogh-Moe (1962) showed that lithium tetraborate is composed of borate structural units. Figure 9.1(a) illustrates schematically the basic structural unit of the borate network which consists of two non-planar six membered rings combined in one group. Two boron atoms and one oxygen atom of the group belong simultaneously to both rings. However the group is twisted slightly and so does not have in itself true mirror-plane symmetry. Inspection of this group shows that there are two types of boron atoms in it; the first has a four-fold coordination with four oxygen atoms linked to one boron atom (figure 9.1(a)) whilst the second boron type is three-fold coordinated. The oxygen atoms act as bridges between identical units to form an infinite three dimensional network. The average boron-oxygen distance in the four-fold coordinated tetrahedron is 1.45 Å and the corresponding average distance found for the three-fold coordinated triangle is 1.39 Å.

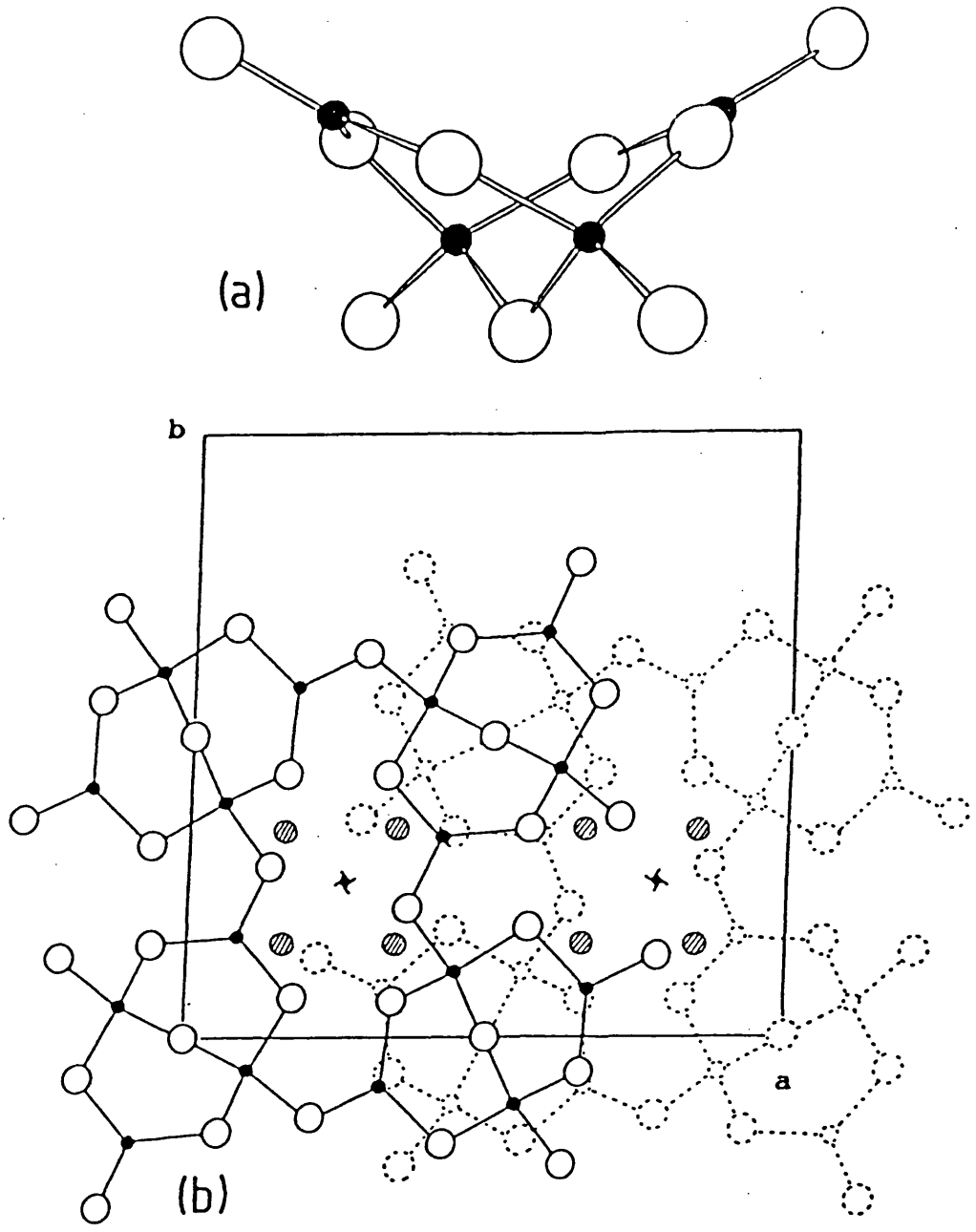

Figure 9.1 : (a) The basic structural unit of the borate networks in lithium tetraborate, as viewed along the a-axis. (b) A projection of the crystal structure along the c-axis. Black spheres represent boron atoms, open spheres represent oxygen atoms, and shaded spheres represent lithium atoms (after Krogh-Moe 1962).

The arrangement of these networks in the lithium tetraborate crystal is shown in figure 1(b) as a projection along the c-axis. The figure illustrates a small arbitrary section of two networks. The broken lines indicate part of a second network, which is a separate, interlocking twin to the first. The unit cell dimensions are signified by the large square. The lithium-oxygen distance estimated by Krogh-Moe (1962) is about 2.1 Å. There are eight molecular units of $Li_2B_4O_7$ per unit cell.

9.3 Experimental Considerations and Results.

9.3.1 Lattice Parameter and Thermal Expansion Measurements.

The lattice parameters a and c of lithium tetraborate have been measured at room temperature using X-ray powder diffractometry and Debye-Scherrer powder photography techniques. A good description of these experimental techniques is given in chapter 17 of the book by Azaroff (1968). Table 9.1 shows values of the interplanar d-spacing of lithium tetraborate which were measured by both techniques. An example of the X-ray diffractometer trace at room temperature is given in figure 9.2. The lattice parameters obtained at room temperature (see table 9.2) are in reasonable agreement with those

Table 9.1 : Interplanar d-spacing in Angstrom units (Å) of indexed planes in lithium tetraborate obtained from (a) X-ray powder (Debye-Scherrer) and (b) X-ray diffractometry methods at room temperature (298K). Results obtained by Krogh-Moe (1968) are included (c) for comparison.

Line no.	Intensity	hkl	d(a)	d(b)	d(c)
1	vvw	020	4.726	4.742	4.740
2	vs	112	4.086	4.082	4.080
3	w	121	3.917	3.923	3.918
4	m	022	3.486	3.487	3.485
5	s	123	2.665	2.669	2.665
6	s	132	2.589	2.592	2.589
7	vvw	040	2.374	2.368	2.369
8	w	141	2.243	2.246	2.243
9	w	233	2.086	2.088	2.086
10	m	224	2.042	2.051	2.040
11	w	134	1.954	1.954	1.951
12	vw	143	1.910	1.911	1.909
13	vvw	125	1.847	1.853	1.851

vvw - very very weak w - weak

m - medium s - sharp

vs - very sharp

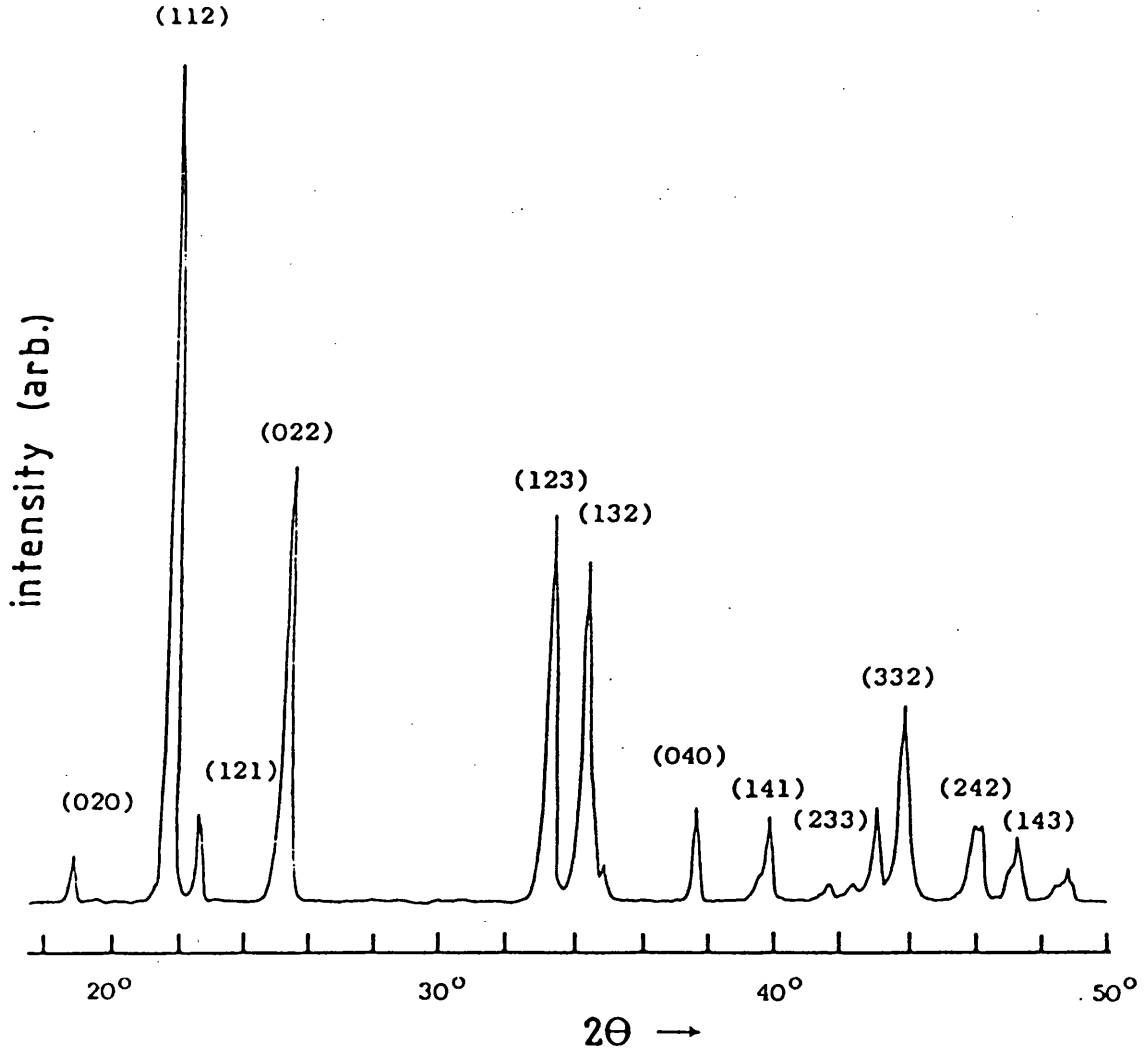

Figure 9.2 : An X-ray diffractometer trace for $Li_2B_4O_7$ powder measured at room temperature (298K).

measured by previous workers (Krogh-Moe 1968, Shorrocks et al. 1981, Bhalla et al. 1985).

The lattice parameters have also been measured as a function of temperature in the range of 80K to 450K using the X-ray diffractometry system (figure 9.3). Within experimental errors the lattice parameters of lithium tetraborate vary almost linearly with temperature and show no indication of a phase transition down to 80K. However the behaviours of the lattice parameters a and c are quite different: a increases and c decreases with temperature respectively. The changes of lattice parameter with respect to temperature have been used to determine the two components α_{11} and α_{33} of the linear thermal expansion coefficient of lithium tetraborate. Room temperature value of α_{11} and α_{33} of this crystal are given in table 9.3. The present results confirm the previous finding that α_{33} is negative (Shorrocks et al. 1981, Emin et al. 1983); this is an unusual feature in the absence of a phase transition and is commonly associated with phonon mode softening. Physically the negative value of α_{33} and positive value of α_{11} indicate clearly how contraction in one principle axis can ensue from large expansion in the other direction. The differences between the linear thermal expansion data (table 9.3) are probably associated with the different experimental technique of measurements and the different ranges of temperature studied. Shorrocks et al. (1981) have measured the linear thermal expansion using X- and

Table 9.2 : The lattice parameters of lithium tetraborate measured at room temperature (298K) using X-ray (a) diffractometry and (b) powder Debye-Scherrer techniques compared to those measured by other workers.

	Present work		Krogh -Moe	Shorrocks et al.	Bhalla et al.
	(a)	(b)	(1968)	(1981)	(1985)
Lattice parameter					
a (Å)	9.479 (±0.020)	9.474 (±0.026)	9.479	9.477 (±0.003)	9.47
c (Å)	10.340 (±0.037)	10.297 (±0.052)	10.280	10.286 (±0.004)	10.26
c/a	1.091	1.086	1.085	1.085	1.083

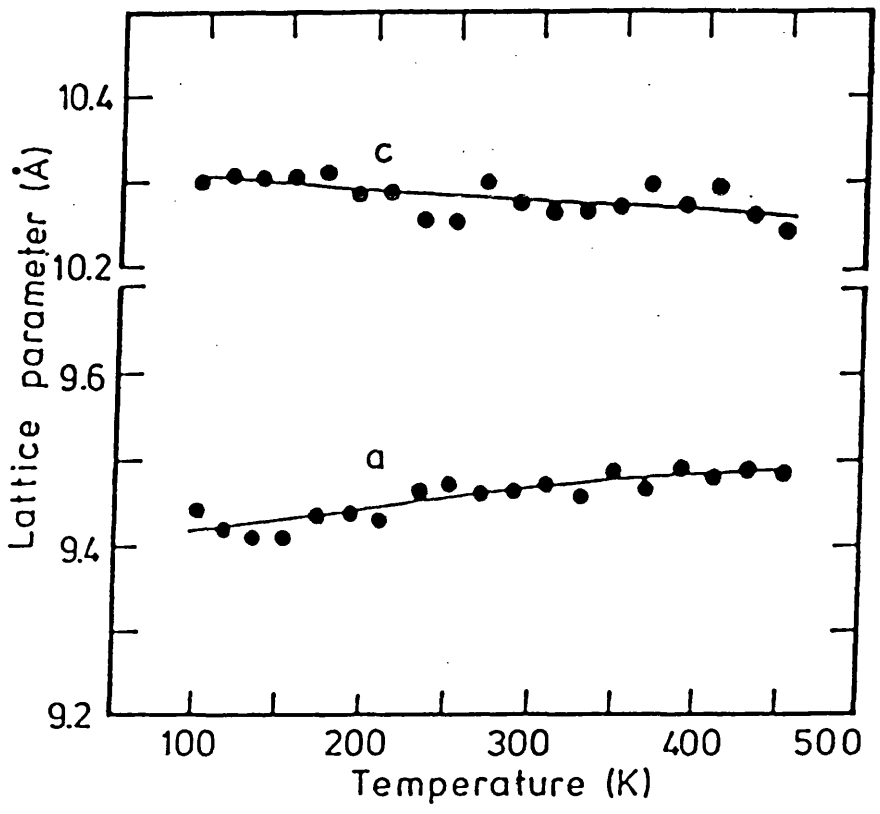

Figure 9.3 : The effect of temperature on the lattice parameters of lithium tetraborate.

Table 9.3 : The room temperature linear thermal expansion tensor components of lithium tetraborate. Data sources (i) Shorrocks et al. (1981), (ii) Emin et al. (1983) and (iii) present work.

Thermal expansion ($\times 10^{-6}$ K^{-1})		Temperature Range	Technique Used	Sources
α_{11}	α_{33}			
12.5	-2.5	-20 - 250°C	Linseis dilatometer	(i)
13.0	-1.5			(ii)
19.8 ($\pm$0.8)	-1.62 ($\pm$0.09)	80 - 450K	X-ray diffractometry	(iii)

Z- bars with Linseis Dilatometer over a temperature range of at least -20 to 250°C whereas Emin et al. (1983) do not give any details of their measurements. The present data for the linear thermal expansion tensor coefficient α_{33} lie between the values obtained by those two groups of workers. However in the case of our measurements α_{11} is somewhat larger but we have obtained the tensor coefficients as the average values α_{11} (=(1/a)(da/dT) and α_{33} (=(1/c)(dc/dT) at 265K (the centre of the temperature range). The other workers did not give any description how they obtained their values of α_{11} but it seems probable that their data were measured only in the neighbourhood of room temperature, so direct comparison is not possible because of the difference in the temperature range of measurement. As mentioned in chapter 2, the thermal expansion of solids is the most obvious consequence of the anharmonicity of lattice vibrations and this can be correlated to the elasticity and thermal Grüneisen parameters γ^{th} which will be discussed later (section 9.4.4).

9.3.2 Crystal Characterisation and Density Measurements.

High optical quality lithium tetraborate single crystals grown from the melt by using the vertical lift technique (Czochralski method) have been obtained from Dr. B. James, G.E.C. Research Centre, United Kingdom. Details of the growth and growth mechanism of this crystal are available elsewhere (Nagel et al. 1977, Garret et al. 1977, Robertson and Young 1982, Adachi et al. 1985). The lithium tetraborate crystals were orientated to an accuracy of 0.5° by the conventional Laue back reflection technique.

The density of lithium tetraborate crystal was determined in two ways; first using Archimedes' principle with toluene as the floatation medium, as 2430 $\pm$ 10 kgm^{-3} at 291K. The theoretical X-ray density is 2436 $\pm$ 8 kgm^{-3}. These results are in reasonable agreement with those reported previously of 2440 kgm^{-3} (Krogh-Moe 1962), 2451 kgm^{-3} (Shorrocks et al. 1981) and 2439 kgm^{-3} (Adachi et al. 1985).

9.3.3 Ultrasonic Wave Velocity and SOEC of a Tetragonal Crystal.

Materials such as lithium tetraborate with 4mm symmetry have eleven independent electro-elastic independent coefficients: six elastic stiffnesses (C_{11}, C_{12}, C_{13}, C_{33}, C_{44}, C_{66}), three piezoelectric (e_{15}, e_{31}, e_{33}), two dielectric constants (ε_{11}, ε_{33}). For a complete determination of all the elastic stiffness constants, nine modes of ultrasonic wave propagation and particle polarisation directions, obtainable from three samples of lithium tetraborate were used. The relationships between the various modes and the elastic constants are given in table 9.3. The first sample is a square faced rectangular parallelepiped having directions of [00$\bar{1}$], [$\bar{1}$10] and [110] with dimensions 14.66mm x 13.66mm x 9.83mm. The second sample is a trapezoidal block of orientation [100], [0$\bar{1}$1] and [011] with dimensions 11.20mm x 14.83mm x 13.67mm and with the angle between the (001) plane and the (011) and (01$\bar{1}$) planes is approximately 42.7°. Both samples are coated with approximately 1000Å of chromium primarily to protect this water soluble crystal. A schematic of these two ultrasonic samples is given in figure 9.4. The third sample is a rectangular block having faces normal to the [001] direction of wave propagation with 14.88mm thickness and is uncoated.

The piezoelectric contribution to effective elastic

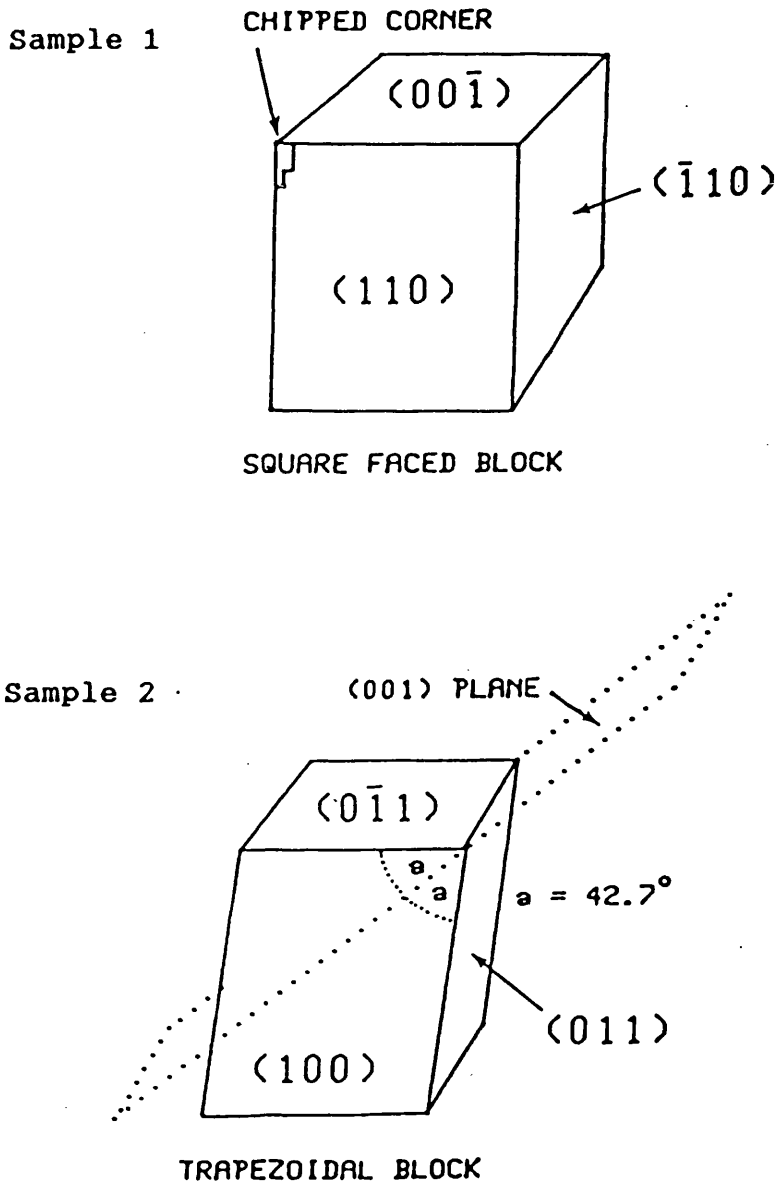

Figure 9.4 : Schematic illustrations of samples 1 and 2 of lithium tetraborate crystal. Both samples were chromium coated. Sample 3 which was uncoated has the same configuration as sample 1.

Table 9.4 : Selected configurational modes of ultrasonic wave propagation N and particle polarisation U directions of tetragonal crystals (4mm symmetry group) and their relation to the effective elastic stiffness constants (ρV^2). V is the measured ultrasonic wave velocity and ρ is a density of crystal.

Mode No.	N	U	Mode	(ρV^2)
1	[100]	[100]	L	C_{11}
2	[100]	[010]	S	C_{66}
3	[100]	[001]	S	$C_{44} + (e_{15})^2/\varepsilon_{11}$
4	[001]	[001]	L	$C_{33} + (e_{33})^2/\varepsilon_{33}$
5	[001]	xy plane	S	C_{44}
6	[110]	[110]	L	$0.5(C_{11}+C_{12}) + C_{66}$
7	[110]	$[1\bar{1}0]$	S	$0.5(C_{11} - C_{12})$
8	[110]	[001]	S	$C_{44}+(e_{15})^2/\varepsilon_{11}$
9	[011]	ϕ (~45°)	QS	$0.5(A+(A^2-B+C^2)^{0.5})$
				$A = C_{44}+0.5(C_{11}+C_{33})$
				$B = (C_{11}+C_{44})(C_{33}+C_{44})$
				$C = C_{13}+C_{44}$

stiffness constants can be significant in the modes of configurations: $\underline{N}[100],\underline{U}[001]$, $\underline{N}[001],\underline{U}[001]$ and $\underline{N}[110],\underline{U}[001]$; elastic stiffness constants measured for these modes are denoted with superscript D and termed as stiffened modes. The unstiffened modes (denoted with superscript E) refer simply to the effective elastic constants to which piezoelectric constants do not contribute. When the subscript is omitted, the corresponding elastic stiffness constants belong to the unstiffened one (there are the same as those denoted by the superscript E). The individual elastic constants C_{11}^{E}, C_{33}^{D}, C_{44}^{E}, C_{44}^{D} and C_{66}^{E} can be obtained from single velocity measurements in pure mode directions; the rest must be deduced from a combination of ultrasonic wave velocity measurements (see table 9.4). The evaluation of elastic stiffness constants C_{33}^{D}, C_{44}^{E}, $(C_{11}+C_{12}+2C_{66})/2$, C' $(=(C_{11}-C_{12})/2)$ and C_{44}^{D} has been carried out using the first sample (1). The second sample (2) was employed to determine the elastic constants C_{11}, C_{66}, C_{44}^{D} and a combination of elastic constants for mode 9 in table 9.4. An extensive range of experiments showed that in the first sample (1) it was not possible to propagate an exponentially decaying echo train for either mode 4 or mode 5 (in table 9.4), and hence to evaluate the elastic constants C_{33}^{D} and C_{44}^{E} as a function the temperature and hydrostatic pressure from measurement made on those modes. Most probably mode conversion occurred along [001] direction in the first sample (1)

disrupting the normally excellent echo trains in this material. However appropriate modes could be satisfactorily propagated in the uncoated sample (3) in which the ultrasonic wave velocities measurements have been carried out to enable determination of the temperature and hydrostatic pressure dependences of the elastic constants C_{33}^D and C_{44}^E.

The ultrasonic wave velocities measurements have been made of modes 4 and 5 (table 9.4) on coated and uncoated samples to obtain the effective elastic constants in both conditions. For mode 5, the uncoated sample gives the room temperature C_{44}^E of 5.81 x 10^{10} Nm^{-2} whilst for the coated sample C_{44}^E is 5.89 x 10^{10} Nm^{-2} , a 2% difference. For the mode 4 (see Table 9.4), the elastic stiffness C_{33}^D for the coated and uncoated samples are 6.80 x 10^{10} Nm^{-2} and 6.82 x 10^{10} Nm^{-2} respectively. The difference between these two values is only about 0.3%. These observation indicate that the effect of coating of the sample does not influence greatly the effective elastic stiffness constants. The elastic stiffness constants of lithium tetraborate obtained at room temperature tabulated in table 9.5 are in reasonable agreement with those quoted in the literature. C_{33}^E itself has been calculated by using piezoelectric and dielectric data of Adachi (1985) by using equation,

$$C_{33}^D = C_{33}^E(1 + (k_{33})^2)$$

where

$$(k_{33})^2 = e_{33}^2/\varepsilon_{33}C_{33}^E.$$

Table 9.5 : The second order elastic stiffness tensor components in units of (10^{10} Nm^{-2}) and elastic compliances in units of 10^{-12} m^2N^{-1} of lithium tetraborate. E and D denote the unstiffened and stiffened modes respectively.

C_{IJ}	Present work 298K	Adachi et al. (1985) 298K	Shorrocks et al. (1981) 293K
Elastic stiffness constants			
C_{11}^E	12.68 ± 0.02	13.50	12.67
C_{12}^E	0.10 ± 0.08	0.36	0.05
C_{13}^E	2.39 ± 0.14	3.35	3.0
C_{33}^D	6.82 ± 0.04		
C_{33}^E	5.62 ± 0.07	5.68	5.39
C_{44}^E	5.81 ± 0.03	5.85	5.50
C_{66}^E	4.57 ± 0.04	4.67	4.60
Elastic compliance constants			
S_{11}	8.6	S_{33}	21.2
S_{12}	0.7	S_{44}	17.2
S_{13}	-4.0	S_{66}	21.9

9.3.4 Temperature and Hydrostatic Pressure Dependences of the Ultrasonic Wave Velocities.

The temperature variation of ultrasonic wave velocities of most of the modes was measured using the pulse echo overlap technique (chapter 3) in the range 4.2K to 298K. The results are presented in figure 9.5 as the relative change of velocity with respect to values measured at 298K. In all cases the velocity measurements taken with decreasing temperature fell on the same line as those obtained with increasing temperature: there is no hysteresis. A set of the elastic stiffness tensor components of lithium tetraborate are plotted for the first time as a function of temperature in figure 9.6. In general the temperature dependences of the elastic stiffnesses of lithium tetraborate do not show the normal behaviour of a crystal.

The effect of hydrostatic pressure on the natural wave velocity of lithium tetraborate is shown in figure 9.7 and the calculated slopes are given in table 9.6. From these values the hydrostatic pressure derivatives (dC_{IJ}/dP) of each mode have been calculated using the equations derived by Tu Hailing and Saunders (1983) and presented in table 9.7 together with the hydrostatic pressure derivatives B_{IJ} in thermodynamic form. The isothermal pressure derivatives of the elastic stiffness tensor components have been calculated by employing

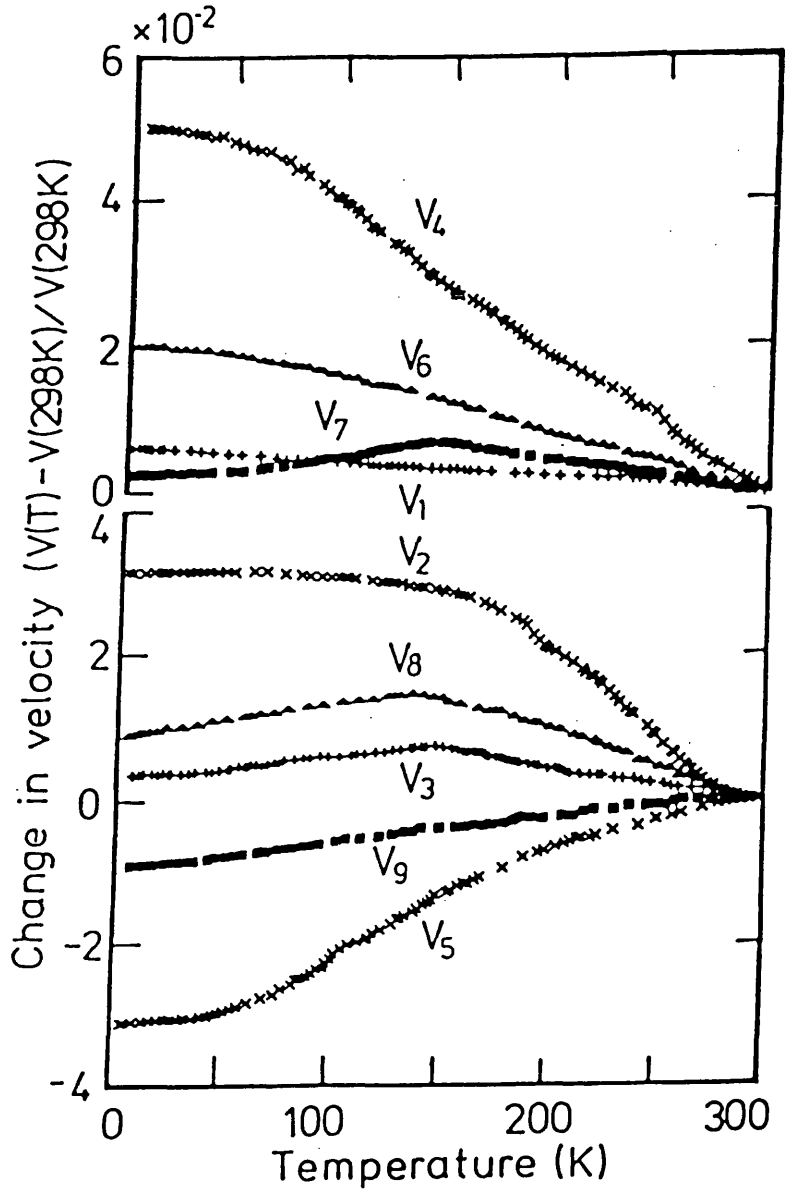

Figure 9.5 : The relative change of ultrasonic wave velocities as a function of temperature of lithium tetraborate. The nomenclature used for the velocity of each mode V_i is that given in table 9.4.

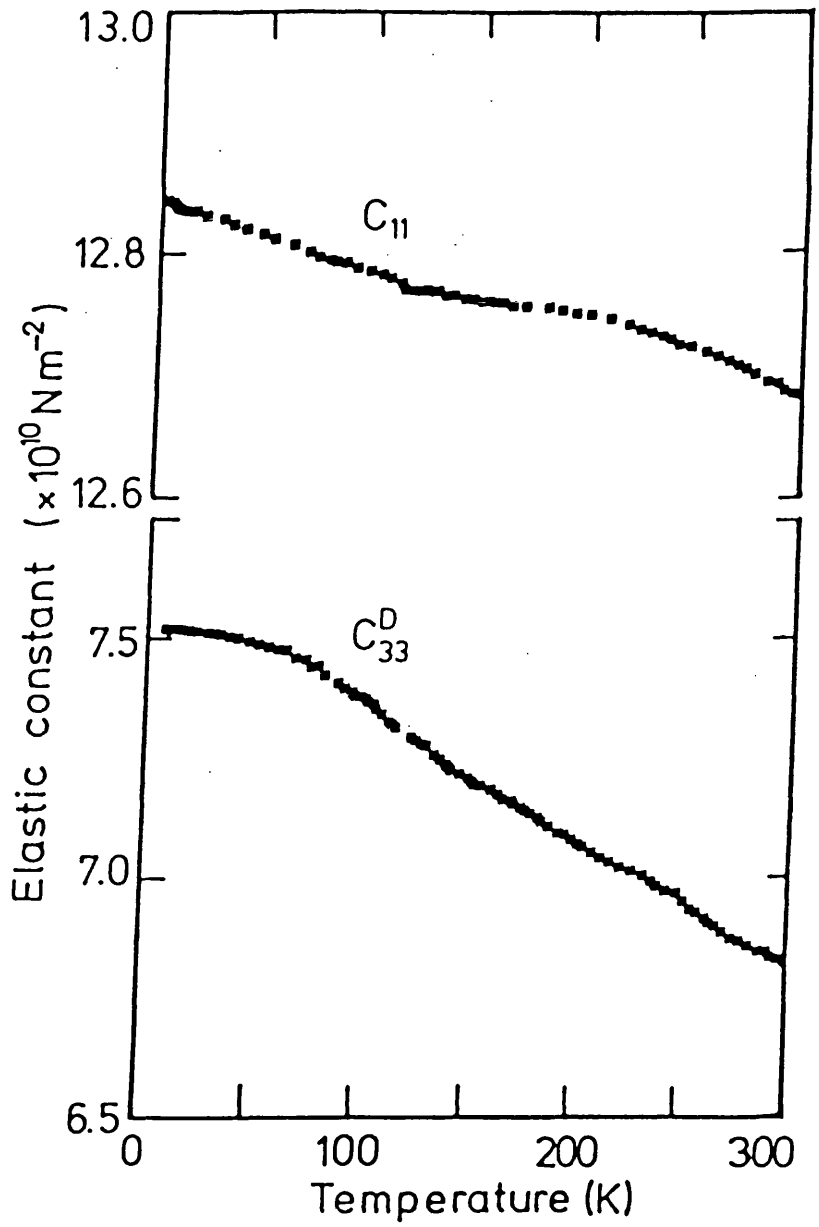

Figure 9.6(a): The temperature dependences of elastic tensor components of lithium tetraborate.

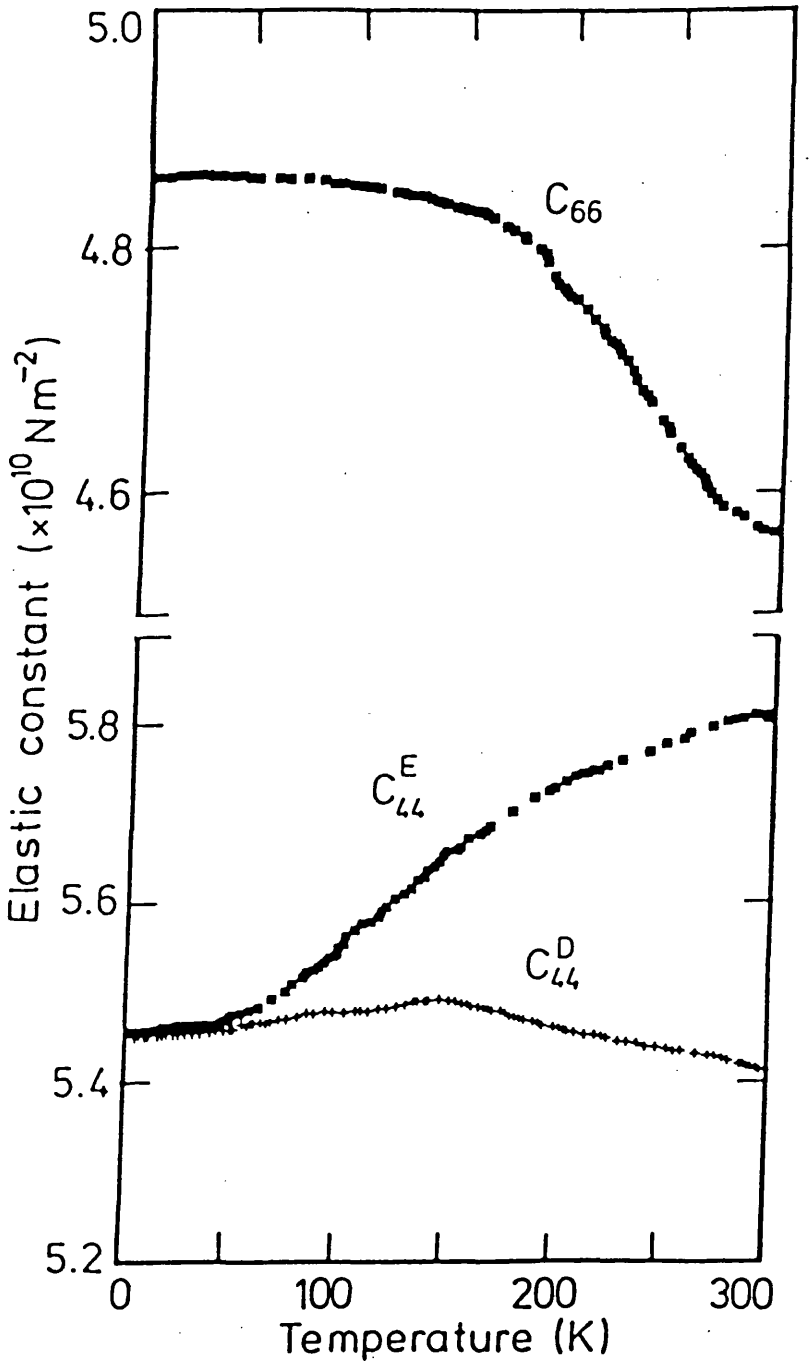

Figure 9.6(b): The temperature dependences of elastic tensor components of lithium tetraborate.

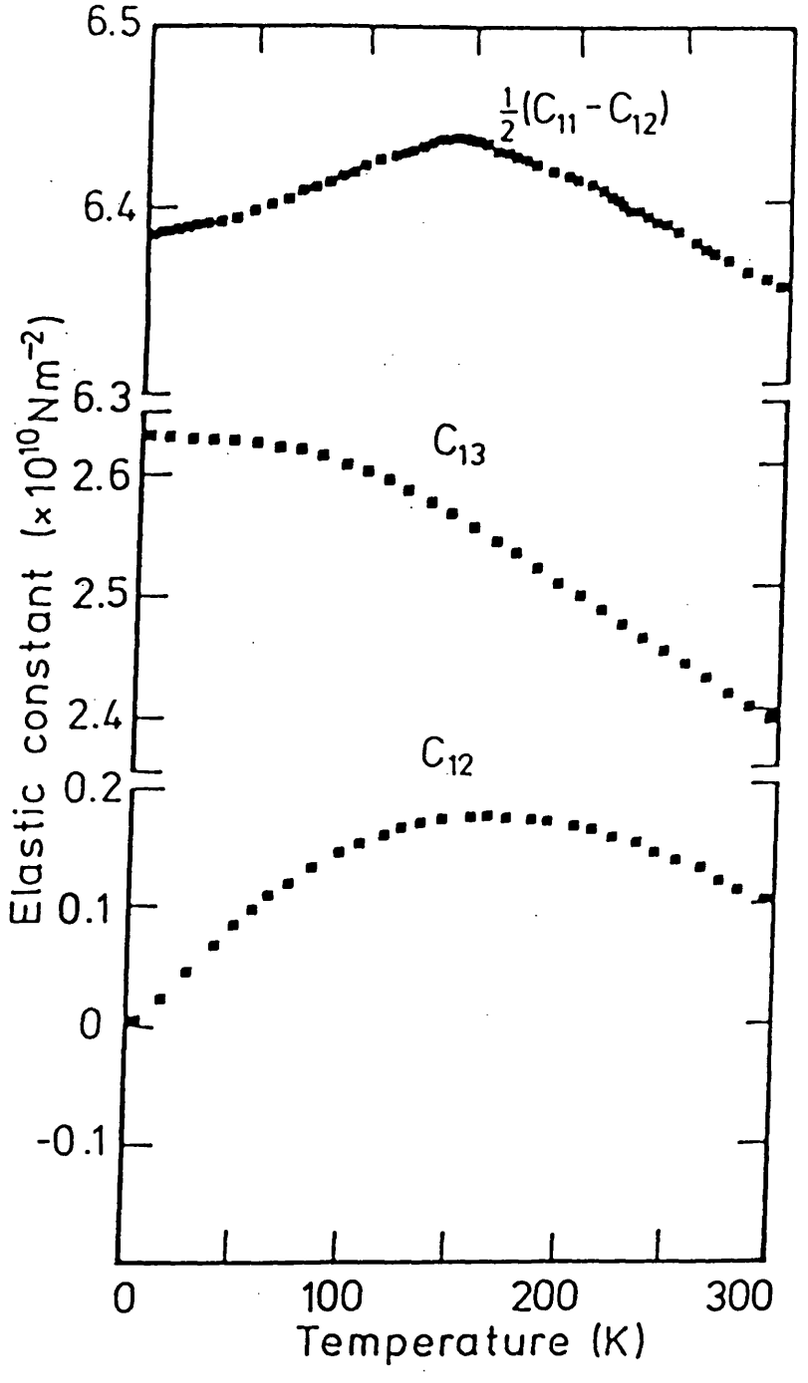

Figure 9.6(c): The temperature dependences of elastic tensor components of lithium tetraborate.

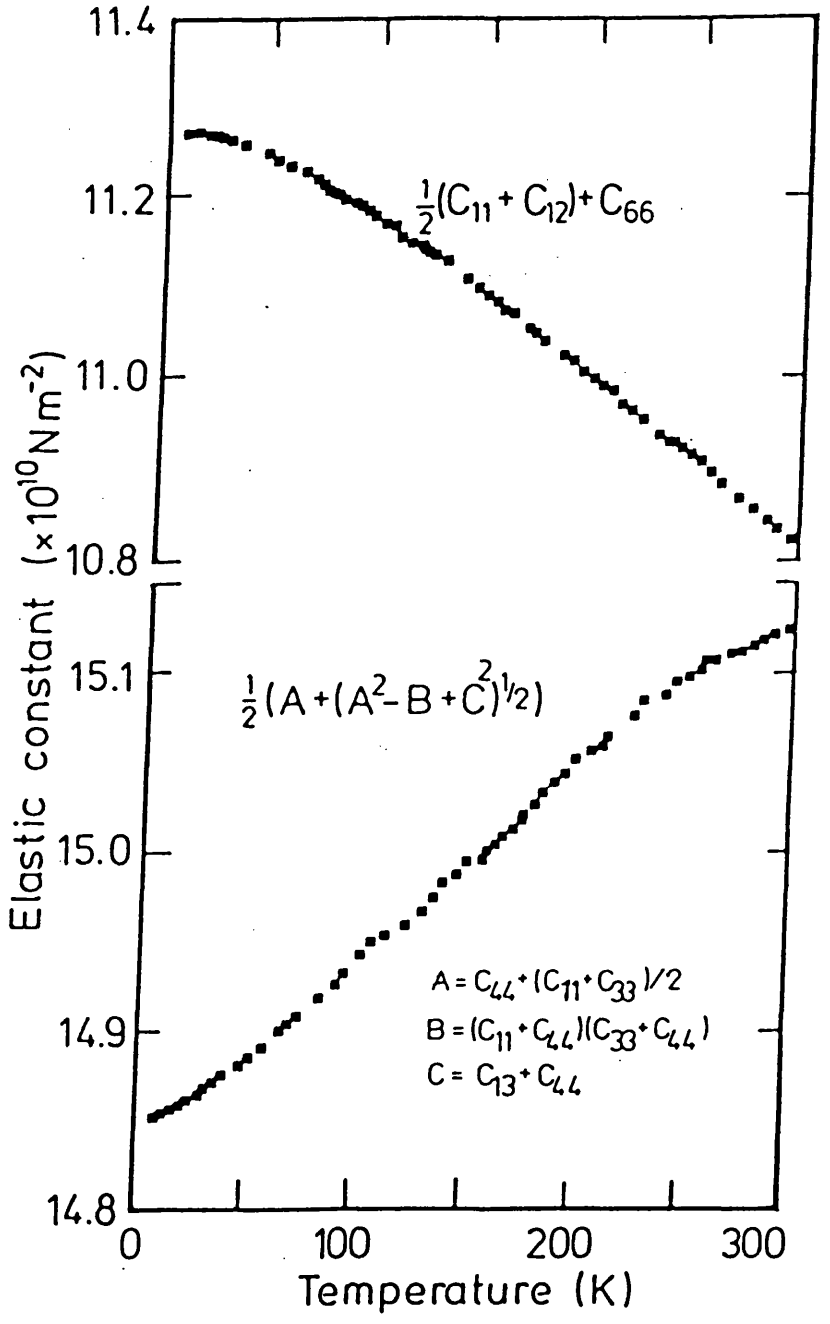

Figure 9.6(d): The temperature dependences of elastic tensor components of lithium tetraborate.

equation (2.28) of chapter 2 (Overton 1962, Anderson 1966) since the thermal expansion and elastic constants as a fuction of temperature have now been measured. As expected the differences between the isothermal and adiabatic constants are not too large. The compression of this crystal estimated at high pressure has been calculated using the Murnaghan equation-of-state (chapter 2) and the result is plotted in figure 9.8. From the plot it can be seen that lithium tetraborate is slightly easier to compress than the other two piezoelectric crystals $AlPO_4$ (chapter 8) and SiO_2 (McSkimin, Andreath and Thurston 1965).

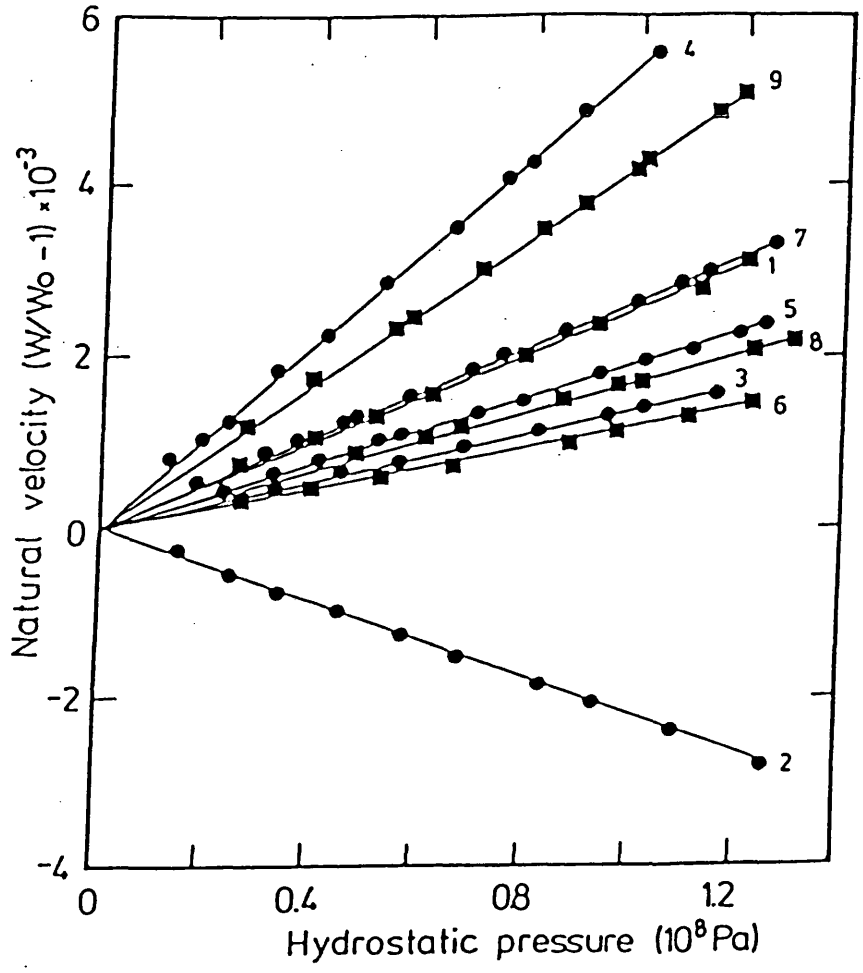

Figure 9.7 : Relative change in natural ultrasonic wave velocity under hydrostatic pressure for $Li_2B_4O_7$. Numbers adjacent to each plot represent to the modes whose propagation and polarisation directions are tabulated in table 9.4. Values of $(\rho W^2)'_{P=0}$ derived from these data are listed in table 9.6.

Table 9.6 : Natural wave velocity W (units ms^{-1}), the initial slope $[W^{-1}(dW/dP)]_{P=0}$ of the hydrostatic pressure dependence of the natural wave velocity (units 10^{-11} m^2N^{-1}), effective elastic stiffness constants $(\rho W^2)_{P=0}$ (units 10^{10} Nm^{-2}) and the hydrostatic pressure derivatives of the second order elastic constant $(d\rho W^2/dP)_{P=0}$ for each ultrasonic mode whose configurations are given in table 9.4 for lithium tetraborate at 298K.

Mode No.	W	$[W^{-1}(dW/dP)]_{P=0}$	$(\rho W^2)_{P=0}$	$(d\rho W^2/dP)_{P=0}$
1	7224	2.55	12.68	8.20
2	4337	-2.21	4.57	-1.42
3	4720	1.35	5.41	2.17
4	5297	5.53	6.82	7.36
5	4889	1.88	5.81	2.03
6	6675	1.18	10.83	3.99
7	5114	2.54	6.36	4.07
8	4697	1.68	5.36	2.51
9	7887	4.27	15.12	13.71

Table 9.7 : The hydrostatic pressure derivatives of the effective $(dC_{IJ}/dP)_{P=0}$ and thermodynamic (B_{IJ}) second order elastic tensor components of lithium tetraborate at 298K. E and D denote the unstiffened and stiffened modes respectively.

dC_{IJ}/dP	Adiabatic	Isothermal	B_{IJ}	Adiabatic
dC_{11}^{E}/dP	8.13	7.94	B_{11}	8.44
dC_{12}^{E}/dP	2.69	2.63	B_{12}	1.68
dC_{13}^{E}/dP	8.94	8.73	B_{13}	8.26
dC_{33}^{D}/dP	7.36	7.17	B_{33}	10.52
dC_{44}^{E}/dP	2.03	1.98	B_{44}	3.80
dC_{66}^{E}/dP	-1.42	1.39	B_{66}	-0.68

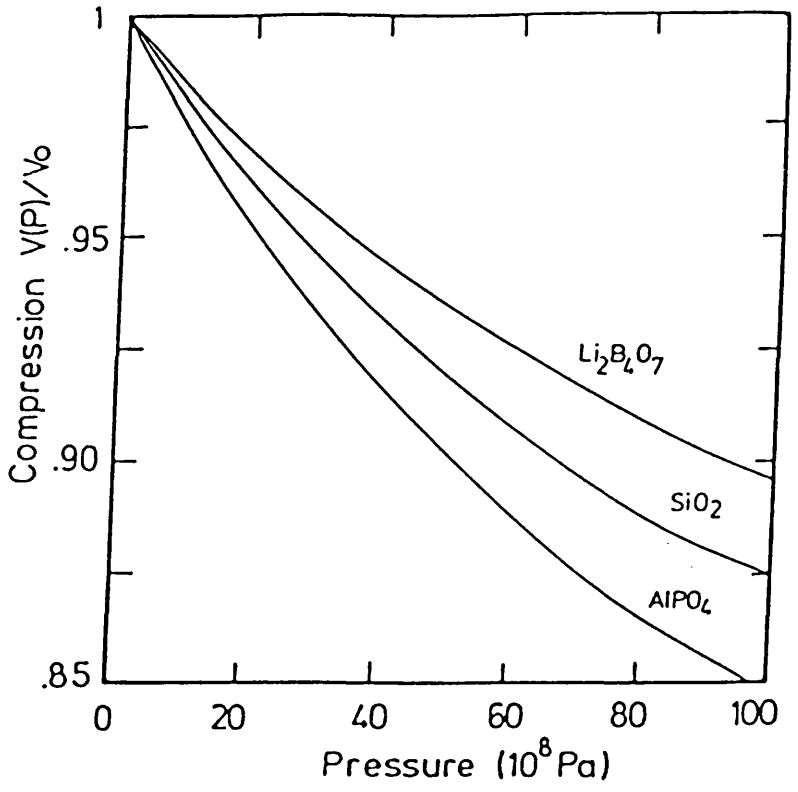

Figure 9.8 : The compression of lithium tetraborate, quartz and berlinite extrapolated up to very high pressures using the Murnaghan equation of state. The basic data of quartz were taken from McSkimin, Andreatch and Thurston (1965).

9.4 Discussion.

9.4.1 Anisotropic Elastic Behaviour of Lithium Tetraborate

The degree of anisotropy of a noncubic crystal can be seen at glance through the behaviour of the ultrasonic wave propagated along various crystal directions. Inspection of the ultrasonic wave velocities in lithium tetraborate shows that the longitudinal wave propagating along the [100] direction is very fast (7224 ms^{-1}) compared to that propagating along the [001] direction which is only 5297 ms^{-1} (table 9.6). This anisotropy is also reflected by the pattern of the elastic stiffness tensor components of $Li_2B_4O_7$; it is particularly significant that C_{11} is much larger than C_{33}. Furthermore $C_{44} > C_{66}$ and $C_{13} > C_{12}$.

Knowledge of the linear compressibilities is useful in gaining more information on the elastic anisotropy because these quantities relate directly the interatomic binding forces and elasticity of solids. For a uniaxial crystal these linear compressibilities, which determine a material's response to a moderate applied stress, are given by β_{XY} in XY plane and β_Z along fourfold Z-axis,

$$\beta_{xy} = S_{11} + S_{12} + S_{13}$$

$$\beta_z = 2S_{13} + S_{33}$$

where the S_{IJ} are the elastic compliances tensor components. Using our elastic data (table 9.5), these two components of linear compressibilities have been calculated: β_z is 1.32 x 10^{-11} m^2N^{-1}, β_{xy} is 0.53 x 10^{-11} m^2N^{-1}. The volume compressibility (the inverse of the bulk modulus) of a uniaxial crystal is given by

$$\beta_v = \beta_z + 2\beta_{xy}$$

For lithium tetraborate β_v is 2.38 x 10^{-11} m^2N^{-1}. At room temperature β_z is about 2.5 times greater than β_{xy}. So it can be seen that under an applied hydrostatic pressure this crystal has a pronounced anisotropic response; it contracts about 2.5 times as much in the Z direction as in directions in the XY plane.

The anisotropic elastic behaviour of lithium tetraborate can also be depicted through the variation of the Young's modulus at various crystal orientations. Young's modulus itself can be defined as the ratio of the longitudinal stress to longitudinal strain (Nye 1960). For a stress applied in a given direction (with direction cosines l_1, l_2, l_3), the Young's modulus (E) of a tetragonal crystal belonging to the 4mm Laue group is given by

$$1/E = (l_1^4 + l_2^4)S_{11} + l_3^4 S_{33} + l_1^2 l_2^2(2S_{12} + S_{66}) + l_3^2(1 - l_3^2)(2S_{13} + S_{44})$$

Figure 9.9 shows, the dependence of Young's modulus upon crystal orientation. The maximum value of Young's modulus at room temperature is found in the XY plane (E_M = 12.82 x 10^{10} Nm^{-2}) while the minimum (E_m = 5.91 x 10^{10} Nm^{-2}), is parallel to the Z axis. Since these two values are so different, again we can see the significant anisotropy for longitudinal deformations (E_M/E_m = 2.17) which is consistent with the ratio of C_{11}/C_{33} (=2.26).

All these anisotropic elastic behaviours of this crystal, ultrasonic wave velocity, elastic stiffness tensor components, compressibilities and Young's modulus must be due to the nature of crystal structure and its interatomic binding. Analysis of the crystalline structure of lithium tetraborate by Krogh-Moe (1962) shows that the structural units of B_4O_7 form a the network layered structure perpendicular to the fourfold direction (figure 9.1). The linear compressibility data of lithium tetraborate suggest that this crystal has relatively weaker interatomic binding forces along the Z direction than those perpendicular to this fourfold axis. In brief all the elastic trends described above are very much in agreement that the concept of the layer-like crystal is a suitable description of the lithium tetraborate structure. In contrast the piezoelectric crystal berlinite (chapter 8) does not show a layer-like structure normal to its uniaxial threefold axis and C_{33}

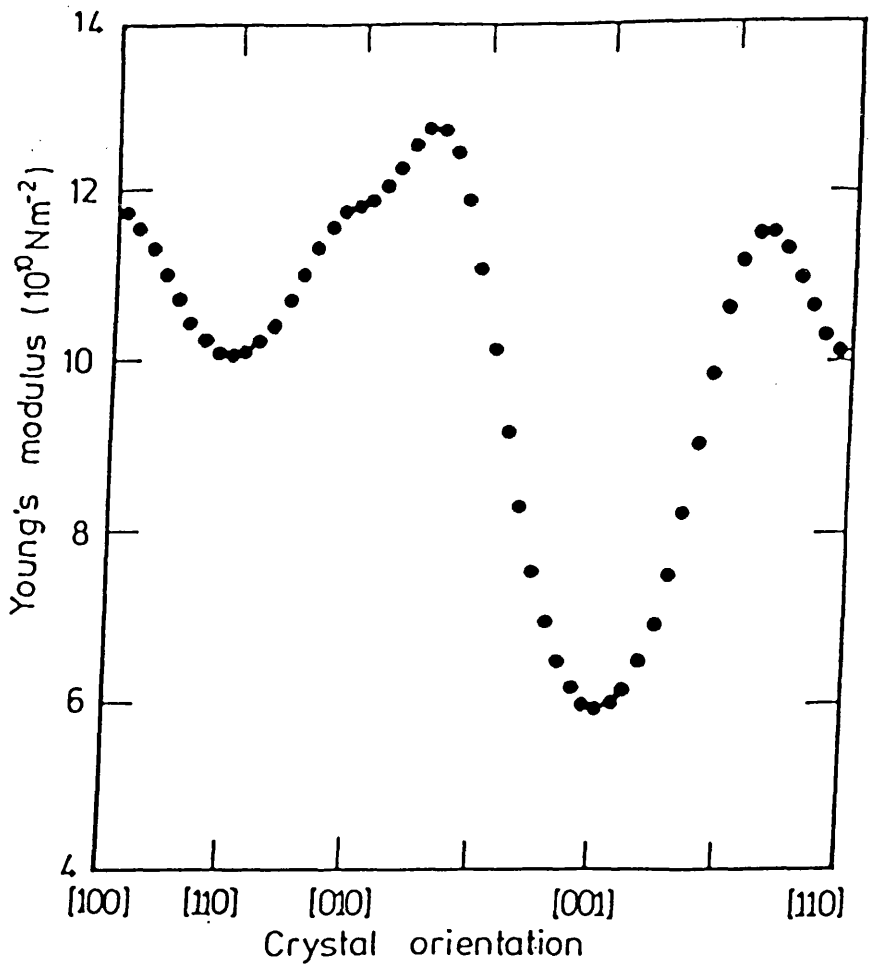

Figure 9.9 : Room temperature Young's modulus of lithium tetraborate in units of 10^{10} Nm^{-2} as a function of crystal orientation.

is greater than C_{11}. Shorrocks et al. (1981) have also treated lithium tetraborate as a layer-like crystal.

However it needs to be emphasised that the layer-like structure of lithium tetraborate is not excessively pronounced since its linear thermal expansion of this crystal is not consistent with the behaviour of linear compressibilities like other layer-like crystal (Bunton and Weintraub 1969, Pace and Saunders 1971, White 1972). Thermal expansion is the result of two effects, namely a strain dependent entropy producing a thermal pressure which is the driving force for thermal expansion, and can be described by Grüneisen functions (section 9.4.3), and the elastic response to this force. Therefore, thermal expansion and linear compressibility tend to be correlated. However this is not true for lithium tetraborate. Normally the thermal expansion tensor components have the same sense as the linear compressibility of solids which show layer-like character i.e. arsenic, antimony, indium or bismuth (Bunton and Weintraub 1969, Pace and Saunders 1971, White 1972). In these materials, the component α_{33} along the Z direction is substantially larger than α_{11}. This is in accord with the well-known fact that in anisotropic crystals the lattice vibrations are more easily excited in the softer direction, so that thermal expansion and linear compressibility are greater in that direction (White 1972). Since the bonds between an atom and its neighbours within a layer are strong compared with those with its

nearest neighbours in the adjacent layer, the elastic stiffness within a layer is substantially larger than that normal to the layers (i.e $C_{11} > C_{33}$ and $S_{33} > S_{11}$, Pace and Saunders 1971). Thus as the temperature is raised from a very low value, the lower-energy lattice vibrations in the soft direction will be the first to be excited, so that α_{33} increases more quickly than α_{11} (Bunton and Weintroub 1969). This can produce a contraction within the layer plane, because the linkage depends on the negative cross-compliance, which leads to negative low-temperature values of α_{11} for antimony and arsenic and very small but positive α_{11} of bismuth. However this is not so for lithium tetraborate; which has the unusual thermal feature that its linear thermal expansion coefficient (table 9.3) is greater along X direction and has negative α_{33} along Z direction in spite of the elastic properties being consistent with a layer-like structure.

9.4.2 Temperature Dependences of the SOEC

Figure 6(a)-(d) shows the variation of the elastic constants with temperature. The stiffness tensor components C_{66}, C_{33}^{D} and C_{13} show a decrease with increasing temperature and flattening out at low temperatures - the usual behaviour found in many crystalline materials. The elastic stiffness tensor component C_{11} exhibits a somewhat unusual feature in the low temperature region: its magnitude increases as the temperature approaches 4.2K rather like that found in many amorphous materials (see chapter 6). Interestingly the shear elastic constant C_{44}^{E} shows a positive gradient in the whole range of temperature studied; this shows that [010] polarized shear acoustic phonons propagated along the [100] direction soften anomalously with decreasing temperature. The shear elastic stiffnesses C' (=$(C_{11}-C_{12})/2$), C_{44}^{D} and also C_{12} exhibit unusual behaviour, that is negative temperature dependences in the range 298K to 170K, a maximum elastic stiffness constant at about 170K and then show positive temperature dependences below 170K. Figure 9.6(b) shows that below 50K within experimental error the temperature derivatives of C_{44}^{D} and C_{44}^{E} are similar. The shear modulus of C_{12} is derived using configurational modes 6 and 7 (table 9.4) and its variation with temperature is similar to that of

the effective elastic stiffness tensor component C_{44}^{D}. The temperature derivatives of second order elastic constants at 298K of this lithium tetraborate crystal are presented in table 9.8.

So far only two other groups of workers have been involved in measuring the elastic stiffness tensor components of lithium tetraborate as a function of temperature. Shorrocks et al. (1981) measured the adiabatic stiffness constants as a function of temperature between -20°C to 80°C; they found that the elastic stiffness C_{33}^{D} shows particularly unusual behaviour with temperature, passing through maximum at about 40°C. Adachi et al. (1985) have also reported the temperature gradients of the elastic constants at room temperature although they do not give any detail of how they did their measurements. It is worthwhile noting that both these groups have only presented their measured data at room temperature: elastic stiffness constants (table 9.5) and their first order temperature coefficients (table 9.9). No further details of the variation of elastic stiffness constants with temperature have been given. The present results complete the data for lithium tetraborate over the entire range of temperature extending from 4.2K to 298K. Since the temperature coefficients of elastic stiffness tensor components obtained at room temperature by both groups are available (see table 9.9), a comparison can be made with our measurements. With the exception of the longitudinal

Table 9.8 : The temperature derivatives of the second order elastic stiffness constants (units of 10^6 $Nm^{-2}K^{-1}$) of lithium tetraborate at 298K.

dC_{IJ}/dT	Uncorrected	Corrected by thermal expansion data
dC_{11}/dT	-8.22	-8.23
dC_{12}/dT	-8.39	-8.40
dC_{13}/dT	-11.57	-11.58
dC_{33}^D/dT	-24.47	-24.46
dC_{44}/dT	+6.28	+6.27
dC_{44}^D/dT	-7.90	-7.91
dC_{66}/dT	-9.97	-9.98
$d((C_{11}-C_{12})/2)/dT$	-5.48	-5.49

Table 9.9 : The temperature coefficients of elastic stiffness tensor components of lithium tetraborate (evaluated at room temperature) of present work and compared with data measured by Shorrocks, Whatmore, Ainger and Young (SWAY 1981) and Adachi, Shiosaki, Kobayashi, Ohnishi and Kawabata (ASKOK 1985).

	Present work	SWAY	ASKOK
Normalized temperature coefficients			
$(1/C_{IJ})(dC_{IJ}/dT)$ (x 10^{-6} K^{-1})			
C_{11}	-65 ± 15	-125	-81.1
C_{12}	-8390 ± 100	-14000	-3370
C_{13}	-485 ± 80	-350	-465
C_{33}	-	+354	+364
C_{33}^{D}	-360 ± 12	-	-
C_{44}	+108 ± 10	-23	-18.1
C_{44}^{D}	-135± 20	-	-
C_{66}	-220 ± 25	-480	-272
Temperature range			
T_{min}	4.2K	-20°C	-
T_{max}	298K	+80°C	-
T_{room}	298K	20°C	25°C
Technique Used	Pulse Echo Overlap	Pulse Echo Overlap	Resonant Frequency

modulus C_{33}^D and shear modulus C_{44} the temperature dependences which we have measured are consistent within experimental error with the gradients at room temperature quoted by Shorrocks et al. (1981) and Adachi et al. (1985) (table 9.9). Any differences between the data are probably due to the defect nature of the samples used and the different measurement techniques; Shorrocks et al. (1981) used a very similar technique to ours. An extensive series of experiments has been carried out here with an aim of duplicating the anomalous behaviour reported for C_{33}^D by Shorrocks et al. (1981). However we have not been able to obtain results for the temperature dependence of C_{33}^D which are comparable with their findings. It is worthwhile remarking here again that the mode 4 (table 9.4), which gives C_{33}, is the very one which could not be propagated cleanly in the coated sample (1); our own results refer to an uncoated sample (3). Unfortunately Shorrocks et al. (1981) do not give any details of whether their samples were coated or uncoated, so it is not clear what their electrical conditions were. Our present work shows that the elastic modulus C_{33}^D increases in usual way as the temperature is decreased and has a zero slope near 4.2K. The clean echo train obtained throughout the temperature range studied gives us confidence that the variation of C_{33}^D with temperature is the correct one for an uncoated sample.

Lithium tetraborate is a piezoelectric crystal and so the possibility of piezoelectric coupling effects on the

acoustic waves propagation has to be considered. In general piezoelectric coupling causes certain modes to be mixed acoustic - electromagnetic ones. In this case an electrical component parallel to the wave propagation vector causes elastic disturbances of the waves; in lithium tetraborate this occurs in modes 3, 4 and 8 as explained in section 9.3.3 (see table 9.4). Hence any unusual temperature dependences of piezolectric and dielectric constants could show up in the behaviour of the effective elastic constants associated with these modes. Information on the variation of piezoelectric and dielectric constants with temperature has been presented by Shorrocks et al. (1981) who measured the two tensor components in the temperature range -20°C to 80°C. In addition Adachi et al. (1985) and other workers (Bhalla et al. 1985) have also measured the electric properties of lithium tetraborate; they obtained complete sets of dielectric property data as a function of frequency at elevated temperature. At low frequencies (100Hz) the dielectric constants change markedly at about -20°C; this turning point temperature is frequency dependent. The room temperature dielectric and piezoelectric constants determined by these three groups are collected in table 9.10. However since complete data for the behaviour of piezoelectric and dielectric constants as a function of temperature needed for a quantitative analysis of our elastic properties measurements is not yet available, it is not yet possible to establish whether or not the

Table 9.10 : Room temperature dielectric and piezoelectric constants of lithium tetraborate as measured by Shorrocks, Whatmore, Ainger and Young (SWAY 1981), Adachi, Shiosaki, Kobayashi, Ohnishi and Kawabata (ASKOK 1985) and Bhalla, Cross and Whatmore (BCW 1985).

	SWAY	ASKOK	BCW
Dielectric constants			
ϵ_{11}/ϵ_o	8.97	8.90	-
ϵ_{33}/ϵ_o	8.15	8.07	10
Temperature range			
T_{min}	-20°C	-	-150°C
T_{max}	+80°C	-	+50°C
Piezoelectric constants (Cm^{-2})			
e_{15}	0.36	0.472	-
e_{31}	0.19	0.290	0.2
e_{33}	0.89	0.928	0.9

unusual behaviour of effective elastic stiffness C_{44}^{D}, C' and C_{12} (figure 9.6b-c) with temperature is due to the electrical properties. Bhalla et al. (1985) have reported that this crystal also exhibits pyroelectric properties which have been measured as a function of temperature between -150°C to 50°C. The temperature dependence of the elastic stiffness tensor components is free from evidence of phase transitions, in agreement with our lattice parameter measurements.

9.4.3 Hydrostatic Pressure Derivatives and Acoustic Vibrational Anharmonic Effects

Generally speaking previous observation indicates that materials having unusual positive temperature dependences of elastic stiffness tensor components often show a related tendency for such components to decrease anomalously under pressure. Examples of this for piezoelectric device crystals include the negative value of dC_{66}/dP and positive value of dC_{66}/dT found for berlinite (chapter 8) and quartz (McSkimin et al. 1965). Another crystal which shows similar acoustic mode softening is the tetragonal crystal paratellurite (TeO_2); its shear elastic stiffness tensor component C' ($=(C_{11}-C_{12})/2$) increases slightly with temperature and decreases with pressure; the shear acoustic phonons modes soften along propagation [110] direction with particle polarisation [$\bar{1}$10] direction (Ohmachi and Uchida 1970, Peercy and Fritz 1974).

A somewhat related behaviour is shown by lithium tetraborate; the elastic constant tensor component C_{44}^E has a positive gradient with temperature (figure 9.6b, table 9.8) indicating softening of these shear acoustic phonons. In contrast to the behaviour of the materials in the preceeding paragraph, dC_{44}/dP is positive (table 9.7). But the shear stiffness constant C_{66} does have a

negative gradient with respect to pressure which can be interpreted as softening of the appropriate shear acoustic phonon propagated in [100] direction with [010] particle polarisation direction. However under the influence of temperature this shear elastic stiffness constant has negative temperature derivatives dC_{66}/dT, so it behaves normally, decreasing with rising temperature. This means that in lithium tetraborate the effects of pressure and temperature are different on these two shear acoustic phonons modes. In each case the influence of pressure and temperature have the opposite sense where on the one hand one specific shear acoustic phonon mode softens with temperature but stiffens with pressure, while on the other hand the other shear acoustic phonon softens with pressure but stiffens with temperature. Softening of the acoustic phonons with both temperature and pressure is not mutually exclusive. Hence the elastic behaviour shown by lithium tetraborate is slightly different from those of the three crystals mentioned before, although it is only the shear acoustic phonons which exhibit soft modes in each of these important materials.

In order to gain more information about the mode softening of C_{66}, measurements have been made of the variation with temperature of the hydrostatic pressure dependence of the velocities of a [010] polarized shear wave propagated along the [100] direction. Similar measurements have also been carried out for the stiffened

mode 3 in table 9.4 corresponding to C_{44}^{D}. These measurements give dC_{66}/dP and dC_{44}^{D}/dP as a function of temperature respectively (figure 9.10, table 9.11). In the temperature range of study (-18°C to 95°C) dC_{66}/dP remains negative; a linear extrapolation of the results suggest that it could reach a (more usual) positive value at about 50K. However this prediction can not be proved yet since the temperature of the pressure system can not be reduced further below about -18°C. dC_{44}^{D}/dP has positive values between 18°C to 99°C and is found to increase somewhat as the temperature is increased. Neither of the temperature dependences of these pressure derivatives of the elastic stiffness tensor components show any marked changes which would correspond to variation in vibrational anharmonicity of these shear modes in the temperature range studied. As emphasised in section 9.4.2, any anomalous elastic behaviour of lithium tetraborate might be due to the interaction of soft mode optic modes or from unusual temperature dependence of electrical properties. A strong soft optic-mode interaction could produce negative derivative of dC_{66}/dP. However to date no reported data on the acoustic and optic phonon dispersion curves have been published.

Indications of shear mode softening with temperature or pressure are usually related to incipient lattice instability which can lead to a phase transition. As discussed in chapter 8, both berlinite and quartz exhibit a second order structural phase transition at about 853K

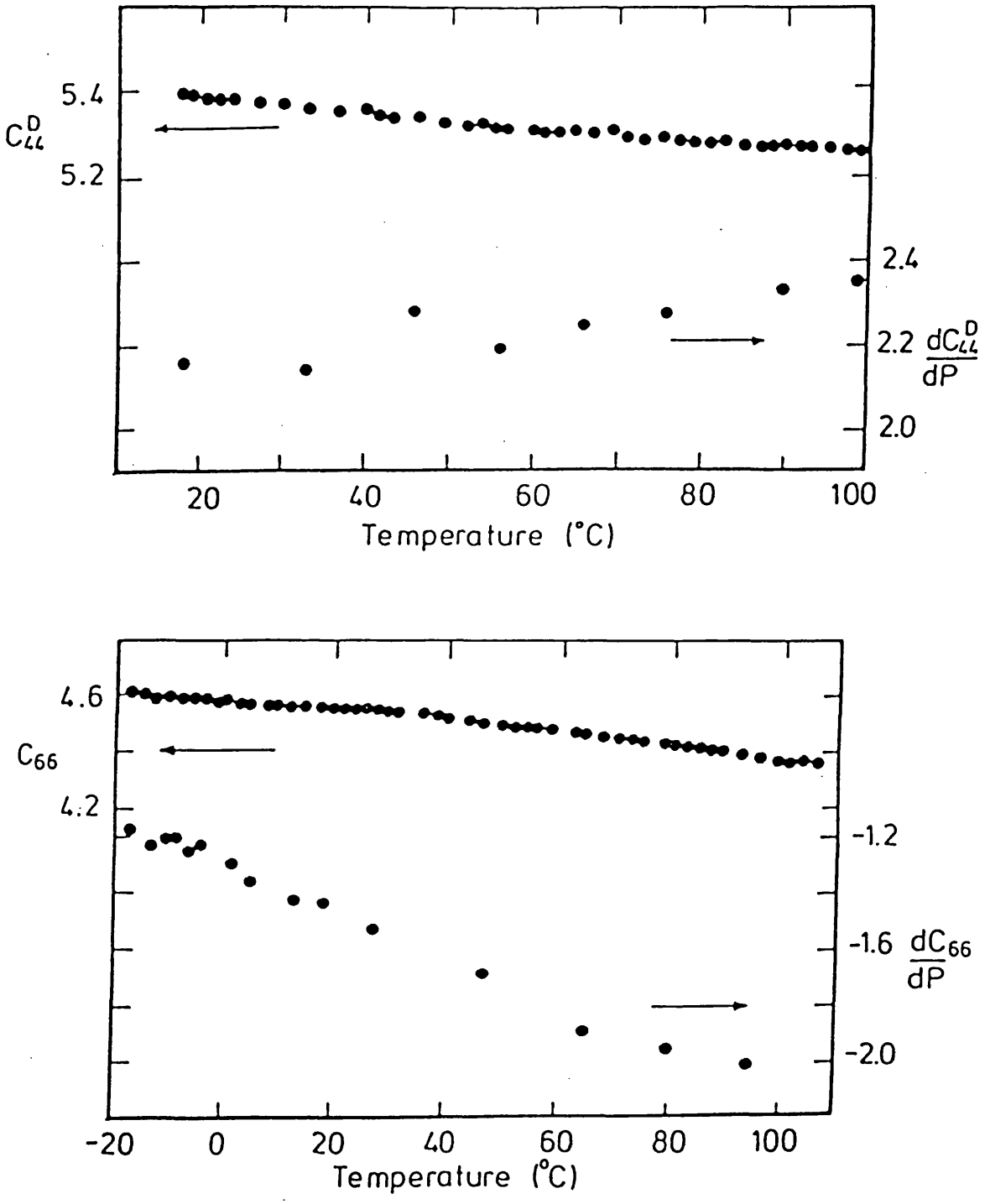

Figure 9.10 : Temperature variation of (a) C_{44}^D and dC_{44}^D/dP and (b) C_{66}^E and dC_{66}^E/dP of lithium tetraborate.

Table 9.11 : Temperature variation of the elastic stiffness constants C_{66} and C_{44}^{D} (in units of 10^{10} Nm^{-2}) and their hydrostatic pressure derivatives for lithium tetraborate single crystals.

T (°C)	C_{66}	dC_{66}/dP
-18	4.62	-1.16
-13	4.60	-1.22
-10	4.59	-1.20
-8	4.59	-1.19
-6	4.59	-1.25
-4	4.58	-1.21
2	4.57	-1.29
5	4.57	-1.35
13	4.56	-1.42
19	4.55	-1.43
27	4.54	-1.52
47	4.50	-1.69
66	4.47	-1.89
80	4.43	-1.95
95	4.38	-2.01

T (°C)	C_{44}^{D}	dC_{44}^{D}/dP
18	5.40	2.16
33	5.36	2.15
45	5.34	2.28
56	5.32	2.19
66	5.31	2.24
76	5.29	2.28
90	5.27	2.34
99	5.26	2.35

(Arnold 1965) driven in part by a soft acoustic mode. The ferroelectric paratellurite crystal exhibits a pressure-induced phase transition at 9 kbar at room temperature which is govern by the softening of the ρV^2 ($(C_{11}-C_{12})/2$) acoustic mode (Peercy and Fritz 1974). This transition is second order in character. Our measurements show that the shear elastic stiffness C_{66} decreases with pressure; this is the first observation of acoustic mode softening with pressure in lithium tetraborate. However no phase transitions have been indicated between 4.2K and the melting point of lithium tetraborate. If this crystal were to behave like paratellurite and have a phase transition induced by pressure, there might be a possibility that a phase transition of lithium tetraborate could take place at high hydrostatic pressures. By utilizing the data obtained for elastic stiffness constant C_{66} and its pressure derivatives and assuming that the elastic stiffness C_{66} would reach a zero value at P_o (where such a phase transition would take place as it does for paratellurite), it can be predicted that this tetragonal crystal might possibly exhibit a phase transition at about 32 kbar.

9.4.4 The Long Wavelength Acoustic Mode and Thermal Grüneisen Parameters of Lithium Tetraborate.

The advantage of having a complete set of second order elastic stiffness tensor components and their hydrostatic pressure derivatives is that they can be used to measure the strain dependences of the lattice vibrational frequencies $\gamma(p,\underline{q})$ accruing from the effect of hydrostatic pressure upon the lattice potential via the generalized Grüneisen parameters (Brugger and Fritz 1967)

$$\gamma(p,\underline{q}) = -\left[\frac{1}{\omega(p,q)}\left[\frac{\partial\omega(p,\underline{q})}{\partial\eta_{ij}}\right]_T\right]_{\eta=0}$$

For a tetragonal crystal belonging to the 4mm Laue group, the elastic Grüneisen parameters of the long wavelength acoustic phonons described in the elastic continuum model (Sheard 1958,) can be written in the following form

$$\begin{aligned}\gamma(p,\underline{N}) = -(2w\beta_\nu)^{-1}\{1 + 2w[&(S_{11} + S_{12} + S_{13})\\ &\times (U_1^2 + U_2^2) + (2S_{13} + S_{33})U_3^2]\\ &- B_{11}(N_1^2U_1^2 + N_2^2U_2^2) - 2B_{12}N_1N_2U_1U_2\\ &- 2B_{13}(N_1N_3U_1U_3 + N_2N_3U_2U_3) - B_{33}N_3^2U_3^2\\ &- B_{44}[(N_1U_3 + N_3U_1)^2 + N_2U_3 + N_3U_2)^2]\\ &- B_{66}(N_1U_2 + N_2U_1)^2\}\end{aligned}$$

where

$$w = C^S_{11}(N_1^2U_1^2 + N_2^2U_2^2) + 2C^S_{12}N_1N_2U_1U_2$$
$$+ 2C^S_{13}(N_1N_3U_1U_3 + N_2N_3U_2U_3) + C^S_{33}N_3^2U_3^2$$
$$+ C^S_{44}[(N_1U_3 + N_3U_1)^2 + (N_2U_3 + N_3U_2)^2]$$
$$+ C^S_{66}(N_1U_2 + N_2U_1)^2.$$

The long wavelength acoustic mode Grüneisen parameters of lithium tetraborate have been computed as a function of crystal orientation and are plotted in figure 9.11. The mode Grüneisen parameters for selected crystal orientations evaluated at room temperature are given in table 9.12. For lithium tetraborate, like other uniaxial crystals, there are two independent components of a Grüneisen tensor, namely $\gamma_\perp$ (= γ_{11} = γ_{22}) and $\gamma_{//}$ (= γ_{33}). The scalar parameter γ (= $2\gamma_{11}+\gamma_{33}$) is the weighted average of the individual mode gammas $\gamma(p,\underline{q})$

$$\gamma = \sum_{p,\underline{q}} \gamma(p,q)c(p,q) \Big/ \sum_{p,\underline{q}} c(p,q)$$

Here

$$c(p,\underline{q}) = kx^2\exp(x)/[\exp(x)-1]^2, \quad [x = \hbar\omega(p,\underline{q})/kT]$$

is the contribution of the mode in branch p and wavevector $\underline{q}$ to the specific heat of the crystal. The

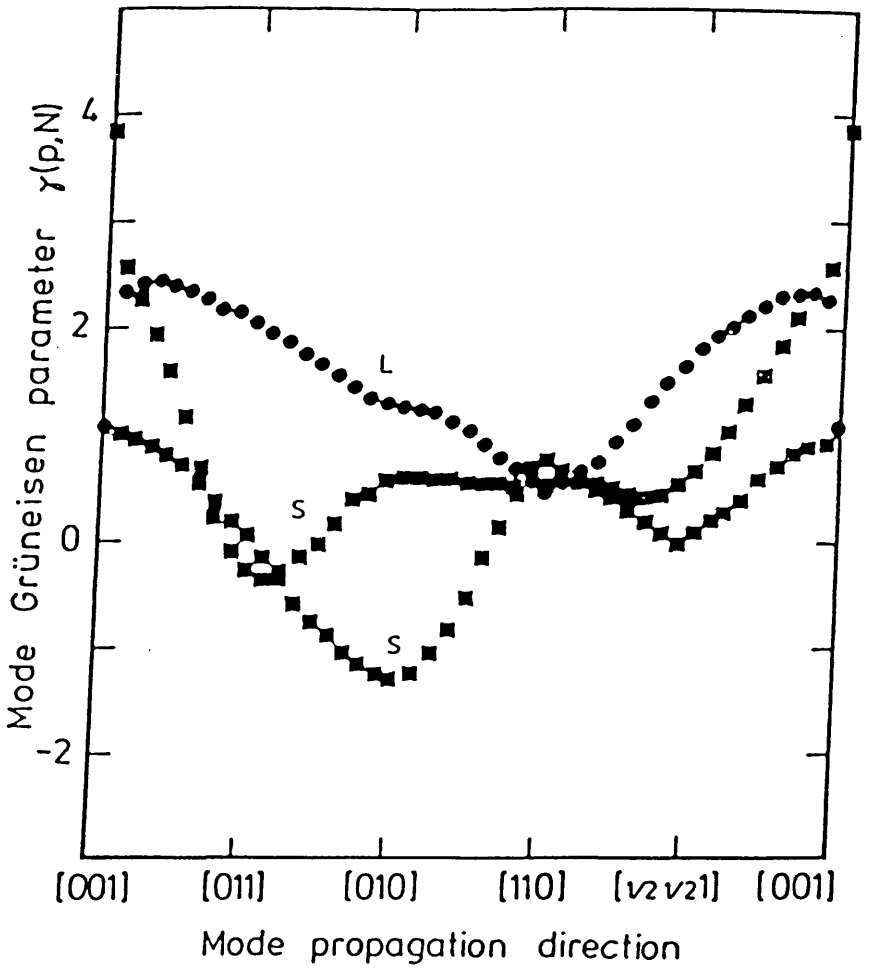

Figure 9.11(a): The long wavelength elastic mode Grüneisen parameters calculated as a function of crystal orientation for a lithium tetraborate single crystal.

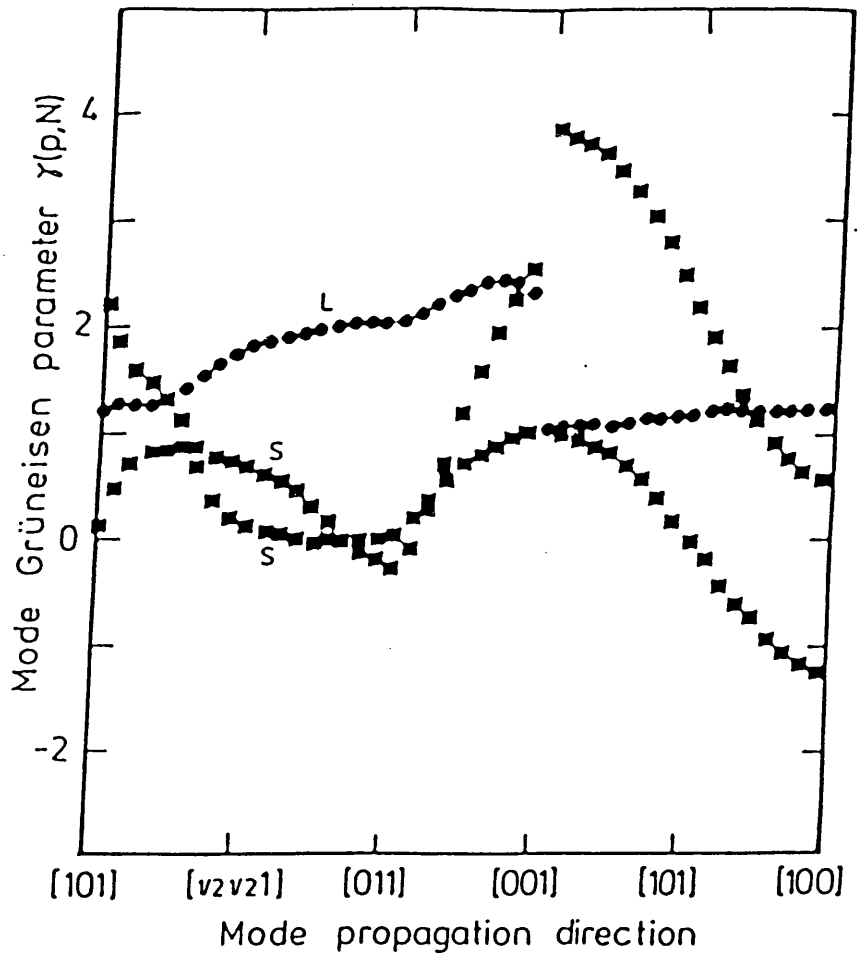

Figure 9.11(b): The long wavelength elastic mode Grüneisen parameters calculated as a function of crystal orientation for a lithium tetraborate single crystal.

Table 9.12 : Directional dependences of the elastic Grüneisen parameters of lithium tetraborate at 298K.

Crystal orientation	Grüneisen parameter		
	shear 1	shear 2	long.
[001]	1.07	3.87	1.07
[101]	2.21	0.05	1.22
[100]	1.29	0.58	1.28
[110]	0.61	0.78	0.52
[011]	0.04	-0.26	2.09

high temperature limit of two components of the mean Grüneisen parameters can obtained by summation over all the zone centre modes $\gamma(p,\underline{q})$ on the acoustic phonon branch using expression of the general form

$$\gamma_H = \frac{1}{3N} \sum \gamma(p, \underline{q})$$

where

$$\gamma(p, \underline{q}) = -(\partial \ln \omega(p, \underline{q}) / \partial \ln V)$$

The summation has been carried out over 26811 modes by dividing the Debye sphere into equal areas with the mode propagation direction centred on each element using a computer programme written by Professor G. A. Saunders. At room temperature we assume that all the modes are classically excited since the elastic Debye temperature θ_D, calculated from low temperature elastic constants, is 302K. For lithium tetraborate the mean Grüneisen parameters in the XY plane and along the Z direction are calculated as 0.62 and 1.40 respectively. The high temperature mean elastic Grüneisen gamma for this crystal is equal to 0.88. A number of interesting features of the acoustic phonons of lithium tetraborate are revealed by these Grüneisen parameters (figure 9.11). The longitudinal mode Grüneisen parameters range between 0.52 to 2.5. The high anisotropy of $\gamma(p,\underline{q})$ is a reflection of the nature of the crystal which has a tendency to show layer-like characteristics (section 9.4.1). As the main

effect of application of hydrostatic pressure is to squeeze the layers together ($\beta_z > \beta_{xy}$), so the influence of the repulsive forces which act between the layers must be especially important. The work done against these forces requires that the energy and frequency of the longitudinal mode propagated down the Z axis should increase substantially when pressure is applied. Hence the mode Grüneisen parameter for this mode is quite large and positive, while those for the X-axis longitudinal mode and Y-axis longitudinal mode are smaller (figure 9.12). The Grüneisen gammas of the shear modes are anomalous in being negative for some directions in the XY plane, achieving minimum values along the X and Y axes; this is a direct consequence of the negative pressure derivative of dC_{66}/dP (table 9.7) and thus of the tendency of the acoustic shear phonons mode propagated in [100] direction with [010] particle polarisation direction to soften under pressure.

As stressed in chapter 2, the anharmonicity of lattice vibrations is responsible for the nonlinear elastic behaviour of a crystal under finite strain and also causes thermal expansion. However, it should be noted that the thermal expansion at a given temperature is determined by summation of the anharmonic effects of all of the excited phonon modes which includes the acoustic modes of the long wavelength limit. At high temperature ($T>\Theta_D$) phonons exist in those optic branches having low enough energy as well as in acoustic branches

in states throughout the Brillouin zone. All these states contribute to thermal expansion. By using the thermal expansion data (table 9.3) and specific heat capacity C_p measured at constant pressure (=3.2 $Jcm^{-3}K^{-1}$) (Bhalla et al. 1985), the thermal Grüneisen parameter γ^{th} (eq. 2.43 and 44) can now be evaluated. Since lithium tetraborate is a uniaxial crystal, there are two principal Grüneisen functions (Barron et al. 1980) (see section 8.3.5). For this crystal the thermal Grüneisen parameter $\gamma_{XY}{}^{th}$ (in the XY plane) has been calculated to be 0.78 and $\gamma_Z{}^{th}$ (along Z axis) as 0.27. Thus the present findings show that the thermal Grüneisen parameter $\gamma_{XY}{}^{th}$ is about three times larger than the one along the Z-axis. Munn (1969) has pointed out that in the direction which has a larger γ^{th} the binding forces are the stronger. This is true in lithium tetraborate for which C_{11} is greater than C_{33}, $S_{33} > S_{11}$ and $\gamma_{XY}{}^{th} > \gamma_Z{}^{th}$. The mean thermal Grüneisen parameter $\bar{\gamma}^{th}$ is given by

$$\bar{\gamma}^{th} = \frac{2\gamma^{th}_{xy}\beta_{xy} + \gamma^{th}_{z}\beta_{z}}{2(S_{11}+S_{12}+S_{13}) + (S_{33}+2S_{13})} = 0.50$$

This mean thermal Grüneisen parameter $\bar{\gamma}^{th}$ is smaller than the mean long wavelength elastic mode $\bar{\gamma}^{el}$ (=0.88): some of the optic phonon modes must have mode Grüneisen parameter γ_i which are less then 0.5 to counteract those of the acoustic phonons in the summation of $\Sigma C_i\gamma_i/\Sigma C_i$ ($= \gamma^{th}$). Here C_i is heat capacity of a mode i.

To conclude, a complete set of elastic stiffness

tensor components of lithium tetraborate as a function of temperature and pressure have been measured. The experimental results show that the influence of temperature and pressure causes unusual behaviour of certain elastic stiffness constants; for instance dC_{44}/dT is positive and dC_{66}/dP is negative. Thus there are indications of softening of certain shear acoustic phonons mode either with temperature or pressure. Much more work needs to be carried out in order to explain the anomalous elastic behaviour which occurs in lithium tetraborate; in particular knowledge of the optic phonons is needed to see if mode softening of optic phonons might be responsible for the unusual elastic properties through an acoustic phonon - optic phonon interaction. However the present study does provide the basic description for understanding the elastic and some aspects of nonlinear acoustic behaviour of lithium tetraborate under the effects of temperature and pressure.

10

ASPECTS OF THE ACOUSTIC MODE SOFTENING

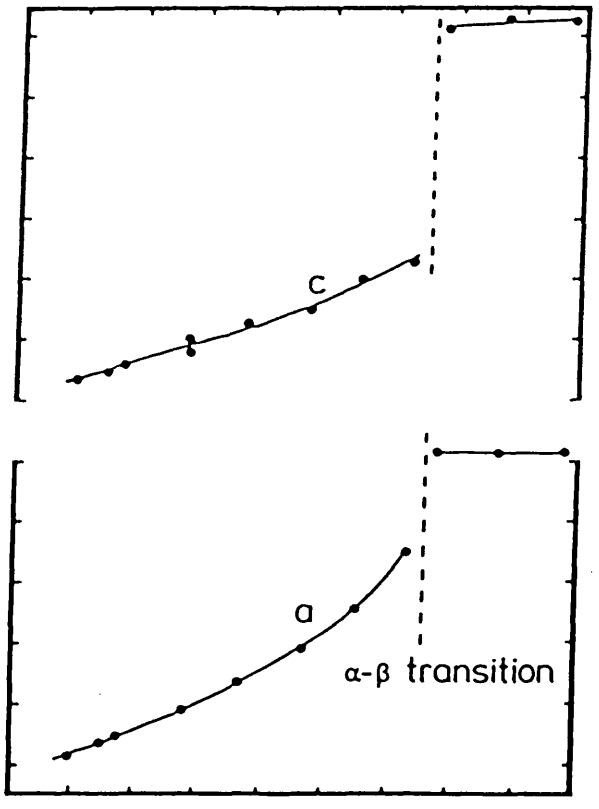

CHAPTER TEN

ASPECTS OF THE ACOUSTIC MODE SOFTENING

Some light has been shed on physical aspects of the elasticity and acoustic mode vibrational anharmonicity at the long wavelength limit in a number of interesting solids which it was anticipated might show acoustic mode softening. The term of mode softening is used simply to mean a normal mode of vibration whose frequency decreases (so that the lattice literally softens with respect to this mode) under the effect of hydrostatic pressure or decreasing temperature or both. This vibrational frequency does not necessarily go to a zero value. The materials investigated have been superionic silver borate glasses, samarium phosphate glasses and single crystals of cubic Ce_3S_4, rhombohedral $AlPO_4$ and tetragonal $Li_2B_4O_7$. For each material the first hydrostatic pressure dependences of the second order elastic constants have been measured successfully and useful knowledge on the interatomic forces and on anharmonic properties has been deduced from the experimental data. The information acquired about the acoustic mode vibrational anharmonicity close to the centre of Brillouin zone of

each solid materials studied has been discussed in terms of mode Grüneisen parameters. The effect of temperature upon the elastic stiffness tensor components has also been considered, especially for samarium phosphate glasses and monocrystalline lithium tetraborate. A number of interesting findings concerning unusual elastic behaviour under the effect of pressure and temperature have been revealed from these ultrasonic experiments and now we present a brief summary of the important results obtained.

Two different series of amorphous materials, silver borate and samarium phosphate glasses, have been studied as a function of composition at room temperature by observing the propagation characteristics of both longitudinal and shear ultrasonic wave velocities. It has been shown that the results when combined with those from other experiments, provide some useful indications about the microscopic nature of these glasses. For the superionic binary silver borate glasses, an increment of mobile silver ions when Ag_2O is included in the recipe changes the coordination of the boron atoms from 3 to 4 (Carini et al. 1984a); this causes the glass to become stiff. However with addition of AgI into the ternary glass networks, the elastic stiffness constants are caused to reduce somewhat. In the case of samarium phosphate glasses, it has been found that the elastic stiffness tensor component C_{11} and the bulk modulus B^S reach minimum values at a composition of about 20 mole%

Sm_2O_3. This feature has been considered to be due to structure change from a three-dimensional cross-linked network to a chain structure typical of the metaphosphate composition; this finds support from Raman spectroscopic studies (Mierzejewski et al. 1988).

It has been suggested that all glasses, at low temperature, possess two-level systems which strongly influence the thermal properties (Phillips 1972, Anderson et al. 1972). Interestingly resonant absorption and relaxation processes have been observed in many glasses, as a result of the interaction of acoustic phonons with such two-level systems. Since the superionic silver borate and samarium phosphate glasses studied here are new ones, part of our work has had the aim of studying their elastic behaviour at low temperature to see if like other glasses, these materials show elastic properties due to the presence of two-level-systems. We have found that both these types of glasses do show unusual behaviour in the lower temperature region (below ~200K); their elastic stiffness tensor components and hence dC_{IJ}/dT increase steadily as the temperature is decreased towards 4.2K. Such a property is compatible with the mechanism of relaxation process caused by the interaction of acoustic waves with two-level systems.

A test of the stability against atomic vibrational frequencies of solids can be made through the inspection of the ultrasonic wave velocities and the elastic stiffness constants as a function of hydrostatic

pressure. Usually the atomic vibrational frequencies increase under external pressure and so dC_{IJ}/dP and hence the anharmonic mode Grüneisen parameters have positive values. However the negative pressure derivative of the shear modulus dC_{44}/dP has been observed in the superionic glasses indicating a slight mode softening. The long wavelength shear acoustic phonon frequencies decrease with hydrostatic pressure and so lead to negative values of the shear γ_S acoustic mode Grüneisen parameter. The longitudinal γ_L of these glasses have the usual positive values. Lambson et al. (1984) have proposed that a strong correlation exists between the mean long wavelength acoustic mode Grüneisen parameter $\bar{\gamma}^{el}$ $(=(\gamma_L+2\gamma_S)/3)$ and the thermal expansion coefficient α for a number of glasses: the present work of these superionic glasses shows excellent agreement with this previously demonstrated linear relationship between $\bar{\gamma}^{el}$ and α. A marked softening of longitudinal and shear acoustic phonons under hydrostatic pressure has also been found in the samarium phosphate glasses; both dC_{11}/dP and dC_{44}/dP are negative and hence so is dB^S/dP. This means physically that these particular glasses become more compressible as the pressure is increased, in contrast with the structurally similar lanthanum phosphate glasses which show normal elastic behaviour with pressure. This anomalous elastic feature under pressure as well as temperature of samarium phosphate glasses probably arises from valence instability or a pressure-varying mixed

valence of the rare-earth samarium ions in these glassy matrix.

Now we turn to discuss the studies made on crystalline solids. First it has been shown that the elastic stiffness tensor components and their hydrostatic pressure derivatives dC_{IJ}/dP of Ce_3S_4 crystal have the same trend and behave normally under pressure as those found in La_3S_4 (Ford et al. 1980) where their dC_{11}/dP > dC_{12}/dP > dC_{44}/dP. The mode Grüneisen gammas in the long wavelength limit for both crystals are all positive at room temperature. Even though Ce_3S_4 crystal does not show any indication of softening acoustic phonons mode under pressure, it has positive temperature derivatives of the longitudinal elastic modulus C_{11} and the shear modulus C' (=$(C_{11}-C_{12})/2$) which means that the associated acoustic phonons soften with temperature (Futterer et al. 1988), and it seems that Ce_3S_4 undergoes a phase transition at very low temperatures.

The search for mode softening has been carried out on two lower symmetry crystals, namely rhombohedral berlinite and tetragonal lithium tetraboratre. The measurements on berlinite extend previous observations that its elastic and physical behaviour is similar to that of quartz which has a similar structure. However it is less stiff elastically than quartz. Furthermore it has been found that berlinite has smaller pressure derivatives of the second order elastic stiffness tensor components; thus application of pressure does not result

in as strong an increase of the stiffness as it does for quartz. Berlinite responds anisotropically under hydrostatic pressure in a similar manner to quartz; a line in the XY plane contracts rather more for a given pressure than one in the threefold Z direction. Large compressibility along the fourfold Z-axis compared those in the XY plane has been found in lithium tetraborate, indicating weaker interatomic bonding along the Z-axis. However its linear thermal expansion tensor components do not behave in this sense and so lithium tetraborate can not be considered simply as a layer-like crystal.

The present observations have shown that only the shear elastic stiffness tensor component C_{66}, of the piezoelectric crystals berlinite and lithium tetraborate, have unusual decrease with increasing hydrostatic pressure (as also found in quartz); the corresponding transverse acoustic phonon modes soften under pressure. This implies that the associated Grüneisen parameters are negative for propagation directions centred around the Y axis. In the case of berlinite (as well as quartz), this behaviour is in good agreement with the anomalous positive temperature dependence of C_{66} where it is consistent with interaction between the transverse - acoustic phonon branch and the optic branch in the same crystallographic Y direction, softening of these particular optic phonons being responsible for the α-β structural transformation which takes place at about 853K. However it has been observed that certain elastic

stiffness tensor components C' (=0.5(C_{11}-C_{12}) and the stiffened C_{44}^{D} of $Li_2B_4O_7$ show rather unusual behaviour and the shear elastic stiffness constant C_{44}^{E} has positive temperature derivatives in the whole temperature range studied. This means that under the influence of temperature the shear acoustic phonons propagated along the [001] direction with particle polarisation on the XY plane show an indication of acoustic phonon mode softening. No phase transition has been observed in our work either on the lattice parameter or elastic stiffness tensor components measurements in temperature range between 4.2K and 298K and also with pressure.

Axial acoustic vibrational anharmonicity and thermal effects have been examined carefully in both the uniaxial crystals, berlinite and lithium tetraborate, by means of the mean elastic and thermal Grüneisen parameters. The difference in magnitudes have been shown to be due basically to high anisotropy of the second order elastic compliances and thermal expansion, and also the difference contribution of individual acoustic and optic phonons modes to the resultant of elastic and thermal Grüneisen parameters.

A suggestion for future work is to continue with a programme whose aim is to provide an individual high order elastic stiffness tensor components of materials in order to obtain a clearer picture of the acoustic mode vibrational anharmonicity. Knowledge of optical phonons has also to be obtained since they also play an important

role to physical, thermal and electrical properties of materials.

REFERENCES

Adachi M., Shiosaki T., Kobayashi H., Ohnishi O. and Kawabata A. (1985) Proc. IEEE Ultrasonic Symposium, 228

Altman H.E. and Beyer R.T. (1976) J. Acoust. Soc. Am. 59, 545

Anderson O.L. (1963) J. Phys. Chem. Solids 24, 909

Anderson O.L. (1965) Physics of Non-Crystalline Solids, (North-Holland, Amsterdam), 179

Anderson O.L. (1966) J. Phys. Chem. Solids, 27, 547

Anderson P.W., Halperin B.I. and Varma C.M. (1972) Phil. Mag. 25, 1

Anderson P.W. (1979) in Condensed Matter, eds. Balian R., Maynard R. and Toulouse G. (Noth Holland: Amsterdam) p. 159

Arnold H. (1965) Z. Kristal. 121, 145

Aschroft N.W. and Mermin N.D. (1976) Solid State Physics, (Saunders College, New York)

Auld B.A. (1973) Acoustic Fields and Waves in Solid. Vol 1 (Wiley, London).

Austin J.B., Salni H. and Pierce R.H.H. (1940) Phys. Rev. 57, 931

Avogadro A., Ferloni P., Ghelfestein M., Magistris A., Szwarc H. and Toscani S. (1983) J. Non-Cryst. Solids 58, 178

Axe J.D. and Shirane G. (1970) Phys. Rev. B 1, 342

Azaroff L.V. (1968) Elements of X-ray Crystallography (McGraw-Hill, London)

Bailey D.S., Soluch W., Lee D.L., Vetelino J.F. and Andle J. (1982) Proc. 36th. Ann. Freq. Control Symposium, 124

Barron T.H.K. (1955) Phil. Mag. 46, 720

Barron T.H.K. and Domb C. (1955) Proc. Royal Soc. A 227, 447

Barron T.H.K., Collin J.G., Smith T.W. and White G.K. (1982) J. Phys. C 15, 4311

Bauer K.H.W., Agodzinski H.J., Dorner B. and Grimm H. (1971) Phys. Status Solidi B 48, 437

Benbattouche N., Saunders G.A. and Sidek H.A.A. (1989) accepted for publication by Phil. Mag.

Bernstein B.T. (1963) Phys. Rev. 132, 50

Bhalla A.S., Cross L.E. and Whatmore R.W. (1985) Jap. J. App. Phys. 24, sup. 24-2, 727

Biscoe J., Pincus A., Smith C. Jr. and Warren B. (1941) J. Amer. Ceram. Soc. 24, 116

Bobovich Y.S. (1962) Optical Spectroscopy 13, 274.

Bogardus E.H. (1965) J. Appl. Phys. 36, 2504.

Borjesson L. and Torrell L.M. (1985) Phys. Lett. A 107, 190

Born M. (1939) J. Chem. Soc. 7, 591

Born M. (1943) Proc. Camb. Philos. Soc. 39, 100

Born M. and Huang K. (1954) Dynamical Theory of Crystal Lattices (Oxford University, Clarendon Press)

Boulos E.N. and Kreidl N.J. (1971) J. Am. Chem. Soc. 54, 368

Bradley C.C. (1969) High Pressure Methods in Solid State Research, (Butterworth, London).

Brassington M.P., Lambson W.A., Miller A.J., Saunders G.A. and Yogurtcu Y.K. (1980), Phil. Mag., 42, 127

Brassington M.P., Miller A.J., Pelzl J. and Saunders G.A. (1981a) J. Non-Cryst. Solids 44, 157

Brassington M.P., Miller A.J. and Saunders G.A (1981b), Phil. Mag., 43, 1049

Brassington M.P., Tu Hailing, Miller A.J. and Saunders G.A. (1981) Mat. Res. Bull. 16, 613

Brassington M.P. (1982) PhD. Thesis, University of Bath.

Bray P.J.(1985) J. Non-Cryst. Solids 75, 29

Bray P.J. and O'Keefe J.G. (1963) Phys. Chem. Glasses 4, 37

Bridge B., Patel N.D. and Waters D.N. (1983) Phys. Stat. Sol. (a) 77, 655

Bridge B. and Higazy A.A. (1986) Phys. and Chem. of Glasses, 27, 1, 1

Bridgman P.W. (1958) The Physics of High Pressure, (Bell and Sons, London).

Brugger K. (1964) Phys. Rev. 133, A1604

Brugger K. (1965) Phys. Rev. 137, A1826

Brugger K. (1965b) J. Appl. Phys. 36, 767

Brugger K. and Fritz T.C. (1967) Phys. Rev. 157, 524

Buerger M.J. (1948) Am. Mineral 33, 751

Bues W. and Gehrke H.W. (1956) Z. Anorg. Allegm. Chemie, 288, 307.

Burns G. (1985) Solid State Physics (Academic Press, New York)

Bunton G.V. and Weintraub S. (1967) J. Phys. C 2, 116

Carini G., Cutroni M., Federico M., Galli G. and Tripodo G. (1983) J. Non-Cryst. Solids, 56, 393

Carini G., Cutroni M., Federico M., Galli G. and Tripodo G. (1984a) PHys. Rev. B 30, 7219

Carini G., Cutroni M., Fontana M. and Rocca F. (1984b) Phys. Rev. B29, 3567

Carini G., Cutroni M., Federico M. and Tripodo G. (1985), Phy. Rev. B 32, 8264

Chang E. and Barsch G.R. (1973) J. Phys. Chem. Solids 34, 1543

Chang Z.P. and Barsch G.R. (1976) IEEE Trans. Sonics and Ultrasonics 23, 127

Chiodelli G., Magistris, A. and Villa M. and Bjorkstam J. (1982), J. Non-Cryst. Solids 51, 143

Chung D.H., Chick B.B. and Silversmith D.J. (1969) Rev. Sci. Instr., 40, 718

Cignini P. and Pistola, G. (1978) Elect. Act., 23, 1099

Comes R., Lambert M. and Gruinier A. (1970) Acta Cryst. A 26, 244

Comins J.D., Macdonald J.E., Lambson E.F., Saunders G.A., Rowsell A.J. and Bridge B. (1987) J. Mat. Sci. 22, 2113.

Corbridge D.E.C. and Lowe E.J. (1954) J. Chem. Soc. 493.

Cottam R.I. and Saunders G.A. (1973) J. Phys. C 6, 2105

Dalba G., Fontana A., Fornasini P., Mariotto G., Masullo M.R. and Rocca, F. (1983) Solid State Ionics, 9/10, 597

Dean P. (1964) Proc. Phys. Soc. Lond. 84, 727

deDecker H.C.J. and MacGillavry C.H. (1941) Rec. Trav. Chim. 60, 153

de Launey J. (1956) Solid State Physics 2, 220

Dernier P.D., Bucher E. and Longinotti L.D. (1975) J. Solid State Chem. 15, 203

Detaint J., Poignant H. and Toudic (1980) Proc. 34th. Ann. Freq. Control Symposium USAERADCOM, Ft. Monmoth, New Jersey

Elliott S.R. (1984) Physics of Amorphous Materials (Longman: London) p. 135

El-Mallawany R.A. and Saunders G.A. (1988) J. Mat. Sci. Letts. 6, 443

Emin C.D.J. and Werner J.F. (1983) An. Freq. Control. Symp. 30, 136

Ermolenko N.N. (1966) in The Structure of Glass vol. 6. ed. by Porai-Koshits E.A. translated from Russia by Boris Urarov E. (Consultants Bureau, New York) p. 52

Fajan K. and Barber S.W. (1952) J. Amer. Chem. Soc. 74, 2761

Fawcett V., Long D.A. and Taylor L.H. (1976) Proc. 5th Int. Conf. Raman Spectroscopy, 112.

Flower S.C., Saunders G.A. and Yogurtcu Y.K. (1985) J. Phys. Chem. Solid 46, 1, 97

Ford P.J., Lambson W.A., Miller A.J, Saunders G.A., Bach H. and Methfessel S. (1980) J. Phys. C 13, L697

Fritz I.J. (1974) J. Phys. Chem. Solids 35, 817

Fukuta K., Ushizawa J., Suzuki H., Ebata Y. and Matsumura S. (1983) Jpn. J. Appl. Phys. 22, Suppl. 22-2, 140

Futterer H., Pelzl J., Bach H., Saunders G.A. and Sidek H.A.A. (1988) J. Mater. Sci. 23, 121

Garber J.A. and Granato A.V. (1975) Phys. Rev. B 11, 10, 3990

Garret J.D., Iyer N.M. and Greedan J.E. (1977) J. Cryst. Growth 41, 225

Gaskel P.H. (1966) Trans. Faraday Soc. 62, 1493

Golding B. and Graebner J.E. (1981) in Amorphous Solids - Low Temperature Properties, ed. Phillips W.A. (Springer, Berlin) p. 107

Grimm H. and Dorner B. (1975) J. Phys. Chem. Solids 36, 407

Hall D.W., Brawer S.A. and Weber M.J. (1982) Phys. Rev. B25, 2828

Hearman R.F.S. (1961) An Introduction of Applied Anisotropic Elasticity (Oxford University Press).

Hughes D.S. and Kelly J.K. (1953) Phys. Rev. 92, 1145.

Hunklinger S. and Arnold W. (1976) in Physical Acoustics: Principle and methods, eds. Mason W.P. and Thurston R.N. vol 12, (Academic Press, London)

Hunklinger S. (1977) Festkorperprobleme 17, 1

Hunklinger S. (1982) J. de Physique 43, C9, 461

Huntington H.B. (1947) Phys. Rev. 72, 321

Huntington H.B. (1958) in Solid State Physics eds. Seitz F. and Turnbull D. (Academic Press Inc., New York) p. 213

IRE Standards on Piezoelectric Crystal (Proc. IRE 46, 764 (1958); 37, 1378, (1949))

Kaga H. (1968) Phys. Rev. 172, 900

Kim K.S. and Bray P.J. (1974), J. Non-Metal, 2, 95

Kittinger E. (1977) Ultrasonics, January, 33

Kittle C. (1956, 1971) Introduction to Solid State Physics (Wiley, London).

Knolmayer E. (1980) Proc. 34th. Ann. Freq. Control Symposium USAERADCOM, Ft. Monmoth, New Jersey

Krogh-Moe J. (1962) Acta Cryst. 15, 190

Krogh-Moe J. (1968) Acta Cyst. 24B, 177

Kurnick S.W. and Meyer C. (1964) J. Phys. Solids 25, 115

Lakkad S.C. (1971) J. Appl. Phys. 42, 4277

Lambson E.F., Saunders G.A., Bridge B. and El-Mallawany R.A. (1984) J. Non Cryst. Solids, 69, 117

Lambson E.F., Lambson W.A., MacDonnald J.E., Gibbs M.R.J. and Saunders G.A. (1986) Phys. Rev. 33, 2380

Lambson E.F. (1988) MPhil. Thesis, University of Bath.

Landau L.D. and Lipshitz E.M. (1958) Statistical Physics (Pergamon, London) chap. XIV

Landau L.D. and Lipshitz E.M. (1970) Theory of Elasticity (Pergamon Press, Oxford).

Lang R., Calvo C. and Datars W.R. (1977) Can. J. Phys. 55, 1613

Leibfried G. and Ludwig W. (1956) Solid State Physics, eds. Seitz F. and Turnbull D., Academic Press, New York, 2, 276

Leibfried G. and Ludwig W. (1961) Solid State Physics, 12, 276

Lewis B., Shorrocks N.M. and Whatmore R.W. (1982) Ultrasonic Symposium, 389

Mackenzie J.D. (1960) ed. Modern Aspects of the Vitreous State (Butterworth, London) chap. 1

Malughani J. and Mercier R. (1984) Solid St. Ionics, 13, 529

Mason W.P. and McSkimin H.J. (1947) J. Acoust. Soc. Am. 19, 469

Mason W.P. (1950) Piezoelectric Crystal and Their Application to Ultrasonics (Van Nostrand, New Jersey), p. 208

Mason W.P. (1957) Physical Acoustics and the Properties of Solids, (Van Nostrand, New York)

May Jr. J.E. (1958) IRE Natl. Conv. Rec. 6, 2, 134

McSkimin H.J., Andreath P. and Thurston R.N. (1965) J. App. Phys. 36, 1624

Methfessel S. (1965) IEEE Trans. Magnetics 1, 144

Mierzejewski A., Saunders G.A., Sidek H.A.A. and Bridge B. (1988) J. Non-Cryst. Solids, 104, 323

Miller A.J., Saunders G.A., Yogurtcu Y.K. and Abey A.E. (1981) Phil. Mag. A 43, 6, 1447

Minami T., Jkeda Y. and Tanaka M. (1982), J. Non-Cryst. Solids, 52, 159

Morke I., Kaldis E. and Wachter P. (1985) J. Mag. and Mag. Mat. 52, 335

Munn R.W. (1969) Adv. Phys. 18, 515

Murnaghan F.D. (1944) Proc. Nat. Acad. Sci. USA, 30, 244

Musgrave M.J.P. (1970) Crystal Acoustics (Holden-Day, San Francisco).

Nagel S.R., Herron L.W., Bergeron C.G. (1977) J. Amer. Ceram. Soc. 3/4, 172

Ng. H.N. and Calvo C. (1976) Can. J. Phys. 54, 638

Nye J.F. (1957, 1960) Physical Properties of Crystals (Oxford Clarendon Press, London).

O'Connel R.M. and Carr P.H. (1977) IEEE Trans. on Sonics and Ultrasonics, 24, 6

Ohmachi Y. and Uchida N. (1970) J. Appl. Phys. 41, 2307

Overton W.C. (1962) J. Chem. Phys. 37, 116

Ovshinsky S.R. (1985) in Physical Properties of Amorphous Materials ed. by Adler D., Schwartz B.B. and Steele M.C. (Plenum Press, New York) p. 121

Pace N.G. and Saunders G.A. (1971) J. Phys. Chem. Solids 32, 1585

Palmer W.G. (1962) Experimental Inorganic Chemistry (Cambridge Univ. Press) p. 201

Papadakis E.P. (1964) J. Appl. Phys. 35, 1474

Papadakis E.P., (1967) J. Acoust. Soc. Amer. 42, 1045

Patel N.D. and Bridge B. (1983) Phys. Chem. of Glasses 24, 130.

Patel N.D., Bridge B. and Waters D.N. (1983) Phys. Chem. of Glasses, 24, 122.

Peach R.C., Emin C.D.J., Werner J.F. and Doherty S.P. (1983) Proc. IEEE Ultrasonic Symp. 521

Peercy P.S. and Fritz I.J. (1974) Phys. Rev. Letts. 32, 9, 446

Phillips W.A. (1972) J. Low Temp. Phys. 7, 351

Phillips W.A. (1981) ed. Topic in Current Physics, Amorphous Solids: Low Temperature Properties (Springer-Verlaq Berlin)

Phillips W.A. (1985) J. Non-Cryst. Solids 77/78, 1329

Phillips W.A. (1987) Rep. Prog. Phys. 50, 1657

Piché L., Maynard R., Hunklinger S. and Jackle J. (1974) Phys. Rev. Lett. 32, 1426

Pohl R.O.(1981) in Topic in Current Physics, Amorphous Solids: Low Temperature Properties ed. Phillips W.A. (Springer-Verlaq Berlin)

Porai-Koshits E.A. (1985) J. Non-Cryst. Solids 73, 79

Ray R.N. (1975) Glass Technology 16, 107.

Raychaudhuri A.K. and Hunklinger S. (1984) Z. Phys. B. Condensed Matter 57, 113

Rivier N. (1987) Adv. Phys. 36, 1, 95

Robertson D.S. and Young I.M. (1982) J. Mater. Sci. 17, 1729

Ryan F.M., Greenberg I.N., Carter F.L. and Miller R.C. (1962) J. Appl. Phys. 33, 3, 864

Salleh M.D.M. (1988) PhD. Thesis, University of Bath.

Samara G.A. and Giardini A.A. (1964) Rev. Sci. Instrum. 35, 989

Sastry B.S.R. and Hummel F.A. (1959) J. Am. Ceram. Soc. 42, 216

Sato Y. and Anderson O.L. (1980) J. Phys. Chem. Solids, 41, 401

Saunders G.A. and Yogurtcu Y.K. (1984) Phys. Rev. B 30, 10, 5734

Saunders G.A. and Yogurtcu Y.K. (1984b) Phys. Rev. B 30, 10, 5734

Schwarzenbach D. (1966) Z. Kristal. 123, 161

Schiraldi A. (1978) Elect. Act., 23, 1039

Scott J.F. (1970) Phys. Rev. Lett. 24, 1107

Scott J.F. (1971) Phys. Rev. B 4, 1360

Seeger A. and Buck O.Z. (1960) Naturforsch, 15A, 1056

Sharan B. and Dutta B.N. (1964) Acta Cryst. 17, 82

Sheard F.W. (1958) Phil. Mag. 3, 1381

Shih G.K. and Su G.J. (1965) Comptes Rendus 48, 7th Cong. Int. du Verre Int., Bruxelles.

Shiosaki T., Adachi M., Kobayashi H., Araki K. and Kawabata A. (1984) Proc. 5th Symp. Ultrasonic Electronics, Tokyo

Shorrocks N.M., Whatmore R.W., Ainger F.W. and Young I.M. (1981) Ultrasonic Symposium, 337

Slonczewski J.C. and Thomas H. (1970) J. Phys. Rev. B 1, 3545

Swanson H.E., Cook M.I., Evans E.H. and De Groot J.H. (1960) Standard X-ray Diffraction Powder Patterns, Nat. Bureau Standards (U.S) Circ. No. 539 (U.S GPO, Washington D.C.) Vol. 10, p. 3

Takahashi T., Nomura E. and Yamamato O. (1972) J. Appl. Electrochem. 2, 51

Thompson J.C. and Bailey K.E. (1978) J. Non-Cryst. Solids 27, 161

Thong N. and Schwarzenbach D. (1979) Acta Cryst. A 35, 658

Thurston R.N. and Brugger T. (1964) Phys. Rev. 133, A1604

Thurston R.N. (1964) Physical Acoustics 1A, (Academic Press, New York).

Thurston R.N., McSkimin H.J. and Andreath P.J. (1966) J. App. Phys. 37, 1

Truell R., Elbaum C. and Chick B.B. (1969) Ultrasonic Methods in Solid State Physics (Academic Press, New York).

Tu Hailing, Saunders G.A., Lambson W.A. and Feigelson R.S. (1982) J. Phys. C 15, 1399

Tu Hailing and Saunders G.A. (1983) Phil. Mag. A 48, 4, 571

Tu Hailing, Saunders G.A. and Bach H. (1984) Phys. Rev. B.29, 1848

Turnbull D. and Cohen M.H. (1960) in Modern Aspects of the Vitreous State ed. Mackenzie J.D. (Butterworth, London) chap. 3, p. 38

van Wazer J.R. and Campanella D.A. (1950) J. Am. Chem. Soc. 72, 665

van Wazer J.R. (1958) Phosphorous and Its Compounds Chemistry, vol 1, (Interscience, New York) p. 754

Wagman D.D., Evans W.H., Parker V.B., Harlow I., Bailey S.M. and Schumm R.H. (1968) Selected Values of Chemical Thermodynamic Properties Circ. No. 270-3 (U.S. GPO, National Bureau of Standards (U.S) Washington, D.C.) P. 215

Wang C.Y. (1967) Rev. Sci. Inst. 38, 24

Wang Hong, Xu Bin, Liu Xiling, Han Jianru, Shan Shuxia and Li Hu (1986) J. Crys. Growth 1, 227

Warren B.E. (1934) J. Amer. Ceram. Soc. 17, 249

Warren B.E. (1941) J. Amer. Ceram. Soc. 24, 256

Wentorf R.H. (1962) Modern Very High Pressure Techniques (Butterworth London)

Weiss G., Hunklinger S. and Lohneysen H.v. (1982) Physica 109 & 110B, 1946

Westerholt K., Bach H., Wendemuth R. and Methfessel S. (1979) Solid State Commun. 31, 961

Westman A.E.R. (1960) in Modern Aspects of the Vitreous State ed. Mackenzie J.D. (Butterworth, London) chap. 4

Whatmore R.W., Shorrocks N.M., Ainger F.W. and Young I.M. (1981) Elect. Lett. 17, 11

White G.K. (1972) J. Phys. C 5, 2731

Wignal G., Rothon R., Longmann G and Woodward G. (1977) J. Mater. Sci. 12, 1039

Wong J. and Angell C.A. (1976) Glass: Structure by Spectroscopy (Dekker).

Wruk N., Futterer H., Bach H., Pelzl J., Hock K.H. and Saunders G.A. (1985) Phonon Physics, eds. Kollar J., Kroo K., Menyhard N., Siklos T., World Scientific Publ., Singapore, p. 293

Yogurtcu Y.K., Tu Hailing, Saunders G.A., Bach H. and Methfessel S. (1984) J. Mat. Sci. Lett. 4, 230.

Yogurtcu Y.K., Saunders G.A. and Riedi P.C. (1985) Phil. Mag. A 52, 6,833

Zachariasen W.H. (1932) J. Amer. Chem. Soc. 54, 3841

Zachariasen W.H. (1935) J. Chem. Phys. 3, 162

Zachariasen W.H. (1940) Acta Cryst. 2, 57

Zachariasen W.H. (1964) Acta Cryst. 17, 749

Zeller R.C. and Pohl R.O. (1971) Phys. Rev. B 4, 2029

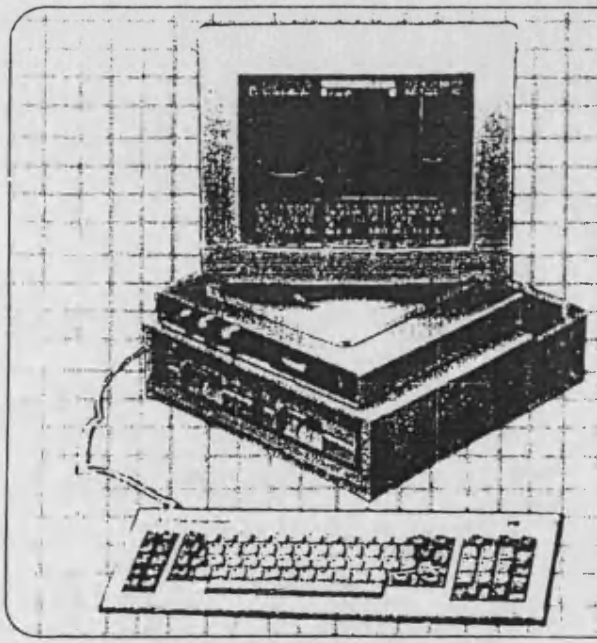

```
550DEFPROC_DISPL
560 IF data=0 THE
570 data=1
580REM ********RE
590 PROC_PROCESS
600PRINTTAB(10);
610PRINTTAB(5)"
620PRINTTAB(5)"
630PRINTTAB(8);L
640PRINTTAB(5);"
650PRINTTAB(11);
" C12 = ";C12/1E
660PRINTTAB(10);
"1E-10;" E- 10 =2
670PRINTTAB(8);"
SOEC":PRINTTAB(8
680PRINTTAB(8)"
DBMP
690PRINTTAB(10)"
AB(8)" C123 + 2C1
700PRINTTAB(2)"
710ENDPROC
720DEFPROC_PRINT
730 IF data=0 THE
740 PROC_PROCESS
750 data=1
760VDU2:*FX6
770PRINT';TAB(10
```

APPENDIX A

COMPUTER PROGRAMME: C.GRUNPAR

The computer programme named C.GRUNPAR written in a BASIC language has been successfully operated in the British Broadcasting Corporation (BBC) computer model 2. The central feature of this computation is the use of the SOEC and their pressure derivatives of a cubic crystal as input data, which provides the convenient link between theoretical and experimental results. This programme is employed to solve Christoffel's equations for the three polarisation vector $\underline{U}$ corresponding to the three normal vibrational modes associated with the propagation direction $\underline{N}$. The calculated polarisation vectors, together with data input are then used to evaluate the ultrasonic wave velocities and the Grüneisen parameters for each of the three modes in cubic crystal. The process is repeated normally in 3° intervals. The primary variables used are:

C11, C12, C44	.... Second order elastic constants
df1, df5, df4	.... Pressure derivative of the SOEC
ro	.... density
vel(i,j)	.... Ultrasonic wave velocities
gru(i,j)	.... Mode Grüneisen parameters
as	.... Degree per step
theta	.... Angle to N from z-axis
phi	.... Angle measured from [110] to [010]

```
 10REM INPUT DATA HERE
 20READ c11,c12,c44
 30READ df1,df5,df4
 40READ ro
 50  DATA 10.857E10,5.87E10,11.15E10
 60 DATA 9.2017,5.0816,0.7465
 70 DATA 7.453E3
 80MODE 3
 90INPUT"Enter degrees per step >"as
100INPUT"Output to printer (Y/N) ? "A$
110nn=135/as
120IF INT(nn)=nn THEN 150
130PRINT';as;" is not a factor of 135"'
140GOTO 90
150DIM vel(3,nn),gru(3,nn),gsum(3),vsum(3)
160DIM A(3,3),V(3),G(3),EV(3,3),EVR(3,3)
170DIM R(3,3),NA(3,3)
180PROCinitialise
190@%=&20207
200CLS
210IF A$="Y" THEN VDU2
220PRINT"theta    phi";TAB(20);"V1";TAB(30);"V2";TAB(40);
230PRINT"V3";TAB(50);"G1";TAB(60);"G2";TAB(70);"G3"
240FORI=0TO79:PRINT"_";:NEXT:PRINT
250VDU 28,0,23,79,3
260NN=90/as
270FOR I%=0 TO NN
280t=45:p=I%*as:REM t,p=theta,phi
290PRINTTAB(2);STR$(t);TAB(9);STR$(p);
300PROCgruneisen(t,p)
310FOR J%=1 TO 3
320vel(J%,I%)=V(J%)
330gru(J%,I%)=G(J%)
340NEXT J%
350PROCoutput
360NEXT I%
370FOR I%=1 TO 45/as
380t=45-I%*as:p=90
390PRINTTAB(2);STR$(t);TAB(9);STR$(p);
400PROCgruneisen(t,p)
410FOR J%=1 TO 3
420vel(J%,NN+I%)=V(J%)
430gru(J%,NN+I%)=G(J%)
440NEXT
450PROCoutput
460NEXT I%
470VDU3
480REM plot results
490MODE4
500ON ERROR GOTO 1020
```

```
 510VDU 23,224,0,0,0,24,24,0,0,0
 520VDU 23,225,102,0,102,102,102,102,62,0
 530xscale=810/nn
 540REPEAT
 550PROCframe
 560PRINTTAB(11,0);"Velocity surface"
 570max=vel(1,0):min=max
 580FOR I%=1 TO nn
 590FOR J%=1 TO 3
 600IF max<vel(J%,I%) THENmax=vel(J%,I%)
 610IF min>vel(J%,I%) THEN min=vel(J%,I%)
 620NEXT:NEXT
 630max=INT(max/100+2)*100
 640min=INT(min/100-1)*100
 650yscale=800/(max-min)
 660@%=&20005
 670PROCscales(max,min)
 680VDU5
 690FOR J%=1 TO nn
 700FOR I%=1 TO 3
 710X%=J%*xscale+200
 720Y%=(vel(I%,J%)-min)*yscale+150
 730MOVEX%-16,Y%+16:PRINTCHR$(224)
 740NEXT:NEXT
 750K=GET
 760CLS
 770VDU4
 780max=gru(1,0):min=max
 790FOR I%=1 TO nn
 800FOR J%=1 TO 3
 810IF max<gru(J%,I%) THENmax=gru(J%,I%)
 820IF min>gru(J%,I%) THEN min=gru(J%,I%)
 830NEXT:NEXT
 840max=INT(max*10+2)/10
 850min=INT(min*10-1)/10
 860yscale=800/(max-min)
 870PROCframe
 880PRINTTAB(10,0);"Gr";CHR$(225);"neisen parameter"
 890@%=&20205
 900PROCscales(max,min)
 910VDU5
 920FOR J%=0 TO nn
 930FOR I%=1 TO 3
 940X%=J%*xscale+200
 950Y%=(gru(I%,J%)-min)*yscale+150
 960MOVEX%-16,Y%+16:PRINTCHR$(224)
 970NEXT:NEXT
 980K=GET
 990CLS
1000VDU4
```

```
1010UNTIL FALSE
1020MODE7
1030ON ERROR OFF
1040END
1050DEF PROCframe
1060MOVE 200,150
1070DRAW 1010,150
1080DRAW 1010,950
1090DRAW 200,950
1100DRAW 200,150
1110FOR I%=230 TO 870 STEP 80
1120MOVE 200,I%:PLOT1,12,0
1130MOVE 1010,I%:PLOT1,-12,0
1140NEXT
1150FOR I%=290 TO 920 STEP 90
1160MOVE I%,150:PLOT1,0,12
1170MOVE I%,950:PLOT1,0,-12
1180NEXT
1190ENDPROC
1200DEF PROCscales(mx,mn)
1210REM y scale first
1220VDU5
1230DN=(max-min)/10
1240N=min
1250FOR I=174 TO 974 STEP 80
1260MOVE 35,I:PRINTN
1270N=N+DN
1280NEXT
1290REM x-axix
1300Y%=140
1310N=0
1320FOR I%=200 TO 740 STEP 90
1330N$=STR$(N):L=LEN(N$)*32
1340X%=I%-L/2
1350MOVEX%,Y%:PRINTN$
1360N=N+15
1370NEXT
1380N=30
1390FOR I%=830 TO 1010 STEP 90
1400N$=STR$(N):L=LEN(N$)*32
1410X%=I%-L/2
1420MOVEX%,Y%:PRINTN$
1430N=N-15
1440NEXT
1450Y%=100
1460RESTORE 1510
1470FOR I=1 TO 4
1480READ X%,D$
1490MOVEX%,Y%:PRINTD$
1500NEXT
```

```
1510DATA 120,"[001]"
1520DATA 450,"[111]"
1530DATA 660,"[110]"
1540DATA 930,"[100]"
1550VDU4
1560PRINTTAB(6,30);"mode propagation direction"
1570ENDPROC
1580DEF PROCoutput
1590FOR J%=1 TO 3
1600PRINTTAB(8+10*J%);V(J%);
1610NEXT
1620FOR J%=1 TO 3
1630PRINTTAB(38+10*J%);G(J%);
1640NEXT
1650PRINT:PRINT
1660ENDPROC
1670DEF PROCgruneisen(theta,phi)
1680theta=RAD(theta):phi=RAD(phi)
1690n3=COS(phi)
1700n2=SIN(phi)*SIN(theta)
1710n1=SIN(phi)*COS(theta)
1720N1=n1*n1:N2=n2*n2:N3=n3*n3
1730REM Christoffel's determinant
1740A(1,1)=N1*c11+N2*c44+N3*c44
1750A(2,2)=N1*c44+N2*c11+N3*c44
1760A(3,3)=N1*c44+N2*c44+N3*c11
1770A(2,3)=n2*n3*(c12+c44)
1780A(1,3)=n1*n3*(c12+c44)
1790A(1,2)=n1*n2*(c12+c44)
1800A(2,1)=A(1,2):A(3,1)=A(1,3):A(3,2)=A(2,3)
1810PROCeigen(3,1E-8)
1820FOR J%=1 TO 3
1830V(J%)=SQR(A(J%,J%)/ro)
1840NEXT J%
1850REM Calculate gruneisen parameter
1860FOR J%=1 TO 3
1870u1=EV(J%,1):U1=u1*u1
1880u2=EV(J%,2):U2=u2*u2
1890u3=EV(J%,3):U3=u3*u3
1900k1=N1*U1+N2*U2+N3*U3
1910ns=(n1*u2+n2*u1)*(n1*u2+n2*u1)
1915nt=(n3*u1+n1*u3)*(n3*u1+n1*u3)
1920k2=(n2*u3+n3*u2)*(n2*u3+n3*u2)+nt+ns
1930k3=2*(n2*n3*u2*u3+n3*n1*u3*u1+n1*n2*u1*u2)
1940W=c11*k1+c44*k2+c12*k3
1950K=C1*k1+C2*k2+C3*k3
1960G(J%)=-(3*B+2*W+K)/(6*W)
1970NEXT J%
1980SOUND1,-10,200,1
1990ENDPROC
2000DEF PROCinitialise
```

```
2010REM Bulk modulus, B
2020B=(c11+2*c12)/3
2030REM Constants for gruneisen
2040C1=-3*B*(1+df1)-c11
2050C2=-3*B*(1+df5)-c44
2060C3=3*B*(1+2*df4-df1)-c12
2070I%=0:J%=0:K%=0:L%=0:P%=0:Q%=0
2080ENDPROC
2090DEF PROCeigen(n,range)
2100LOCAL I%,J%,K%,L%,P%,Q%,X,theta,max
2110FOR I%=1 TO n
2120FOR J%=1 TO n
2130IF I%=J% THEN EV(I%,J%)=1 ELSE EV(I%,J%)=0
2140NA(I%,J%)=A(I%,J%)
2150NEXT:NEXT
2160norm=FNnorm(n)
2170REPEAT
2180onorm=norm
2190REM find largest modulus in upper partition
2200max=0
2210FOR I%=1 TO n-1
2220FOR J%=I%+1 TO n
2230IF max<ABS(A(I%,J%)) THEN max=ABS(A(I%,J%)):P%=I%:Q%=J%
2240NEXT:NEXT
2250REM calculate rotation angle, theta
2260d=A(P%,P%)-A(Q%,Q%)
2270IF d=0 THEN theta=PI/4 ELSE theta=ATN(2*A(P%,Q%)/d)/2
2280VDU4
2290REM Calculate new matrix elements
2300sin=SIN theta:cos=COS theta:sin2=sin*sin:cos2=cos*cos
2310FOR I%=1 TO n
2320IF (I%=P%) OR (I%=Q%) THEN 2360
2330NA(I%,P%)=A(I%,P%)*cos+A(I%,Q%)*sin
2340NA(I%,Q%)=-A(I%,P%)*sin+A(I%,Q%)*cos
2350NA(P%,I%)=NA(I%,P%):NA(Q%,I%)=NA(I%,Q%)
2360NEXT
2370NA(P%,P%)=A(P%,P%)*cos2+2*A(P%,Q%)*sin*cos+A(Q%,Q%)*sin2
2380NA(Q%,Q%)=A(P%,P%)*sin2-2*A(P%,Q%)*sin*cos+A(Q%,Q%)*cos2
2390NA(P%,Q%)=(A(Q%,Q%)-A(P%,P%))*cos*sin+A(P%,Q%)*(cos2-sin2)
2400NA(Q%,P%)=NA(P%,Q%)
2410FOR I%=1 TO n
2420FOR J%=I% TO n
2430A(I%,J%)=NA(I%,J%)
2440A(J%,I%)=A(I%,J%)
2450NEXT:NEXT
2460
2470REM generate rotation matrix R
2480FOR I%=1 TO n
2490FOR J%=I% TO n
2500IF I%=J% THEN R(I%,J%)=1 ELSE R(I%,J%)=0:R(J%,I%)=0
```

```
2510NEXT:NEXT
2520R(P%,P%)=COS theta
2530R(Q%,Q%)=R(P%,P%)
2540R(P%,Q%)=SIN theta
2550R(Q%,P%)=-R(P%,Q%)
2560REM calculate multiple rotation matrix
2570FOR I%=1 TO n
2580FOR J%=1 TO n
2590EVR(I%,J%)=0
2600FOR K%=1 TO n
2610EVR(I%,J%)=EVR(I%,J%)+R(I%,K%)*EV(K%,J%)
2620NEXT:NEXT:NEXT
2630FOR I%=1 TO n
2640FOR J%=1 TO n
2650EV(I%,J%)=EVR(I%,J%)
2660NEXT:NEXT
2670REM Check to see if matrix A is diagonalised
2680norm=FNnorm(n)
2690UNTIL ABS(onorm-norm)<range
2700FOR I%=1 TO n-1
2710max=0
2720FOR J%=I% TO n
2730IF max<A(J%,J%) THEN max=A(J%,J%):K%=J%
2740NEXT
2750X=A(K%,K%):A(K%,K%)=A(I%,I%):A(I%,I%)=X
2760FOR L%=1 TO n
2770X=EV(K%,L%):EV(K%,L%)=EV(I%,L%):EV(I%,L%)=X
2780NEXT:NEXT
2790ENDPROC
2800DEF FNnorm(n)
2810LOCAL S
2820S=0
2830FOR I%=1 TO n
2840S=S+A(I%,I%)*A(I%,I%)
2850NEXT
2860=S
```

APPENDIX B

COMPUTER PROGRAMME: G.ELASTIC

This programme evaluates the elastic properties and acoustic mode vibrational anharmonicity (in terms of the mode Grüneisen parameter) of glasses system. The calculation is straightforward due to the isotropic properties of glass.

Nomenclature of Computer Programme:

RHO	.... Density
L	.... Thickness of sample
LMF, SMF	.... Pulse echo overlapping frequencies
LMG, SMG4	.... Gradient of frequency-pressure plot
vel	.... Ultrasonic wave velocity
C11, C12, C44	.... Second order elastic constants
S11, S12, S44	.... Elastic compliance constants
BM	.... Bulk modulus
dC_{IJ}/dP	.... Pressure derivative of the SOEC
C_{IJK}	.... Third order elastic constant
gama(i), avg	.... Mode Grüneisen parameters

```
 10CLS
 20 data=0
 30REPEAT
 40 *FX15,0
 50MODE7
 60 VDU19,0,6;0;
 70 VDU19,1,0;0;
 80 PRINTTAB(4,1);CHR$(141)" ELASTIC PROPERTIES OF GLASS"
 90PRINTTAB(4,2);CHR$(141)" ELASTIC PROPERTIES OF GLASS"
100PRINTTAB(6,3)" (c) H.A.A Sidek  1986 "
110PRINTTAB(16,5)"MENU"
120PRINTTAB(6,7)"1. ENTER DATA FROM KEYBOARD"
130PRINTTAB(6,9)"2. DISPLAY PRESENT DATA"
140PRINTTAB(6,11)"3. DISPLAY OUTPUT ON SCREEN "
150PRINTTAB(6,13)"4. PRINT OUTPUT (PRINTER)"
160PRINTTAB(6,15)"5. SAVE DATA (DISK)"
170PRINTTAB(6,17)"6. LOAD DATA (DISK)"
180PRINTTAB(3,21)"< PRESS THE NO. OF YOUR CHOICE >"
190 VDU 23,1,0;0;0;0;
200REPEAT
210 Z$=GET$
220 V=VAL(Z$)
230 UNTIL V>0 AND V<7
240IFV=1 THEN MODE3:PROC_INPUT
250IFV=2 THEN MODE3:PROC_PRESENT
260IFV=3 THEN MODE3:PROC_DISPLAY
270IFV=4 THEN MODE3:PROC_PRINT
280IFV=5 THEN MODE3:PROC_SAVE
290IFV=6 THEN MODE3: PROC_LOAD
300REM IFV=7 THEN MODE3: PROC_LOAD
310UNTIL FALSE
320DEFPROC_INPUT
330CLS
340 @%=&820509
350 data=1
360 PRINT" DATA INPUT ":PRINT'
370INPUT"  Sample ff ";M$
380 INPUT"  Density of sample (kgm-3) ";RHO
390 INPUT"  Thickness of sample (mm) ";L
400 INPUT"  Longitudinal mode frequency (kHz) ";LMF
410 INPUT"  Shear mode frequency  (kHz)   ";SMF4
420 SMFD=SMF4
430 INPUT"  Gradient 1/w*dw/dp for longitudinal mode (E-11)m2 N-1 ";LMG
440 INPUT"  Gradient 1/w*dw/dp for shear mode (E-11)m2 N-1 ";SMG4
450 SMGD=SMG4
460
470 L=L*1E-3:LMF=LMF*1E3:SMF4=SMF4*1E3:SMFD=SMFD*1E3:LMG=LMG*1E-11:
480SMG4=SMG4*1E-11:SMGD=SMGD*1E-11
490PRINT:PRINT'" *** < press the space bar > *** ": REPEAT UNTIL GET=32
500ENDPROC
```

```
510DEFPROC_DISPLAY
520 IF data=0 THEN PRINTTAB(5,5)" ***  WARNING *** "
530PRINTTAB(5,7)" PLEASE INPUT YOUR DATA "
535FOR I=1 TO 2500:NEXT I :ENDPROC
540 data=1
550REM *******RESULT *********
560 PROC_PROCESS
570PRINTTAB(10);" ELASTIC PROPERTIES OF ";M$;" AT ROOM TEMPERATURE "
580PRINTTAB(5)" Density (kgm-3)";TAB(29);" Thickness ( E-3 m )"
590PRINTTAB(10);RHO;TAB(36);L/1E-3
600PRINTTAB(5)" Long. vel (ms-1) ";TAB(29);" Shear vel 4 (ms-1) ";
610PRINTTAB(50);" Shear vel 1 (ms-1) "
620PRINTTAB(8);LV;TAB(33);SV4;TAB(55);SVD
630PRINTTAB(5);" Elastic constant (E10 Nm-2) ";TAB(39);
640PRINTTAB(39);" Elastics complience (E-10 m2 N-)"
650PRINTTAB(11);" C11 = ";C11/1E10;TAB(42);" S11 = ";S11/1E-10
660PRINTTAB(11);" C44 = ";C44/1E10;TAB(42);" S44 = ";S44/1E-10
670PRINTTAB(11);" C12 = ";C12/1E10;TAB(42);" S12 = ";S12/1E-10
680PRINTTAB(10);" Anisotropic ratio ";AIR
690PRINTTAB(10)" Bulk modulus ";BM/1E10 ;" E 10 Nm-2"
700PRINTTAB(10);" Volume compressibility ";KV/1E-10;" E- 10 m2 N-1"
710PRINTTAB(10);" Linear compressibility ";KL/1E-10;" E- 10 m2 N-1"
720PRINTTAB(8);" dCl/dp = ";DLP;TAB(29);" ds4/dp = ";DS4P;
730PRINTTAB(50);" dC'/dp = ";DSDP:PRINTTAB(5)" Effective SOEC";
740PRINTTAB(35)" Thermodynamic SOEC":PRINTTAB(8)" dC11/dp = ";DC11P
750PRINTTAB(40)" B11 = ";B11
760PRINTTAB(8)" dC44/dp = ";DC44P;TAB(40)" B44 = ";B44
770PRINTTAB(8)" dC12/dp = ";DC12P;TAB(40)" B12 = ";B12
780PRINTTAB(10)" Combination of TOEC ( E 11 Nm-2 ) "
790PRINTTAB(8)" C111 + 2C112 = ";T1/1E11
800PRINTTAB(8)" C144 + 2C166 = ";T2/1E11
810PRINTTAB(8)" C123 + 2C112 = ";T3/1E11
820PRINTTAB(2)"  *** < press the space bar > ***  "
830REPEAT UNTIL GET=32
840ENDPROC
850DEFPROC_PRINT
860 IF data=0 THEN PRINTTAB(5,5)" ***  WARNING *** "
870PRINTTAB(5,7)" PLEASE INPUT YOUR DATA "
880FOR I=1 TO 2500:NEXT I :PROC_INPUT
890 PROC_PROCESS
900 data=1
910VDU2:*FX6
920PRINT';TAB(10);"ELASTIC PROPERTIES OF ";M$;". "
930PRINTTAB(10);:FOR I=1 TO 45:PRINT"_";:NEXT I
940 PRINT':PRINT'
950PRINTTAB(10);"Density (kgm-3)" ;TAB(36);RHO
960PRINT';TAB(10);"Thickness (E-3 m )";TAB(36);L/1E-3
970PRINT';TAB(10);"Elastic constants ":PRINTTAB(13);"(E 10 Nm-2)"
980PRINTTAB(10);"C11 ";TAB(36);C11/1E10
990PRINTTAB(10);"C12 ";TAB(36);C12/1E10
1000PRINTTAB(10);"C44 ";TAB(36);C44/1E10
```

```
1010PRINTTAB(10);"C' = 0.5(C11-c12) ";TAB(36);CD/1E10
1020PRINTTAB(10);"Bulk modulus B ";TAB(36);BM/1E10
1030PRINT';TAB(10);"Elastic compliances ":PRINTTAB(13);"(E-10 m2 N-1)"
1040PRINTTAB(10);"S11 ";TAB(36);S11/1E-10
1050PRINTTAB(10);"S12 ";TAB(35);S12/1E-10
1060PRINTTAB(10);"S44 ";TAB(36);S44/1E-10
1070REM PRINT';TAB(10);"Anisotropic ratio ";TAB(36);AIR
1080REM PRINT';TAB(10);"Bulk modulus B ";TAB(36);BM/1E10
1090REM PRINT';TAB(10);"Linear compressibility  ";TAB(36);KL/1E-10
1100PRINT';TAB(10);"Hydrostatic pressure derivatives "
1110PRINT';TAB(10);"dC11/dp";TAB(36);DC11P
1120PRINTTAB(10);"dC12/dp";TAB(36);DC12P
1130PRINTTAB(10);"dC44/dp";TAB(36);DC44P
1140PRINTTAB(10);"dB/dp";TAB(36);DBDP
1150PRINT';TAB(10);"B11";TAB(36);B11:PRINTTAB(10);"B12";
1160PRINTTAB(36);B12:PRINTTAB(10);"B44";TAB(36);B44
1170PRINTTAB(10);"Volume compress.   K ";TAB(36);KV/1E-10
1180PRINTTAB(10);"Linear compress.   l ";TAB(36);KL/1E-10
1190PRINT';TAB(10);"Combination of TOEC ":PRINTTAB(13);"(E 11 Nm-2)"
1200PRINT';TAB(10);"C111 + 2C112 ";TAB(36);T1/1E11
1210PRINTTAB(10);"C144 + 2C166 ";TAB(36);T2/1E11
1220PRINTTAB(10);"C123 + 2C112 ";TAB(36);T3/1E11
1230PRINT';TAB(10);"Gama(l) ";TAB(36);GAL
1240PRINT TAB(10);"Gama(s) ";TAB(36);GAS
1250PRINT TAB(10);"Mean Gruneisen parameter ";TAB(36);AVG
1260 VDU3:FOR I=1 TO 3000 :NEXT I
1270 ENDPROC
1280DEFPROC_PROCESS
1290@%=&20309
1300 REM ***** DATA PROCESSOR ****
1310 REM  L=L*1E-3:LMF=LMF*1E3:SMF4=SMF4*1E3:SMFD=SMFD*1E3
1320LMG=LMG*1E-11:SMG4=SMG4*1E-11:SMGD=SMGD*1E-11
1330CL=RHO*(2*L*LMF)^2:CT4=RHO*(2*L*SMF4)^2:CTD=RHO*(2*L*SMFD)^2
1340C11=CL-CT4+CTD:C44=CT4:C12=CL-CT4-CTD
1350LV=2*L*LMF:SV4=2*L*SMF4:SVD=2*L*SMFD
1360AIR=0.5*(C11-C12)/C44:DES=(C11-C12)*(C11+2*C12)
1370S11=(C11+C12)/DES:S12=-C12/DES:S44=1./C44
1380BM=.33333*(C11+2*C12):KV=1./BM:KL=.33333*KV:E=1./S11:NIU=-S12*E
1390DLP=2*CL*LMG+CL/(C11+2*C12):DS4P=2*CT4*SMG4+CT4/(C11+2*C12)
1400DSDP=2*CTD*SMGD+CTD/(C11+2*C12)
1410DC11P=DLP-DS4P+DSDP:DC44P=DS4P:DC12P=DLP-DS4P-DSDP
1420DBDP=.33333*(DC11P+2*DC12P)
1430T=S11+2*S12:B11=DC11P+1+T*C11:B44=DC44P+1+T*C44:B12=DC12P-1+T*C12
1440T1=-3*BM*B11:T2=-3*BM*B44:T3=-3*BM*B12
1450  DEL=0.5*BM*(B11-1.):GAL=-0.1667+DEL/C11
1460DES=0.5*BM*(B44-1.):GAS=-0.1667+DES/C44:AVG=(GAL+2.*GAS)/3.
1470 REM
1480ENDPROC
1490DEFPROC_SAVE
1500 IF data=0 THEN PRINTTAB(5,5)"***  WARNING ***"
1510PRINTTAB(5,7)" PLEASE INPUT YOUR DATA FIRST "
```

```
1520FOR I=1 TO 2500: NEXT I :PROC_INPUT
1530CLS
1540PRINTTAB(5,5)"ENTER THE NAME OF THE FILE"
1550PRINTTAB(10,7)"YOU WISH TO SAVE"
1560INPUT file$
1570channel% = OPENOUT(file$)
1580PRINT£ channel%,M$,RHO,L
1590PRINT£ channel%,LMF,SMF4,SMFD
1600PRINT£ channel%,LMG,SMG4,SMGD
1610PRINT£ channel%,LMF2,SMF42,SMFD2
1620CLOSE£ channel%
1630ENDPROC
1640DEFPROC_LOAD
1650 data=1
1660CLS
1670PRINTTAB(5,5)"ENTER THE NAME OF THE FILE"
1680PRINTTAB(10,7)"YOU WISH TO LOAD"
1690INPUT file$
1700flen%=100
1710channel% = OPENIN(file$)
1720 INPUT£ channel%,M$,RHO,L
1730 INPUT£ channel%,LMF,SMF4,SMFD
1740 INPUT£ channel%,LMG,SMG4,SMGD
1750INPUT£ channel%,LMF2,SMF42,SMFD2
1760CLOSE£ channel%
1770ENDPROC
1780REM FINISH 22.2.86 5.36 PM. DEE**TEE FRIDAY
1790 DEFPROC_FORMAT
1800 REM
1810 ENDPROC
1820DEFPROC_PRESENT
1830 IF data=0 THEN PRINTTAB(5,5)"***  WARNING ***":
1840PRINTTAB(5,7)" PLEASE INPUT YOUR DATA FIRST "
1850FOR I=1 TO 2500: NEXT I :PROC_INPUT
1860 data=1
1870 PROC_PROCESS
1880 CLS
1890PRINTTAB(1,3)" ELASTIC CONSTANT OF  GLASSY SYSTEM"
1900@%=&820309
1910PRINT"  Present sample : ";M$
1920PRINT"  Density        : ";RHO;"  kgm-3. "
1930PRINT"  Thickness      : ";L/1E-3;"  E-3 m. "
1940PRINT"  Longitudinal mode frequency   : ";LMF/1E3 ;" kHz. "
1950 PRINT"  Shear mode frequency         : ";SMF4/1E3;" kHz. "
1960 PRINT"  Shear mode frequency   (C')   : ";SMFD/1E3;" kHz. "
1970PRINT"  Gradient 1/w*dw/dp for longitudinal mode : ";LMG/1E-11;
1980PRINT"  E-11 m2 N-1."
1990PRINT"  Gradient 1/w*dw/dp for shear mode    : ";SMG4/1E-11;
2000PRINT"  E-11 m2 N-1."
2010PRINT""  *** < Press the space bar > *** ":REPEAT UNTIL GET=32
2020ENDPROC
```

APPENDIX C

Room temperature elastic data of 10 mole% La_2O_3 (B2), 15 mole% La_2O_3 (B3) phosphate glasses and a ceramic of 30 mole% Sm_2O_3-P_2O_5 (A6).

	B2	B3	A6
Density (kgm^{-3})	3346	3413	3731
Elastic constants ($\times 10^{10}$ Nm^{-2})			
C_{11}	6.589	6.763	7.49
C_{12}	2.437	2.154	2.96
C_{44}	2.076	2.305	2.26
Bulk modulus B^s	3.821	3.690	4.47
Poisson's ratio	0.270	0.241	0.28
Elastic compliances ($\times 10^{-10}$ m^2N^{-1})			
S_{11}	0.190	0.175	0.172
S_{12}	-0.051	-0.042	-0.049
S_{44}	0.482	0.434	0.440
Volume compressibility	0.262	0.271	0.224
Linear compressibility	0.087	0.090	0.075
Hydrostatic pressure derivatives			
dC_{11}/dP	2.193	3.557	1.33
dC_{12}/dP	1.968	3.300	1.76
dC_{44}/dP	0.113	0.128	-0.21
dB^s/dP	2.043	3.386	1.62
B_{11}	3.768	5.168	2.89
B_{12}	1.181	2.495	0.98
B_{44}	1.294	1.337	0.95
Grüneisen parameter			
γ_L	0.469	0.804	0.23
γ_S	-0.063	-0.064	-0.38
Mean $(\gamma_L + 2\gamma_S)/3$	0.114	0.225	-0.17

PUBLICATIONS

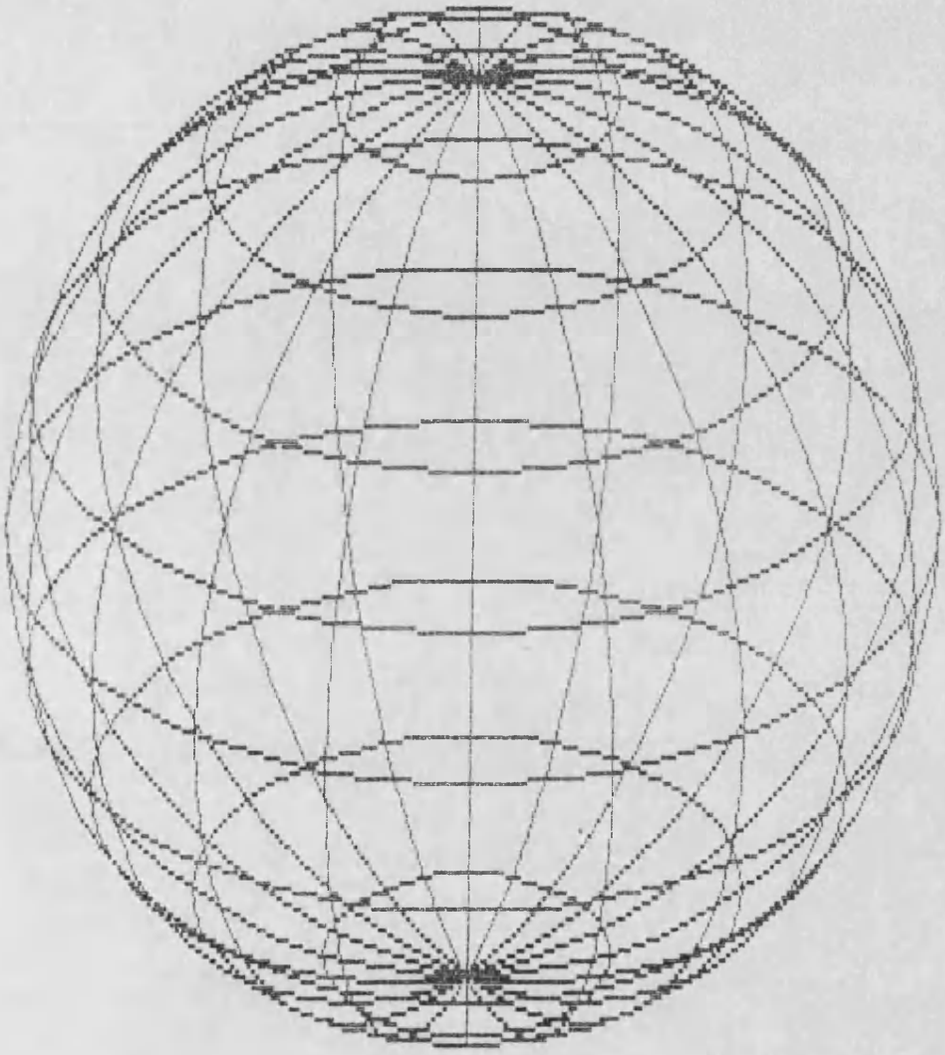

PUBLICATION.

Elastic Behaviour Under Pressure of Superionic Glasses
G.A. Saunders, H.A.A. Sidek, J.D. Comins, G. Carini and M. Federico
Phil. Mag. B56, 1, 1-13, (1987)

Elastic Behaviour Under Hydrostatic Pressure and Acoustic Mode Vibrational Anharmonicity of Single-Crystal Berlinite
H.A.A. Sidek, G.A. Saunders, Wang Hong, Xu Bin and Han Jianru
Phys. Rev. B36, 7612-7619, (1987)

Valence Instability of Samarium Ion In A Phosphate Glasses
A. Mierzejewski, I.J. Mummar G.A. Saunders and H.A.A. Sidek
6th. International Meeting on Solid State Ionincs, Garmisch-Partenkirchen, September 6-11, (1987)

The Elastic Behaviour of Ce_3S_4 and La_3S_4
H. Futterer, J. Pelzl, H. Bach, G.A. Saunders and H.A.A. Sidek
J. Mat. Sci. 23, 121-125, (1988)

Samarium Ion Valence Instability in a Glassy Matrix
H.A.A. Sidek, G.A. Saunders, R.N. Hampton, R.C.J. Draper and B. Bridge
Phil. Mag. Letts., 57, 49-53, (1988)

Vibrational Properties of Samarium Phosphate Glasses
A. Mierzejewski, G.A. Saunders, H.A.A. Sidek and B. Bridge
J. Non-Cryst. Solids, 104, 323-332, (1988)

Electrical Conductivity and Dielectric Constant of Samarium Phosphate Glasses
H.A.A. Sidek, I.T. Collier, R.N. Hampton, G.A. Saunders and B. Bridge
accepted by Phil. Mag. (1988)

Valence Instability of Samarium Ion in A Phosphate Glass
A. Mierzejewski, G.A. Saunders, H.A.A. Sidek, R.N. Hampton and I.J. Mummar
Solid State Ionics, 28, (1988)

Electrical Properties of Samarium Phosphate Glasses
H.A.A. Sidek, I.T. Collier, R.N. Hampton, G.A. Saunders and B. Bridge
11th. European Conference on Thermophysical Properties, Umea, Sweden, Jun, (1988)

Anharmonicity of Acoustic Modes in vitreous TeO_2
N.E. Benbattauche, G.A. Saunders and H.A.A. Sidek
accepted for publication by Phil. Mag.

Temperature Dependences of the Second Order Elastic Constants of Samarium Phosphate Glasses
H.A.A. Sidek and G.A. Saunders
- to be published

Elastic Properties of Lithium Tetraborate
H.A.A. Sidek, G.A. Saunders and B. James
- to be published

The Effect of Hydrostatic Pressure on the Dielectric Constants and their Temperature Dependences of Phosphate and Tellurite Glasses
R.N. Hampton, I.T. Collier, H.A.A. Sidek and G.A. Saunders
- to be published